# THEORY OF ELECTRON LOCALIZATION

# IN DISORDERED SYSTEMS

by

WOLFRAM TILL ARNOLD

A DISSERTATION

Presented to the Department of Physics
and the Graduate School of the University of Oregon
in partial fulfillment of the requirements
for the degree of
Doctor of Philosophy

August 2000

"Theory of Electron Localization in Disordered Systems," a dissertation prepared by Wolfram Till Arnold in partial fulfillment of the requirements for the Doctor of Philosophy degree in the Department of Physics. This dissertation has been approved and accepted by:

---

Prof. Roger Haydock, Chair of the Examining Committee

---

Date

Committee in charge:
Prof. Roger Haydock, Chair
Prof. Dietrich Belitz
Prof. J. David Cohen
Prof. Janice Cuny
Prof. Stephen D. H. Hsu

Accepted by:

---

Dean of the Graduate School

©2000 Wolfram Till Arnold

An Abstract of the Dissertation of

Wolfram Till Arnold for the degree of Doctor of Philosophy

in the Department of Physics to be taken August 2000

Title: THEORY OF ELECTRON LOCALIZATION IN DISORDERED SYSTEMS

Approved: _____

Prof. Roger Haydock

The effects of disorder penetrate many areas of physics. A question of fundamental interest is how disorder affects the conductance of a material.

In this dissertation, we have studied the quantum mechanical transmittance of disordered samples which dominates the conductance in the low-temperature regime where phase-destroying, inelastic scattering events are infrequent. When the phase is conserved, disorder may eventually lead to a localization of the wavefunction, and hence insulating behavior, through destructive interference between different components of the wavefunction.

While many phenomena are attributed to an interplay of disorder and carrier interactions, non-interacting models, specifically the Anderson model, display surprising complexity and despite a large body of research, some aspects have remained inconclusive.

For the Anderson model, our findings indicate that in one dimension, all states are exponentially localized. In two dimensions, the states are localized with

a power law at low disorders, which turns into an exponential law at a disorder strength of about $W \geq 12$. A mobility edge between center-of-band states and edge states persists up to the highest studied disorder of $W = 30$, indicating a qualitative difference in the localization. In three dimensions, the states are delocalized up to a disorder of around $W = 8$. Beyond that, the system exhibits only power-law localization up the highest disorder considered, $W = 24$. A sharp mobility edge exists and moves outward with increasing disorder. This supports a qualitative difference between center-of-band states and edge states.

In the second part of this dissertation, we address recent experimental findings of an apparent 2D metal-insulator transition in high-mobility Silicon MOSFETs. Owing to the low carrier density, electron-electron interaction effects are considered to play an important role in this effect. Using a simple interacting model based on the Hubbard Hamiltonian and including temperature, we can apply the same techniques as before and find a qualitative separation between a conductive and an insulating regime depending on the interaction strength.

The computations have been carried out with a new parallel implementation of the recursion method that can handle systems of previously unprecedented size, e.g. $10^{15}$ degrees of freedom and exhibits outstanding, linear parallel speedup up to 128 processors.

# CURRICULUM VITA

NAME OF AUTHOR: Wolfram Till Arnold

PLACE OF BIRTH: Usingen, Germany

DATE OF BIRTH: 1971

GRADUATE AND UNDERGRADUATE SCHOOLS ATTENDED:

University of Oregon
Universität Ulm, Germany

DEGREES AWARDED:

Doctor of Philosophy, 2000, University of Oregon
Diplom, 1998, Universität Ulm
Master of Arts, 1997, University of Oregon
Vordiplom, 1992, Universität Ulm

AREAS OF SPECIAL INTEREST:

Disordered, interacting condensed matter systems
Numerical approaches to many-body problems
Large-scale sparse matrix computation
Parallel processing

PROFESSIONAL EXPERIENCE:

Research Assistant, Department of Physics, University of Oregon, Eugene, 1996-1999

Teaching Assistant, Department of Physics, University of Oregon, Eugene, 1995-1996

Software Development and Technology Consulting, Inwave Corp., Eugene, Oregon, 1997

Software Development, Siemens Corp., Munich, Germany, 1993

AWARDS AND HONORS:

Study-abroad stipend, Baden-Württemberg–Oregon exchange program, 1994

PUBLICATIONS:

W. T. Arnold, R. Haydock, "A parallel, object-oriented implementation of the dynamic recursion method" In D. Caromel, R. Oldehoeft, and M. Tholburn, editors, *Computing in Object-Oriented Parallel Environments. Second International Symposium, ISCOPE 98. Proceedings*, pages 199–206, Berlin, Germany, 1998. Springer-Verlag.

# ACKNOWLEDGEMENTS

First and foremost I am deeply indebted to my mother and father, Jutta and Robert Arnold, who never tired to lend support wherever needed throughout this decade of my college and university education. They share credit in my earning this degree and this accomplishment is as much theirs as mine.

I would like to thank my advisor, Roger Haydock, for welcoming me into his research group and extending his trust, for giving me much latitude in making design choices in the computational aspects of this research, for patiently teaching me his view of physics, and for discussing interesting topics "over tea" throughout the years. His family is credited for the occasional invitation for lunch or to the symphony which have contributed to the very pleasant atmosphere.

I am grateful for the excellent lecture courses by Dietrich Belitz and Michael Raymer; I thank Janice Cuny and John Conery for introducing me to parallel computing. The Computational Science Institute has been supportive in providing access to its computational facilities, administered by the capable hands of Craig Thornley. Chris Nex deserves credit for brainstorming the initial form of PARP during my 1995 stay in Cambridge; Sameer Shende has been invaluable in teaching me the ins and outs of profiling parallel applications.

The support of the administrative staff at the Materials Science Institute, Lucy Biggs-Glassberg, Suzi Creech and formerly Kristi Mikkelsen, as well as at the physics department, Sandee Thompson and Jani Calavan, through their unparalleled efficiency and friendly expertise has been invaluable.

Much credit belongs to many fellow students whom I have had the honor to

become friends with. Out of the many that must remain unnamed, I would like to mention Parvez Anandam, Klaus Engenhardt, Xudong Fan, Christoph Greiner, Tom Loftus, Rajesh Narayanan, Kimon and Phedon Palinginis, Ramasubramaniam Rajagopal, Elizabeth "Betsy" Raymond, Sharon Sessions, Sameer Shende, Weidong Yang for stimulating and diverse discussions, technical assistance and numerous memorable moments spent together. Dietrich Belitz, J. David Cohen, Stephen Gregory and Yoram Lubianiker are thanked for helpful comments and discussion.

Furthermore, I would like to thank the former staff of the Advanced Computing Laboratory at the Los Alamos National Laboratory, notably Theresa Ayala, Peter Beckman, Tim Cleland, Julian Cummings, Scott Haney, William Humphrey, Steve Karmesin, Rod Oldehoeft, John Reynders, Suvas Vajracharya and Timothy Williams for giving me the opportunity to work with them in summer 1999 at Los Alamos and to use their computational facility without which some of the present research would not have been possible.

Among the many friends outside the university, I would like to highlight Pam Smith and Tim Whitley who have made me part of their family and welcomed me warmly into the Eugene community at the beginning of my stay.

This work was supported by the National Science Foundation Materials Theory Program under grant no. DMR-9319246, and by the Office of Science and Technology Infrastructure under grant no. STI-9413532.

# DEDICATION

To

my dear Mother, Father and Brothers

TABLE OF CONTENTS

Chapter Page

I. INTRODUCTION . . . . . 1

II. MODELS OF DISORDER AND TRANSPORT PROPERTIES . . . 4

2.1. Introduction . . . . . 4
2.2. The Anderson Model . . . . . 5
2.3. Scaling Arguments . . . . . 8
2.4. Non-Scaling Approaches . . . . . 13
2.5. Interaction Effects . . . . . 13
2.6. The Hubbard Model and Random-Alloy Analogy . . . . . 16
2.7. Conductance and Transmittance . . . . . 19

III. HOW TO EFFICIENTLY COMPUTE TRANSMITTANCES FROM GIANT SPARSE MATRICES . . . . . 22

3.1. Introduction . . . . . 22
3.2. The Recursion Method . . . . . 25
3.3. Projected Quantities and Lead States . . . . . 30
3.4. Projected Density of States and Related Theory . . . . . 34
3.5. Transmittance . . . . . 40
3.6. Identification of Ghosts . . . . . 42
3.7. Tools . . . . . 44

IV. TRANSMITTANCE IN DISORDERED SYSTEMS—RESULTS . . . 46

4.1. Introduction . . . . . 46
4.2. Interrelation of Localization and Ghosting . . . . . 48
4.3. Computation of Transmittance and Inferred Localization . . . 53
4.4. Transmittance of Disordered 1D System . . . . . 54
4.5. Transmittance of Disordered 2D System . . . . . 60
4.6. Transmittance of Disordered 3D System . . . . . 67
4.7. Mobility Edge Trajectory . . . . . 75
4.8. A Model for Conductance of a 2D Disordered, Interacting System 78

Page

V. THE PARALLEL RECURSION PROJECT . . . . . 82

5.1. Introduction . . . . . 82
5.2. Design . . . . . 83
5.3. Performance Results . . . . . 88

VI. DISCUSSION AND CONCLUSION . . . . . 92

APPENDIX

A. TRANSMITTANCE PLOTS FOR DISORDERED 1D SYSTEM . . 96

B. TRANSMITTANCE PLOTS FOR DISORDERED 2D SYSTEM . . 108

C. TRANSMITTANCE PLOTS FOR DISORDERED 3D SYSTEM . . 152

BIBLIOGRAPHY . . . . . 199

POCKET MATERIAL

# LIST OF FIGURES

Figure Page

1. (a) Ordered Potential Wells; (b) Disordered Potential Wells; (c) Distribution of Disordered Potential . . . . . 6

2. A Typical Wavefunction $\psi$ in the Anderson Lattice: (a) Extended State, (b) State at Low Disorder, (c) Localized State at High Disorder . . . . . 8

3. Temperature Dependencies of Resistivities for Various Electron Densities . . . . . 15

4. (a) Bimodal Disorder Distribution and (b) Transitions in Random Alloy Model . . . . . 17

5. Hubbard Density of States, Filling at $T = 0$, $k_BT \sim I$ and Site Occupation (Schematic) . . . . . 18

6. Transformation to the Chain . . . . . 28

7. Spatial Distribution of Vector Components for $\mathbf{u}_0$, $\mathbf{u}_1$, $\mathbf{u}_2$, $\mathbf{u}_3$, $\mathbf{u}_4$, $\mathbf{u}_5$, $\mathbf{u}_{10}$ . . . . . 29

8. Lead-Sample Arrangement for Computation of Transmittance in 2D . 33

9. Distribution of Number of Good Eigenvalues vs. Ghosts for $W = 0$ and $W = 50$ for a 2D System at 1000 Levels . . . . . 48

10. Effect of High Ghost Count on Localization, Example in 1D, $W = 4$, $E \in [-1.5, 1.5]$ . . . . . 52

11. Ghost Count, $n_{\text{gh}}$, and Effective Level Number, $n_{\text{eff}}$ for 1D, $W = 1$ at Various $\epsilon_{\text{gh}}$ . . . . . 56

12. $\langle \log t_N \rangle_E$ vs. $N$ in 1D, $W = 1$, $E \in [-0.5, 0.5]$ . . . . . 56

13. Ghost Count, $n_{\text{gh}}$, and Effective Level Number, $n_{\text{eff}}$ for 1D, $W = 2$ at Various $\epsilon_{\text{gh}}$ . . . . . 57

14. $\langle \log t_N \rangle_E$ vs. $N$ in 1D, $W = 2$, $E \in [-0.5, 0.5]$ . . . . . 57

Page

15. Ghost Count, $n_{\text{gh}}$, and Effective Level Number, $n_{\text{eff}}$ for 1D, $W = 4$ at Various $\epsilon_{\text{gh}}$ . . . . . 58

16. $\langle \log t_N \rangle_E$ vs. $N$ in 1D, $W = 4$, $E \in [-0.5, 0.5]$ . . . . . 58

17. Ghost Count, $n_{\text{gh}}$, and Effective Level Number, $n_{\text{eff}}$ for 1D, $W = 8$ at Various $\epsilon_{\text{gh}}$ . . . . . 59

18. $\langle \log t_N \rangle_E$ vs. $N$ in 1D, $W = 8$, $E \in [-0.5, 0.5]$ . . . . . 59

19. Ghost Count, $n_{\text{gh}}$, and Effective Level Number, $n_{\text{eff}}$ for 2D, $W = 4$ at Various $\epsilon_{\text{gh}}$ . . . . . 61

20. $\langle \log t_N \rangle_E$ vs. $N$ in 2D, $W = 4$, $E \in [-0.5, 0.5]$ . . . . . 62

21. Ghost Count, $n_{\text{gh}}$, and Effective Level Number, $n_{\text{eff}}$ for 2D, $W = 8$ at Various $\epsilon_{\text{gh}}$ . . . . . 62

22. $\langle \log t_N \rangle_E$ vs. $N$ in 2D, $W = 8$, $E \in [-0.5, 0.5]$ . . . . . 63

23. Ghost Count, $n_{\text{gh}}$, and Effective Level Number, $n_{\text{eff}}$ for 2D, $W = 12$ at Various $\epsilon_{\text{gh}}$ . . . . . 63

24. $\langle \log t_N \rangle_E$ vs. $N$ in 2D, $W = 12$, $E \in [-0.5, 0.5]$ . . . . . 64

25. Ghost Count, $n_{\text{gh}}$, and Effective Level Number, $n_{\text{eff}}$ for 2D, $W = 16$ at Various $\epsilon_{\text{gh}}$ . . . . . 64

26. $\langle \log t_N \rangle_E$ vs. $N$ in 2D, $W = 16$, $E \in [-0.5, 0.5]$ . . . . . 65

27. Ghost Count, $n_{\text{gh}}$, and Effective Level Number, $n_{\text{eff}}$ for 2D, $W = 20$ at Various $\epsilon_{\text{gh}}$ . . . . . 65

28. $\langle \log t_N \rangle_E$ vs. $N$ in 2D, $W = 20$, $E \in [-0.5, 0.5]$ . . . . . 66

29. Ghost Count, $n_{\text{gh}}$, and Effective Level Number, $n_{\text{eff}}$ for 2D, $W = 30$ at Various $\epsilon_{\text{gh}}$ . . . . . 66

30. $\langle \log t_N \rangle_E$ vs. $N$ in 2D, $W = 30$, $E \in [-0.5, 0.5]$ . . . . . 67

31. Ghost Count, $n_{\text{gh}}$, and Effective Level Number, $n_{\text{eff}}$ for 3D, $W = 4$ at Various $\epsilon_{\text{gh}}$ . . . . . 69

32. $\langle \log t_N \rangle_E$ vs. $N$ in 3D, $W = 4$, $E \in [-0.5, 0.5]$ . . . . . 69

Page

33. Ghost Count, $n_{\text{gh}}$, and Effective Level Number, $n_{\text{eff}}$ for 3D, $W = 8$ at Various $\epsilon_{\text{gh}}$ . . . . . 70

34. $\langle \log t_N \rangle_E$ vs. $N$ in 3D, $W = 8$, $E \in [-0.5, 0.5]$ . . . . . 70

35. Ghost Count, $n_{\text{gh}}$, and Effective Level Number, $n_{\text{eff}}$ for 3D, $W = 12$ at Various $\epsilon_{\text{gh}}$ . . . . . 71

36. $\langle \log t_N \rangle_E$ vs. $N$ in 3D, $W = 12$, $E \in [-0.5, 0.5]$ . . . . . 71

37. Ghost Count, $n_{\text{gh}}$, and Effective Level Number, $n_{\text{eff}}$ for 3D, $W = 16$ at Various $\epsilon_{\text{gh}}$ . . . . . 72

38. $\langle \log t_N \rangle_E$ vs. $N$ in 3D, $W = 16$, $E \in [-0.5, 0.5]$ . . . . . 72

39. Ghost Count, $n_{\text{gh}}$, and Effective Level Number, $n_{\text{eff}}$ for 3D, $W = 20$ at Various $\epsilon_{\text{gh}}$ . . . . . 73

40. $\langle \log t_N \rangle_E$ vs. $N$ in 3D, $W = 20$, $E \in [-0.5, 0.5]$ . . . . . 73

41. Ghost Count, $n_{\text{gh}}$, and Effective Level Number, $n_{\text{eff}}$ for 3D, $W = 24$ at Various $\epsilon_{\text{gh}}$ . . . . . 74

42. $\langle \log t_N \rangle_E$ vs. $N$ in 3D, $W = 24$, $E \in [-0.5, 0.5]$ . . . . . 74

43. Mobility Edge Trajectory for 2D . . . . . 76

44. Mobility Edge Trajectory for 3D . . . . . 76

45. Transmittance vs. Energy and Comparison with Global Density of States in 2D at $W = 12$ . . . . . 77

46. Transmittance vs. Energy and Comparison with Global Density of States in 3D at $W = 4, 16$ . . . . . 78

47. Resistance vs. Temperature for Hubbard Random Alloy Model in 2D 80

48. Index Tree Structure and Parallel Data Partitioning Concepts . . . . 86

49. Performance Test on 12-Node SGI Power Challenge . . . . . 90

50. Performance Test on 128-Node SGI Origin 2000 . . . . . 90

51. $\langle \log t_N \rangle_E$ vs. $N$ in 1D, $W = 1$, $E \in [-3.5, -2.5]$ . . . . . 96

Page

52. $\langle \log t_N \rangle_E$ vs. $N$ in 1D, $W = 1$, $E \in [-2.5, -1.5]$ . . . . . 97
53. $\langle \log t_N \rangle_E$ vs. $N$ in 1D, $W = 1$, $E \in [-1.5, -0.5]$ . . . . . 97
54. $\langle \log t_N \rangle_E$ vs. $N$ in 1D, $W = 1$, $E \in [-0.5, 0.5]$ . . . . . 97
55. $\langle \log t_N \rangle_E$ vs. $N$ in 1D, $W = 1$, $E \in [0.5, 1.5]$ . . . . . 98
56. $\langle \log t_N \rangle_E$ vs. $N$ in 1D, $W = 1$, $E \in [1.5, 2.5]$ . . . . . 98
57. $\langle \log t_N \rangle_E$ vs. $N$ in 1D, $W = 1$, $E \in [2.5, 3.5]$ . . . . . 98
58. $\langle \log t_N \rangle_E$ vs. $N$ in 1D, $W = 2$, $E \in [-3.5, -2.5]$ . . . . . 99
59. $\langle \log t_N \rangle_E$ vs. $N$ in 1D, $W = 2$, $E \in [-2.5, -1.5]$ . . . . . 99
60. $\langle \log t_N \rangle_E$ vs. $N$ in 1D, $W = 2$, $E \in [-1.5, -0.5]$ . . . . . 99
61. $\langle \log t_N \rangle_E$ vs. $N$ in 1D, $W = 2$, $E \in [-0.5, 0.5]$ . . . . . 100
62. $\langle \log t_N \rangle_E$ vs. $N$ in 1D, $W = 2$, $E \in [0.5, 1.5]$ . . . . . 100
63. $\langle \log t_N \rangle_E$ vs. $N$ in 1D, $W = 2$, $E \in [1.5, 2.5]$ . . . . . 100
64. $\langle \log t_N \rangle_E$ vs. $N$ in 1D, $W = 2$, $E \in [2.5, 3.5]$ . . . . . 101
65. $\langle \log t_N \rangle_E$ vs. $N$ in 1D, $W = 4$, $E \in [-4.5, -3.5]$ . . . . . 101
66. $\langle \log t_N \rangle_E$ vs. $N$ in 1D, $W = 4$, $E \in [-3.5, -2.5]$ . . . . . 101
67. $\langle \log t_N \rangle_E$ vs. $N$ in 1D, $W = 4$, $E \in [-2.5, -1.5]$ . . . . . 102
68. $\langle \log t_N \rangle_E$ vs. $N$ in 1D, $W = 4$, $E \in [-1.5, -0.5]$ . . . . . 102
69. $\langle \log t_N \rangle_E$ vs. $N$ in 1D, $W = 4$, $E \in [-0.5, 0.5]$ . . . . . 102
70. $\langle \log t_N \rangle_E$ vs. $N$ in 1D, $W = 4$, $E \in [0.5, 1.5]$ . . . . . 103
71. $\langle \log t_N \rangle_E$ vs. $N$ in 1D, $W = 4$, $E \in [1.5, 2.5]$ . . . . . 103
72. $\langle \log t_N \rangle_E$ vs. $N$ in 1D, $W = 4$, $E \in [2.5, 3.5]$ . . . . . 103
73. $\langle \log t_N \rangle_E$ vs. $N$ in 1D, $W = 4$, $E \in [3.5, 4.5]$ . . . . . 104
74. $\langle \log t_N \rangle_E$ vs. $N$ in 1D, $W = 8$, $E \in [-5.5, -4.5]$ . . . . . 104

Page

75. $\langle \log t_N \rangle_E$ vs. $N$ in 1D, $W = 8$, $E \in [-4.5, -3.5]$ . . . . . 104
76. $\langle \log t_N \rangle_E$ vs. $N$ in 1D, $W = 8$, $E \in [-3.5, -2.5]$ . . . . . 105
77. $\langle \log t_N \rangle_E$ vs. $N$ in 1D, $W = 8$, $E \in [-2.5, -1.5]$ . . . . . 105
78. $\langle \log t_N \rangle_E$ vs. $N$ in 1D, $W = 8$, $E \in [-1.5, -0.5]$ . . . . . 105
79. $\langle \log t_N \rangle_E$ vs. $N$ in 1D, $W = 8$, $E \in [-0.5, 0.5]$ . . . . . 106
80. $\langle \log t_N \rangle_E$ vs. $N$ in 1D, $W = 8$, $E \in [0.5, 1.5]$ . . . . . 106
81. $\langle \log t_N \rangle_E$ vs. $N$ in 1D, $W = 8$, $E \in [1.5, 2.5]$ . . . . . 106
82. $\langle \log t_N \rangle_E$ vs. $N$ in 1D, $W = 8$, $E \in [2.5, 3.5]$ . . . . . 107
83. $\langle \log t_N \rangle_E$ vs. $N$ in 1D, $W = 8$, $E \in [3.5, 4.5]$ . . . . . 107
84. $\langle \log t_N \rangle_E$ vs. $N$ in 1D, $W = 8$, $E \in [4.5, 5.5]$ . . . . . 107
85. $\langle \log t_N \rangle_E$ vs. $N$ in 2D, $W = 4$, $E \in [-5.5, -4.5]$ . . . . . 108
86. $\langle \log t_N \rangle_E$ vs. $N$ in 2D, $W = 4$, $E \in [-4.5, -3.5]$ . . . . . 109
87. $\langle \log t_N \rangle_E$ vs. $N$ in 2D, $W = 4$, $E \in [-3.5, -2.5]$ . . . . . 109
88. $\langle \log t_N \rangle_E$ vs. $N$ in 2D, $W = 4$, $E \in [-2.5, -1.5]$ . . . . . 109
89. $\langle \log t_N \rangle_E$ vs. $N$ in 2D, $W = 4$, $E \in [-1.5, -0.5]$ . . . . . 110
90. $\langle \log t_N \rangle_E$ vs. $N$ in 2D, $W = 4$, $E \in [-0.5, 0.5]$ . . . . . 110
91. $\langle \log t_N \rangle_E$ vs. $N$ in 2D, $W = 4$, $E \in [0.5, 1.5]$ . . . . . 110
92. $\langle \log t_N \rangle_E$ vs. $N$ in 2D, $W = 4$, $E \in [1.5, 2.5]$ . . . . . 111
93. $\langle \log t_N \rangle_E$ vs. $N$ in 2D, $W = 4$, $E \in [2.5, 3.5]$ . . . . . 111
94. $\langle \log t_N \rangle_E$ vs. $N$ in 2D, $W = 4$, $E \in [3.5, 4.5]$ . . . . . 111
95. $\langle \log t_N \rangle_E$ vs. $N$ in 2D, $W = 4$, $E \in [4.5, 5.5]$ . . . . . 112
96. $\langle \log t_N \rangle_E$ vs. $N$ in 2D, $W = 8$, $E \in [-8.5, -7.5]$ . . . . . 112
97. $\langle \log t_N \rangle_E$ vs. $N$ in 2D, $W = 8$, $E \in [-7.5, -6.5]$ . . . . . 112

Page

98. $\langle \log t_N \rangle_E$ vs. $N$ in 2D, $W = 8$, $E \in [-6.5, -5.5]$ . . . . . 113
99. $\langle \log t_N \rangle_E$ vs. $N$ in 2D, $W = 8$, $E \in [-5.5, -4.5]$ . . . . . 113
100. $\langle \log t_N \rangle_E$ vs. $N$ in 2D, $W = 8$, $E \in [-4.5, -3.5]$ . . . . . 113
101. $\langle \log t_N \rangle_E$ vs. $N$ in 2D, $W = 8$, $E \in [-3.5, -2.5]$ . . . . . 114
102. $\langle \log t_N \rangle_E$ vs. $N$ in 2D, $W = 8$, $E \in [-2.5, -1.5]$ . . . . . 114
103. $\langle \log t_N \rangle_E$ vs. $N$ in 2D, $W = 8$, $E \in [-1.5, -0.5]$ . . . . . 114
104. $\langle \log t_N \rangle_E$ vs. $N$ in 2D, $W = 8$, $E \in [-0.5, 0.5]$ . . . . . 115
105. $\langle \log t_N \rangle_E$ vs. $N$ in 2D, $W = 8$, $E \in [0.5, 1.5]$ . . . . . 115
106. $\langle \log t_N \rangle_E$ vs. $N$ in 2D, $W = 8$, $E \in [1.5, 2.5]$ . . . . . 115
107. $\langle \log t_N \rangle_E$ vs. $N$ in 2D, $W = 8$, $E \in [2.5, 3.5]$ . . . . . 116
108. $\langle \log t_N \rangle_E$ vs. $N$ in 2D, $W = 8$, $E \in [3.5, 4.5]$ . . . . . 116
109. $\langle \log t_N \rangle_E$ vs. $N$ in 2D, $W = 8$, $E \in [4.5, 5.5]$ . . . . . 116
110. $\langle \log t_N \rangle_E$ vs. $N$ in 2D, $W = 8$, $E \in [5.5, 6.5]$ . . . . . 117
111. $\langle \log t_N \rangle_E$ vs. $N$ in 2D, $W = 8$, $E \in [6.5, 7.5]$ . . . . . 117
112. $\langle \log t_N \rangle_E$ vs. $N$ in 2D, $W = 8$, $E \in [7.5, 8.5]$ . . . . . 117
113. $\langle \log t_N \rangle_E$ vs. $N$ in 2D, $W = 12$, $E \in [-9.5, -8.5]$ . . . . . 118
114. $\langle \log t_N \rangle_E$ vs. $N$ in 2D, $W = 12$, $E \in [-8.5, -7.5]$ . . . . . 118
115. $\langle \log t_N \rangle_E$ vs. $N$ in 2D, $W = 12$, $E \in [-7.5, -6.5]$ . . . . . 118
116. $\langle \log t_N \rangle_E$ vs. $N$ in 2D, $W = 12$, $E \in [-6.5, -5.5]$ . . . . . 119
117. $\langle \log t_N \rangle_E$ vs. $N$ in 2D, $W = 12$, $E \in [-5.5, -4.5]$ . . . . . 119
118. $\langle \log t_N \rangle_E$ vs. $N$ in 2D, $W = 12$, $E \in [-4.5, -3.5]$ . . . . . 119
119. $\langle \log t_N \rangle_E$ vs. $N$ in 2D, $W = 12$, $E \in [-3.5, -2.5]$ . . . . . 120
120. $\langle \log t_N \rangle_E$ vs. $N$ in 2D, $W = 12$, $E \in [-2.5, -1.5]$ . . . . . 120

Page

121. $\langle \log t_N \rangle_E$ vs. $N$ in 2D, $W = 12$, $E \in [-1.5, -0.5]$ . . . . . 120
122. $\langle \log t_N \rangle_E$ vs. $N$ in 2D, $W = 12$, $E \in [-0.5, 0.5]$ . . . . . 121
123. $\langle \log t_N \rangle_E$ vs. $N$ in 2D, $W = 12$, $E \in [0.5, 1.5]$ . . . . . 121
124. $\langle \log t_N \rangle_E$ vs. $N$ in 2D, $W = 12$, $E \in [1.5, 2.5]$ . . . . . 121
125. $\langle \log t_N \rangle_E$ vs. $N$ in 2D, $W = 12$, $E \in [2.5, 3.5]$ . . . . . 122
126. $\langle \log t_N \rangle_E$ vs. $N$ in 2D, $W = 12$, $E \in [3.5, 4.5]$ . . . . . 122
127. $\langle \log t_N \rangle_E$ vs. $N$ in 2D, $W = 12$, $E \in [4.5, 5.5]$ . . . . . 122
128. $\langle \log t_N \rangle_E$ vs. $N$ in 2D, $W = 12$, $E \in [5.5, 6.5]$ . . . . . 123
129. $\langle \log t_N \rangle_E$ vs. $N$ in 2D, $W = 12$, $E \in [6.5, 7.5]$ . . . . . 123
130. $\langle \log t_N \rangle_E$ vs. $N$ in 2D, $W = 12$, $E \in [7.5, 8.5]$ . . . . . 123
131. $\langle \log t_N \rangle_E$ vs. $N$ in 2D, $W = 12$, $E \in [8.5, 9.5]$ . . . . . 124
132. $\langle \log t_N \rangle_E$ vs. $N$ in 2D, $W = 16$, $E \in [-11.5, -10.5]$ . . . . . 124
133. $\langle \log t_N \rangle_E$ vs. $N$ in 2D, $W = 16$, $E \in [-10.5, -9.5]$ . . . . . 124
134. $\langle \log t_N \rangle_E$ vs. $N$ in 2D, $W = 16$, $E \in [-9.5, -8.5]$ . . . . . 125
135. $\langle \log t_N \rangle_E$ vs. $N$ in 2D, $W = 16$, $E \in [-8.5, -7.5]$ . . . . . 125
136. $\langle \log t_N \rangle_E$ vs. $N$ in 2D, $W = 16$, $E \in [-7.5, -6.5]$ . . . . . 125
137. $\langle \log t_N \rangle_E$ vs. $N$ in 2D, $W = 16$, $E \in [-6.5, -5.5]$ . . . . . 126
138. $\langle \log t_N \rangle_E$ vs. $N$ in 2D, $W = 16$, $E \in [-5.5, -4.5]$ . . . . . 126
139. $\langle \log t_N \rangle_E$ vs. $N$ in 2D, $W = 16$, $E \in [-4.5, -3.5]$ . . . . . 126
140. $\langle \log t_N \rangle_E$ vs. $N$ in 2D, $W = 16$, $E \in [-3.5, -2.5]$ . . . . . 127
141. $\langle \log t_N \rangle_E$ vs. $N$ in 2D, $W = 16$, $E \in [-2.5, -1.5]$ . . . . . 127
142. $\langle \log t_N \rangle_E$ vs. $N$ in 2D, $W = 16$, $E \in [-1.5, -0.5]$ . . . . . 127
143. $\langle \log t_N \rangle_E$ vs. $N$ in 2D, $W = 16$, $E \in [-0.5, 0.5]$ . . . . . 128

Page

144. $\langle \log t_N \rangle_E$ vs. $N$ in 2D, $W = 16$, $E \in [0.5, 1.5]$ . . . . . 128
145. $\langle \log t_N \rangle_E$ vs. $N$ in 2D, $W = 16$, $E \in [1.5, 2.5]$ . . . . . 128
146. $\langle \log t_N \rangle_E$ vs. $N$ in 2D, $W = 16$, $E \in [2.5, 3.5]$ . . . . . 129
147. $\langle \log t_N \rangle_E$ vs. $N$ in 2D, $W = 16$, $E \in [3.5, 4.5]$ . . . . . 129
148. $\langle \log t_N \rangle_E$ vs. $N$ in 2D, $W = 16$, $E \in [4.5, 5.5]$ . . . . . 129
149. $\langle \log t_N \rangle_E$ vs. $N$ in 2D, $W = 16$, $E \in [5.5, 6.5]$ . . . . . 130
150. $\langle \log t_N \rangle_E$ vs. $N$ in 2D, $W = 16$, $E \in [6.5, 7.5]$ . . . . . 130
151. $\langle \log t_N \rangle_E$ vs. $N$ in 2D, $W = 16$, $E \in [7.5, 8.5]$ . . . . . 130
152. $\langle \log t_N \rangle_E$ vs. $N$ in 2D, $W = 16$, $E \in [8.5, 9.5]$ . . . . . 131
153. $\langle \log t_N \rangle_E$ vs. $N$ in 2D, $W = 16$, $E \in [9.5, 10.5]$ . . . . . 131
154. $\langle \log t_N \rangle_E$ vs. $N$ in 2D, $W = 16$, $E \in [10.5, 11.5]$ . . . . . 131
155. $\langle \log t_N \rangle_E$ vs. $N$ in 2D, $W = 20$, $E \in [-12.5, -11.5]$ . . . . . 132
156. $\langle \log t_N \rangle_E$ vs. $N$ in 2D, $W = 20$, $E \in [-11.5, -10.5]$ . . . . . 132
157. $\langle \log t_N \rangle_E$ vs. $N$ in 2D, $W = 20$, $E \in [-10.5, -9.5]$ . . . . . 132
158. $\langle \log t_N \rangle_E$ vs. $N$ in 2D, $W = 20$, $E \in [-9.5, -8.5]$ . . . . . 133
159. $\langle \log t_N \rangle_E$ vs. $N$ in 2D, $W = 20$, $E \in [-8.5, -7.5]$ . . . . . 133
160. $\langle \log t_N \rangle_E$ vs. $N$ in 2D, $W = 20$, $E \in [-7.5, -6.5]$ . . . . . 133
161. $\langle \log t_N \rangle_E$ vs. $N$ in 2D, $W = 20$, $E \in [-6.5, -5.5]$ . . . . . 134
162. $\langle \log t_N \rangle_E$ vs. $N$ in 2D, $W = 20$, $E \in [-5.5, -4.5]$ . . . . . 134
163. $\langle \log t_N \rangle_E$ vs. $N$ in 2D, $W = 20$, $E \in [-4.5, -3.5]$ . . . . . 134
164. $\langle \log t_N \rangle_E$ vs. $N$ in 2D, $W = 20$, $E \in [-3.5, -2.5]$ . . . . . 135
165. $\langle \log t_N \rangle_E$ vs. $N$ in 2D, $W = 20$, $E \in [-2.5, -1.5]$ . . . . . 135
166. $\langle \log t_N \rangle_E$ vs. $N$ in 2D, $W = 20$, $E \in [-1.5, -0.5]$ . . . . . 135

Page

167. $\langle \log t_N \rangle_E$ vs. $N$ in 2D, $W = 20$, $E \in [-0.5, 0.5]$ . . . . . 136
168. $\langle \log t_N \rangle_E$ vs. $N$ in 2D, $W = 20$, $E \in [0.5, 1.5]$ . . . . . 136
169. $\langle \log t_N \rangle_E$ vs. $N$ in 2D, $W = 20$, $E \in [1.5, 2.5]$ . . . . . 136
170. $\langle \log t_N \rangle_E$ vs. $N$ in 2D, $W = 20$, $E \in [2.5, 3.5]$ . . . . . 137
171. $\langle \log t_N \rangle_E$ vs. $N$ in 2D, $W = 20$, $E \in [3.5, 4.5]$ . . . . . 137
172. $\langle \log t_N \rangle_E$ vs. $N$ in 2D, $W = 20$, $E \in [4.5, 5.5]$ . . . . . 137
173. $\langle \log t_N \rangle_E$ vs. $N$ in 2D, $W = 20$, $E \in [5.5, 6.5]$ . . . . . 138
174. $\langle \log t_N \rangle_E$ vs. $N$ in 2D, $W = 20$, $E \in [6.5, 7.5]$ . . . . . 138
175. $\langle \log t_N \rangle_E$ vs. $N$ in 2D, $W = 20$, $E \in [7.5, 8.5]$ . . . . . 138
176. $\langle \log t_N \rangle_E$ vs. $N$ in 2D, $W = 20$, $E \in [8.5, 9.5]$ . . . . . 139
177. $\langle \log t_N \rangle_E$ vs. $N$ in 2D, $W = 20$, $E \in [9.5, 10.5]$ . . . . . 139
178. $\langle \log t_N \rangle_E$ vs. $N$ in 2D, $W = 20$, $E \in [10.5, 11.5]$ . . . . . 139
179. $\langle \log t_N \rangle_E$ vs. $N$ in 2D, $W = 20$, $E \in [11.5, 12.5]$ . . . . . 140
180. $\langle \log t_N \rangle_E$ vs. $N$ in 2D, $W = 30$, $E \in [-17.5, -16.5]$ . . . . . 140
181. $\langle \log t_N \rangle_E$ vs. $N$ in 2D, $W = 30$, $E \in [-16.5, -15.5]$ . . . . . 140
182. $\langle \log t_N \rangle_E$ vs. $N$ in 2D, $W = 30$, $E \in [-15.5, -14.5]$ . . . . . 141
183. $\langle \log t_N \rangle_E$ vs. $N$ in 2D, $W = 30$, $E \in [-14.5, -13.5]$ . . . . . 141
184. $\langle \log t_N \rangle_E$ vs. $N$ in 2D, $W = 30$, $E \in [-13.5, -12.5]$ . . . . . 141
185. $\langle \log t_N \rangle_E$ vs. $N$ in 2D, $W = 30$, $E \in [-12.5, -11.5]$ . . . . . 142
186. $\langle \log t_N \rangle_E$ vs. $N$ in 2D, $W = 30$, $E \in [-11.5, -10.5]$ . . . . . 142
187. $\langle \log t_N \rangle_E$ vs. $N$ in 2D, $W = 30$, $E \in [-10.5, -9.5]$ . . . . . 142
188. $\langle \log t_N \rangle_E$ vs. $N$ in 2D, $W = 30$, $E \in [-9.5, -8.5]$ . . . . . 143
189. $\langle \log t_N \rangle_E$ vs. $N$ in 2D, $W = 30$, $E \in [-8.5, -7.5]$ . . . . . 143

Page

190. $\langle \log t_N \rangle_E$ vs. $N$ in 2D, $W = 30$, $E \in [-7.5, -6.5]$ . . . . . 143
191. $\langle \log t_N \rangle_E$ vs. $N$ in 2D, $W = 30$, $E \in [-6.5, -5.5]$ . . . . . 144
192. $\langle \log t_N \rangle_E$ vs. $N$ in 2D, $W = 30$, $E \in [-5.5, -4.5]$ . . . . . 144
193. $\langle \log t_N \rangle_E$ vs. $N$ in 2D, $W = 30$, $E \in [-4.5, -3.5]$ . . . . . 144
194. $\langle \log t_N \rangle_E$ vs. $N$ in 2D, $W = 30$, $E \in [-3.5, -2.5]$ . . . . . 145
195. $\langle \log t_N \rangle_E$ vs. $N$ in 2D, $W = 30$, $E \in [-2.5, -1.5]$ . . . . . 145
196. $\langle \log t_N \rangle_E$ vs. $N$ in 2D, $W = 30$, $E \in [-1.5, -0.5]$ . . . . . 145
197. $\langle \log t_N \rangle_E$ vs. $N$ in 2D, $W = 30$, $E \in [-0.5, 0.5]$ . . . . . 146
198. $\langle \log t_N \rangle_E$ vs. $N$ in 2D, $W = 30$, $E \in [0.5, 1.5]$ . . . . . 146
199. $\langle \log t_N \rangle_E$ vs. $N$ in 2D, $W = 30$, $E \in [1.5, 2.5]$ . . . . . 146
200. $\langle \log t_N \rangle_E$ vs. $N$ in 2D, $W = 30$, $E \in [2.5, 3.5]$ . . . . . 147
201. $\langle \log t_N \rangle_E$ vs. $N$ in 2D, $W = 30$, $E \in [3.5, 4.5]$ . . . . . 147
202. $\langle \log t_N \rangle_E$ vs. $N$ in 2D, $W = 30$, $E \in [4.5, 5.5]$ . . . . . 147
203. $\langle \log t_N \rangle_E$ vs. $N$ in 2D, $W = 30$, $E \in [5.5, 6.5]$ . . . . . 148
204. $\langle \log t_N \rangle_E$ vs. $N$ in 2D, $W = 30$, $E \in [6.5, 7.5]$ . . . . . 148
205. $\langle \log t_N \rangle_E$ vs. $N$ in 2D, $W = 30$, $E \in [7.5, 8.5]$ . . . . . 148
206. $\langle \log t_N \rangle_E$ vs. $N$ in 2D, $W = 30$, $E \in [8.5, 9.5]$ . . . . . 149
207. $\langle \log t_N \rangle_E$ vs. $N$ in 2D, $W = 30$, $E \in [9.5, 10.5]$ . . . . . 149
208. $\langle \log t_N \rangle_E$ vs. $N$ in 2D, $W = 30$, $E \in [10.5, 11.5]$ . . . . . 149
209. $\langle \log t_N \rangle_E$ vs. $N$ in 2D, $W = 30$, $E \in [11.5, 12.5]$ . . . . . 150
210. $\langle \log t_N \rangle_E$ vs. $N$ in 2D, $W = 30$, $E \in [12.5, 13.5]$ . . . . . 150
211. $\langle \log t_N \rangle_E$ vs. $N$ in 2D, $W = 30$, $E \in [13.5, 14.5]$ . . . . . 150
212. $\langle \log t_N \rangle_E$ vs. $N$ in 2D, $W = 30$, $E \in [14.5, 15.5]$ . . . . . 151

Page

213. $\langle \log t_N \rangle_E$ vs. $N$ in 2D, $W = 30$, $E \in [15.5, 16.5]$ . . . . . 151

214. $\langle \log t_N \rangle_E$ vs. $N$ in 2D, $W = 30$, $E \in [16.5, 17.5]$ . . . . . 151

215. $\langle \log t_N \rangle_E$ vs. $N$ in 3D, $W = 4$, $E \in [-7.5, -6.5]$ . . . . . 152

216. $\langle \log t_N \rangle_E$ vs. $N$ in 3D, $W = 4$, $E \in [-6.5, -5.5]$ . . . . . 153

217. $\langle \log t_N \rangle_E$ vs. $N$ in 3D, $W = 4$, $E \in [-5.5, -4.5]$ . . . . . 153

218. $\langle \log t_N \rangle_E$ vs. $N$ in 3D, $W = 4$, $E \in [-4.5, -3.5]$ . . . . . 153

219. $\langle \log t_N \rangle_E$ vs. $N$ in 3D, $W = 4$, $E \in [-3.5, -2.5]$ . . . . . 154

220. $\langle \log t_N \rangle_E$ vs. $N$ in 3D, $W = 4$, $E \in [-2.5, -1.5]$ . . . . . 154

221. $\langle \log t_N \rangle_E$ vs. $N$ in 3D, $W = 4$, $E \in [-1.5, -0.5]$ . . . . . 154

222. $\langle \log t_N \rangle_E$ vs. $N$ in 3D, $W = 4$, $E \in [-0.5, 0.5]$ . . . . . 155

223. $\langle \log t_N \rangle_E$ vs. $N$ in 3D, $W = 4$, $E \in [0.5, 1.5]$ . . . . . 155

224. $\langle \log t_N \rangle_E$ vs. $N$ in 3D, $W = 4$, $E \in [1.5, 2.5]$ . . . . . 155

225. $\langle \log t_N \rangle_E$ vs. $N$ in 3D, $W = 4$, $E \in [2.5, 3.5]$ . . . . . 156

226. $\langle \log t_N \rangle_E$ vs. $N$ in 3D, $W = 4$, $E \in [3.5, 4.5]$ . . . . . 156

227. $\langle \log t_N \rangle_E$ vs. $N$ in 3D, $W = 4$, $E \in [4.5, 5.5]$ . . . . . 156

228. $\langle \log t_N \rangle_E$ vs. $N$ in 3D, $W = 4$, $E \in [5.5, 6.5]$ . . . . . 157

229. $\langle \log t_N \rangle_E$ vs. $N$ in 3D, $W = 4$, $E \in [6.5, 7.5]$ . . . . . 157

230. $\langle \log t_N \rangle_E$ vs. $N$ in 3D, $W = 8$, $E \in [-9.5, -8.5]$ . . . . . 157

231. $\langle \log t_N \rangle_E$ vs. $N$ in 3D, $W = 8$, $E \in [-8.5, -7.5]$ . . . . . 158

232. $\langle \log t_N \rangle_E$ vs. $N$ in 3D, $W = 8$, $E \in [-7.5, -6.5]$ . . . . . 158

233. $\langle \log t_N \rangle_E$ vs. $N$ in 3D, $W = 8$, $E \in [-6.5, -5.5]$ . . . . . 158

234. $\langle \log t_N \rangle_E$ vs. $N$ in 3D, $W = 8$, $E \in [-5.5, -4.5]$ . . . . . 159

235. $\langle \log t_N \rangle_E$ vs. $N$ in 3D, $W = 8$, $E \in [-4.5, -3.5]$ . . . . . 159

Page

236. $\langle \log t_N \rangle_E$ vs. $N$ in 3D, $W = 8$, $E \in [-3.5, -2.5]$ . . . . . 159
237. $\langle \log t_N \rangle_E$ vs. $N$ in 3D, $W = 8$, $E \in [-2.5, -1.5]$ . . . . . 160
238. $\langle \log t_N \rangle_E$ vs. $N$ in 3D, $W = 8$, $E \in [-1.5, -0.5]$ . . . . . 160
239. $\langle \log t_N \rangle_E$ vs. $N$ in 3D, $W = 8$, $E \in [-0.5, 0.5]$ . . . . . 160
240. $\langle \log t_N \rangle_E$ vs. $N$ in 3D, $W = 8$, $E \in [0.5, 1.5]$ . . . . . 161
241. $\langle \log t_N \rangle_E$ vs. $N$ in 3D, $W = 8$, $E \in [1.5, 2.5]$ . . . . . 161
242. $\langle \log t_N \rangle_E$ vs. $N$ in 3D, $W = 8$, $E \in [2.5, 3.5]$ . . . . . 161
243. $\langle \log t_N \rangle_E$ vs. $N$ in 3D, $W = 8$, $E \in [3.5, 4.5]$ . . . . . 162
244. $\langle \log t_N \rangle_E$ vs. $N$ in 3D, $W = 8$, $E \in [4.5, 5.5]$ . . . . . 162
245. $\langle \log t_N \rangle_E$ vs. $N$ in 3D, $W = 8$, $E \in [5.5, 6.5]$ . . . . . 162
246. $\langle \log t_N \rangle_E$ vs. $N$ in 3D, $W = 8$, $E \in [6.5, 7.5]$ . . . . . 163
247. $\langle \log t_N \rangle_E$ vs. $N$ in 3D, $W = 8$, $E \in [7.5, 8.5]$ . . . . . 163
248. $\langle \log t_N \rangle_E$ vs. $N$ in 3D, $W = 8$, $E \in [8.5, 9.5]$ . . . . . 163
249. $\langle \log t_N \rangle_E$ vs. $N$ in 3D, $W = 12$, $E \in [-10.5, -9.5]$ . . . . . 164
250. $\langle \log t_N \rangle_E$ vs. $N$ in 3D, $W = 12$, $E \in [-9.5, -8.5]$ . . . . . 164
251. $\langle \log t_N \rangle_E$ vs. $N$ in 3D, $W = 12$, $E \in [-8.5, -7.5]$ . . . . . 164
252. $\langle \log t_N \rangle_E$ vs. $N$ in 3D, $W = 12$, $E \in [-7.5, -6.5]$ . . . . . 165
253. $\langle \log t_N \rangle_E$ vs. $N$ in 3D, $W = 12$, $E \in [-6.5, -5.5]$ . . . . . 165
254. $\langle \log t_N \rangle_E$ vs. $N$ in 3D, $W = 12$, $E \in [-5.5, -4.5]$ . . . . . 165
255. $\langle \log t_N \rangle_E$ vs. $N$ in 3D, $W = 12$, $E \in [-4.5, -3.5]$ . . . . . 166
256. $\langle \log t_N \rangle_E$ vs. $N$ in 3D, $W = 12$, $E \in [-3.5, -2.5]$ . . . . . 166
257. $\langle \log t_N \rangle_E$ vs. $N$ in 3D, $W = 12$, $E \in [-2.5, -1.5]$ . . . . . 166
258. $\langle \log t_N \rangle_E$ vs. $N$ in 3D, $W = 12$, $E \in [-1.5, -0.5]$ . . . . . 167

Page

259. $\langle \log t_N \rangle_E$ vs. $N$ in 3D, $W = 12$, $E \in [-0.5, 0.5]$ . . . . . 167
260. $\langle \log t_N \rangle_E$ vs. $N$ in 3D, $W = 12$, $E \in [0.5, 1.5]$ . . . . . 167
261. $\langle \log t_N \rangle_E$ vs. $N$ in 3D, $W = 12$, $E \in [1.5, 2.5]$ . . . . . 168
262. $\langle \log t_N \rangle_E$ vs. $N$ in 3D, $W = 12$, $E \in [2.5, 3.5]$ . . . . . 168
263. $\langle \log t_N \rangle_E$ vs. $N$ in 3D, $W = 12$, $E \in [3.5, 4.5]$ . . . . . 168
264. $\langle \log t_N \rangle_E$ vs. $N$ in 3D, $W = 12$, $E \in [4.5, 5.5]$ . . . . . 169
265. $\langle \log t_N \rangle_E$ vs. $N$ in 3D, $W = 12$, $E \in [5.5, 6.5]$ . . . . . 169
266. $\langle \log t_N \rangle_E$ vs. $N$ in 3D, $W = 12$, $E \in [6.5, 7.5]$ . . . . . 169
267. $\langle \log t_N \rangle_E$ vs. $N$ in 3D, $W = 12$, $E \in [7.5, 8.5]$ . . . . . 170
268. $\langle \log t_N \rangle_E$ vs. $N$ in 3D, $W = 12$, $E \in [8.5, 9.5]$ . . . . . 170
269. $\langle \log t_N \rangle_E$ vs. $N$ in 3D, $W = 12$, $E \in [9.5, 10.5]$ . . . . . 170
270. $\langle \log t_N \rangle_E$ vs. $N$ in 3D, $W = 16$, $E \in [-12.5, -11.5]$ . . . . . 171
271. $\langle \log t_N \rangle_E$ vs. $N$ in 3D, $W = 16$, $E \in [-11.5, -10.5]$ . . . . . 171
272. $\langle \log t_N \rangle_E$ vs. $N$ in 3D, $W = 16$, $E \in [-10.5, -9.5]$ . . . . . 171
273. $\langle \log t_N \rangle_E$ vs. $N$ in 3D, $W = 16$, $E \in [-9.5, -8.5]$ . . . . . 172
274. $\langle \log t_N \rangle_E$ vs. $N$ in 3D, $W = 16$, $E \in [-8.5, -7.5]$ . . . . . 172
275. $\langle \log t_N \rangle_E$ vs. $N$ in 3D, $W = 16$, $E \in [-7.5, -6.5]$ . . . . . 172
276. $\langle \log t_N \rangle_E$ vs. $N$ in 3D, $W = 16$, $E \in [-6.5, -5.5]$ . . . . . 173
277. $\langle \log t_N \rangle_E$ vs. $N$ in 3D, $W = 16$, $E \in [-5.5, -4.5]$ . . . . . 173
278. $\langle \log t_N \rangle_E$ vs. $N$ in 3D, $W = 16$, $E \in [-4.5, -3.5]$ . . . . . 173
279. $\langle \log t_N \rangle_E$ vs. $N$ in 3D, $W = 16$, $E \in [-3.5, -2.5]$ . . . . . 174
280. $\langle \log t_N \rangle_E$ vs. $N$ in 3D, $W = 16$, $E \in [-2.5, -1.5]$ . . . . . 174
281. $\langle \log t_N \rangle_E$ vs. $N$ in 3D, $W = 16$, $E \in [-1.5, -0.5]$ . . . . . 174

Page

282. $\langle \log t_N \rangle_E$ vs. $N$ in 3D, $W = 16$, $E \in [-0.5, 0.5]$ . . . . . 175
283. $\langle \log t_N \rangle_E$ vs. $N$ in 3D, $W = 16$, $E \in [0.5, 1.5]$ . . . . . 175
284. $\langle \log t_N \rangle_E$ vs. $N$ in 3D, $W = 16$, $E \in [1.5, 2.5]$ . . . . . 175
285. $\langle \log t_N \rangle_E$ vs. $N$ in 3D, $W = 16$, $E \in [2.5, 3.5]$ . . . . . 176
286. $\langle \log t_N \rangle_E$ vs. $N$ in 3D, $W = 16$, $E \in [3.5, 4.5]$ . . . . . 176
287. $\langle \log t_N \rangle_E$ vs. $N$ in 3D, $W = 16$, $E \in [4.5, 5.5]$ . . . . . 176
288. $\langle \log t_N \rangle_E$ vs. $N$ in 3D, $W = 16$, $E \in [5.5, 6.5]$ . . . . . 177
289. $\langle \log t_N \rangle_E$ vs. $N$ in 3D, $W = 16$, $E \in [6.5, 7.5]$ . . . . . 177
290. $\langle \log t_N \rangle_E$ vs. $N$ in 3D, $W = 16$, $E \in [7.5, 8.5]$ . . . . . 177
291. $\langle \log t_N \rangle_E$ vs. $N$ in 3D, $W = 16$, $E \in [8.5, 9.5]$ . . . . . 178
292. $\langle \log t_N \rangle_E$ vs. $N$ in 3D, $W = 16$, $E \in [9.5, 10.5]$ . . . . . 178
293. $\langle \log t_N \rangle_E$ vs. $N$ in 3D, $W = 16$, $E \in [10.5, 11.5]$ . . . . . 178
294. $\langle \log t_N \rangle_E$ vs. $N$ in 3D, $W = 16$, $E \in [11.5, 12.5]$ . . . . . 179
295. $\langle \log t_N \rangle_E$ vs. $N$ in 3D, $W = 20$, $E \in [-13.5, -12.5]$ . . . . . 179
296. $\langle \log t_N \rangle_E$ vs. $N$ in 3D, $W = 20$, $E \in [-12.5, -11.5]$ . . . . . 179
297. $\langle \log t_N \rangle_E$ vs. $N$ in 3D, $W = 20$, $E \in [-11.5, -10.5]$ . . . . . 180
298. $\langle \log t_N \rangle_E$ vs. $N$ in 3D, $W = 20$, $E \in [-10.5, -9.5]$ . . . . . 180
299. $\langle \log t_N \rangle_E$ vs. $N$ in 3D, $W = 20$, $E \in [-9.5, -8.5]$ . . . . . 180
300. $\langle \log t_N \rangle_E$ vs. $N$ in 3D, $W = 20$, $E \in [-8.5, -7.5]$ . . . . . 181
301. $\langle \log t_N \rangle_E$ vs. $N$ in 3D, $W = 20$, $E \in [-7.5, -6.5]$ . . . . . 181
302. $\langle \log t_N \rangle_E$ vs. $N$ in 3D, $W = 20$, $E \in [-6.5, -5.5]$ . . . . . 181
303. $\langle \log t_N \rangle_E$ vs. $N$ in 3D, $W = 20$, $E \in [-5.5, -4.5]$ . . . . . 182
304. $\langle \log t_N \rangle_E$ vs. $N$ in 3D, $W = 20$, $E \in [-4.5, -3.5]$ . . . . . 182

Page

305. $\langle \log t_N \rangle_E$ vs. $N$ in 3D, $W = 20$, $E \in [-3.5, -2.5]$ . . . . . 182
306. $\langle \log t_N \rangle_E$ vs. $N$ in 3D, $W = 20$, $E \in [-2.5, -1.5]$ . . . . . 183
307. $\langle \log t_N \rangle_E$ vs. $N$ in 3D, $W = 20$, $E \in [-1.5, -0.5]$ . . . . . 183
308. $\langle \log t_N \rangle_E$ vs. $N$ in 3D, $W = 20$, $E \in [-0.5, 0.5]$ . . . . . 183
309. $\langle \log t_N \rangle_E$ vs. $N$ in 3D, $W = 20$, $E \in [0.5, 1.5]$ . . . . . 184
310. $\langle \log t_N \rangle_E$ vs. $N$ in 3D, $W = 20$, $E \in [1.5, 2.5]$ . . . . . 184
311. $\langle \log t_N \rangle_E$ vs. $N$ in 3D, $W = 20$, $E \in [2.5, 3.5]$ . . . . . 184
312. $\langle \log t_N \rangle_E$ vs. $N$ in 3D, $W = 20$, $E \in [3.5, 4.5]$ . . . . . 185
313. $\langle \log t_N \rangle_E$ vs. $N$ in 3D, $W = 20$, $E \in [4.5, 5.5]$ . . . . . 185
314. $\langle \log t_N \rangle_E$ vs. $N$ in 3D, $W = 20$, $E \in [5.5, 6.5]$ . . . . . 185
315. $\langle \log t_N \rangle_E$ vs. $N$ in 3D, $W = 20$, $E \in [6.5, 7.5]$ . . . . . 186
316. $\langle \log t_N \rangle_E$ vs. $N$ in 3D, $W = 20$, $E \in [7.5, 8.5]$ . . . . . 186
317. $\langle \log t_N \rangle_E$ vs. $N$ in 3D, $W = 20$, $E \in [8.5, 9.5]$ . . . . . 186
318. $\langle \log t_N \rangle_E$ vs. $N$ in 3D, $W = 20$, $E \in [9.5, 10.5]$ . . . . . 187
319. $\langle \log t_N \rangle_E$ vs. $N$ in 3D, $W = 20$, $E \in [10.5, 11.5]$ . . . . . 187
320. $\langle \log t_N \rangle_E$ vs. $N$ in 3D, $W = 20$, $E \in [11.5, 12.5]$ . . . . . 187
321. $\langle \log t_N \rangle_E$ vs. $N$ in 3D, $W = 20$, $E \in [12.5, 13.5]$ . . . . . 188
322. $\langle \log t_N \rangle_E$ vs. $N$ in 3D, $W = 24$, $E \in [-15.5, -14.5]$ . . . . . 188
323. $\langle \log t_N \rangle_E$ vs. $N$ in 3D, $W = 24$, $E \in [-14.5, -13.5]$ . . . . . 188
324. $\langle \log t_N \rangle_E$ vs. $N$ in 3D, $W = 24$, $E \in [-13.5, -12.5]$ . . . . . 189
325. $\langle \log t_N \rangle_E$ vs. $N$ in 3D, $W = 24$, $E \in [-12.5, -11.5]$ . . . . . 189
326. $\langle \log t_N \rangle_E$ vs. $N$ in 3D, $W = 24$, $E \in [-11.5, -10.5]$ . . . . . 189
327. $\langle \log t_N \rangle_E$ vs. $N$ in 3D, $W = 24$, $E \in [-10.5, -9.5]$ . . . . . 190

Page

328. $\langle \log t_N \rangle_E$ vs. $N$ in 3D, $W = 24$, $E \in [-9.5, -8.5]$ . . . . . 190
329. $\langle \log t_N \rangle_E$ vs. $N$ in 3D, $W = 24$, $E \in [-7.5, -6.5]$ . . . . . 190
330. $\langle \log t_N \rangle_E$ vs. $N$ in 3D, $W = 24$, $E \in [-6.5, -5.5]$ . . . . . 191
331. $\langle \log t_N \rangle_E$ vs. $N$ in 3D, $W = 24$, $E \in [-5.5, -4.5]$ . . . . . 191
332. $\langle \log t_N \rangle_E$ vs. $N$ in 3D, $W = 24$, $E \in [-4.5, -3.5]$ . . . . . 191
333. $\langle \log t_N \rangle_E$ vs. $N$ in 3D, $W = 24$, $E \in [-3.5, -2.5]$ . . . . . 192
334. $\langle \log t_N \rangle_E$ vs. $N$ in 3D, $W = 24$, $E \in [-2.5, -1.5]$ . . . . . 192
335. $\langle \log t_N \rangle_E$ vs. $N$ in 3D, $W = 24$, $E \in [-1.5, -0.5]$ . . . . . 192
336. $\langle \log t_N \rangle_E$ vs. $N$ in 3D, $W = 24$, $E \in [-0.5, 0.5]$ . . . . . 193
337. $\langle \log t_N \rangle_E$ vs. $N$ in 3D, $W = 24$, $E \in [0.5, 1.5]$ . . . . . 193
338. $\langle \log t_N \rangle_E$ vs. $N$ in 3D, $W = 24$, $E \in [1.5, 2.5]$ . . . . . 193
339. $\langle \log t_N \rangle_E$ vs. $N$ in 3D, $W = 24$, $E \in [2.5, 3.5]$ . . . . . 194
340. $\langle \log t_N \rangle_E$ vs. $N$ in 3D, $W = 24$, $E \in [3.5, 4.5]$ . . . . . 194
341. $\langle \log t_N \rangle_E$ vs. $N$ in 3D, $W = 24$, $E \in [4.5, 5.5]$ . . . . . 194
342. $\langle \log t_N \rangle_E$ vs. $N$ in 3D, $W = 24$, $E \in [5.5, 6.5]$ . . . . . 195
343. $\langle \log t_N \rangle_E$ vs. $N$ in 3D, $W = 24$, $E \in [6.5, 7.5]$ . . . . . 195
344. $\langle \log t_N \rangle_E$ vs. $N$ in 3D, $W = 24$, $E \in [7.5, 8.5]$ . . . . . 195
345. $\langle \log t_N \rangle_E$ vs. $N$ in 3D, $W = 24$, $E \in [8.5, 9.5]$ . . . . . 196
346. $\langle \log t_N \rangle_E$ vs. $N$ in 3D, $W = 24$, $E \in [9.5, 10.5]$ . . . . . 196
347. $\langle \log t_N \rangle_E$ vs. $N$ in 3D, $W = 24$, $E \in [10.5, 11.5]$ . . . . . 196
348. $\langle \log t_N \rangle_E$ vs. $N$ in 3D, $W = 24$, $E \in [11.5, 12.5]$ . . . . . 197
349. $\langle \log t_N \rangle_E$ vs. $N$ in 3D, $W = 24$, $E \in [12.5, 13.5]$ . . . . . 197
350. $\langle \log t_N \rangle_E$ vs. $N$ in 3D, $W = 24$, $E \in [13.5, 14.5]$ . . . . . 197

Page

351. $\langle \log t_N \rangle_E$ vs. $N$ in 3D, $W = 24$, $E \in [14.5, 15.5]$ . . . . . 198

# CHAPTER I

# INTRODUCTION

Disorder in all generality is a feature that many physical systems share. Nature rarely supplies materials in pristine purity or order. Even with advanced processing techniques, some impurities, lattice dislocations and other imperfections are often a fact of life.

Aspects of disorder in solids therefore pervade many areas of physics. Entire subbranches of condensed matter physics are dedicated to the study of systems whose prime characteristic is disorder, such as amorphous substances and glasses. In other areas, disorder is more of a nuisance because, for example, it may increase the electrical losses in conductors, reduce the reflectivity of mirrors or spoil certain phenomena altogether.

In this dissertation, we concern ourselves with the impact of disorder on the electrical conduction in metal-like model systems in the low-temperature elastic scattering regime. The physics of disordered systems is rich, yet many mathematical tools developed for ordered systems fail to capture disorder-related phenomena or are altogether inapplicable in the presence of disorder. In some cases, a perturbative treatment may be possible, but to the present day considerable challenges persist in analytical approaches to systems with intermediate, moderate disorder. Under these circumstances, numerical analysis often remains the last resort.

Disorder can produce spontaneous fluctuations which can be so large that

the mean of the fluctuating physical quantity itself loses its usefulness. This is a hallmark of disordered, mesoscopic systems (Janssen, 1998). In these cases one often must consider the entire distribution of the quantity, because isolated realizations are no longer representative. This problem also affects computer simulations that, constrained by the efficiency of the algorithms and the performance of the available machines, often have to content themselves with tiny sample sizes that are sometimes questionable approximations to the thermodynamic limit.

In the present dissertation, we attempt to circumvent these problems by simulating systems of unprecedented size thanks to an efficient algorithm and a novel, parallel implementation thereof.

Under certain circumstances, the effects of disorder on physical quantities can not be considered in isolation but only in conjunction with interactions between charge carriers. This seems to be the case in recent experimental findings of an apparent metal-insulator transition in two dimensions (Kravchenko et al., 1994, 1995; Simmons et al., 1998b,a). As part of this dissertation, we attempt to build a model that qualitatively describes this phenomenon by including both disorder and a special type of electron-electron interaction.

The remainder of this dissertation is organized as follows. In Chapter II, we introduce two specific models for disordered systems, the Anderson model and the Hubbard model, that will form the basis for the subsequent investigation. We also mention concepts of electron transport and discuss relevant literature. In Chapter III, we describe our computational techniques and how we calculate the quantum mechanical transmittance which we will use to characterize the localization of electronic states. In Chapter IV we present and comment the results of these

calculations. Chapter V describes the design and performance of the main computer code that was developed for the purpose of this study, the parallel recursion project. Finally, we discuss our results in the context of previous findings in this field and give concluding remarks in Chapter VI.

All programs the author wrote for the purposes for this study, including the parallel recursion code are included on the CD in the Pocket Material.

# CHAPTER II

# MODELS OF DISORDER AND TRANSPORT PROPERTIES

## 2.1 Introduction

In order to explain the rich experimental phenomena in disordered systems it is often not sufficient to consider the implications of disorder in isolation but in many cases interactions between the charge carriers play a role as well. In particular, the occurrence of a metal-insulator transition may be the result of competing effects (Edwards et al., 1998; Mott, 1990).

Nonetheless, a certain understanding of fundamental concepts may be derived from the study of simplified models. The Anderson model presented in Sec. 2.2 disregards all interactions. Despite its apparent simplicity, it displays surprisingly complex physics which continues to be the subject of debate even four decades after the model's first introduction. The present contribution to this large body of research seeks to elucidate the nature of the localization of states as disorder is increased and their dimensional dependence.

Another model that includes a special type of interaction was given by Hubbard which we will employ in Sec. 2.6 in an attempt at a qualitative understanding of recent experimental findings of an apparent metal-insulator transition in two dimensions described briefly in Sec. 2.5.

## 2.2 The Anderson Model

This simple single-electron model of disorder is due to Anderson (1958). It has been widely studied for the fundamental effects of lattice disorder on the localization of the single-electron wavefunction.

The model is based on a tight binding-type square (2D) or simple cubic (3D) lattice with a Hamiltonian,

$$H = \sum_i \varepsilon_i c_i^\dagger c_i + v \sum_{\langle i,j \rangle} c_i^\dagger c_j \,, \tag{2.1}$$

where $c_i^\dagger$ and $c_i$ are the electron creation and annihilation operators on site $i$, respectively. The first term represents potential energy with $\varepsilon_i$ the on-site energy; the second term corresponds to kinetic energy with $v$ the overlap integral between neighboring wavefunctions and $\langle i, j \rangle$ denoting summation over nearest neighbors.

In the Anderson model, the disorder is introduced by selecting the $\varepsilon_i$ from a box distribution of width $W$, the disorder strength, cf. Fig. 1c. The disorder is purely diagonal; the off-diagonal coefficients, $v$, are kept constant and will be set to unity throughout this dissertation.

For simple cubic or square lattices, the coordination of each lattice site is six and four, respectively. Eq. (2.1) can be written in site representation with each operator $c_i$ corresponding to a lattice vector. The Hamiltonian matrix $H$ will then be sparse, containing only six or four entries per row and column. The size of the matrix corresponds to the size of the block of material considered. Tackling this problem numerically will require efficient algorithms designed for very large sparse matrices such as the Lanczos and recursion methods introduced in Chapter III.

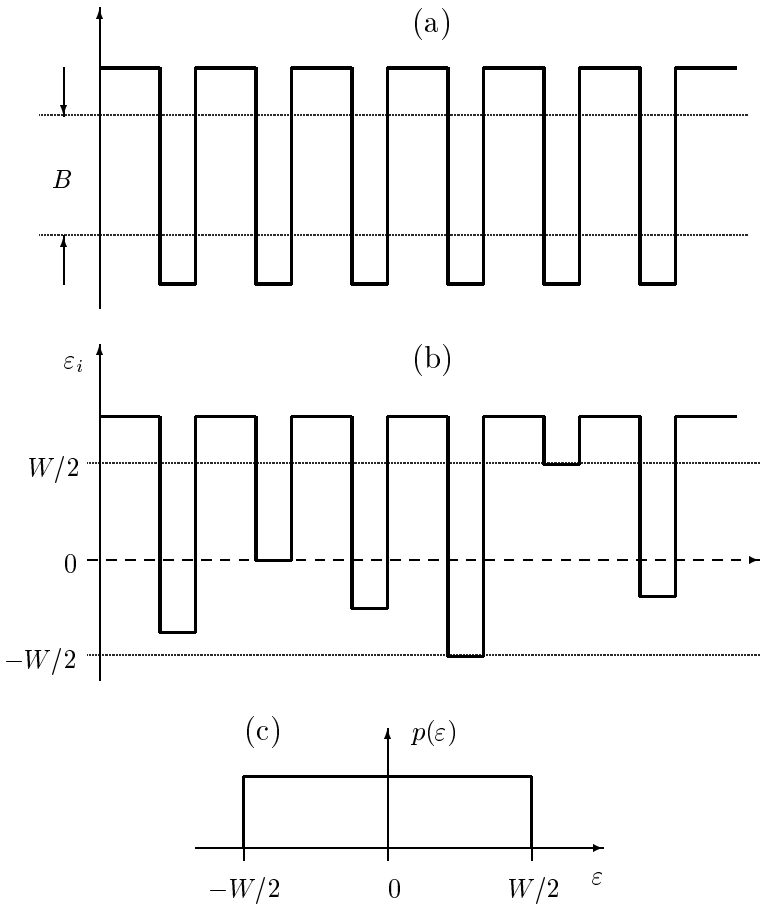


FIGURE 1. (a) Ordered potential wells and single-electron bandwidth $B$; (b) Disordered potential wells with disorder strength $W$; (c) Distribution of disordered potential

The Anderson model could be pictured as an $n$-ary alloy with each atom having a different on-site energy but constant overlap integrals between atoms, cf. Figs. 1a,b. The bandwidth of the disordered system is given as the sum of the bandwidth $B$ of the ordered system—resulting from the overlap of adjacent atomic orbitals—and the spread of the disordered potential distribution, $W$, which permits isolated states to exist at any energy with magnitude up to $W/2$ above or below the ordered bandwidth $B$. These extremal states are rare, the density of states decays exponentially in the Lifshitz tails (Lifshitz, 1963).

The Anderson model describes a scenario where interactions are absent and thus only elastic scattering may occur. We review two mechanisms by which the single-particle wavefunction may become localized under these circumstances.

In a periodic, ordered system, the solutions of the single-electron Schrödinger equation will extend unabated through the system. If the Fermi level separates an occupied region from an unoccupied one in the band, a current can flow through the system. Without any scattering on impurities, phonons or other electrons, the resistance in such a system will be zero. If a small amount of disorder is introduced, elastic scattering off the impurities will typically lead to a complicated stationary state of the wavefunction, but at least in higher dimensions the envelope suffers little attenuation. As the amount of disorder is increased, the scattering produced off random impurities may eventually lead to destructive interference and a decay of the envelope of the wavefunction. The state has then become localized, cf. Fig. 2 (Anderson, 1958; Edwards et al., 1998; Mott, 1990).

Another mechanism for localization is also possible. States in deep wells are effectively localized because an electron in such a state may escape only by tunneling due to the absence of any inelastic effects or thermal activation. Since deep wells are a rare realization of the disordered potential, a possible receiver state may be far away. Quantum mechanics tells us that the tunnel probability decreases exponentially with the width of the barrier.

The Anderson model has formed the basis for a number of studies and proposed theories to explain the fundamental behavior of wavefunctions in disordered systems in various dimensions. We will mention those relevant to the present work in the next section.

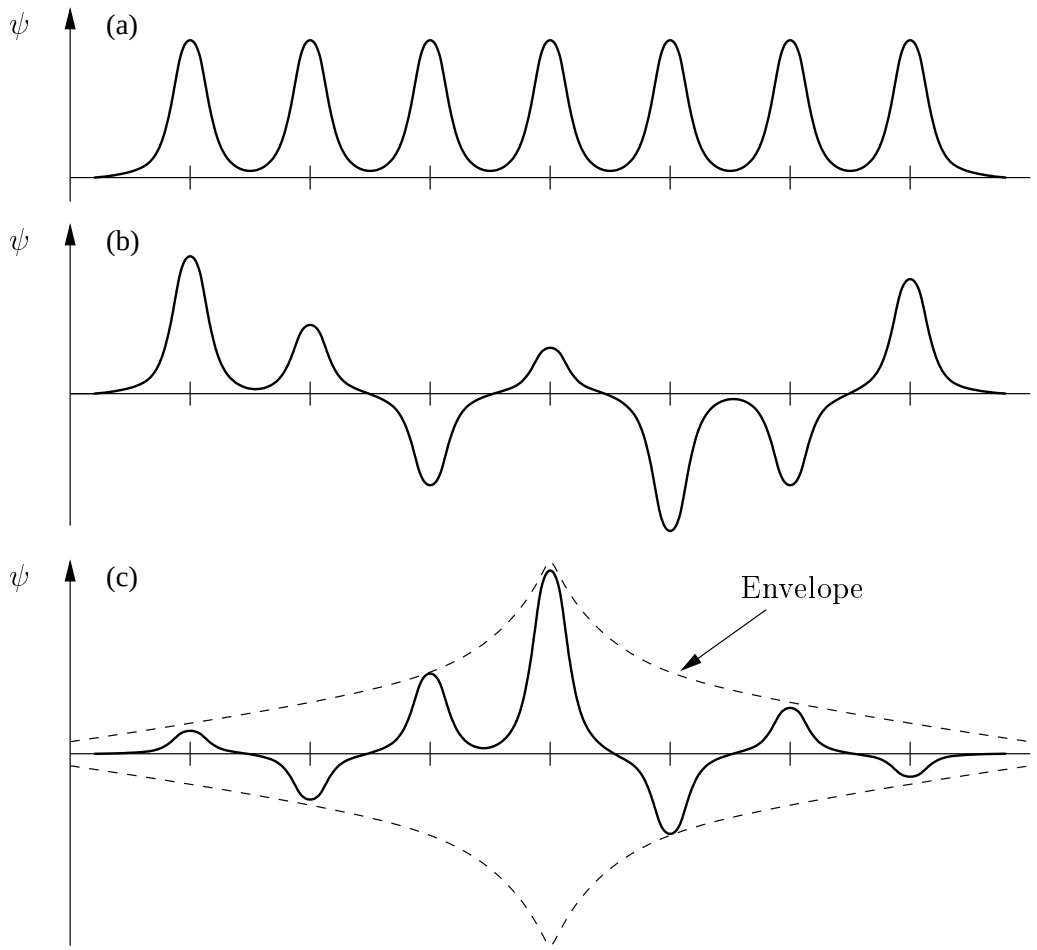


FIGURE 2. A typical wavefunction $\psi$ in the Anderson lattice: (a) extended state, (b) state at low disorder, (c) localized state at high disorder

## 2.3 Scaling Arguments

### 2.3.1 Single-Parameter Scaling Hypothesis

Abrahams, Anderson, Licciardello, and Ramakrishnan (1979) have formulated a theory based on a "single-parameter scaling" hypothesis. According to this theory, the scaling of the dimensionless conductance $g$ (see Sec. 2.7) can be described by a scaling function $\beta(g(L)) = d\ln g/d(\ln L)$ whose only parameter is $g$. $L$ is the linear size of a $d$-dimensional block of material with conductance $g(L)$.

The asymptotics of the $\beta$-function can be derived from physical arguments: In the conducting case, the situation is expected to be Ohmic, $g \sim L^{d-2}$, so that $\beta = d - 2$. In the insulating case, the conductance can be expected to be exponential, $g \sim e^{-L/\xi}$, so that $\beta = \ln g$. Under the assumption of a monotonic cross-over between the extremal cases, the predictions then are: (a) in one dimension, all states are exponentially localized at any finite disorder; (b) in three dimensions, the $\beta$-function has a zero so that there exists a phase transition between delocalized and exponentially localized states at a finite critical disorder $W_c$; (c) the two-dimensional case is border-line, but no true metallic states should exist. Despite a considerable body of literature on this subject, the scaling hypothesis remains unproven. In particular, the scaling argument of the conductance is concerned only with amplitudes but not with phases (Godin, 1988; Haydock, 1986). In the presence of phase-destroying events this may not matter; in the Anderson model, however, all processes are elastic and localization comes about as a result of interference. A break-down of scaling was also observed numerically as a result of boundary effects in systems smaller than the phase correlation length (MacKinnon and Kramer, 1983).

The single-parameter scaling theory has been subjected to a number of numerical tests, notably using two different methods, the transfer matrix method and the method of level spacing statistics.

### 2.3.2 Transfer Matrix Method

The transfer matrix method was developed and applied to the Anderson model in a series of papers (MacKinnon and Kramer, 1983; Zdetsis et al., 1985;

Bulka et al., 1987; Kramer et al., 1990). It is based on dividing the two or three-dimensional sample into $n$ strips or bars of width $M$ or cross-section $M \times M$, respectively. Then a solution to the Schrödinger equation can be written in terms of $(d-1)$-dimensional matrices $A_n$ given by the recurrence

$$A_{n+1} = (E - H_n)A_n - A_{n-1}\,. \tag{2.2}$$

A transfer matrix $T_n$ between different strips can be defined as

$$\begin{pmatrix} A_{n+1} \\ A_n \end{pmatrix} = T_n \begin{pmatrix} A_n \\ A_{n-1} \end{pmatrix}\,. \tag{2.3}$$

The product matrix $M_n = T_1 \ldots T_n$ is then an expression for the matrix elements of the resolvent between both ends of the sample. In the limit of $n \to \infty$, the smallest eigenvalue of $M_n M_n^\dagger$ is related to the *asymptotic exponential decay length* $\lambda_M$ by $e^{2n/\lambda_M}$. The authors then proceed with a scaling analysis assuming the renormalized localization length $\Lambda(M,W) = \lambda_M(W)/M$ is independent of $W$ and $M$ and can be written as a scaling function $f(\xi(E,W)/M)$ where $\xi(E,W)$ is the scaling parameter, in some sense a localization length, although that concept is ill-defined for extended states. They back up this hypothesis by using $\xi$ as a fitting parameter to make individual $(\lambda_M, W)$ data sets fall on a single curve in a plot of $\Lambda$ vs. $\xi/M$. This is interpreted as universality of the scaling function.

There are some problems with this analysis, however. Godin (1988) has pointed out that since the individual data sets overlap by very little in the resulting curve of the scaling function, this procedure might be argued to be a fit with the same number of free parameters as data sets included. The localization length

enters as a parameter, it is not actually measured nor are individual wavefunctions considered. Unfortunately, the references (MacKinnon and Kramer, 1983; Bulka et al., 1987; Kramer et al., 1990) compute only statistical errors from the fitting procedure. Kramer et al. (1990) states that the results for $\xi$ have an unknown error bar and it is not clear if the numerics may not introduce a systematic component too. In particular, it has not been addressed in any of these references, to what extent the results are dependent on the arithmetic precision used. Furthermore, in the transfer matrix calculations, an exponential behavior is always assumed, but at low disorders, MacKinnon and Kramer (1983) find localization lengths that are orders of magnitude larger than the largest system size considered.

### 2.3.3 Level Spacing Statistics

Another approach focuses on the distributions of the spacings $s$ between neighboring eigenlevels. The basic idea is that metallic states obey a different level spacing distribution than insulating states. The specifics of these distributions depend on correlations or lack thereof between the states. In an ordered lattice, all states are extended throughout the sample and as a result of their orthogonality, in finite systems their levels will stack up at well-separated, discrete energies. The asymptotic level distribution in this case is given by the Wigner surmise, $P_W(s) = (\pi s/2)\exp(-\pi s^2/4)$ (see Shklovskii et al., 1993; Zharekeshev and Kramer, 1997, and references therein), where the spacing $s$ is measured in units of the average spacing, $\langle s \rangle$. In the other extreme of tightly localized, insulating states, the correlation between the states is lost and their energy spacings follow that of an uncorrelated, random process, the one-event Poisson distribution, $P_P(s) = e^{-s}$.

Shklovskii et al. (1993) have postulated that there is a universal intermediate distribution at the critical disorder $W_c$. Subsequent investigations have used the Lanczos method (cf. Chapter III) to diagonalize lattice samples of up to $100^3$ sites and verified the size-independence of the critical distribution which was used to determine the critical disorder at $W_c \approx 16.4$ in the band center (Zharekeshev and Kramer, 1995, 1997).

### 2.3.4 Other Studies and Comment

With the exception of Bulka et al. (1987); Zdetsis et al. (1985), all of the other studies cited in this section have investigated the transition only in the band center. Zharekeshev and Kramer (1997) justify averaging over a range of energies $|E| < 6$ citing the results of Bulka et al. (1987) according to which the critical disorder is largely energy-independent over this range. To the author's knowledge no recent work has been conducted on the nature of the transition at the mobility edge in 3D.

The nature of disorder-induced metal-insulator transitions with and without interactions have been studied with field theoretical techniques based on the non-linear $\sigma$-model which uses perturbation expansions. For a review, see (Belitz and Kirkpatrick, 1994). The analysis derives critical exponents but does not yield a value for the critical disorder in the Anderson transition.

All of these studies use statistical and scaling arguments. The author is not aware of any recent investigations that have examined the nature of the states directly.

## 2.4 Non-Scaling Approaches

Haydock (1986) has conducted an analytic perturbative analysis of the nature of the localization in 2D and 3D at low disorder. He finds in 2D that the decay of the wavefunction undergoes a power law-to-exponential transition. Near the mobility edge, the localization length has a $\sqrt{E}$ dependence. In three dimensions, there are extended states and exponentially localized states separated by a mobility edge.

By numerically computing the quantum mechanical transmittance of a sample with leads on both ends, Godin (1988); Godin and Haydock (1992) have investigated the localization of states in the band tails in 2D and found evidence for a pseudo-mobility edge.

The core of the present work analyzes the localization of states across the entire band in 1D, 2D and 3D directly using transmittance coefficients.

## 2.5 Interaction Effects

In 1994, Kravchenko et al. (1994, 1995) jolted the physics community by announcing evidence for a metal-insulator transition in two dimensions, Fig. 3. Their experimental system consisted of high-mobility MOSFETs which were of unprecendented high quality such that they were operational down to very low carrier densities of around $10^{11}\mathrm{cm}^{-2}$. In the inversion layer of these transistors, carriers are quantum confined in the third dimension, making this one of the best experimentally accessible two-dimensional systems. A similar phenomenon was subsequently observed along the two-dimensional interface of GaAs-AlGaAs heterostructures (Simmons et al., 1998b,a). The data can be rescaled to fall on a

single curve with two branches. This was interpreted as a telltale signature of a phase transition in the framework of one-parameter scaling. However, according to the one-parameter scaling theory by Abrahams et al. (1979), no metallic states and no phase transition should exist in two-dimensional systems. The later observation of a re-entrant transition by Hamilton et al. (1999) threw some doubt on the simple phase transition conjecture and hints that the truth may be more complicated. Possibly, several effects are competing against one another.

The debate has since focused on the effects of electron-electron interactions, which are strongest if the electron density is low, and their interplay with disorder. Often both effects are in competition with one another leading to a variety of phenomena. We briefly mention a few and then proceed in Secs. 2.6 and 4.8 to propose a simple model in an attempt at a qualitative understanding of these experimental findings.

If the electron gas is very tenuous, the mean separation between carriers, $r$, is large. The long-ranged nature of the Coulomb interaction ($\sim 1/r$) dominates over kinetic energy ($\sim 1/r^2$), and in the extremal case the electrostatic forces may freeze the electrons into a self-assembled crystalline arrangement, the Wigner crystal (Mott, 1990). Such a configuration has one highly conducting mode, namely where the entire crystal moves through the conductor. If, however, the crystal is stuck ("pinned") at local impurities, the system becomes highly insulating, but may revert to its conducting mode if the external potential is large enough to overcome the associated energy scale, the depinning voltage.

In another scenario, where wavefunctions are strongly localized by interference due to ambient disorder, an electron-electron inelastic scattering event may

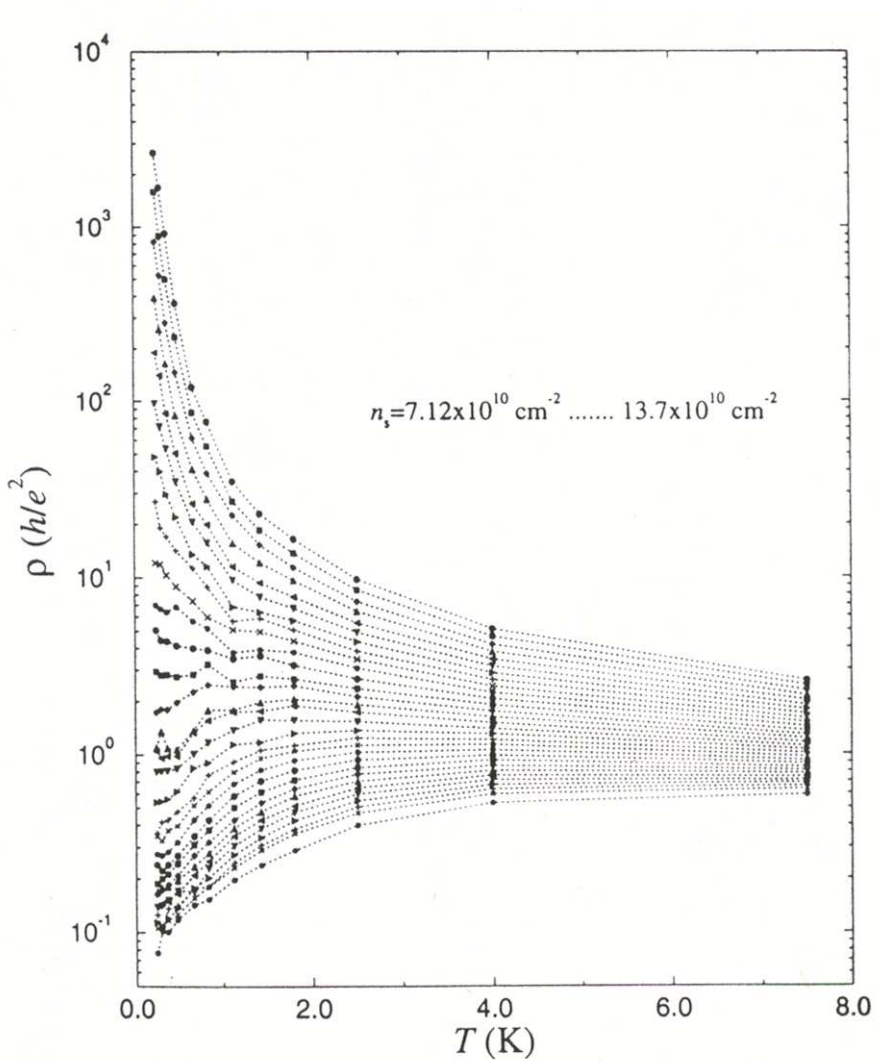


FIGURE 3. Temperature dependencies of resistivities for various electron densities, from (Kravchenko et al., 1995)

transfer a localized particle to a state whose maximum amplitude is centered a few sites away. The localization length will then have effectively been extended. In that sense, electron-electron interaction can have a delocalizing effect.

In a numerical study, Vojta and Epperlein (1998) diagonalized a Hamiltonian containing both long-ranged Coulomb interactions and Anderson disorder in an energetically pre-selected Hartree-Fock basis. The authors found that weak

Coulomb interactions can *enhance* the conductance of highly localized states at high disorder.

## 2.6 The Hubbard Model and Random-Alloy Analogy

Hubbard (1963, 1964a,b, also referred to as Hubbard I,II,III) in a series of papers has proposed a simple Hamiltonian that includes a form of electron-electron interaction,

$$H = \sum_{i,\sigma} (\varepsilon + \frac{1}{2} I c^{\dagger}_{i,-\sigma} c_{i,-\sigma})\, c^{\dagger}_{i,\sigma} c_{i,\sigma} + \sum_{\langle i,j \rangle,\sigma} v_{i,j}\, c^{\dagger}_{i,\sigma} c_{j,\sigma}\,, \tag{2.4}$$

where $\varepsilon$ is the binding energy, $I$ the electron-electron Coulomb potential, and $v_{i,j} = v$ the hopping energy which we take again to be constant and only to extend to nearest neighbors, as in the Anderson Hamiltonian denoted by $\langle i, j \rangle$. The spin quantum number $\sigma$ enters here to include the possibility of double occupation of a state. By construction of the special interaction term in the Hubbard Hamiltonian, two electrons experience an interaction only when they occupy the same orbital in which case their spins must be anti-parallel. Although inspired by the Coulomb repulsion, the range of this interaction is point-like, opposed to the typical $1/r$ long-ranged Coulomb law. However, in materials with a large dielectric constant such as silicon, one can argue that the effective Coulomb-interaction becomes more short-ranged due to Thomas-Fermi screening (Ziman, 1979) and so this term in Eq. (2.4) may be a plausible, if somewhat uncontrolled approximation.

At this point, we are still facing a multi-electron problem. To simplify further, Hubbard III has introduced the *random-alloy analogy* in which one imagines the $\downarrow$-electrons to be frozen into the lattice at random positions, creating a disor-

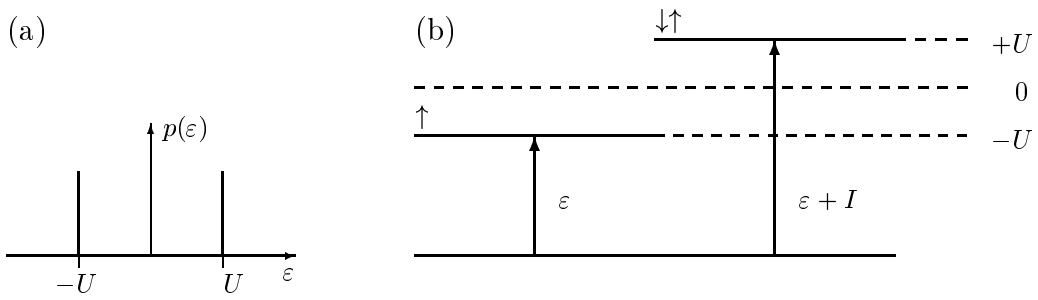


FIGURE 4. (a) Bimodal disorder distribution and (b) transitions in random alloy model

dered background potential for an ↑-electron. We may ask what the bounds on the validity of this approximation are. Consider an atom hosting a ↓-electron. The atom has then a transition energy of $\varepsilon + I$. If the ↓-electron were to move off that atom, the resonance would shift to $\varepsilon$. If the switching between either resonance is slow, then the resonances will be slightly broadened but distinct. The approximation thus holds when the kinetic energy is low compared to the interaction strength $I$. If the switching rate is fast, the two transitions merge into one.

Assuming the approximation is valid, an ↑-electron will then see an effective potential of either $\varepsilon$ at an unoccupied site, or $\varepsilon + I$ at a site occupied by a ↓-electron. In other words, the problem thus becomes a single-particle problem with disorder, where the disorder potential now is bimodal, cf. Fig. 4a. If we reset the zero of the energy scale to $\varepsilon + I/2$, we can define the disorder potential $U_i$ at site $i$ in terms of a single parameter $U$, Fig. 4b,

$$U_i \quad = \quad \begin{cases} +U = \varepsilon + I, & \downarrow\uparrow \\ -U = \quad \varepsilon, & \uparrow \ . \end{cases} \tag{2.5}$$

We have thus mapped the interacting many-body problem onto a disordered single-particle one. The disorder now represents the disordered *electron-electron*

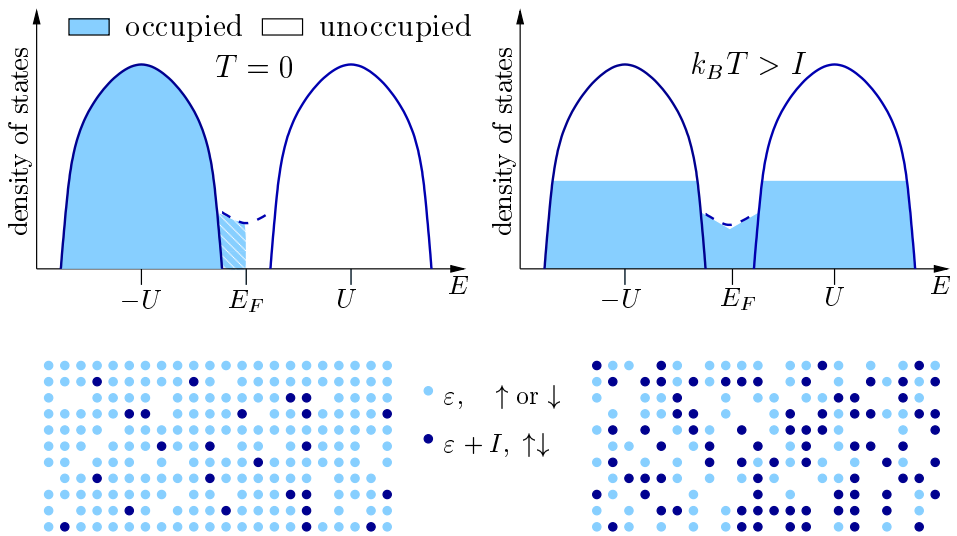


FIGURE 5. Hubbard density of states, filling at $T = 0$, $k_B T \sim I$ and site occupation (schematic)

*potential*, not lattice disorder as in the Anderson model. The two transition energies will produce a bimodal density of states, Fig. 5. If we fill up the single-particle states to the Fermi level $E_F$, at zero temperature only the lower band will be occupied, corresponding to the $\uparrow$-electrons sitting in singly occupied orbitals. At higher temperature, when $k_B T \sim I$, both bands will have roughly equal occupation, Fig. 5 (right panel), both transitions become equally likely and we expect to find a roughly equal number of singly and doubly occupied orbitals. Due to residual quantum fluctuations, there may be occasional doubly occupied sites even at lowest temperatures, as schematically depicted in the bottom panel of Fig. 5.

We will expand on these ideas to construct a model for conductance in a disordered, interacting two-dimensional system in Sec. 4.8.

## 2.7 Conductance and Transmittance

The Drude model of electrical conductivity (Ashcroft and Mermin, 1976) views electrons as classical ballistic particles that undergo a random momentum change within a relaxation time $\tau$. The average drift velocity $\langle v \rangle$ under the influence of an external field $E$ then equals $eE\tau/m$. With a carrier number density $n$, we obtain the current density as $j = en\langle v \rangle$. Dividing by the field yields the Drude conductivity,

$$\sigma = \frac{ne^2\tau}{m}\,. \tag{2.6}$$

This simple theory is valid for the metallic conductivity if both elastic and inelastic events are present. As a classical theory, however, it fails to account for effects of quantum interference that will attenuate a wave passing through a random array of scatterers. The latter is captured, however, in the transmittance $|t|^2$ and reflectance $|r|^2$. As an electron wave $e^{ikx}$ impinges on a potential barrier (in 1D), there will be a backscattered part, $re^{-ikx}$, and a transmitted part, $te^{ikx}$. The coefficients $r$, $t$ are complex and contain both an amplitude attenuation and a phase shift. Unitarity requires that $|r|^2+|t|^2 = 1$. The barrier can be a complicated array of scatterers, but since all processes are elastic, the foregoing argument always holds.

Using the transmittance, one can derive a formula for the quantum conductance. The argument follows Kirkman and Pendry (1984); Godin (1988). Consider a linear conductor across which a voltage difference of $\Delta V$ is applied. This will provoke a change $\Delta\mu$ in the chemical potential giving rise to an accumulation of $\Delta N$ carriers proportional to the density of states available at the Fermi level

$n(E_F)$,

$$\Delta N = n(E_F)\Delta\mu = en(E_F)\Delta V\,. \tag{2.7}$$

External fields typically do not penetrate into the conductor because of screening (Ziman, 1979). The conduction electrons do not feel a force exerted by an external field but rather, by quantum mechanics, scurry around at the Fermi velocity due to their kinetic energy, $v_F\hbar = \partial E/\partial k$. The density of states furthermore is given by the curvature of the band, $n(E)\pi = \partial k/\partial E$. A current now results from the $\Delta N$ electrons moving along the gradient in the chemical potential at velocity $v_F$, but only the fraction $|t|^2$ will arrive at the opposite lead. Thus,

$$I = ev_F\Delta N|t|^2\,. \tag{2.8}$$

The conductance $G$ is then given by

$$G \quad = \quad \frac{I}{\Delta V} \quad = \quad \frac{e^2}{\pi\hbar}|t|^2\,. \tag{2.9}$$

Landauer (1957, 1970); Anderson et al. (1980) have derived a similar formula but in lieu of $|t|^2$, it contains $|t|^2/|r|^2$. There has been some argument as to which formula is correct. The latter form has been criticized for yielding a diverging conductance if $|r|^2 \cong 0$ for highly transmissive samples. The maximum conductance however should be finite as the current is carried by states at the Fermi level and their number is limited by a finite density of states. (Landauer, 1981) in an attempt to resolve the conflict attributes the factor of $|r|^2$ to the local accumulation of charge in a self-consistent treatment. But he concedes that the form given in Eq. (2.9) is adequate for the behavior over long distances. Godin (1988) also discusses

this issue in some depth. We will employ the form of Eq. (2.9) since our primary focus in not on microscopic details but rather long-range behavior.

In the context of conductances of disordered systems it should be noted that Thouless (1974) has introduced a dimensionless conductance $g$ which is based on the observation that the eigenlevels of conducting states will shift in response to a change in boundary conditions from periodic to antiperiodic while while insulating (localized) states will be less sensitive to such a change, commensurate with the decay of their wavefunction over the width of the sample. His result was a linear relationship to the conductance $G$,

$$g \quad = \quad \frac{\hbar}{e^2} G \,. \tag{2.10}$$

# CHAPTER III

# HOW TO EFFICIENTLY COMPUTE TRANSMITTANCES FROM GIANT SPARSE MATRICES

## 3.1 Introduction

The study of disordered systems is complicated by the fact that mesoscopic systems exhibit large fluctuations in physical quantities (Janssen, 1998). This particularly affects computational efforts to analyze the nature of asymptotic limits using material samples whose size is limited by the CPU time and memory requirements for a particular algorithm.

Several standard approaches rely on diagonalizing the large sparse Hamiltonian matrices for the Anderson model introduced in Sec. 2.2 to derive, e.g. level spacing statistics (Zharekeshev and Kramer, 1999) or dimensionless conductances.

Unfortunately, the calculation of eigenvalues (or eigenstates) commands a relatively high computational price which imposes narrow limits on the largest tractable system size, such as $100^3$ (Zharekeshev and Kramer, 1997) which is considered state-of-the-art.

Typical diagonalization schemes (Wilkinson, 1985) often proceed in a two-step fashion where in the first step, the initial matrix is brought into a tridiagonal form and, in a second step, the tridiagonal matrix is diagonalized. A frequently used technique is the Lanczos method (Wilkinson, 1985; Cullum and Willoughby, 1985) for tridiagonalization, followed by a bisection algorithm to diagonalize the result (Nex, 1984; Cullum and Willoughby, 1985).

For very large matrices with upward of $10^6$ elements, the Lanczos method has become very popular in recent years because of its low demands on computer memory, in particular also in cases where the matrix elements can be computed on the fly rather than need to be held in storage. The reason for this economical memory usage lies in the Lanczos algorithm's iterative nature: It produces a tridiagonalization of the matrix successively, element by element, requiring the storage of only two vectors of the transformation matrix, cf. Sec. 3.2. This contrasts with other methods such as Householder reduction or Givens rotation which produce tridiagonal forms or the QR/QL algorithms that diagonalize directly (Wilkinson, 1985; Press et al., 1999). These methods operate on all matrix elements simultaneously and therefore need to hold the original and the result matrix in memory at all times. In addition, the most computation-intensive operation in the Lanczos method are matrix-vector multiplications which are of order $O(N^2)$, with N the number of entries per vector, while other methods contain matrix-matrix multiplications which are of order $O(N^3)$.

All these advantages of the Lanczos method come at a price, however, and that price is the emergence of spurious, artifactual multiplicities in the converged eigenvalues (Cullum and Willoughby, 1985). These spurious multiplicities, aptly named "ghosts," are the result of a loss of orthogonality in the successively generated basis vectors. While there are various ways to reorthogonalize the basis vectors, these techniques tend to defeat some of the CPU time and storage advantages that made the Lanczos method so attractive in the first place and, more importantly, are often unnecessary as there are more clever ways to deal with ghosts, cf. Secs. 3.6, 4.2.

An efficient implementation of the Lanczos method for large sparse matrices, as we use them in this dissertation, must account for and exploit the sparseness of these matrices. This turns out to be a non-trivial problem if a parallel distribution of the data is desired at the same time, and the implementation is supposed to operate in generic dimensions. At the core of such an implementation lies a design for storing vector components and matrix elements that allows a cache-efficient matrix-vector multiplication. These premises have formed the foundation of the *Parallel Recursion Project* (PARP) whose aim it was to supply a framework and library at a high level of abstraction so that it can be easily adapted for a variety of problems while supplying an efficient underlying machinery for parallel execution, cf. Chapter V.

While the Lanczos method is typically employed to obtain eigenvalues, the singular focus on eigenvalues also detracts from physical insights that can be learned from the tridiagonal matrix already. The quest for eigenvalues using the Lanczos method is furthermore unnecessarily expensive, as in order to obtain convergence, many iterations over already explored state space are needed. In many cases of mesoscopic and macroscopic systems, eigenvalues do not supply the most useful picture of the underlying physics, for they are strongly affected by minute changes in the (microscopic) boundary conditions which may not be mirrored in a corresponding change of the physical properties of the system. Global quantities such as transmittances, transition probabilities or distributions of eigenvalues may prove more illustrative.

An approach that employs the Lanczos recursion but concentrates on the study of the tridiagonal matrix and quantities derived from it has become known

as the *recursion method* (Haydock, 1980). It is related to the theory of orthogonal polynomials and continued fractions. In the next sections, we will describe the recursion method and show how it can be employed for the study of disordered systems.

## 3.2 The Recursion Method

In this section, we will introduce the recursion method to tridiagonalize large sparse matrices. In Secs. 3.3, 3.4, 3.5, we then explore quantities of interest that can be computed without explicit diagonalization.

Given a Hamiltonian matrix $H$, defined in some basis $\{\phi_i\}$, e.g. a lattice representation, cf. Fig. 6, we seek a new set of basis vectors $(\mathbf{u}_0, \mathbf{u}_1, \ldots, \mathbf{u}_n, \mathbf{u}_{n+1})$ in which the Hamiltonian assumes a tridiagonal form,

$$J = \begin{pmatrix} a_0 & b_1 & & & \\ b_1 & a_1 & b_2 & & \\ & b_2 & a_2 & & \\ & & & \ddots & b_n \\ & & & b_n & a_n \end{pmatrix} . \tag{3.1}$$

To reiterate, the motivation for tridiagonalizing the Hamiltonian is due to the computational advantages this technique bears for very large matrices as will become clear in a moment.

We begin by selecting a starting vector $\mathbf{u}_0$, normalized to unity. We will see later in Sec. 3.3 that the choice of $\mathbf{u}_0$ plays an important role in determining what kind of information can be extracted from the tridiagonal matrix $J$ directly. To

leap ahead, we divulge that $\mathbf{u}_0$ *projects out* the subspace of interest.

The diagonal matrix element between $\mathbf{u}_0$ and $H$ is defined as

$$a_0 = \mathbf{u}_0^\dagger H \mathbf{u}_0 \,. \tag{3.2}$$

We construct a new orthogonal basis vector $\mathbf{u}_1$ by projecting $\mathbf{u}_0$ onto $H$ and subtracting the diagonal contribution,

$$b_1 \mathbf{u}_1 = (H - a_0)\mathbf{u}_0 \,. \tag{3.3}$$

Normalization of $\mathbf{u}_1$ yields $b_1$,

$$b_1 = \sqrt{[(H - a_0)\mathbf{u}_0]^\dagger [(H - a_0)\mathbf{u}_0]} \,. \tag{3.4}$$

For $n > 1$, the procedure continues in general as

$$b_{n+1}\mathbf{u}_{n+1} = (H - a_n)\mathbf{u}_n - b_n \mathbf{u}_{n-1} \,, \tag{3.5}$$

where

$$a_n = \mathbf{u}_n^\dagger H \mathbf{u}_n \,, \tag{3.6}$$

$$b_{n+1} = \sqrt{[(H - a_n)\mathbf{u}_n - b_n \mathbf{u}_{n-1}]^\dagger [(H - a_n)\mathbf{u}_n - b_n \mathbf{u}_{n-1}]} \,. \tag{3.7}$$

To illustrate the origin of Eq. (3.5), we rewrite it as

$$H \mathbf{u}_n = b_{n+1}\mathbf{u}_{n+1} + a_n \mathbf{u}_n + b_n \mathbf{u}_{n-1} \,. \tag{3.8}$$

The product $H\mathbf{u}_n$ is a linear combination of *only* $\mathbf{u}_{n+1}$, $\mathbf{u}_n$ and $\mathbf{u}_{n-1}$. By subtracting the contributions parallel to $\mathbf{u}_n$ and $\mathbf{u}_{n-1}$, therefore, the vector $\mathbf{u}_{n+1}$ has been constructed orthogonally to the former two, and furthermore to all previous vectors $\mathbf{u}_0, \mathbf{u}_1, \ldots, \mathbf{u}_{n-1}$.

This latter statement may not be immediately obvious. The proof follows by induction: Suppose the vectors $\mathbf{u}_0, \mathbf{u}_1, \ldots, \mathbf{u}_n$ have been orthonormalized. We have to show that the vector $\mathbf{u}_{n+1}$ constructed according to Eq. (3.5) is orthogonal to all $\mathbf{u}_m$ for $m < n-1$, i.e. the scalar product $\mathbf{u}_m^\dagger \mathbf{u}_{n+1}$ must be zero:

$$\begin{aligned} b_{n+1}\mathbf{u}_m^\dagger \mathbf{u}_{n+1} &= \mathbf{u}_m^\dagger H\mathbf{u}_n - a_n \mathbf{u}_m^\dagger \mathbf{u}_n - b_n \mathbf{u}_m^\dagger \mathbf{u}_{n-1} && (3.9)\\ &= (H\mathbf{u}_m)^\dagger \mathbf{u}_n && (3.10)\\ &= 0\,, \qquad \text{q.e.d.} \end{aligned}$$

On the right hand side of Eq. (3.9) we have substituted in Eq. (3.5); the last two terms are zero by our assumption. In line (3.10), we have used the Hermiticity of $H$. The product $H\mathbf{u}_m$ will have components along $\mathbf{u}_{m-1}$, $\mathbf{u}_m$ and $\mathbf{u}_{m+1}$, all of which have zero overlap with $\mathbf{u}_n$, again by the assumption.

This construction is reminiscent of the Gram-Schmidt orthogonalization procedure, but, while in Gram-Schmidt any new vector has to be orthonormalized with respect to all previous vectors, in the case of the recursion basis any new vector needs to be orthogonalized only against the two previous ones. All other scalar products are automatically zero. The three-term recurrence relation Eq. (3.5) produces a new basis $\{\mathbf{u}_n\}$ in which the matrix has only diagonal elements $\{a_n\}$ and symmetrical side diagonals $\{b_n\}$. The side diagonals will always be symmetrical if the matrix $H$ is Hermitian, as is the case for all Hamiltonians. The matrix $J$ is

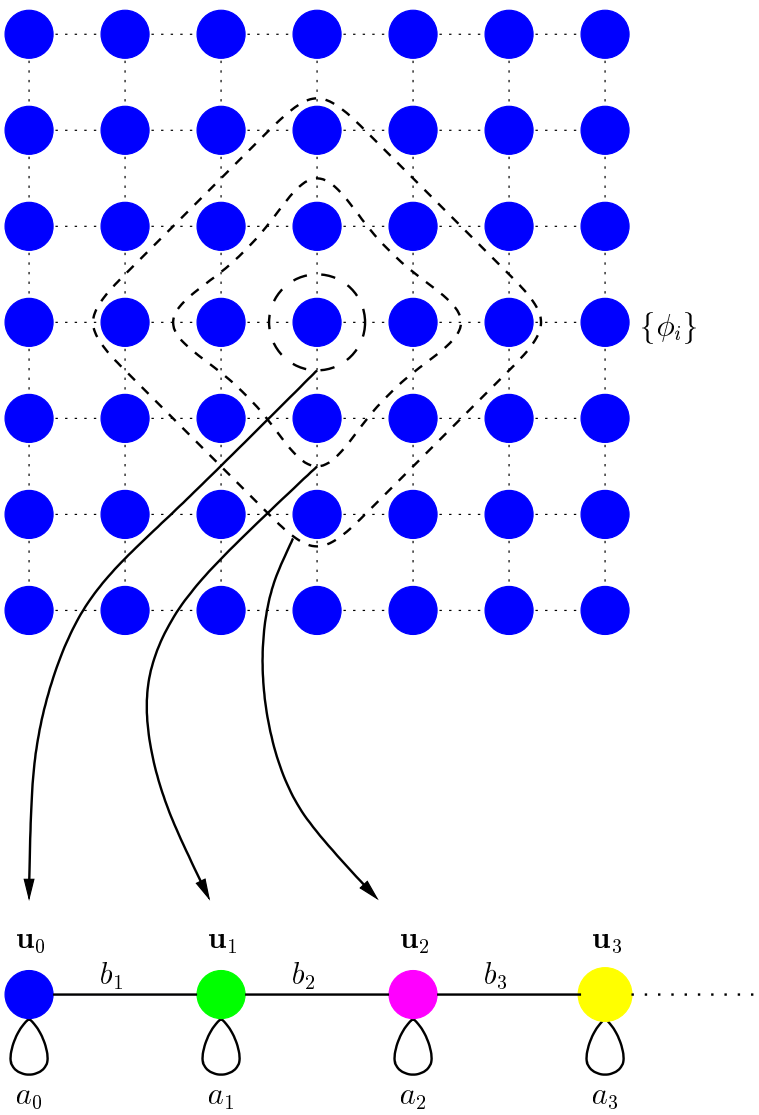


FIGURE 6. Transformation to the chain

called *tridiagonal*.

The transformation to a tridiagonal matrix can be graphically represented as the transformation of a $d$-dimensional lattice into a one-dimensional semi-infinite chain model. The basis states $\{\mathbf{u}_n\}$ form the nodes of the chain model whose diagonal matrix elements are the coefficients $\{a_n\}$ and the coupling between sites is provided by $\{b_n\}$, see Fig. 6. In the lattice basis $\{\phi_i\}$ of the Hamiltonian, each

FIGURE 7. Spatial distribution of vector components for $\mathbf{u}_0$, $\mathbf{u}_1$, $\mathbf{u}_2$, $\mathbf{u}_3$, $\mathbf{u}_4$, $\mathbf{u}_5$, $\mathbf{u}_{10}$

vector $\mathbf{u}_n$ is defined by its components $\{u_n^i\}_i$ on the lattice sites,

$$\mathbf{u}_n = \sum_i u_n^i \phi_i \qquad \text{i.e.} \qquad \mathbf{u}_n = \begin{pmatrix} u_n^1 \\ u_n^2 \\ \vdots \\ u_n^j \\ \vdots \end{pmatrix} . \tag{3.11}$$

If $\mathbf{u}_0$ is chosen to consist only of a single non-zero component located on a single site, i.e. $\mathbf{u}_0 = \phi_0$, the vectors $\{\mathbf{u}_n\}_{n=1}$ form "shells" around the starting site, intuitively representing the "interaction" of increasingly distant environments with the state of projection. Figure 7 shows the spatial distribution of the components of the vector $\mathbf{u}_n$ after several iterations. We can see that there is an approximate relationship between recursion index $n$ and distance from the starting state $r$. This is the result of the orthogonality of the basis vectors, in reminiscence of spherical waves.

The three-term recurrence spells a tremendous computational opportunity:

Only two basis vectors have to be held in memory at any given time. In addition, if the matrix is highly sparse and some or all of its elements can be generated on the fly or are constant, the matrix-vector multiplication in $H\mathbf{u}_n$ involves only few operations of order $O(kN)$ with $k$ the typical number of entries per row and column of $H$, and $N$ the number of elements in the vector $\mathbf{u}_n$. In the case of the Anderson model considered for square and simple cubic lattice systems in this dissertation, these two condition are met: The off-diagonal elements are constant, and the coordination $k$ is four or six. Furthermore, the diagonal matrix elements can be stored where they are needed, namely together with the each component of $\mathbf{u}_n$ and $\mathbf{u}_{n-1}$, thereby increasing the concentration of relevant data in the processor cache and hence execution speed. These observations have led to the Parallel Recursion Project which is described in further detail in Chapter V.

While we deploy the recursion method in the present dissertation in a computational context, it shall be noted that it is a handy tool also for analytical studies. Also, in cases where other approaches relying on lattice symmetries and $\vec{k}$-space break down, the applicability and usefulness of the recursion method has been demonstrated (Heine, 1980).

## 3.3 Projected Quantities and Lead States

Let us now turn our attention to the kinds of quantities we can extract from the tridiagonal matrix $J$. As already indicated in Sec. 3.2 above, the starting vector determines the interpretation of quantities computed from the tridiagonal matrix.

### 3.3.1 A Word on Lanczos

In a typical Lanczos diagonalization scheme, the elements of the starting vector are usually chosen randomly. The idea is to have the starting vector overlap with as large a number of eigenvectors of the original matrix as possible, because only those eigenvectors are contained in the projected subspace of the recursion basis and can be converged from eigenvectors of the tridiagonal matrix. In other words, eigenvectors that are exactly orthogonal to the starting vector will never be detected by the Lanczos method. The *Lanczos phenomenon* (Parlett, 1998; Cullum and Willoughby, 1985) says that the eigenvalues of the tridiagonal matrix will eventually converge to eigenvalues of the original matrix, for eigenvalues whose states are represented in the projected subspace. Thus, this projection is more a nuisance than a feature in traditional matrix diagonalization applications of Lanczos.

In order to achieve convergence for all eigenvalues of a matrix with $M$ elements, it is typically necessary to complete $2M$ iterations. With periodic boundary conditions and a randomly distributed stating vector, this means that the system is traversed by the recursion basis many times. One should think that one sweep across all of state space should be enough to explore it exhaustively. The strict insistance on eigenvalues thereby blocks more economical avenues to gather the relevant information.

### 3.3.2 The Significance of Projection in the Recursion Method

In a recursion method calculation, the setup is principally different. Typically a highly singluar starting vector is chosen, e.g. one that has a component on only

one site of the lattice representation. The basis states $\{\mathbf{u}_n\}$ are constructed by a single sweep through the system. No explicit boundary conditions other than the specific choice of starting vector are imposed, and the basis explores state space unencumbered. The informational content of the resulting tridiagonal matrix is that of the whole system projected onto the starting vector.

This projection is exploited as a feature in that the physical properties of the state projected onto are highlighted. For example, in the investigation of a surface, it makes sense to construct a subspace projected onto a surface state to study how the surface affects the rest of the system. Similarly, one can project onto specific disturbances of the system to analyze its response, e.g. the removal of an electron from a Heisenberg spin chain (Haydock, 2000). Projecting on gap states or impurity states yields information about how electronic characteristics of the system change as a result of their presence.

### 3.3.3 Projection, Transmittance and Lead States

In this dissertation, we study transmittances to assess the low-temperature quantum conductance of disordered systems. To that effect, we need to consider how the states in leads to and from the sample couple with the sample's own electronic states. The natural choice for projection is hence a state representing the connection to the lead. The construction of the projected subspace will then automatically include only those states with a non-zero overlap with the lead state or, in other words, only those participating in transport of electrons injected by this lead. In the absence of inelastic scattering events, all other states of the system are irrelevant for this purpose.

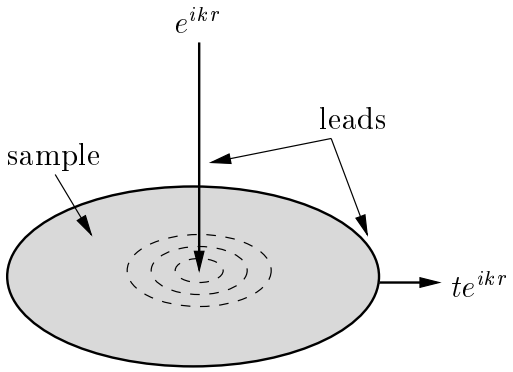


FIGURE 8. Lead-sample arrangement for computation of transmittance in 2D

In research looking for a mobility edge in 2-d disordered systems, Godin (1988); Godin and Haydock (1992) included two leads for incoming and outgoing current, respectively, which led to a more involved form of the recursion method, called block recursion.

In the present case, we use a generalized notion of the leads: We choose a starting state that has non-zero weight on only a single site. This site represents the input lead, injecting a wave packet into the system. By constructing the orthogonal basis, this disturbance then propagates through states coupled to the initial (lead) state. After $N$ recursions, the last constructed state, $\mathbf{u}_N$ is taken as the opposing lead state. This state is not point-like but distributed across many sites with the largest components concentrated along a spherical (circular in 2-d) surface with a radius $\sim N$. A corresponding experimental setup is shown in Fig. 8.

It is these two states, coupled by intervening states of the system, between which we will calculate a transmittance in Sec. 3.5. First, however, we will take a brief detour and present select aspects of other quantities such as the projected

density of states that can be derived from the tridiagonal matrix and related theory.

## 3.4 Projected Density of States and Related Theory

We mentioned previously that useful quantities can be extracted from the tridiagonal matrix $J$ without diagonalization. In Sec. 3.5 we will compute the transmittance of a disordered system from $J$ which forms the basis for further analysis in Chapter IV. In the present section, we will turn to computing distributions of eigenvalues directly, notably the *projected density of states* (PDOS).

### 3.4.1 Density of States

In conjunction with the Schrödinger Equation a physical system is completely described by its Hamiltonian operator, $\hat{H}$. For the present purpose it is useful to define an equivalent operator, the *Resolvent*:

$$\hat{R}(z) \quad \equiv \quad (z - \hat{H})^{-1} \quad \equiv \quad \frac{1}{z - \hat{H}} \tag{3.12}$$

Let $\{|\psi_n\rangle\}$ be a complete set of eigenstates in Dirac notation with eigenvalues $\{\lambda_n\}$ of $\hat{H}$. We can then rewrite the Resolvent in spectral representation,

$$\hat{R}(z) \quad = \quad \sum_n \frac{|\psi_n\rangle\langle\psi_n|}{z - \lambda_n}\,. \tag{3.13}$$

The resolvent possesses simple poles along the real axis at each eigenvalue $\lambda_n$. In an infinitely large system, the eigenvalues become dense, forming a band. The Resolvent will then exhibit a branch cut for the width of the band. These observations indicate a relation to the density of states (DOS) of the system: For

a discrete spectrum, the density of states consists of discrete $\delta$-functions at the location of the poles of the Resolvent; for a continuous spectrum the $\delta$-spikes fuse into a smooth function. A mathematically rigorous relation can be established by a limiting procedure approaching the singularities of the Resolvent from above and below the real axis. Noting that

$$\lim_{\epsilon\to 0}\frac{1}{z\pm i\epsilon}=\mathcal{P}\frac{1}{z}\mp i\pi\delta(z)\,, \tag{3.14}$$

where the principal value $\mathcal{P}f(x)$ is defined in terms of the Cauchy principal value integral as

$$\mathcal{P}\int_{-\infty}^{\infty}f(x)\,dx=\lim_{\epsilon\to 0}\left(\int_{-\infty}^{-\epsilon}f(x)\,dx+\int_{\epsilon}^{\infty}f(x)\,dx\right)\,, \tag{3.15}$$

we discover from Eq. (3.13) that the imaginary part of the Resolvent becomes a sum of $\delta$-functions, using the limiting procedure of Eq. (3.14),

$$\mp\frac{1}{\pi}\mathrm{Im}\left[\lim_{\epsilon\to 0}\hat{R}(z\pm i\epsilon)\right] \quad = \quad \sum_n\delta(z-\lambda_n) \quad \equiv \quad N(z)\,. \tag{3.16}$$

The expression on the right-hand-side is the (global) density of states $N(z)$.

### 3.4.2 Projected or Local Density of States

A quantity derived from the *global* density of states, Eq. (3.16) is the *projected* or *local* density of states (PDOS). The PDOS is weighted by the projection of the eigenstates $\{|\psi_n\rangle\}$ onto some state $|\mathbf{u}\rangle$, hence the name:

$$N_{|\mathbf{u}\rangle}(z) \quad \equiv \quad \sum_n|\langle\psi_n|\mathbf{u}\rangle|^2\,\delta(z-\lambda_n) \tag{3.17}$$

The projected density of states thus defined incorporates both local information by means of the overlaps with $|\mathbf{u}\rangle$ as well as global information through the distribution of eigenstates. It is a unique quantity and suited for studying the interplay of the specifics of a certain state $|\mathbf{u}\rangle$ with the rest of the system at large. It can be used to measure the system's response to a disturbance brought on by the presence of the state $|\mathbf{u}\rangle$. In a generalized sense, if the states are substituted for operators ("operator recursion") (Annett et al., 1994; Haydock and Kim, 1995), the resulting quantity is a *projected density of transitions* which has been employed to tackle many-body quantum problems, such as a Heisenberg spin chain. The transitions induced therein by the removal of an electron can be calculated by projecting onto the annihilation operator (Haydock, 2000).

The emphasis on the projected density of states stems from a neat relationship to the tridiagonal matrix $J$. In the previous Subsection, we have shown how the global Resolvent is related to the global density of states. If we consider a *projected Resolvent*,

$$R_{|\mathbf{u}\rangle}(z) \quad \equiv \quad \langle \mathbf{u}|\hat{R}(z)|\mathbf{u}\rangle \quad = \quad \langle \mathbf{u}|\frac{1}{z-H}|\mathbf{u}\rangle\,, \tag{3.18}$$

then, by Eqs. (3.16, 3.17) the projected density of states emerges simply as

$$N_{|\mathbf{u}\rangle}(z) \quad = \quad \mp\frac{1}{\pi}\mathrm{Im}\lim_{\epsilon\to 0}\langle \mathbf{u}|(z\pm i\epsilon-\hat{H})^{-1}|\mathbf{u}\rangle\,. \tag{3.19}$$

If now the state $|\mathbf{u}\rangle$ is chosen to be the starting state $\mathbf{u}_0$ of the recursion basis and we revert to matrix notation, then by straightforward linear algebra, the matrix element $\mathbf{u}_0^\dagger(z-H)^{-1}\mathbf{u}_0$ equals the top left matrix element of the inverse of

$(z - J)$, since the $\mathbf{u}_0, \mathbf{u}_1, \ldots, \mathbf{u}_n$ form the transformation matrix to $J$,

$$\mathbf{u}_0^\dagger (z - H)^{-1} \mathbf{u}_0 \quad = \quad \mathbf{e}_0^\dagger (z - J)^{-1} \mathbf{e}_0 \,, \tag{3.20}$$

where $\mathbf{e}_0^\dagger = (1, 0, 0, \ldots), \ldots$, the unit vectors in the $J$ basis. The top left element of an inverse matrix is easily obtained with the help of an expansion in cofactors. The result is a continued fraction expansion (Haydock, 1980),

$$\mathbf{e}_0^\dagger (E - J)^{-1} \mathbf{e}_0 \quad = \quad \cfrac{1}{(E - a_0) - \cfrac{b_1^2}{(E - a_1) - \cfrac{b_2^2}{(E - a_2) - \cfrac{b_3^2}{\vdots}}}} \,, \tag{3.21}$$

where the coefficients $\{a_n\}$ and $\{b_n\}$ are the ones appearing in the tridiagonal matrix $J$, Eq. (3.1).

The projected density of states converges quickly with the number of levels in the continued fraction. Its convergence is, in fact, exponential so that the PDOS computed from a finite chain model approximates that of an infinite chain model with exponentially increasing quality. It is this remarkable piece of mathematics that permits the study of truly infinite systems with just a finite number of computations.

An interesting corollary to the exponential convergence is that an error occurring somewhere down the chain can at most have an exponentially weak effect on the projected density of states. This is true for any kind of error, e.g. rounding error, ghosting, or the error due to termination of the chain at a finite level (Te and Haydock, 1994). The cumulative error remains finite. One might phrase

this as *exponential insensitivity* to disturbances down the chain, reminiscent of the black body theorem which states that the electro-magnetic mode density in a cavity is insensitive to the shape of the boundary (von Laue, 1914). This raises an interesting possibility: In order to conserve memory, one could truncate the basis vectors $\mathbf{u}_n$ at every step, retaining only the largest components. This way, simulating potentially infinite systems becomes a realistic option. This process has been termed *dynamic recursion* because of its dynamically changing basis set.

### 3.4.3 Orthogonal Polynomials

The projected density of states introduced in the previous quantity is a distribution that can be used to compute moments such as the average energy, etc. There is a set of polynomials $P_0, P_1, \ldots, P_n$ associated with this distribution such that the polynomials obey an orthonormality relation defined by the scalar product,

$$\langle P_n | P_m \rangle \quad \equiv \quad \int P_n(E) P_m(E) N_{\mathbf{u}_0}(E)\, dE \quad = \quad \delta_{nm}\,. \tag{3.22}$$

The projected density of states $N_{\mathbf{u}_0}(E)$ plays the role of the measure in this integral. There is a large body of literature on the subject of orthogonal polynomials and the connection with the moments of the distribution. For completeness, we mention a few more facts without proof, referring the reader to Akhiezer (1965); Chihara (1978); Shohat (1943) for details.

The polynomials $\{P_n\}$ in Eq. (3.22) satisfy a recurrence relation as well. This can be seen if we consider a solution $\Psi$ to the Schrödinger equation,

$$H\Psi = E\Psi\,, \tag{3.23}$$

on the chain. The expansion coefficients of $\Psi$ in the basis $\{\mathbf{u}_n\}$ are precisely the orthogonal polynomials that satisfy Eq. (3.22),

$$\Psi = \sum_n P_n \mathbf{u}_n \,. \tag{3.24}$$

By substituting the three-term recurrence in the form of Eq. (3.8) into the Schrödinger Equation (3.23) and collecting terms for each $\mathbf{u}_n$, we retain

$$b_{n+1} P_{n+1} = (E - a_n) P_n - b_n P_{n-1} \,. \tag{3.25}$$

Because the recurrence has three terms, there are two linearly independent solutions. Conventionally one defines two sets of polynomials $P_n$ and $Q_n$ with the initial conditions $P_{-1} = 0$, $P_0 = 1$, $Q_0 = 0$, $Q_1 = 1$. A quantity which permits the characterization of the nature of the localization of the state is given by the Christoffel function,

$$\lambda_N \quad \equiv \quad \frac{1}{\sum_{n=0}^{N-1} P_n^2(E)} \,. \tag{3.26}$$

With Eq. (3.24), we note that the Christoffel function approximates the inverse of the normalization of $\Psi$. If the state is localized, we would expect $\lambda_N$ to approach a constant; if the state is extended, $\lambda_N$ should grow linearly with $N$. But this criterion always depends on the specific initial conditions chosen for $P_n$. In the next section we will introduce the transmittance for that same purpose. The advantage is that the transmittance is independent of initial conditions.

## 3.5 Transmittance

The quantum mechanical transmittance, as introduced in Sec. 2.7, lies at the heart of our study of the low-temperature quantum conductance in disordered media.

Transmittances or closely related quantities can be calculated from transfer matrices that describe the attenuation of a wave by a slab of material. In the chain model, we can define a transfer matrix between successive nodes as follows (cf. Fig. 6):

Suppose a set of amplitudes $\{\phi_n\}$ describes a solution of the Schrödinger equation along the chain with eigenvalue $E$, i.e. the amplitudes obey a three-term recurrence like Eq. 3.25,

$$b_{n+1}\phi_{n+1} = (E - a_n)\phi_n - b_n\phi_{n-1}\,. \tag{3.27}$$

Then, the scattering between the amplitudes $\phi_{n-1}$, $\phi_n$ and $\phi_{n+1}$ can be related by a $2 \times 2$ matrix $\tau_n$,

$$\begin{pmatrix} \phi_{n+1} \\ \phi_n \end{pmatrix} = \tau_n \begin{pmatrix} \phi_n \\ \phi_{n-1} \end{pmatrix}\,. \tag{3.28}$$

By comparison with Eq. (3.27), the elements of $\tau_n$ can be derived:

$$\tau_n = \begin{pmatrix} \dfrac{E - a_n}{b_{n+1}} & \dfrac{b_n}{b_{n+1}} \\ 1 & 0 \end{pmatrix} \tag{3.29}$$

The transfer matrix $\tau_n$ is an equivalent statement to the tree-term recurrence, Eq. (3.27). It provides a way to calculate the amplitude $\phi_{n+1}$ given the amplitudes

$\phi_n$ and $\phi_{n-1}$. By continued application of transfer matrices, we can "unroll" the recurrence and relate the initial conditions for the solution, expressed by choices for $\phi_0$ and $\phi_{-1}$, to the amplitudes $\phi_{n+1}$ and $\phi_n$. Defining

$$T_n \equiv \prod_{m=n}^{0} \tau_m = \tau_n \tau_{n-1} \ldots \tau_1 \tau_0 \,, \tag{3.30}$$

we have

$$\begin{pmatrix} \phi_{n+1} \\ \phi_n \end{pmatrix} = T_n \begin{pmatrix} \phi_0 \\ \phi_{-1} \end{pmatrix} . \tag{3.31}$$

The matrix $T_n$ is non-Hermitian, but $T_n^\dagger T_n$ is. In the limit $n \to \infty$, the eigenvalues of $T_n^\dagger T_n$ will be reciprocals of each other, with the smaller one corresponding to the transmittance $t_n$ (Anderson et al., 1980; Janssen, 1998). For the chain model, the transmittance depends on the coefficient chosen for $b_0$ that enters $\tau_0$. The physical significance of $b_0$ is that of a coupling parameter to the lead. If the lead and the conductor are not impedance-matched, the transmittance will not equal unity even for a perfect conductor. What is more, it does not appear to be possible to impedance-match a lead consisting of just one lattice site. Godin (1988); Godin and Haydock (1992) included infinite leads and then were able to choose a bandwidth for the lead larger than that of the disordered conductor. In practice, however, this issue has little implication, since we will always consider ratios of transmittances; more precisely, integrals over the logarithm of the transmittance, cf. Sec. 4.3.

## 3.6 Identification of Ghosts

The finite precision of computer arithmetic produces a peculiar side-effect in the Lanczos/recursion algorithm. As previously mentioned in the Introduction to this Chapter, the orthogonality of the Lanczos basis $\{\mathbf{u}_n\}$ is quickly lost due to rounding errors in the finite-precision computer arithmetic. It is then possible that the dimension of the invariant subspace fails to grow by one at every iteration. As a result, newly constructed vectors $\mathbf{u}_{m>n}$ may pick up components of previous basis vectors which will either re-introduce an already converged eigenvector, thereby creating a spurious multiple or, more mysteriously, may create a completely artifactual eigenvalue that appears spontaneously just to disappear and then reappear elsewhere. These spurious eigenvalues are numerical artifacts and aptly named "ghosts."

As we shall see in Sec. 4.2, the rate of ghosting is affected by the disorder in the system and has an impact on the calculation of the transmittance in a disordered sample. We therefore need a means to identify and account for ghosts.

According to the excellent work by Cullum and Willoughby (1985), there are two types of ghosts: Since in exact arithmetic, a symmetric tridiagonal matrix possesses only non-degenerate eigenvalues, any numerically occurring multiplicities greater than one in an eigenvalue are therefore by definition all ghosts. The second type of ghosts are spurious eigenvalues that occur singly. The latter kind of eigenvalue may spontaneously appear, converge for a while before jumping elsewhere.

Both kinds of ghosts can be identified by the criterion laid out in Cullum and Willoughby (1985, Chapter 4). Defining a matrix $\hat{J}$, which is obtained from the tridiagonal matrix $J$ by deleting the first row and column, the criterion states

that ghosts are all those eigenvalues of $J$ which are also eigenvalues of $\hat{J}$ within the numerical precision. The reasoning is that ghosts are those eigenstates that appear somewhere down the chain, but not right at the beginning when orthogonality is still strong. Therefore, these ghost eigenstates have no overlap with the starting state. All eigenstates of $\hat{J}$, too, have zero overlap with the starting state by construction. Eigenvalues occurring both in $J$ and $\hat{J}$ are thus designated as ghosts.

While the basic concept sounds straightforward enough, in practice the decision when eigenvalues of $J$ and $\hat{J}$ can be viewed as identical becomes more tricky a task. Obviously "equality" must be defined in terms of the accuracy of the arithmetic employed. This is not an exact science but draws on empirical insights. We define $\epsilon_{\rm gh}$,

$$|\lambda - \hat{\lambda}| \quad < \quad \epsilon_{\rm gh}\,, \tag{3.32}$$

where $\lambda$ and $\hat{\lambda}$ refer to eigenvalues of $J$ and $\hat{J}$, respectively. Cullum and Willoughby (1985, Chapter 4) recommend an $\epsilon_{\rm gh}$ for identifying ghosts, and an $\epsilon_{\rm conv}$ for the accuracy in the convergence of eigenvalues,

$$\epsilon_{\rm gh} \quad \equiv \quad (n+1000)\,||J||\,\epsilon_M \tag{3.33}$$

$$\epsilon_{\rm conv} \quad \equiv \quad \sqrt{n+1000}\,||J||\,\epsilon_M\,, \tag{3.34}$$

where $\epsilon_M$ is twice the floating point accuracy of the machine arithmetic. Typically, on machines conforming to the IEEE floating point standard, $\epsilon_M \approx 10^{-16}$ for double precision arithmetic. $||J||$ is the norm of $J$, defined as the matrix element with maximum magnitude; $n$ the length of $J$. This formula is motivated by the cumulative rounding error that is likely to have accumulated by the time an eigenvalue

is extracted and depends on the number of operations which is proportional to the size of the matrix $n$ and its scale $||J||$. The factor of 1000 appears to be empirical. It is then sensible define as equal eigenvalues $\lambda$ and $\hat{\lambda}$ that fall within this error bar.

Despite the careful analysis by Cullum and Willoughby (1985), the number of ghosts identified this way in the disordered systems considered in this dissertation is sensitive to variation of $\epsilon_{\rm gh}$ and $\epsilon_{\rm conv}$. As we will see in Sec. 4.2, this ghost count enters the final results. We therefore need an error estimate of the uncertainty in the number of ghosts detected. We accomplish this by re-computing the ghost count using $\epsilon_{\rm gh}^{<} = 0.1\epsilon_{\rm gh}$ and $\epsilon_{\rm gh}^{>} = 10\epsilon_{\rm gh}$ and take the spread of the resulting values as an error bar.

## 3.7 Tools

Before we present results and discussion in the next Chapters IV, VI, we mention computer programs we have used and adapted from other sources.

The identification of ghosts was done with the help of the `bisec` routine of the Fortran 77 source code to Cullum and Willoughby (1985). The code is available on Netlib at Argonne National Laboratory, `http://www.netlib.org/lanczos/lesub`.

The eigenvalues of the combined transfer matrix Eq. (3.30) which can be very small or very big were obtained using the technique for stably calculating the roots of a quadratic equation given in Press et al. (1999, Chapter 5.6) which is not as trivial as it appears at first glance.

The random number generator used to produce the realizations of the disor-

der in PARP follows an encryption method for non-linear bit mixing by the same authors (Press et al., 1999, Chapter 7.5). The standard linear congruential algorithm supplied with most operating systems had insufficient period for the large number of random values required.

The fits for the plots in Chapter IV involved error bars in both the abscissa and ordinate values. We used the fitting routines of ODRPACK (Boggs et al., 1992) for that purpose. These algorithms are based on weighted orthogonal distance regression, which provide better stability than the standard least squares method. The source code is available at Netlib as well, `http://www.netlib.org/odrpack/`.

All programs the author wrote for the purposes for this study, including the parallel recursion code are included on the CD in the Pocket Material.

# CHAPTER IV

# TRANSMITTANCE IN DISORDERED SYSTEMS—RESULTS

## 4.1 Introduction

In this Chapter, we will present the detailed results of our study of transmittances in the Anderson model in 1D, 2D and 3D and in the 2D Hubbard model. One central objective of this dissertation was to analyze the localization of the states directly via their ability to transmit quantum mechanical wave packets through the sample, rather than to infer their properties indirectly by statistical means. We found this approach revealing.

Nonetheless, the results were subtle and difficult to obtain. As pointed out by Janssen (1998), mesoscopic systems will display large fluctuations in physical quantities. To be precise, Janssen (1998) defines "mesoscopic" as a size smaller than the system's phase coherence length. In the artificial Anderson model, the latter, however, in infinite. This definition notwithstanding, we will employ the term more loosely in the sense that a system is mesoscopic when the fluctuations in physical quantities become so large that mean values lose their expressiveness and the associated distributions need to be considered. This is a consequence of insufficient self-averaging. In the asymptotic limit of infinitely large systems, however, we expect to recover self-averaging and fluctuations should diminish. Conversely, one might say that whenever fluctuations die down, some measure of proximity to the asymptotic limit has been established.

This argument breaks down, however, when the system undergoes a phase

transition. Fluctuations in critical quantities are expected on all length scales—a feature which sparked the development of renormalization group theory (Wilson and Kogut, 1974). Conversely, if fluctuations do not persist to largest scales, one can argue that the respective quantity does not display critical behavior.

Our approach of employing the recursion method allowed us to computationally investigate systems of unprecendented size, in an attempt to outgrow the mesoscopic regime. In 3D, we considered systems of $8 \times 800^3 \approx 4 \times 10^9$ lattice sites, corresponding to a maximum length of 800 nodes in the chain model. To the author's knowledge, the biggest system in the published literature for the 3D Anderson model contained only $100^3 = 10^6$ lattice sites and was part of a statistical analysis, (Zharekeshev and Kramer, 1997).

The remainder of this Chapter is organized as follows: In Sec. 4.2 we will explain how the ghosting phenomenon described in Sec. 3.6 interacts with highly localized states in a disordered system. The understanding gained thereby is tested on the one-dimensional disordered system and we unambiguously recover the expected exponential localization. In Sec. 4.3 we describe how the computations were done and present the results for the transmittance in the band center in Secs. 4.4, 4.5, 4.6 for one, two, and three dimensions respectively. Plots for the transmittance in other energy intervals have been relegated to Appendices A, B, C. In Sec. 4.7 we will summarize our results in the mobility edge trajectory. Finally, in Chapter 4.8, we describe our model for the 2D interacting system and present findings.

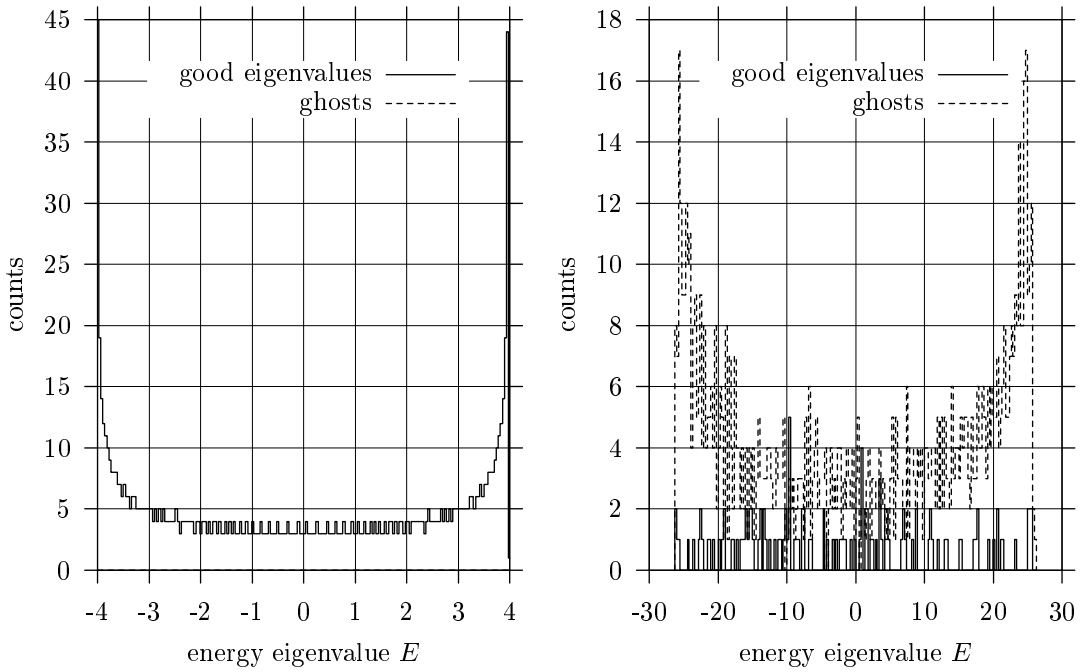


FIGURE 9. Distribution of number of good eigenvalues vs. ghosts for $W = 0$ (left) and $W = 50$ (right) for a 2D system at 1000 levels

## 4.2 Interrelation of Localization and Ghosting

In the course of our study of disordered systems based on the Anderson model, we have noticed an interesting correlation between the disorder strength $W$ and the prevalence of ghosts. As a prelude to the results presented in the following Secs., we contrast the eigenvalue and ghost distributions for two extremal cases.

As Fig. 9 shows, the ordered case ($W = 0$, 2D) does not exhibit any ghosting, while the number of ghosts in the strongly disordered 2D-system ($W = 50$) by far exceeds the number of non-spurious, "good" eigenvalues.

The following is an explanation of this observed disorder-dependence. To the best of the author's knowledge, the argument is original.

In the ordered system, all electronic states are delocalized and extend through-

out the sample. In the absence of scattering centers or boundaries, the recursion basis will propagate outward from the starting site forming roughly concentric "shells" around it which are naturally orthogonal. Under these circumstances, ghosting is bound to be minimal as long as the average magnitude of the components in the recursion basis is large compared to the relative machine accuracy—a condition that is satisfied in the present calculations. Since an unbounded system does not have discrete eigenvalues, the eigenvalues computed from the tridiagonal matrix will never converge but keep interleaving one another for successive recursions.

In the opposite extreme of high disorder, most states of the system will be strongly localized. Specifically, the spatial extent of the Wannier functions of states overlapping with the starting state is bound to be fairly limited. The recursion basis will soon have mapped out the reach of these states. At that point, the corresponding eigenvalues converge. Because there are only very few or no states that seep out into other areas of the system, the recursion basis remains confined to the localized wavefunctions overlapping the starting state. As iterations go on, new basis vectors are likely to return to an already explored state, and the associated eigenvalue will then re-converge a second time. In the worst case, the basis becomes "trapped" in a narrow region of state space and, unable to to break out of this confinement, the recursion grinds on just to produce more ghosts at a rate of one per level.

This worst-case scenario occurs when the states overlapping the starting state are very highly localized across all energies. We argue that the localization length of these states can be approximately estimated from the rate of ghosting, namely

a ghost will occur roughly after the same number of iterations it takes for the basis to move from the "center" of the localized wavefunction to the "end," i.e. to traverse its localization length.

In contrast to an unbounded recursion calculation, to obtain eigenvalues in a Lanczos calculation, the spatial expansion of the recursion basis has to be restricted by boundary conditions. The system is effectively confined to a box and the Lanczos basis will encounter the walls and "reflect" off them. In order to converge all or most eigenvalues, the iterations have to be continued until the number of Lanczos basis vectors approximately equals two to three times the number of matrix elements $M$, (Cullum and Willoughby, 1985; Zharekeshev and Kramer, 1999). If, for example, the matrix corresponds to a square lattice of linear extent $N$ so that $M = N^2$, then the basis will have explored the system within $N$ recursions. Obtaining converged eigenvalues, however, forces the basis to re-explore this space another $N(N-1)$ times. The basis thereby returns to previously visited sites and the likelihood to produce ghosts is much raised. Even in an ordered system, therefore, such a Lanczos calculation will be fraught with a non-zero rate of ghosting. This setup, typical for Lanczos-based diagonalizations, illustrates the price of forgone efficiency paid by insistence upon converging eigenvalues.

The prevalence of ghosting in disordered systems exhibiting localization of wavefunctions has bearing on the use of the quantum mechanical transmittance $t_n$ derived from the recursion basis as a probe to detect such localization. In Sec. 3.5, we have constructed the transmittance as the smaller eigenvalues of the product of transfer matrices, Eq. (3.30). Each of the transfer matrices $\tau_m$ describes the transport of an incident wave from one chain node to the next. The correspondence

between the transmittance thus derived and the envelope of the wave function in real space is based on the assumption that successive nodes on the chain (successive vectors in the recursion basis) represent consecutive orthogonal linear combinations of the lattice basis whose dominant contributions originate from a roughly circular (spherical in 3D) set of lattice sites at consecutive radii from the starting state.

This one-to-one mapping between recursion level index $n$ and radius $\vec{r}$, however, breaks down when the recursion basis becomes overcomplete, because then successive basis vectors do not necessarily correspond to consecutive radii in the lattice representation. This is when ghosts appear; the recursion basis starts revisiting lattice sites that were already included in a previous recursion vector. The associated transfer matrix $\tau_n$ then fails to adequately describe the attenuation with respect to sites at a further radius, but rather at the same or a lesser radius which would make the wavefunction appear *less localized!* The need to compensate for ghosting becomes obvious.

Since the apparition of a ghost at a certain recursion index means that no new state space (no new lattice sites) was included in that iteration, we need to disregard this iteration in the transmittance. We therefore compute an *effective level number* $n_{\text{eff}}$ from the actual level number $n_{\text{act}}$ and the total number of ghosts that have appeared up to this point $n_{\text{gh}}$, as computed by the procedure described in Sec. 3.6,

$$N \equiv n_{\text{eff}} = n_{\text{act}} - n_{\text{gh}} . \tag{4.1}$$

For the remainder of this Chapter, we always refer to this corrected, effective level number when speaking of "level number" and denote it by $N$.

To illustrate the significance of this correction, we show as an example the

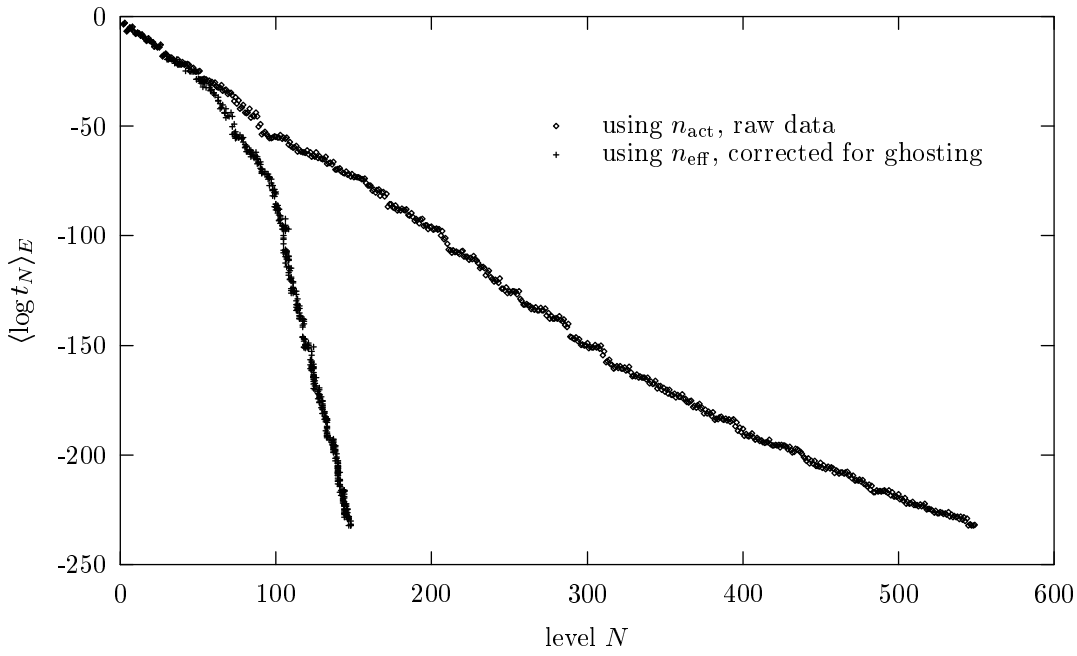


FIGURE 10. Effect of high ghost count on localization, example in 1D, $W = 4$, $E \in [-1.5, 1.5]$, averaged over 5000 sample points

results of the transmittance computed for a one-dimensional disordered system with disorder strength $W = 4$. In Fig. 10, we plot the averaged logarithm of the transmittance versus both the effective level number and the actual level number. According to theory (Landauer, 1970; Abrahams et al., 1979; Anderson et al., 1980; Haydock, 1986), all states in 1D should be exponentially localized. The figure shows that the averaged logarithm of the transmittance becomes a straight line—verifying exponential behavior—only if we use the corrected effective level number. The ghost count correction is therefore critical to correctly characterize the localization of the wavefunction.

## 4.3 Computation of Transmittance and Inferred Localization

In the next three Secs., we present the results of transmittance calculations for the one, two and three-dimensional Anderson model at various disorders. All data was obtained by a recursion calculation using PARP on a lattice system with Anderson disorder, followed by an evaluation of the small eigenvalue of the product transfer matrices $T_N^\dagger T_N$ as explained in Sec. 3.5 and denoted by $t_N$ in the following. Since the transmittances are distributed roughly according to a log-normal distribution (Haydock, 1986; Janssen, 1998), we need to average over $\log t_N$. The averaging was done over energy intervals of width $\Delta E = 1$ in units of the off-diagonal matrix elements of $H$ at 1000 equidistant sample points. The results are plotted against the effective level number $N$. The error bar on the horizontal axis was derived as described in Sec. 3.6, but for readability only every tenth error bar is drawn. The error bar on the vertical axis was estimated by doubling the sampling frequency. The resulting uncertainty, however, was less than the size of the data point markers in the plots.

For each disorder value we show a plot of the ghost count and derived effective level number for various values of $\epsilon_{\mathrm{gh}}$ as defined by Eq. (3.33). The $\epsilon_{\mathrm{gh}}$ recommended by Cullum and Willoughby (1985) is marked with "C&W;" error bars were computed from the values for $\epsilon_{\mathrm{gh}}$'s directly above and below.

Then, the individual plots of $\langle \log t_N \rangle$ follow, one per energy interval. The energy intervals were selected for each disorder to cover most of the bandwidth, given by the Lifshitz edges. In all cases it was very evident where the projected density of states became exponentially small, resulting in strongly exponentially decaying transmittances that in most cases led to numerical underflows before the

end of the total available chain length.

In order to gain a better feeling for the character of the localization, for 2D and 3D the data was plotted against both a linear axis and a logarithmic axis side-by-side. The idea is that for exponential localization,

$$t_N = t_0 \, e^{-N/\xi} \,, \tag{4.2}$$

the plot on linear abscissa should produce a straight line with the negative reciprocal localization length $\xi$ as slope. For weaker, power-law localization,

$$t_N = bN^{-\alpha} \tag{4.3}$$

the plot on logarithmic abscissa should produce a straight line with a slope of $-\alpha$, the power.

In practice it turned out that in many cases particularly in 3D the distinction between the two types of localization was very subtle, and a convincing judgement could not always be made. Whenever a clear trend was observable in the author's opinion, straight lines were fit. Sometimes, however, the data displayed steps of different regimes and occasionally multiple trends were fit. In other cases still, where localization was fairly subtle, both power law and exponential behavior seemed equally likely. To highlight this ambiguity, sometimes both cases were fit.

## 4.4 Transmittance of Disordered 1D System

In this section, we present the results of transmittance calculations for the one-dimensional Anderson model at disorders $W = 1, 2, 4, 8$. Even though in 1D,

the calculation is inexpensive, we computed only 1000 recursion levels, because beyond that the ghost count becomes very high and no new information is learned from further recursions. At 1000 levels, we unambiguously verified exponential localization. In fact, in the plots of the ghost count, Figs. 11, 13, 15, 17, we recognize that at disorder $W = 2$ the ghost count overtakes the effective level number at around 500, in $W = 4$ at around 150 and at $W = 8$ at around 50. The crossing means that the procedure has become very inefficient and explores little new state space. We also note that the uncertainty in the ghost identification seems to mysteriously vanish at 600 levels in $W = 4$ and at 100 levels in $W = 8$. The reason for that is presently unknown, but we believe that the data above this threshold probably has little credibility.

This effect manifests itself in kinks at around $N = 150$ in the data at $W = 4$, e.g. in Figs. 67–71, and at $N = 50$ for $W = 8$ in Figs. 75–83. The long shallower tail in these figures may not be real. Nonetheless, even on the tail the localization length is very short, only a few lattice sites, so that the discrepancy may not have much impact.

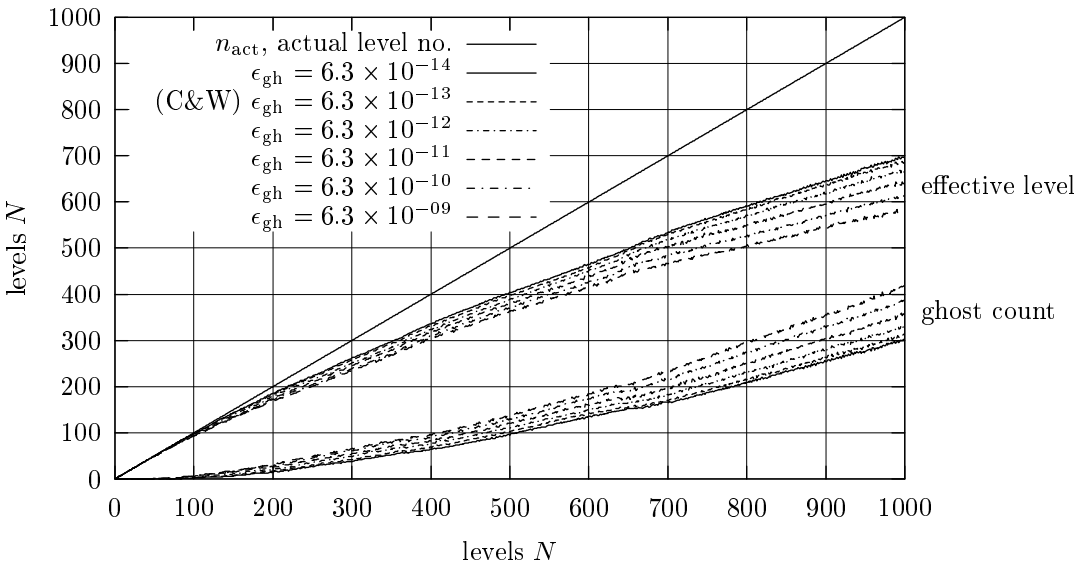


FIGURE 11. Ghost count, $n_{\rm gh}$, and effective level number, $n_{\rm eff}$ for 1D, $W = 1$ at various $\epsilon_{\rm gh}$

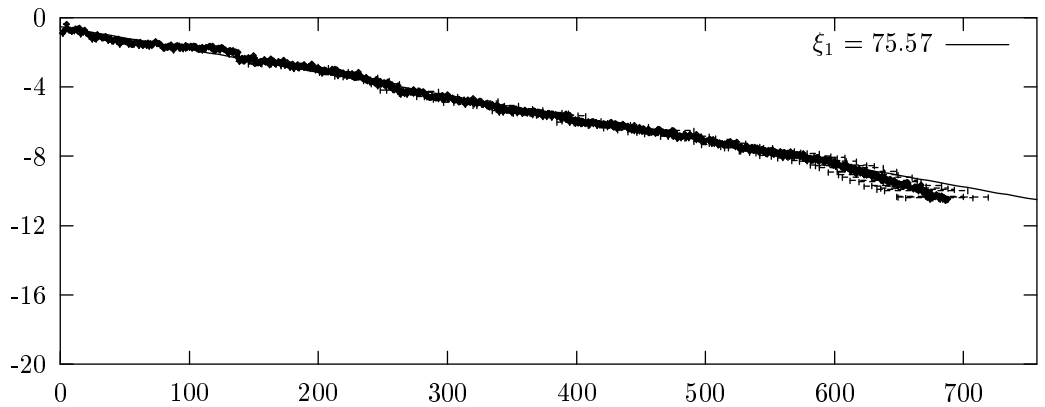


FIGURE 12. $\langle \log t_N \rangle_E$ vs. $N$ in 1D, $W = 1$, $E \in [-0.5, 0.5]$

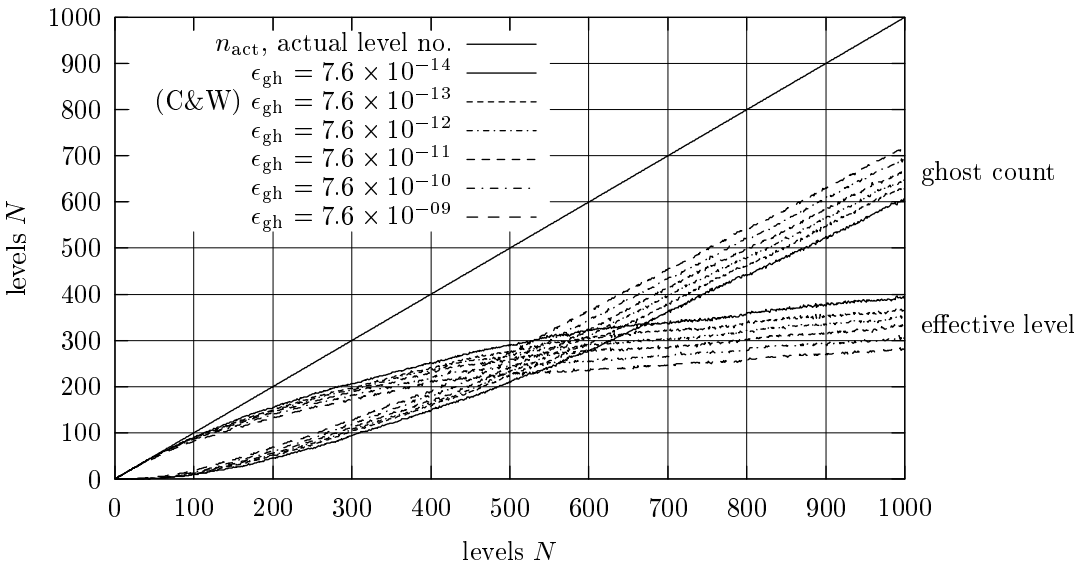


FIGURE 13. Ghost count, $n_{\rm gh}$, and effective level number, $n_{\rm eff}$ for 1D, $W = 2$ at various $\epsilon_{\rm gh}$

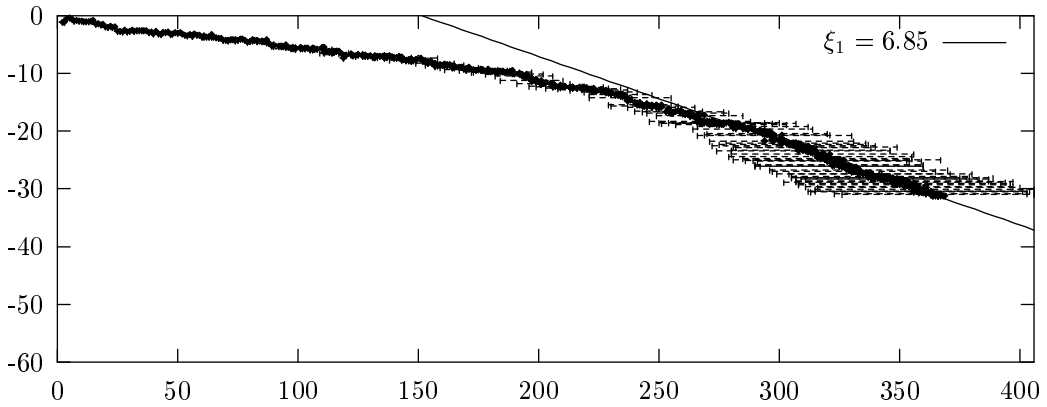


FIGURE 14. $\langle \log t_N \rangle_E$ vs. $N$ in 1D, $W = 2$, $E \in [-0.5, 0.5]$

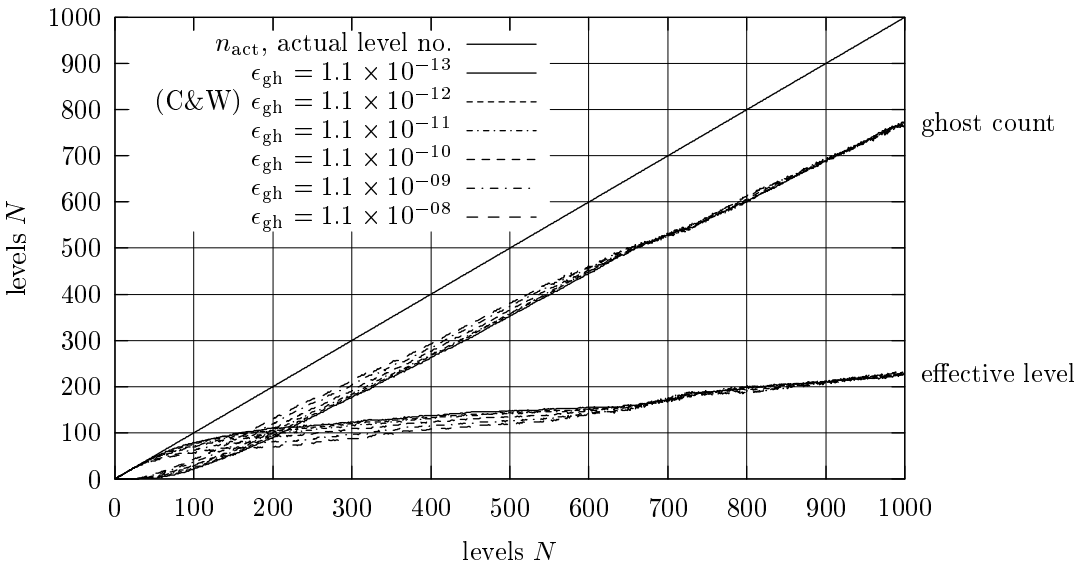


FIGURE 15. Ghost count, $n_{\rm gh}$, and effective level number, $n_{\rm eff}$ for 1D, $W = 4$ at various $\epsilon_{\rm gh}$

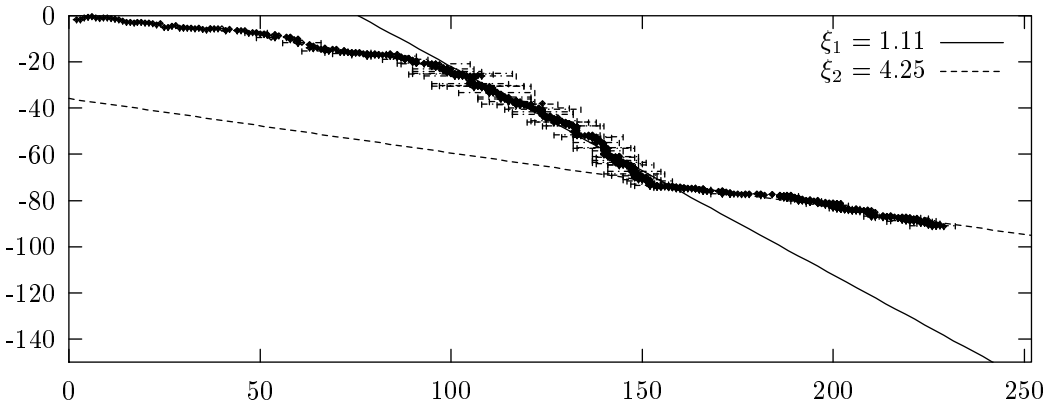


FIGURE 16. $\langle \log t_N \rangle_E$ vs. $N$ in 1D, $W = 4$, $E \in [-0.5, 0.5]$

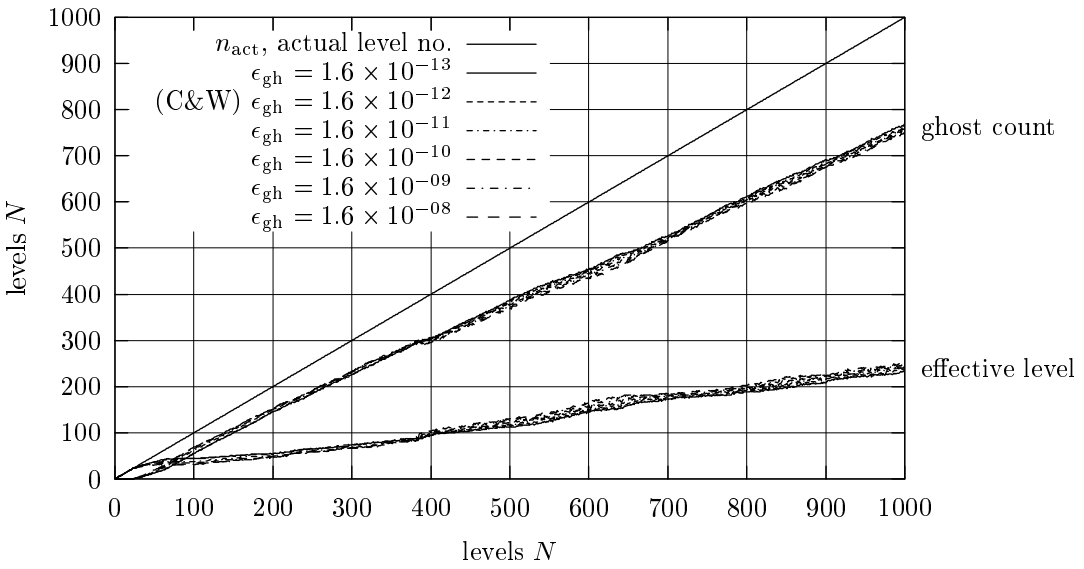


FIGURE 17. Ghost count, $n_{\rm gh}$, and effective level number, $n_{\rm eff}$ for 1D, $W = 8$ at various $\epsilon_{\rm gh}$

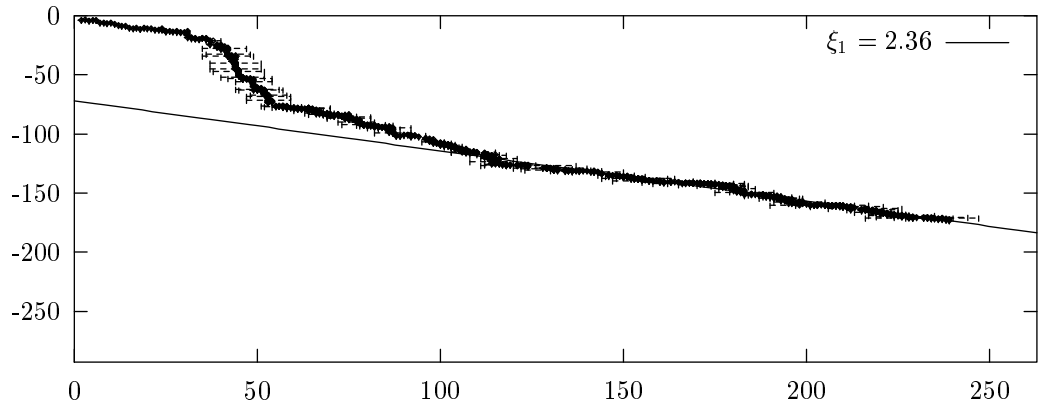


FIGURE 18. $\langle \log t_N \rangle_E$ vs. $N$ in 1D, $W = 8$, $E \in [-0.5, 0.5]$

## 4.5 Transmittance of Disordered 2D System

In 2D, we observe in the ghost counts, Figs. 19, 21, 23, 25, 27, 29, that $n_{\mathrm{gh}}$ crosses $n_{\mathrm{eff}}$ for $W = 16$ at 1000, for $W = 20$ at 500 and for $W = 30$ at 250. In particular at $W = 30$, $n_{\mathrm{eff}}$ becomes practically flat at $\sim 200$. This finds an expression in Figs. 182–212 where the transmittance turns almost vertical with a massive error bar. In all of these plots at $W = 30$, the behavior is clearly exponential with localization lengths ranging from approximately 5–15.

At $W = 20$, localization in the central band region, Figs. 156–178 is recognizably exponential as well with localization lengths in the range 15–30.

The same is true for $W = 16$, now with longer localization lengths 35–70 in Figs. 136–150. The localization length is largest in the band center and drops towards the tails, down to 12–20 in Figs. 134, 135, 151, 152.

At $W = 12$ the situation starts to become less clear-cut. In some cases such as Figs. 123, 124, 127, 129 a clear curvature in the plots with linear abscissa seems to prevail and the power-law fits have powers in the range $-3 \ldots -6$. In the cases where an exponential was fit, Figs. 116–121, 125, 126, 128, $\xi \sim 70 \ldots 130$. In Fig. 24, the band center, we fitted both an exponential law and a power law and the results of either are in line with the other cases at this disorder. It is therefore quite well possible that even at these large system sizes, power-law and exponential behavior may not be numerically discriminated at this disorder.

At disorder $W = 8$, we can again fit to fairly moderate power laws with $\alpha = -1 \ldots -3$, Figs. 100, 102, 103, 105, 106. Alternatively, the exponential fits of Figs. 107, 108 yield $\xi = 251, 171$. The results in cases where both was fit, Figs. 101, 22, were again in line with the other fits. We note that at the mobility edge, Figs.

98, 99, 109, 110 the powers get markedly stronger (-2.9, -4.8) and the localization lengths get shorter $\sim 4$.

Lastly, at $W = 4$, all states in the center seem to follow a power law with small $\alpha$ between $-0.1$ and $-0.9$, Figs. 86–94, while the tail region is strongly localized, Figs. 85, 95.

In summary, our data indicates a smooth cross over from weakly localized to strongly localized. Exponential localization does not seem to appear at low disorders such as $W = 4$. This is not necessarily inconsistent with (MacKinnon and Kramer, 1983) since they found, under the *a priori assumption* of exponential behavior, localization lengths of $10^6$ at $W = 2$ which was many times larger than their system size.

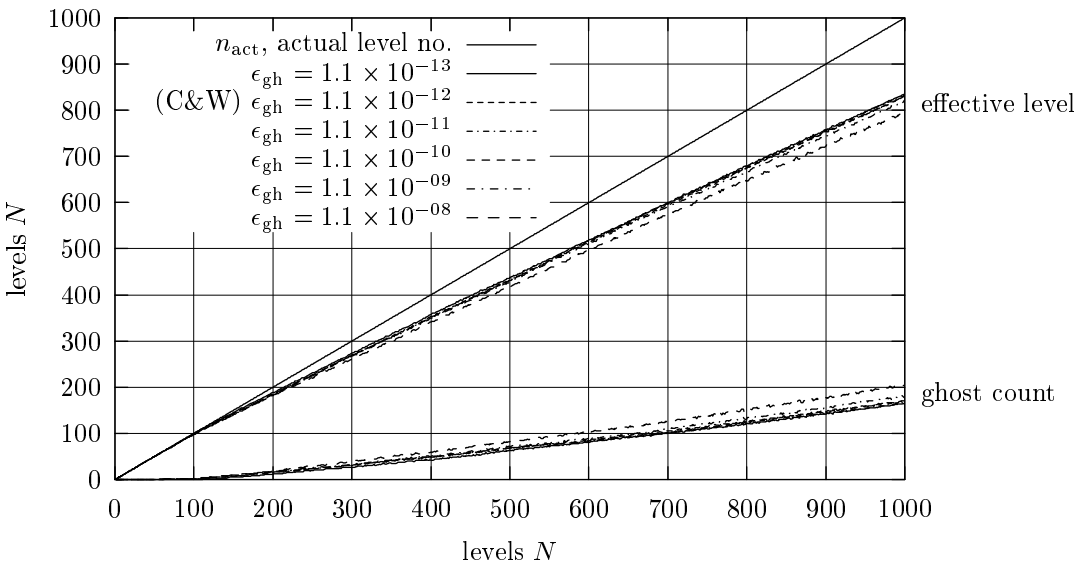


FIGURE 19. Ghost count, $n_{\mathrm{gh}}$, and effective level number, $n_{\mathrm{eff}}$ for 2D, $W = 4$ at various $\epsilon_{\mathrm{gh}}$

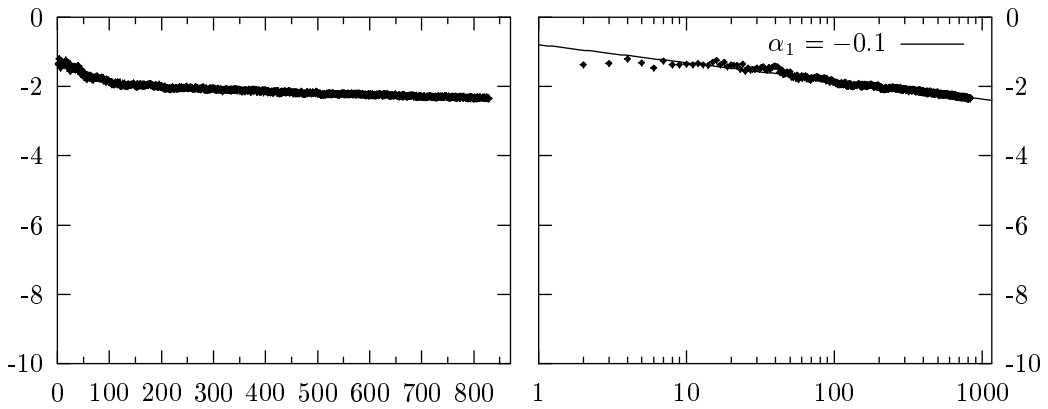


FIGURE 20. $\langle \log t_N \rangle_E$ vs. $N$ in 2D, $W = 4$, $E \in [-0.5, 0.5]$

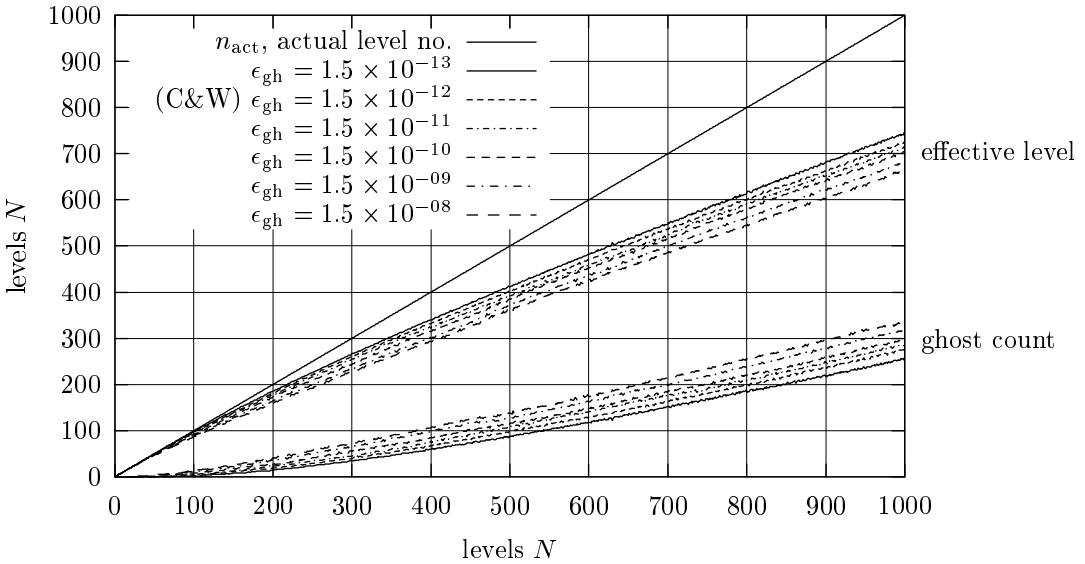


FIGURE 21. Ghost count, $n_{\rm gh}$, and effective level number, $n_{\rm eff}$ for 2D, $W = 8$ at various $\epsilon_{\rm gh}$

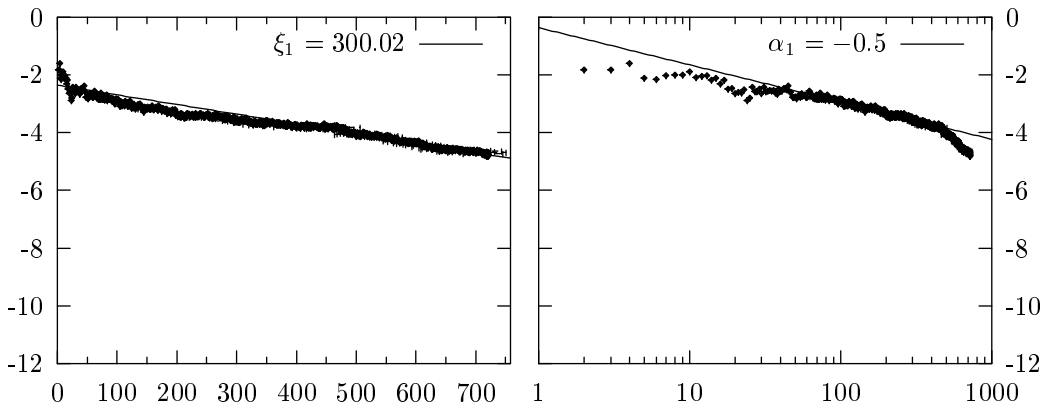


FIGURE 22. $\langle \log t_N \rangle_E$ vs. $N$ in 2D, $W = 8$, $E \in [-0.5, 0.5]$

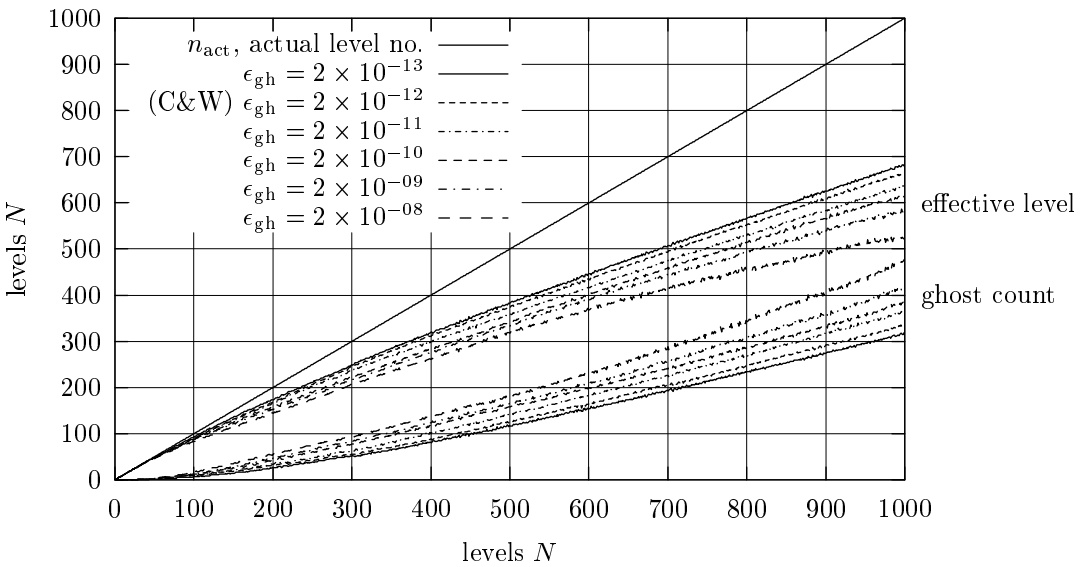


FIGURE 23. Ghost count, $n_{\rm gh}$, and effective level number, $n_{\rm eff}$ for 2D, $W = 12$ at various $\epsilon_{\rm gh}$

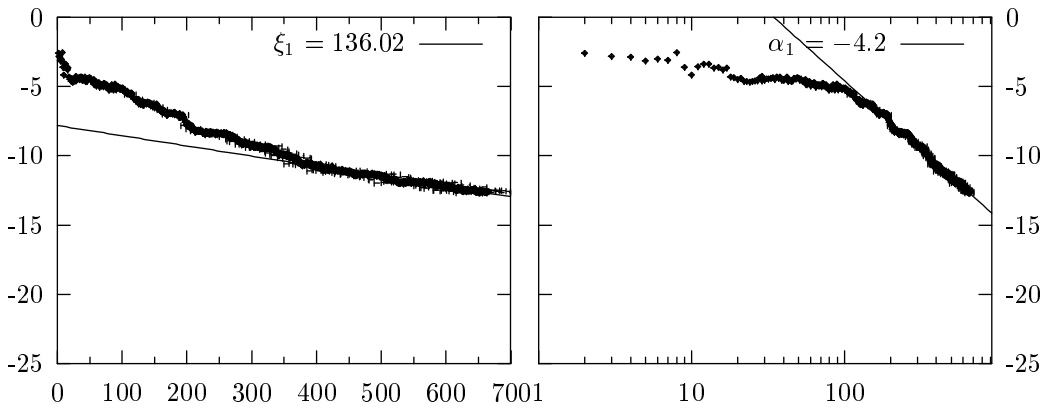


FIGURE 24. $\langle \log t_N \rangle_E$ vs. $N$ in 2D, $W = 12$, $E \in [-0.5, 0.5]$

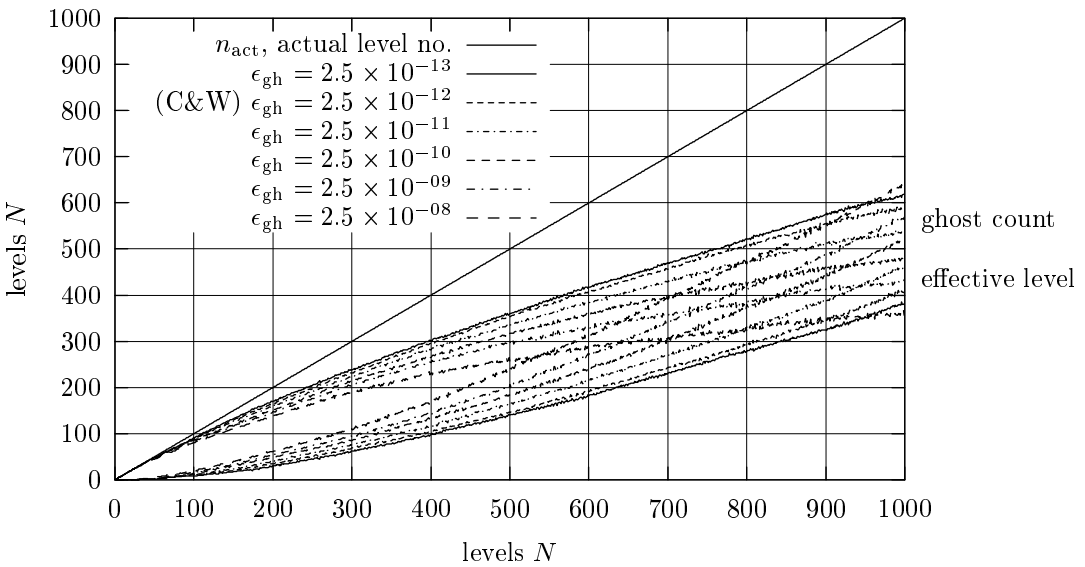


FIGURE 25. Ghost count, $n_{\rm gh}$, and effective level number, $n_{\rm eff}$ for 2D, $W = 16$ at various $\epsilon_{\rm gh}$

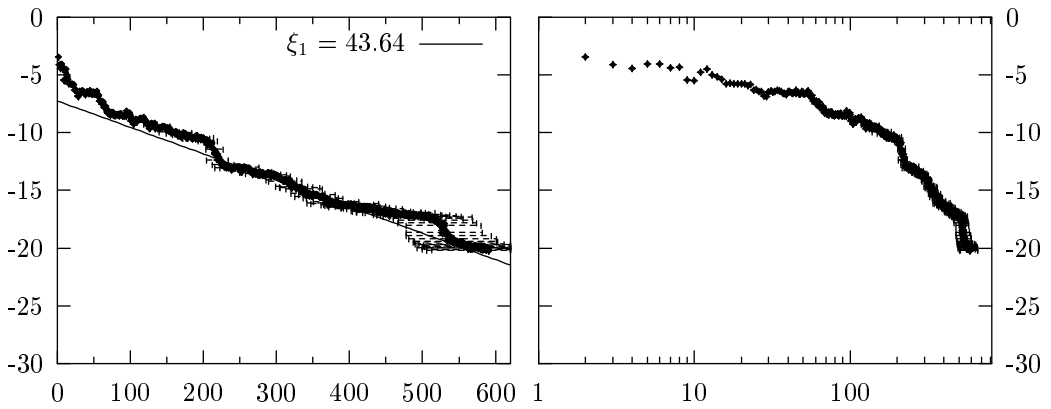


FIGURE 26. $\langle \log t_N \rangle_E$ vs. $N$ in 2D, $W = 16$, $E \in [-0.5, 0.5]$

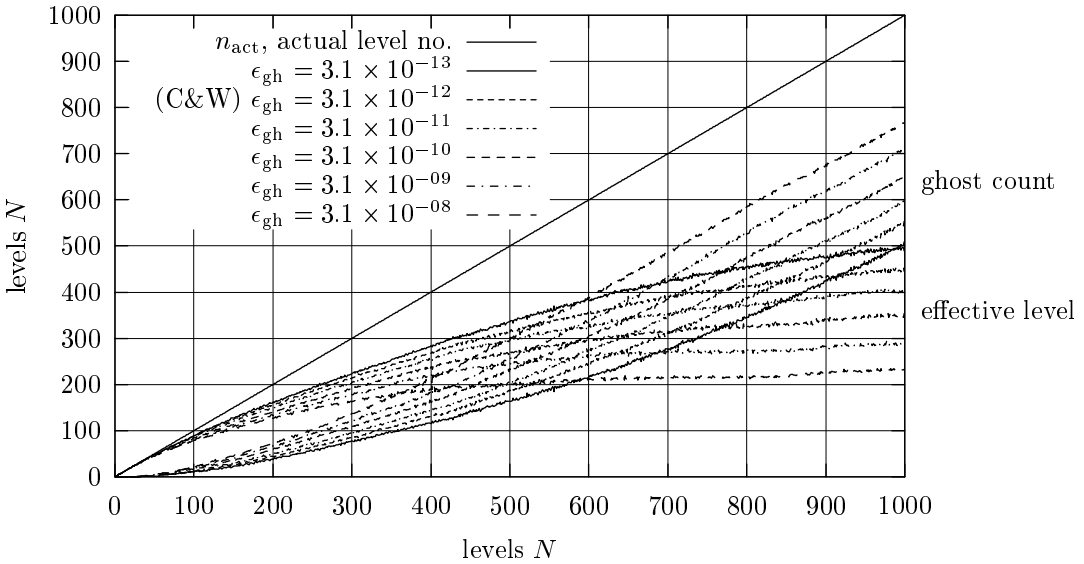


FIGURE 27. Ghost count, $n_{\rm gh}$, and effective level number, $n_{\rm eff}$ for 2D, $W = 20$ at various $\epsilon_{\rm gh}$

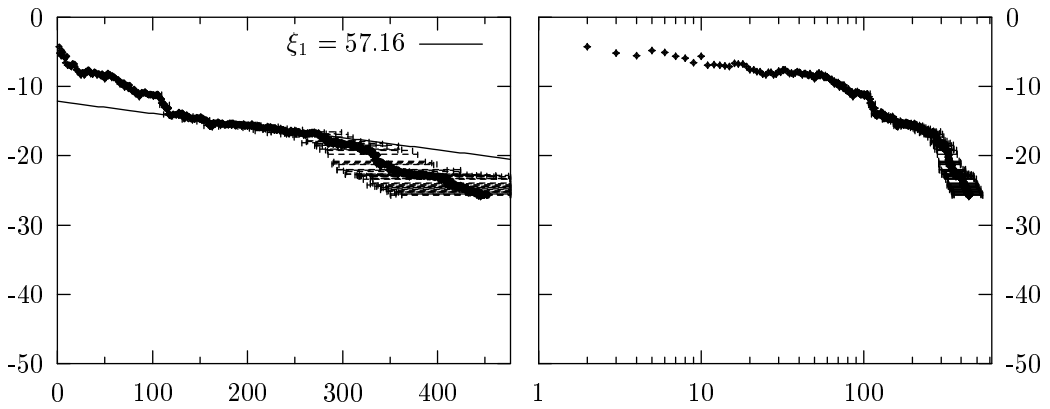


FIGURE 28. $\langle \log t_N \rangle_E$ vs. $N$ in 2D, $W = 20$, $E \in [-0.5, 0.5]$

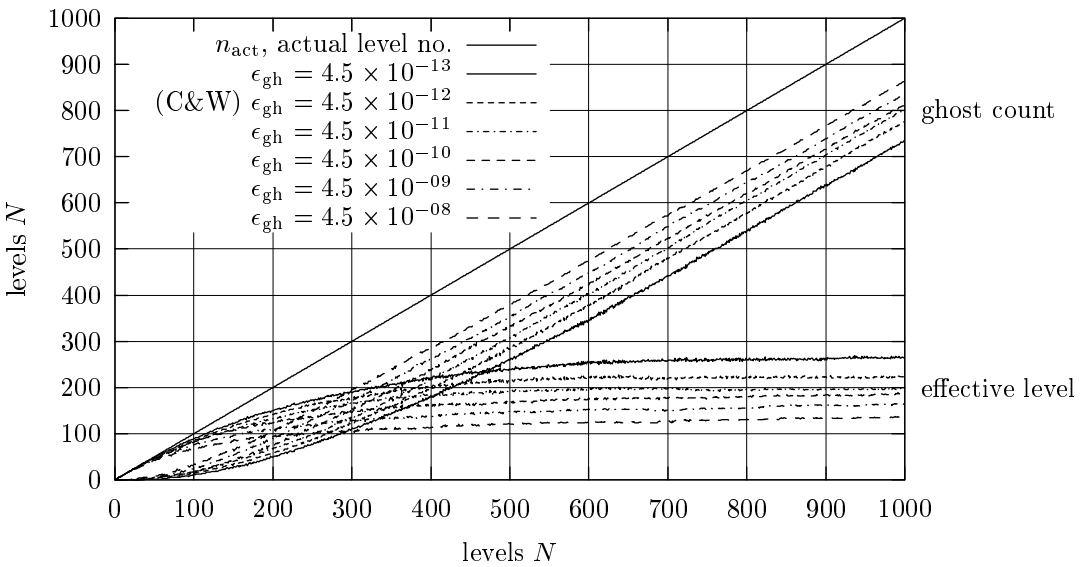


FIGURE 29. Ghost count, $n_{\rm gh}$, and effective level number, $n_{\rm eff}$ for 2D, $W = 30$ at various $\epsilon_{\rm gh}$

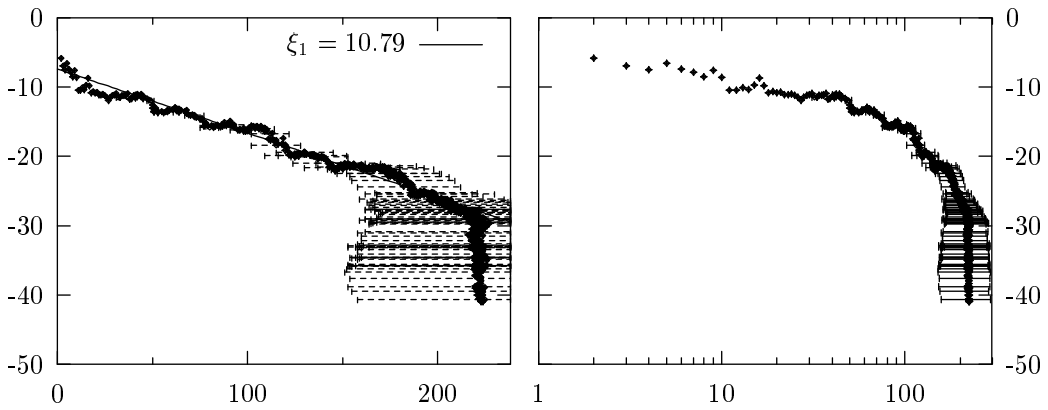


FIGURE 30. $\langle \log t_N \rangle_E$ vs. $N$ in 2D, $W = 30$, $E \in [-0.5, 0.5]$

## 4.6 Transmittance of Disordered 3D System

In 3D the data is in many respects the cleanest. It is the most weakly localized system, and the fluctuations are the lowest which may perhaps be a result of the fact that self-averaging is most well preserved.

Figs. 217–227 display what can without question be taken as extended states. Powers, where fitted, are around 0.1; in Fig. 227 an exponential was fitted with $\xi \approx 10^5$, larger than the system size. At the band tail, Figs. 216, 228 the localization is markedly stronger although it is still not clear if power-law or exponential. Most likely the cross-over between delocalized-to-localized happens part-way through the averaging interval, as the mobility edge is fairly sharp, so that the averaged behavior may not be characteristic in these intervals.

The situation is very similar indeed for $W = 8$ where there is effectively no localization in the center, Figs. 233–245. Approaching the mobility edge, Figs. 232, 246, the power is approximately $-3$.

At $W = 12$, we find powers between $-0.1 \ldots -0.8$, Figs. 251–266 with the exception of Fig. 267, while the tail states are now exponentially localized with

$\xi = 3$, Figs. 250, 268.

For $W = 16$ localization in the band center is becoming stronger and so is the ambiguity regarding its true nature. Power-law fits, Figs. 273–281, 283–291 have very moderate powers of magnitude less than unity. Near the tail region we have a strong power law, Figs. 272, 292 we find a significant but unambiguous power of $\approx -9$.

For $W = 20$ we still find mostly clear evidence for power law behavior, Figs. 297–299, 301, 303–314, 316, 318, 319 at powers in the range $-0.6 \ldots -3$, all in all not much different from $W = 16$. The claims in the literature of a critical disorder at $W = 16.5$ at which the localization is supposed to become exponential does not seem to be supported by our data. The data is, however, consistent with Haydock (1986) who predicts a gradual changeover from delocalized-to-power law-to-exponential. We note furthermore a strong power law in Figs. 296, 320 of $\approx -30$ in the tail region.

Finally, for $W = 24$ the situation is again little changed. We find predominantly power law behavior with marginally larger powers $\alpha = -3.8 \ldots -1$, Figs. 324–326, 328–331, 333–344, 346–349. At the mobility edge, we find distinct power laws around $-60$ in Figs. 323,350.

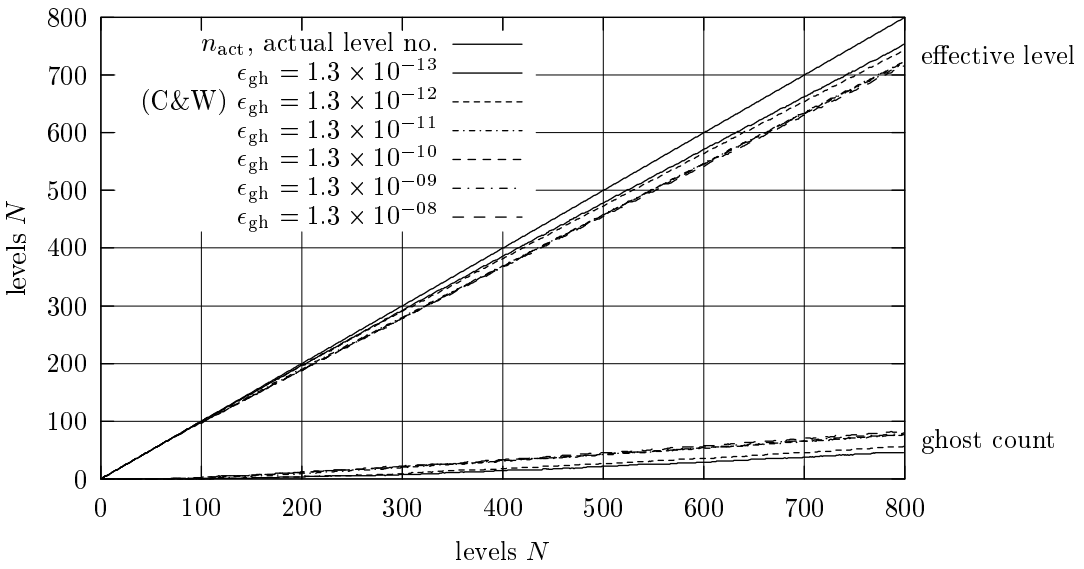


FIGURE 31. Ghost count, $n_{\rm gh}$, and effective level number, $n_{\rm eff}$ for 3D, $W = 4$ at various $\epsilon_{\rm gh}$

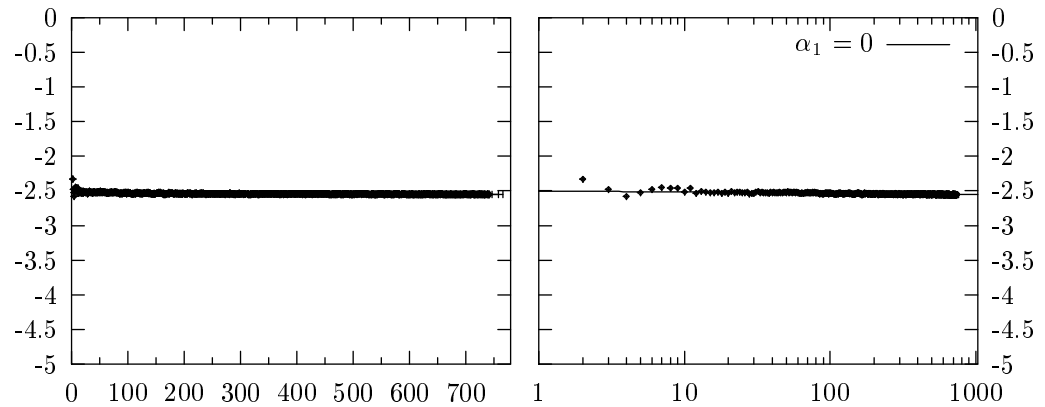


FIGURE 32. $\langle \log t_N \rangle_E$ vs. $N$ in 3D, $W = 4$, $E \in [-0.5, 0.5]$

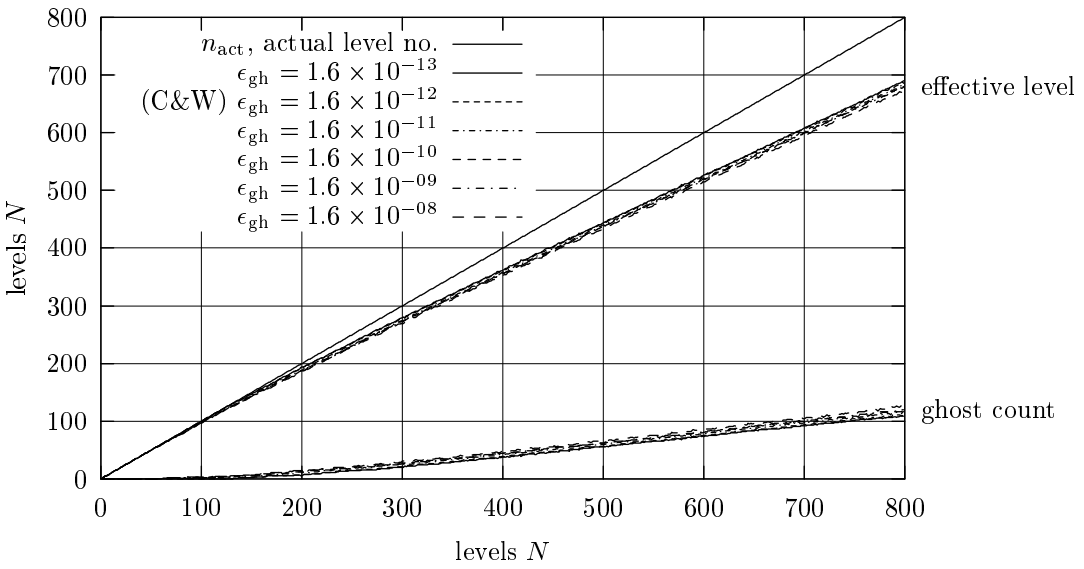


FIGURE 33. Ghost count, $n_{\rm gh}$, and effective level number, $n_{\rm eff}$ for 3D, $W = 8$ at various $\epsilon_{\rm gh}$

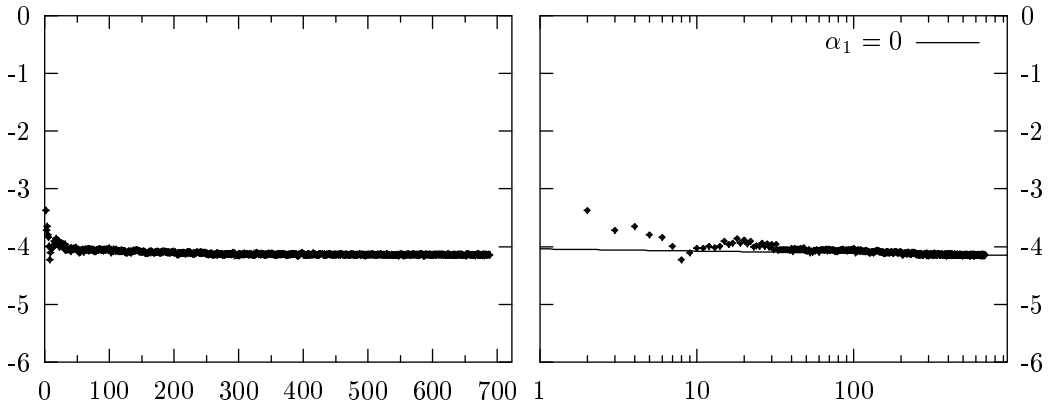


FIGURE 34. $\langle \log t_N \rangle_E$ vs. $N$ in 3D, $W = 8$, $E \in [-0.5, 0.5]$

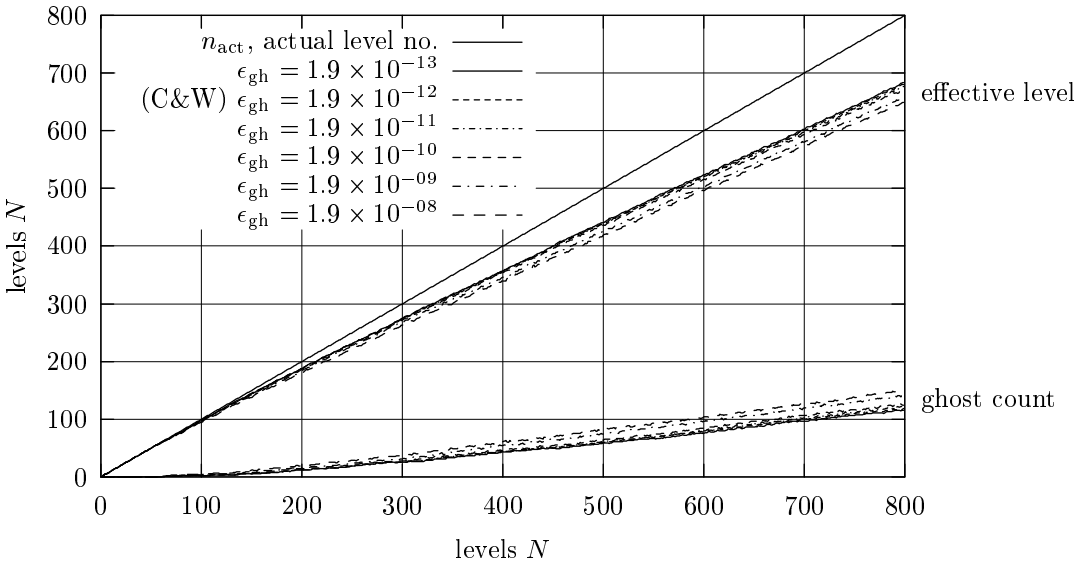


FIGURE 35. Ghost count, $n_{\rm gh}$, and effective level number, $n_{\rm eff}$ for 3D, $W = 12$ at various $\epsilon_{\rm gh}$

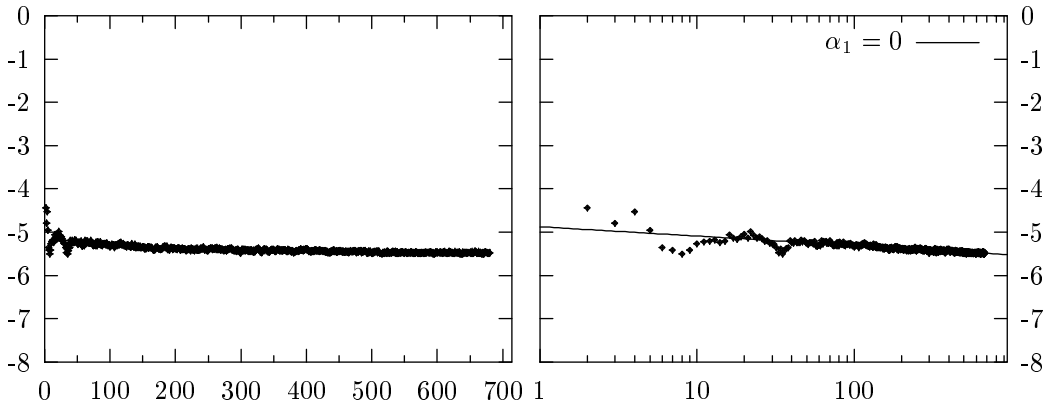


FIGURE 36. $\langle \log t_N \rangle_E$ vs. $N$ in 3D, $W = 12$, $E \in [-0.5, 0.5]$

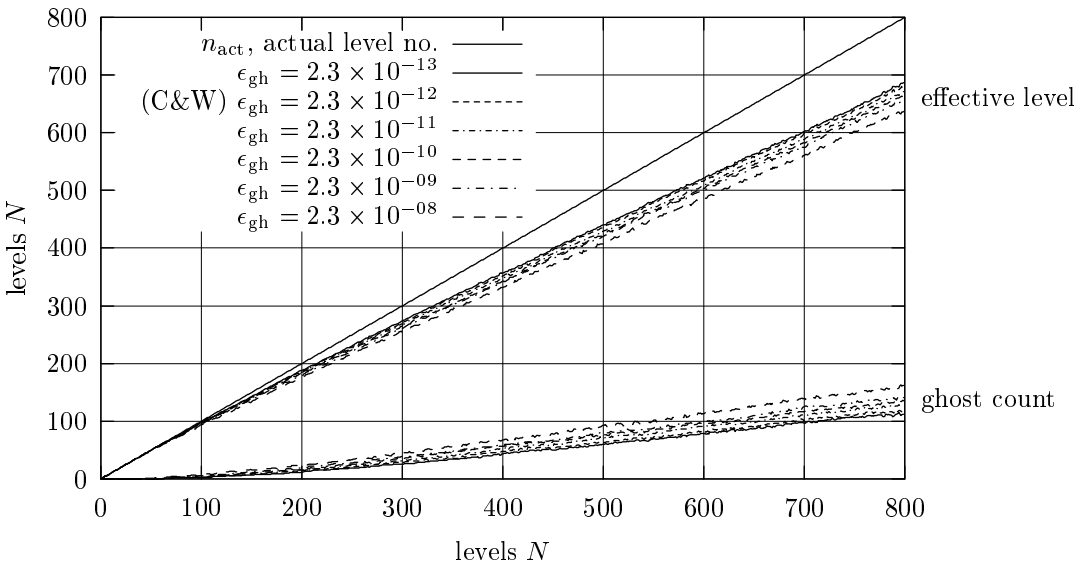


FIGURE 37. Ghost count, $n_{\rm gh}$, and effective level number, $n_{\rm eff}$ for 3D, $W = 16$ at various $\epsilon_{\rm gh}$

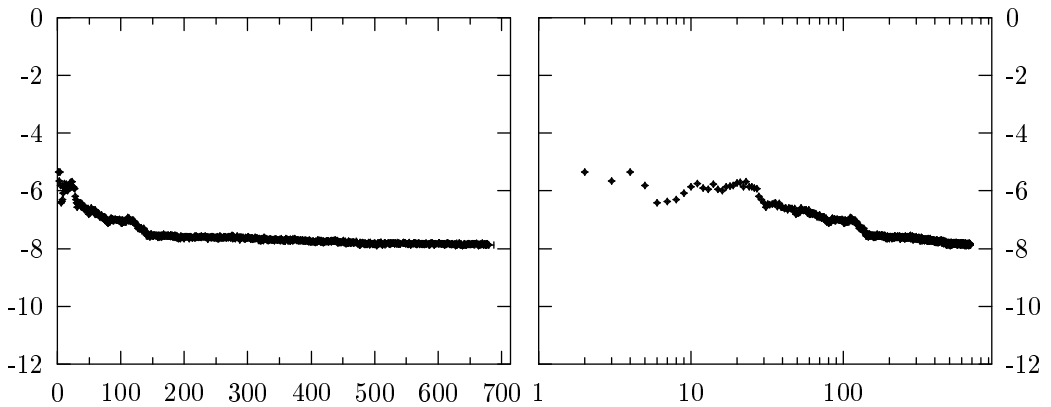


FIGURE 38. $\langle \log t_N \rangle_E$ vs. $N$ in 3D, $W = 16$, $E \in [-0.5, 0.5]$

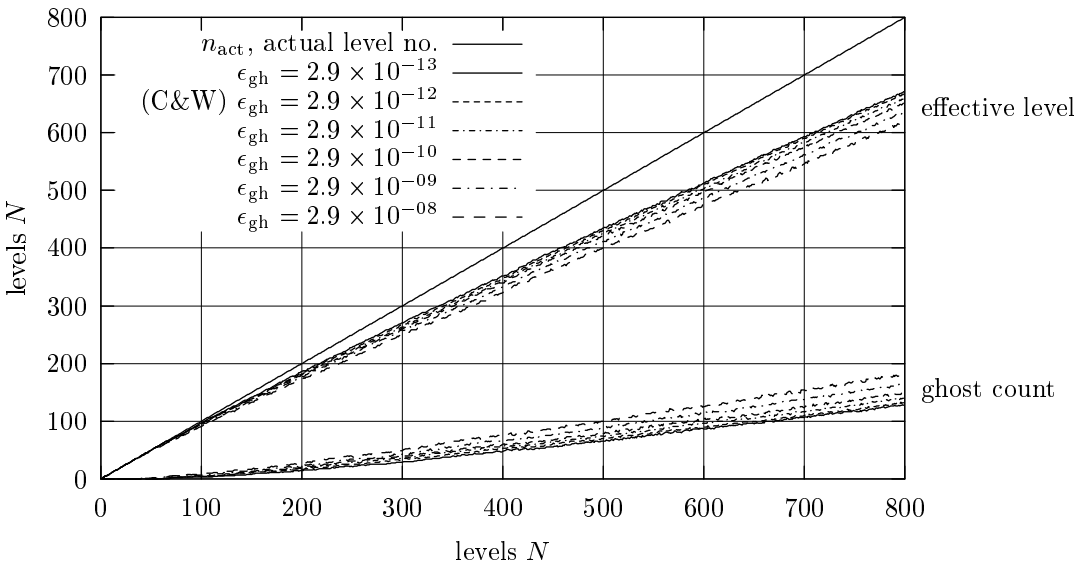


FIGURE 39. Ghost count, $n_{\rm gh}$, and effective level number, $n_{\rm eff}$ for 3D, $W = 20$ at various $\epsilon_{\rm gh}$

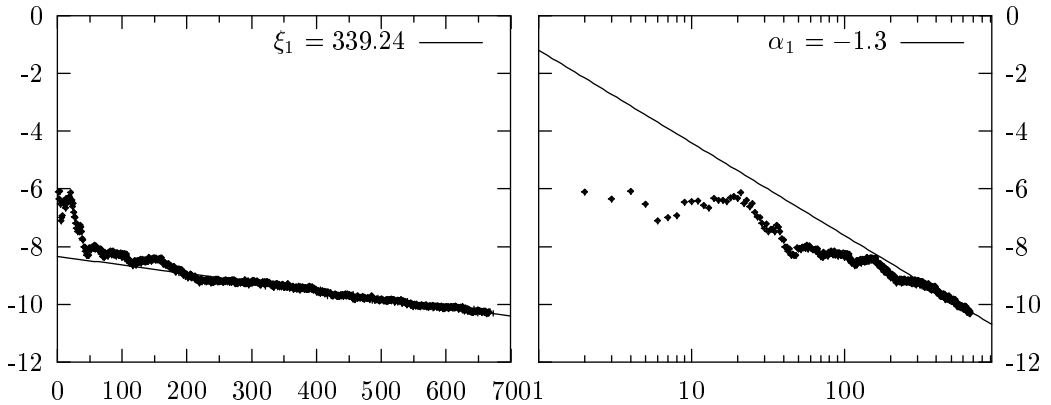


FIGURE 40. $\langle \log t_N \rangle_E$ vs. $N$ in 3D, $W = 20$, $E \in [-0.5, 0.5]$

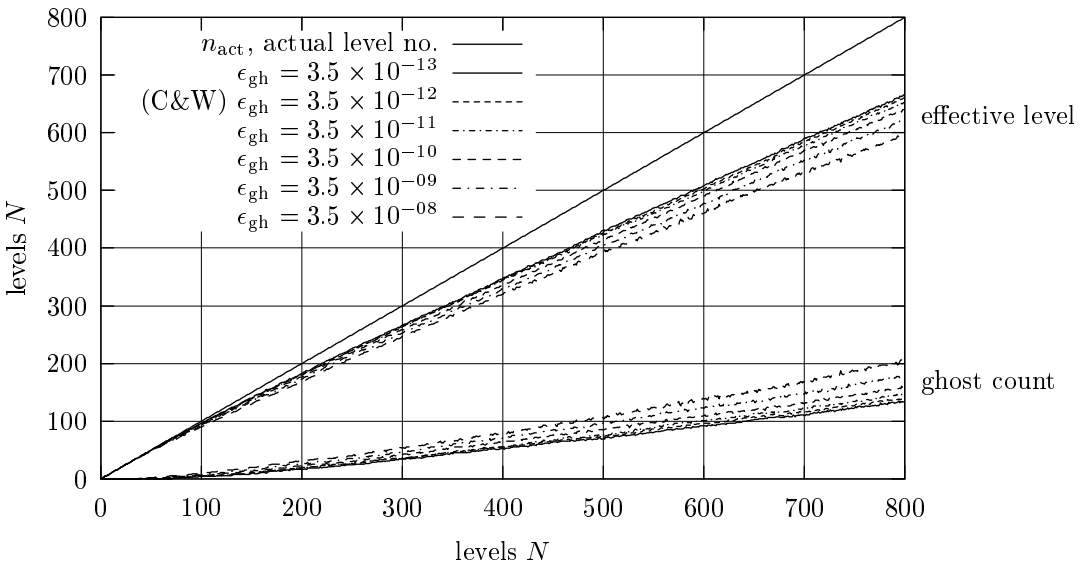


FIGURE 41. Ghost count, $n_{\rm gh}$, and effective level number, $n_{\rm eff}$ for 3D, $W = 24$ at various $\epsilon_{\rm gh}$

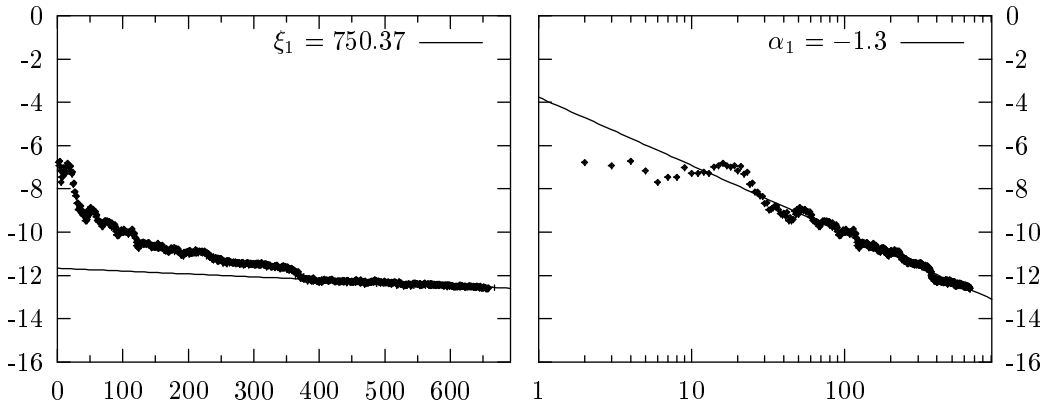


FIGURE 42. $\langle \log t_N \rangle_E$ vs. $N$ in 3D, $W = 24$, $E \in [-0.5, 0.5]$

## 4.7 Mobility Edge Trajectory

We now turn to an analysis of the mobility edges observed in the data for 2D and 3D. We have seen that in all cases, there was a very strong exponential localization at extremal energies, i.e. we can write for the transmittance in the tail region,

$$t_N = t_0 e^{-N/\xi}\,, \tag{4.4}$$

where $t_0$ is the average transmittance in the band center. Given the kinetic energy of an electron near the mobility edge on the localized side, $E - E_c = (\hbar k)^2/2m$, where $E_c$ is the critical energy, and identifying the localization length $\xi$ with the wavenumber $k$ in this extremal regime, we can identify the mobility edge by fitting the exponential part of the transmittance spectrum according to,

$$\left[\log \frac{t_N}{t_0}\right]^2 = \frac{2mN^2}{\hbar^2}(E - E_c)\,. \tag{4.5}$$

This fit was easy and unambiguous in most cases as plots according to this formula displayed a marked kink at $E_c$, with the exception of the one-dimensional case. There, the curve was rounded and no clear determination could be made. We take this as evidence for the absence of a mobility edge in 1D.

The results of these fits together with the Lifshitz edges are shown in Figs. 43, 44 for 2D and 3D, respectively. We note that at all investigated disorders, this mobility edge trajectory keeps moving outward and does not appear to join in the band center, in contrast to Bulka et al. (1987).

Mott (1990) and others have stated that the transition at the mobility edge is due to a drop-off in the density of states and therefore not surprising. We would

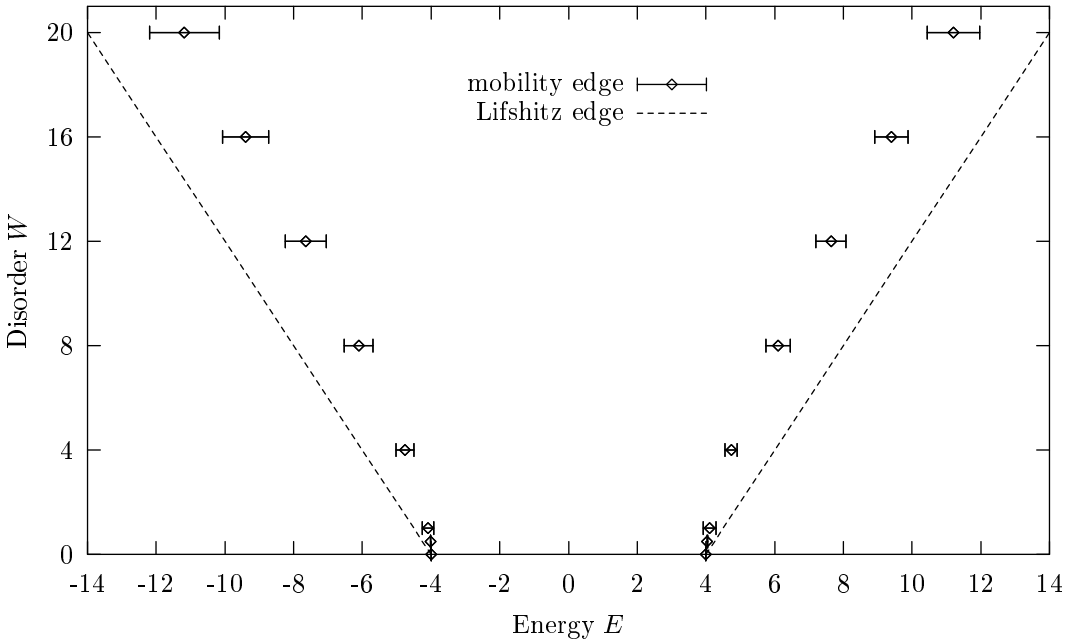


FIGURE 43. Mobility edge trajectory for 2D

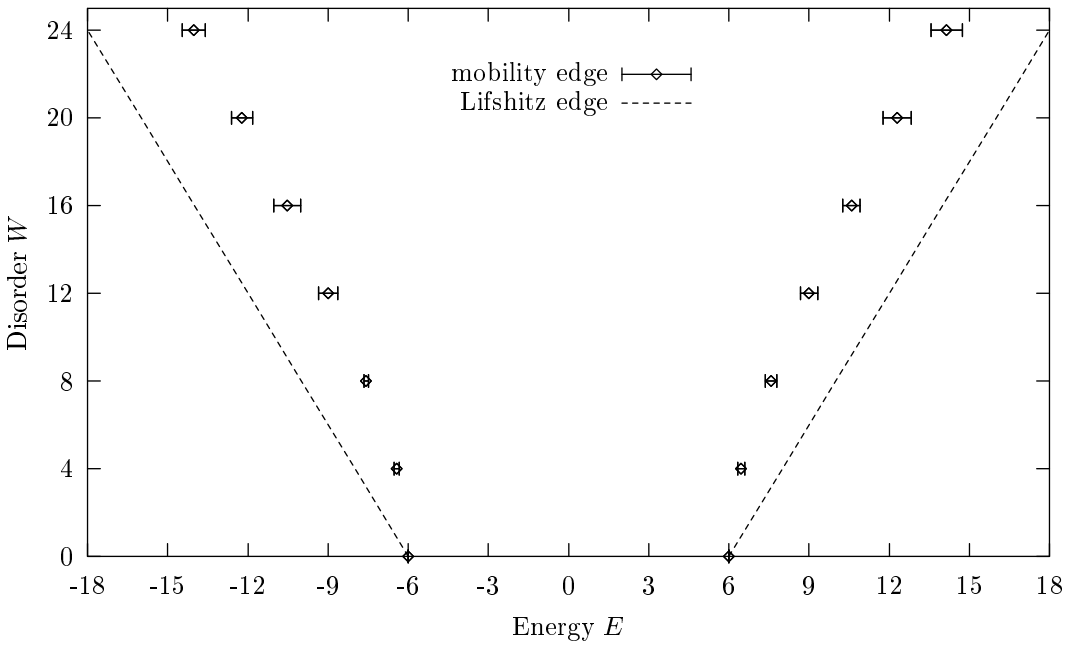


FIGURE 44. Mobility edge trajectory for 3D

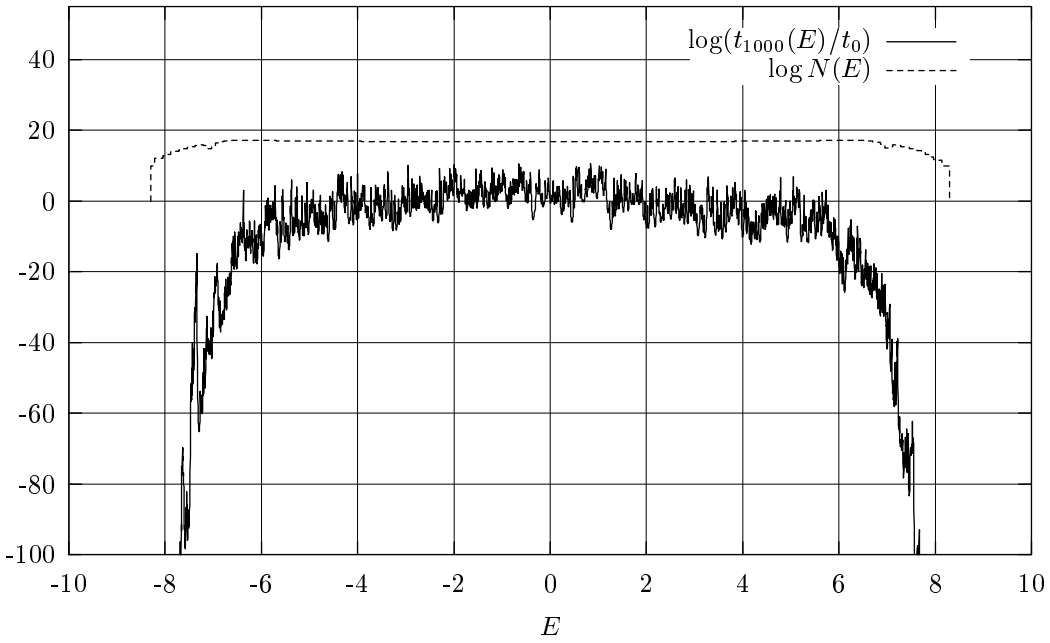


FIGURE 45. Transmittance vs. energy and comparison with global density of states in 2D at $W = 12$

like to refine this statement. In Figs. 45, 46, we have plotted $\log t_N/t_0$ against energy, where we used for $t_N$ the transmittance evaluated at $N = 1000$ levels in 2D and $N = 800$ levels in 3D. Superimposed on the same plot are the global density of states for the same disorder. For the latter we used the eigenvalue histogram obtained from a Lanczos calculation in a bounded box of $262144 = 2^{18}$ lattice sites. Due to CPU time constraints (the diagonalization ran for about a week), we computed the eigenvalues after only 262144 iterations. Therefore the central part of the spectrum is not fully converged which, however, is of no concern here, since we are only interested in the tail region where eigenvalues converge much sooner.

These figures show that the decay in the transmittance cannot be generally attributed to the decline of the global density of states. Rather, it is a result of the decline of the *projected* density of states. The projection is on the lead state

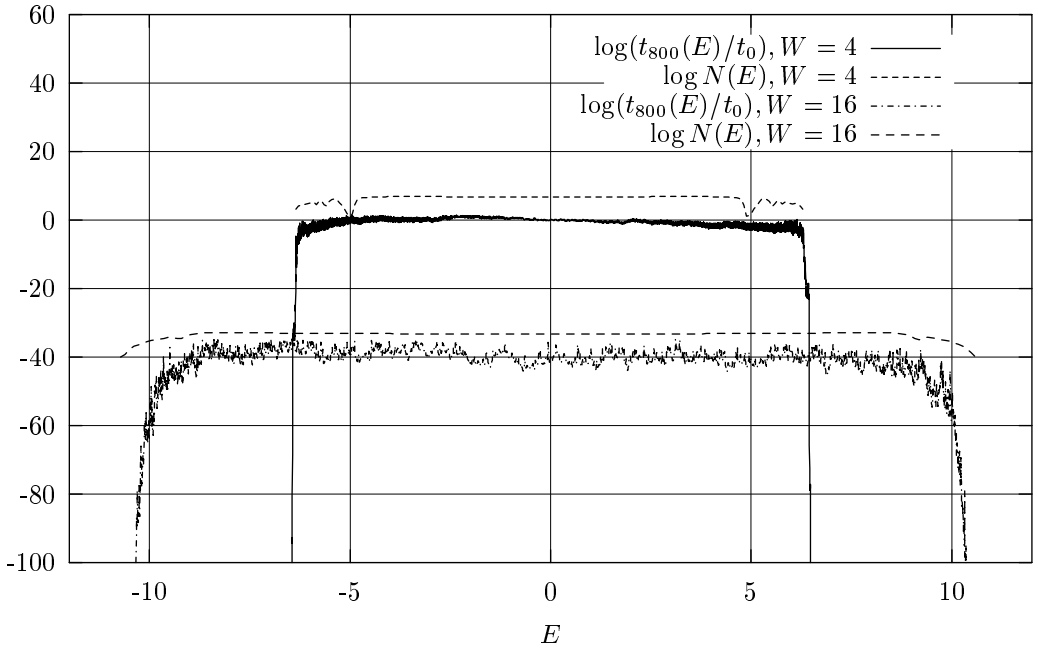


FIGURE 46. Transmittance vs. energy and comparison with global density of states in 3D at $W = 4, 16$

(cf. Sec.3.3) which excludes all states that do not overlap with the lead and would therefore not participate in current transport. These remaining states, however, do add up to a sizeable density of states in the tails, and therefore the global density of states extends beyond the mobility edge we observe. It is interesting to note also that this discrepancy becomes more prominent at higher disorder as Fig. 46 shows. This is a result of the onset of localization which causes fewer states to overlap with the lead state.

## 4.8 A Model for Conductance of a 2D Disordered, Interacting System

We recall the two scenarios depicted in Fig. 5: At zero temperature, inelastic scattering events are rare, although not entirely absent due to residual quantum fluctuations. At higher higher temperature, on the right panel, inelastic scattering

events are more frequent. Since this process is thermally driven we can estimate the probability for an electron to be activated across the energy barrier $U$ as $e^{-U/T}$, where we have set $k_B = 1$. The inverse of that quantity can be understood as the number $n_i$ of hops on the lattice an electron can make before it is scattered inelastically. The asymptotics of this generalized inelastic scattering length are correct: At $T = \infty$, $n_i = 1$, i.e. the electron suffers inelastic scattering at every hop, in the other extreme, at $T = 0$, $n_i = \infty$ there is no inelastic scattering.

If we take $n_i$ as a length along the chain, we can find the dimensionless resistance due to elastic disorder scattering within a chunk of material corresponding to a chain of length $n_i$ by Eq. (2.9), as

$$R_{n_i} \quad = \quad \frac{1}{|t_{n_i,U}|^2} \, . \tag{4.6}$$

The transmittance $t_{n_i,U}$ is calculated in the sense of Sec. 3.5 for a chain model computed from a 2D lattice with the binary disorder distribution of Eq. (2.5). The temperature $T$ thus defines the size of the sample for which the above resistance formula holds, i.e. for which the resistance is purely due to quantum interference. Beyond that size, inelastic scattering events occur and the phase is destroyed. For a sample composed of a juxtaposition of $m$ chunks of size $n_i$, the resistances add to the total of $R = mR_{n_i}$. Utilizing Eq. (4.6), we obtain for the resistance of a sample of size $L$:

$$R \quad = \quad \frac{L}{|t_{n_i,U}|^2 \, n_i} \quad = \quad \frac{Le^{-U/T}}{|t_{n_i,U}|^2} \tag{4.7}$$

Figure 47 shows the result of our calculations of a chain length of 2800, corresponding to a 2D system of $5600^2 \approx 3 \times 10^7$ lattice sites. The transmittance

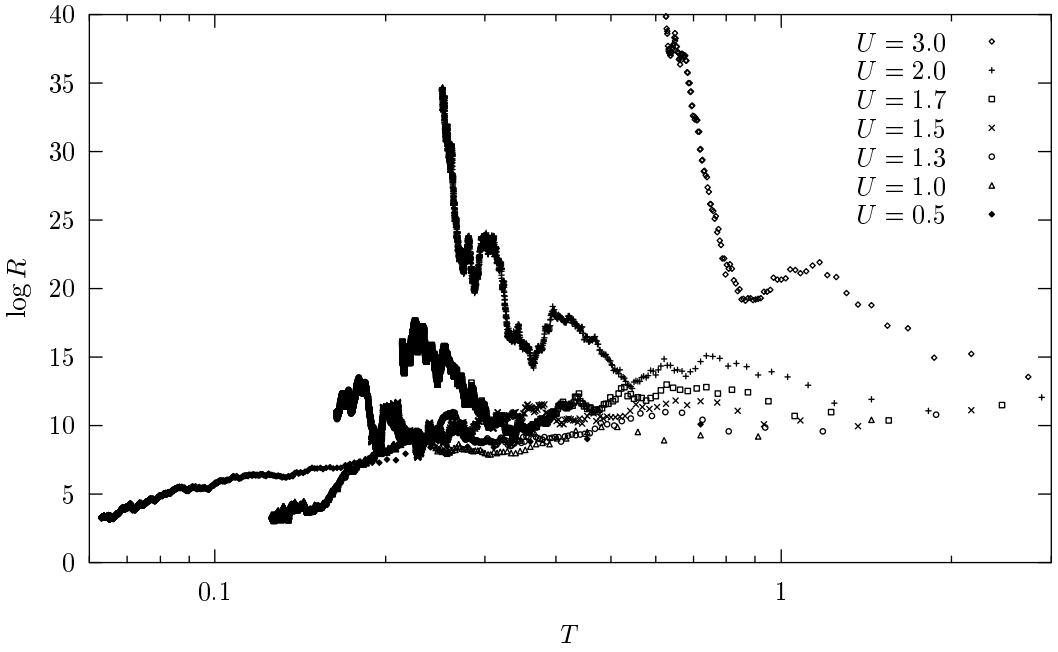


FIGURE 47. Resistance vs. temperature for Hubbard random alloy model in 2D

was log-averaged over a small energy interval of width $2U/L$ around the Fermi level.

We can observe that there is a qualitative distinction between small and large values of $U$ corresponding to weak and strong electron-electron interaction, respectively. In the former case the resistance appears to drop towards lower temperature, in the latter is rises steeply. There is an intermediate regime for values $U = 1.3, 1.5, 1.7$ where fluctuations are large and no clear trend is recognizable. We attribute the qualitative distinction to the interplay of the relevant energy scales, $U$, $k_B T$ and kinetic energy.

At this point it is uncertain if this data would support the phase transition hypothesis. Further study will be needed to refine the model. Our primary aim was to test if our model captures the essential ingredients that are necessary to

obtain an at least qualitative understanding of the processes that led to the two different regimes in the experimental data by Kravchenko et al. (1995); Simmons et al. (1998b).

We have used the Hubbard model and the random-alloy analogy in conjunction with a simple model for the temperature-dependence of the inelastic scattering length as a minimalistic approach to a theory including the key ingredients of some form of electron-electron interaction and disorder. We believe there is a qualitative correspondence between our results and the experimental data. The real situation may still be more complicated than our model is capable of capturing and quantitative agreement is still distant. In particular the question as to whether or not a true quantum phase transition occurs, we are unable to answer conclusively at this stage. The data seem to indicate that this is not the case, and this is in line with other recent work, e.g. (Altshuler et al., 2000). The debate over this system has been controversial and interesting developments in the future are to be expected.

# CHAPTER V

# THE PARALLEL RECURSION PROJECT

## 5.1 Introduction

In this dissertation, we have used the recursion method to simulate very large systems of $4 \times 10^9$ lattice sites that are beyond the reach of more traditional methods. The recursion method has been deployed successfully in a variety of applications and holds great potential for systems of huge state space, systems that lack symmetry and others that can benefit from its inherent projection feature that reduces an overwhelmingly large combinatorial explosion to a manageable information density.

To facilitate future lattice-based applications of the recursion method and to perpetuate the software design and development conducted for the purpose of this dissertation, the author has designated these efforts to the Parallel Recursion Project (PARP) in the hope that others may benefit and development can continue.

The recursion method falls in the group of techniques that exploit the concept of physical locality which is a prerequisite for algorithms whose complexity scales as $O(N)$ (Ordejón, 1998).

In this chapter we present the basic ideas behind the implementation of PARP and report data on its parallel performance scaling. A previous version has been described (Arnold and Haydock, 1998).

## 5.2 Design

We recall the three-term recurrence Eq. (3.5),

$$b_{n+1}\mathbf{u}_{n+1} = (H - a_n)\mathbf{u}_n - b_n\mathbf{u}_{n-1}\,. \tag{5.1}$$

The most time consuming step in this equation is the matrix-vector multiplication $H\mathbf{u}_n$.

While the Cambridge Recursion Library by Nex (1984) supplies an excellent package of supporting routines that are needed for typical recursion method-based studies, such as routines for diagonalization or Gaussian quadrature integration, the task of devising an efficient storage scheme and implementation of the matrix vector multiply was left to the user.

At least for lattice-based systems, PARP is an attempt at alleviating this drudgery. The design of PARP was approached from an abstract and modular level afforded by the object-oriented facilities of C++ (Stroustrup, 1997). We have implemented a general matrix-vector multiply with associated storage mechanisms in generic dimension for simple cubic lattice symmetry. Other Bravais lattices such as face-centered cubic or body-centered cubic could easily be added.

One of the main challenges was storage management of the vector $\mathbf{u}_n$ which is highly sparse. For the purposes of this dissertation, only the diagonal matrix elements need to be stored. The non-zero off-diagonal elements are constant and their location in the matrix is encoded in the way the vector elements are stored.

This last point deserves further discussion: Assuming some arbitrary but fixed enumeration scheme for lattice sites, the matrix is a representation of the

lattice. Links to neighbors are mapped to off-diagonal matrix elements; the value associated with a site itself is mapped to a diagonal matrix element. In the language of graph theory, the matrix represents a connectivity matrix whose associated graph is given by the lattice. The diagonal elements in the matrix are the nodes of the graph and the off-diagonal elements are the edges interlinking the nodes, cf. also Fig. 6.

The remaining problem then is one of enumeration. A $d$-dimensional graph must be mapped to a semi-infinite set of discrete numbers—the computer memory locations—in such a way that the retrieval of neighbors to a node is optimized, since this is the critical operation in the matrix-vector multiplication. We recall that to compute an element of the result vector, $v^i$,[1] we must sum over all elements of $\mathbf{u}_n$ and multiply with the associated matrix-elements,

$$v^i = \sum_j H_{ij} u^j \,. \tag{5.2}$$

Since $H$ is highly sparse, only very few off-diagonal elements $H_{ij}$ are non-zero, namely precisely those that represent links to nearest neighbors. Hence, efficiency in the neighbor-lookup and storage procedure is critical.

From a performance standpoint, data that is needed at the same time should be stored as closely together as possible. In other words, if the locality of the physical problem, where the neighbors to each node are just one hop away, can be approximately preserved in the mapping to memory, execution speed will be optimal.

---

[1]For the purpose of this discussion we have dropped the recursion index $n$ and denote references to elements by a superscript.

As the steep rise in CPU speeds has outpaced the speed of dynamic random access memory chips, hardware designs have introduced a memory hierarchy with cascading layers of access speed and size: First and second-level cache, main memory, possibly remote memory at different processing elements, and virtual memory on disk. Efficient navigation of this memory hierarchy is no trivial task for data-intensive applications, but critical for optimal performance.

In the PARP, we have solved this problem in generic dimensions by organizing access to the components of $\mathbf{u}_n$ through a tree structure. At its lowest level, the tree indexes subunits of the lattice, "clusters," which hold the vector elements and diagonal matrix elements and are stored as unit. Their size is chosen to fit well within the machine's cache memory. The matrix-vector multiply then proceeds in units of these clusters where the interior nodes of a cluster are traversed first, because all of their neighbors will reside inside the same cluster. The exterior nodes will require lookup of nodes in neighboring clusters. The tree hierarchy assists in finding such neighbors quickly, namely in $O(\log n_{\mathrm{cl}})$ operations where $n_{\mathrm{cl}}$ is the total number of clusters.

If PARP is used for a recursion calculation, the vector $\mathbf{u}_0$ typically has only one non-zero component. After the first matrix-vector multiplication, its neighbors will also acquire non-zero components, then their neighbors, and so on. Successive vectors have their biggest elements located on roughly concentric shells around the starting site, cf. Fig. 7. As the vector grows, the lattice expands and more cluster units have to be allocated and new branches may have to be added to the tree.

Figure 48 depicts the arrangement of the data structure and the indexing of the graph by the tree.

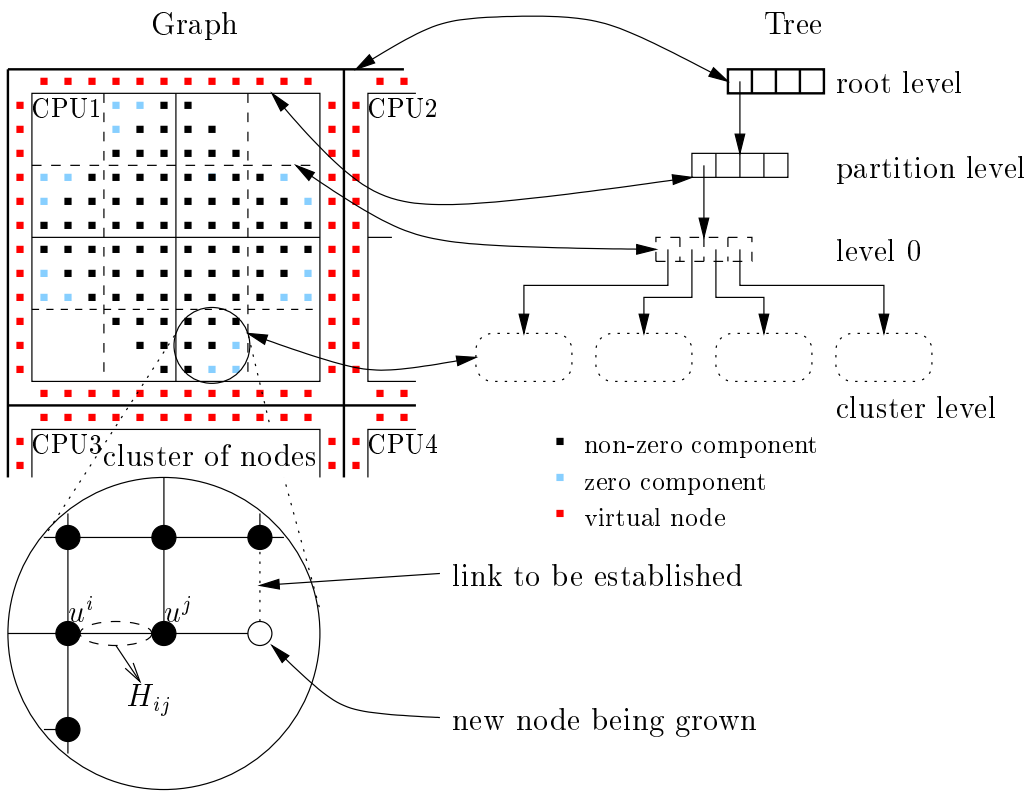


FIGURE 48. Index tree structure and parallel data partitioning concepts

The tree arrangement also makes it easy to distribute work across multiple processors. Subbranches of the tree can be split off at a certain level, called the *partition* or *concurrent branch* level in PARP, and assigned to different processors.

PARP uses POSIX threads (Kleiman et al., 1996; Cortesi et al., 1999, Chapters 10, 13) for concurrent processing. The operating system will schedule multiple threads across multiple CPUs if available, and the execution can proceed in parallel. The thread model of PARP uses a master thread to coordinate a number of worker threads. Each worker thread has a task queue on which the master thread will deposit pointers to "concurrent" subbranches of the tree as they are allocated. During the work cycle, each thread will then compute the matrix-vector multiply

on its list of concurrent subbranches, return the accumulated results for the coefficients $a_n$ and $b_n$ to the master thread and then wait for the next cycle. The fact that each worker thread "owns" its data ensures that the memory affinity remains high and little swapping of cached data is necessary.

Looking up neighbors across the partition boundary would theoretically involve reading from another thread's data while that thread may be writing to it. This is called a race condition and is considered an error because data integrity may be lost. Therefore, facilities must be provided that make threads block each other using mutual exclusion locks on shared data. If the shared data is accessed many times by multiple threads, locking may provoke a lot of thread contention and have a negative effect on performance. In PARP, therefore, we use a layer of "virtual" nodes around each partition block that contains a copy of the respective neighbors' data. In an updating phase after the multiplication has finished, each thread updates its virtual nodes by *reading* from the neighbors' data. This avoids all data races and thus the need for exclusion locks.

The idea to let each worker own a private list of jobs (partition pointers) was a radical redesign over the former version described in Arnold and Haydock (1998). The effects were rewarding in that the parallel speedup is now linear up to the maximum number of 128 processors PARP was tested on. Performance charts are shown in the next section.

The bottleneck in the earlier version was clearly excessive cache invalidation as partitions were assigned to different threads at each iteration. In addition, no virtual nodes were used and therefore each single cross-partition neighbor lookup required locking. Although there was little contention, the overhead of acquir-

ing and releasing the locks became significant due to the high frequency of lock invocation which was on the order of $10^9$ for a 3D recursion problem of 100 levels.

A tool that proved invaluable for the performance analysis and to discover and quantify the details of the bottlenecks mentioned in the preceding paragraph, were the "Tuning and Analysis Utilities" (TAU) developed by Shende et al. (1998); Shende (1999); Malony and Shende (2000).[2] TAU supplies a number of source code macros that will time sections of source code, count events or trace function invocations. A graphical user interface is provided to display and analyze the gathered performance data in many different ways. The per-thread and per-function charts are particularly useful. TAU also handily copes with the complicated data structure names of C++ template code. In summary, it is an understatement to say that the present performance of PARP would not have been conceivable without the in-depth performance analysis made available by TAU.

## 5.3 Performance Results

In order to achieve peak performance on NUMA (non-uniform memory access) machines, such as the Silicon Graphics Origin 2000 (Heinrich, 1997, 1996; Cortesi and Fier, 1998; Cortesi et al., 1999, Part I), that have increased latency for retrieval of data from remote memory, it is critical to utilize a memory allocator that will allocate memory locally to each processor. Surprisingly this is not usually the default behavior. Even on multi-processor machines with uniform memory access, there may still be a benefit due to the avoidance of memory fragmentation and better cache reuse on a per-processor basis.

[2]Source code available at: http://www.cs.uoregon.edu/research/paracomp/tau/

Since PARP allocates all of its data using `vector` and `deque` container classes of the standard C++ library (ISO/IEC/ANSI, 1998), the default allocator for these classes must be overridden by a thread-aware allocator that will reserve memory local to each thread. In the SGI implementation of the standard C++ library, an allocator class `pthread_alloc` is available that does just that.

For more general use, it may be better to override the system default at the `malloc()` level through which all allocation requests are routed. The Hoard library[3] is a drop-in replacement for `malloc()` and deploys its magic transparently to the user. The threaded version of the Linux run-time library `glibc6` also already contains thread-specific allocation mechanisms. For our tests on the Origin 2000, we have employed the `pthread_alloc` allocator supplied by SGI which gave satisfactory performance.

Figures 49, 50 show the performance results for three-dimensional recursion calculations in terms of wallclock run time versus number of processors $n_p$ in a double-logarithmic plot. Lines drawn between data points serve as a guide to the eye only. In Fig. 50, a $1/n_p$ dependence is also shown for comparison. We can see that in all cases the slopes are constant, proving that we did indeed achieve linear speedup which by Amdahl's law (Amdahl, 1988) is the maximal possible value. It also means that the sections of sequential code in between parallel sections are negligible. Thereby we have achieved our design objectives.

The slight disturbances at the bottom of Fig. 49 are due to processes of other users that were run at the same time, reducing the number of physical CPU's effectively available to the PARP job.

---

[3]Berger (2000)

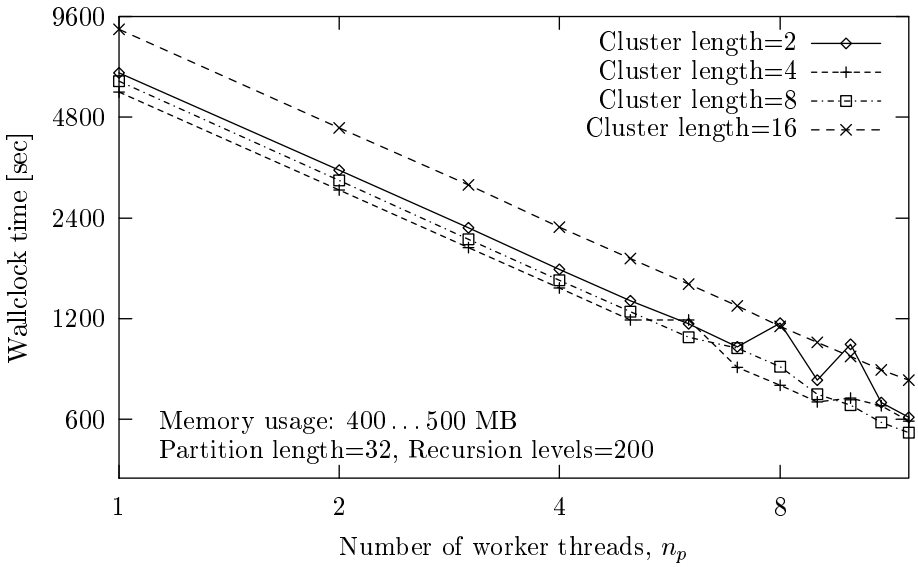


FIGURE 49. Performance test on 12-node SGI Power Challenge with 75Mhz R8000 CPUs, "Aeros" at UO Computational Science Institute

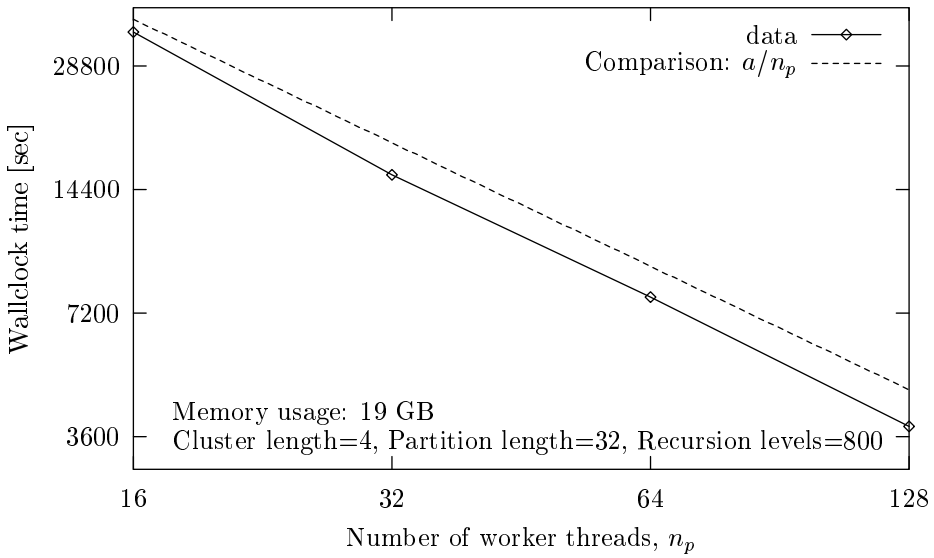


FIGURE 50. Performance test on 128-node SGI Origin 2000 with 250Mhz R10000 CPUs, "Nirvana" at Los Alamos National Laboratory

The first data point at 16 processing elements in Fig. 50 is not representative, because the total allocation of 19 GB of memory was larger than the total memory available at the 16 processing elements (256 MB each) combined. As a result, the operating system allocated some memory at other processing elements that did not participate in the PARP job. Due to the non-uniform memory access architecture, however, there is an increased latency for access to this memory so that the job was proportionally slower than the other tests run at higher number of processors. The maximally achievable speedup is still linear.

The author gratefully acknowledges the use of the Nirvana cluster and the kind support by the staff at the Advanced Computing Laboratory at the Los Alamos National Laboratory where the 128-node tests were carried out.

# CHAPTER VI

## DISCUSSION AND CONCLUSION

We summarize the results presented in Chapter IV for the Anderson model:

1. In 1D, all states are exponentially localized at all disorder strengths. Although we do observe that the localization depends more strongly on the energy as we move into the band tails, we could not fit a mobility edge with the method described in Sec. 4.7, because there was no distinct kink in the transmittance vs. energy plot. We must therefore conclude that our data does not support the existence of a mobility edge in 1D.

2. In 2D, we observe that in the band center states are weakly power law-localized at low disorder and obey a clear exponential law at higher disorder $W \geq 16$. In the band tails, the localization is exponential with an energy-dependent localization length. In the central band region, the localization sets in as weak power law at the lowest disorder $W = 4$ and turns into exponential localization around $W = 12$. A mobility edge was fitted and we do not observe that it curves inward at hight disorder. Comparing the mobility edge at select disorders to the total density of states, we find that the mobility edge occurs before the (global) density of states drops off sharply. We conclude that the localization of the states qualitatively differs between the band center and the band edge and that a mobility edge exists.

3. In 3D, we observe that at low disorders $W = 4, 8$ the states are delocalized in the band center. At disorders above that states become gradually more

localized but remain more power law-like than exponential throughout the range of investigated disorders up to $W = 24$. In the band tails, we find energy-dependent exponential localization which allowed us to fit a mobility edge trajectory. Just as in 2D, is does not appear to curve inwards at high disorder. Our observations do not seem to support an abrupt change in the character of the localization in the band center as would be expected if a phase boundary were present.

The findings of a mobility edge in 2D are in line with the predictions by Haydock (1986) and numerical results by Godin (1988); Godin and Haydock (1992).

Our results in 2D and 3D seem to be at odds with numerous other numerical and theoretical studies which assert the existence of a mobility edge in the band center in 3D and exponential localization throughout in 2D (Abrahams et al., 1979; MacKinnon and Kramer, 1983; Zdetsis et al., 1985; Bulka et al., 1987; Kramer et al., 1990; Belitz and Kirkpatrick, 1994; Zharekeshev and Kramer, 1997; Janssen, 1998). Can this discrepancy be reconciled? Our data does not exclude that a phase boundary may exist in the band center in 3D. Our data seems to indicate, however, that it must lie at disorders much higher than those considered. In 2D, on the other hand, the data points to a power-law-to-exponential transition that would be in conflict with one-parameter scaling. As to the numerical studies carried out to date, in particular those deriving a closed mobility edge trajectory, we would like to point out that these findings were obtained with relatively tiny systems compared to those studied in the present work (Bulka et al., 1987). Kramer et al. (1990) mention that the error bar for the scaling parameter is large and unknown with the transfer matrix method. The studies done with the Lanczos method (Zharekeshev

and Kramer, 1997, 1999) do not discuss the issue of ghosting that emerged as an important aspect of localization studies with the Lanczos or recursion methods. Furthermore most studies in the literature were of a statistical nature which can be influenced in systematic ways by machine rounding errors. Unfortunately, most authors do not discuss this potential source of systematic errors. We propose to repeat those calculations with different arithmetic precisions.

In addition, numerical studies employing the transfer matrix method or the Lanczos method with box boundary conditions are limited to very few sample sizes, because the computations have to be restarted from scratch for each size. The scaling or statistical analysis therefore rests upon a dearth of data points in this respect. As a result of the special nature of boundary conditions in recursion calculations, the techniques used in this dissertation supply data points for all sizes of the lattice sample between 2 and 1000 in linear dimension.

Our evidence supports that power-law localization is likely both in 2D and 3D. Wavefunctions with power-law decay of the envelope are mathematically troublesome as their normalization is infinite and there is no length scale associated with them. We suggest that the critical disorder observed in previous transfer matrix and level statistics calculations may be extrapolations, based on an assumption of exponential behavior.

Furthermore, in the transfer matrix calculations, an exponential behavior is always assumed, but at low disorders, MacKinnon and Kramer (1983) find localization lengths that are orders of magnitude larger than the largest system size considered. It would appear that this does not rule out a weaker, power-law type of localization, particularly since weak exponential behavior and power law behav-

ior are hard to separate numerically. In fact, the propagation of rounding errors in a strip recursion may itself be an exponential process and might easily dominate over a subtle power law localization.

The author is unaware of any recent research that computes the localization of the states directly rather than assuming certain predicated scaling behavior in conjunction with a statistical analysis.

Our findings with the 2D Hubbard model and random alloy analogy suggest that this model does indeed contain the necessary physical processes that lead to a separation of branches for the resistance as a function of temperature and density. However, further work will be necessary to refine this idea and to obtain quantitative results.

Finally, we demonstrated convincingly that the Parallel Recursion Project is well suited for large-scale spare matrix calculations and that the author's design of the parallel algorithm and data distribution achieves practically the maximal theoretically possible linear speedup in the number of processors. The author is not aware of any other published matrix package capable of handling similar problem sizes whose performance scales linearly up to 128 processors.

# APPENDIX A

## TRANSMITTANCE PLOTS FOR DISORDERED 1D SYSTEM

This Appendix contains data plots of transmittance calculations in one-dimensional disordered systems at various disorder strengths, averaged at 1000 sample points over energy intervals across the entire band, as described in Sec. 4.4.

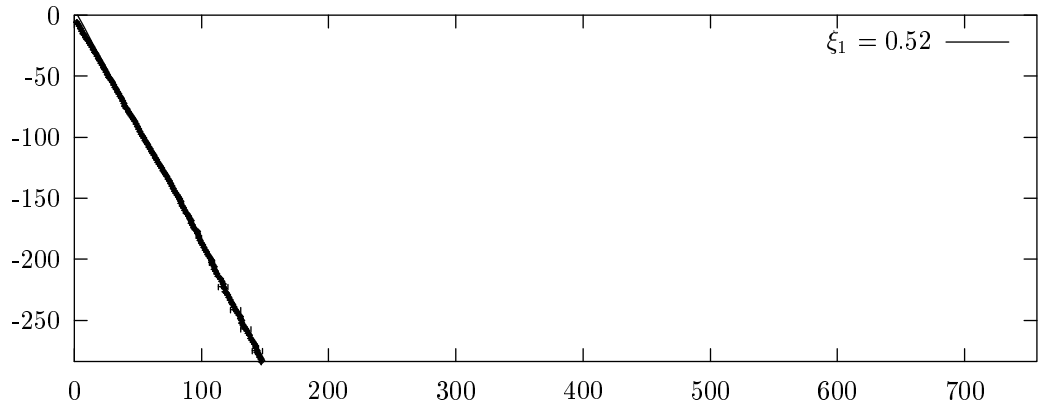


FIGURE 51. $\langle \log t_N \rangle_E$ vs. $N$ in 1D, $W = 1$, $E \in [-3.5, -2.5]$

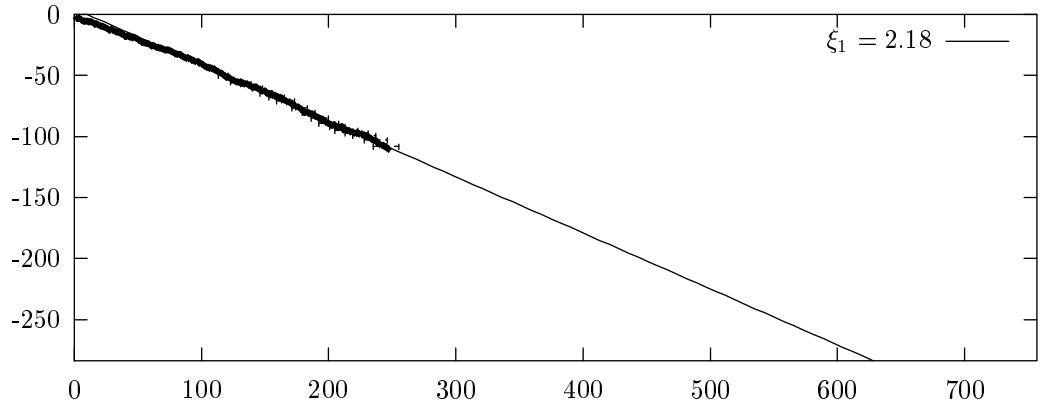


FIGURE 52. $\langle \log t_N \rangle_E$ vs. $N$ in 1D, $W = 1$, $E \in [-2.5, -1.5]$

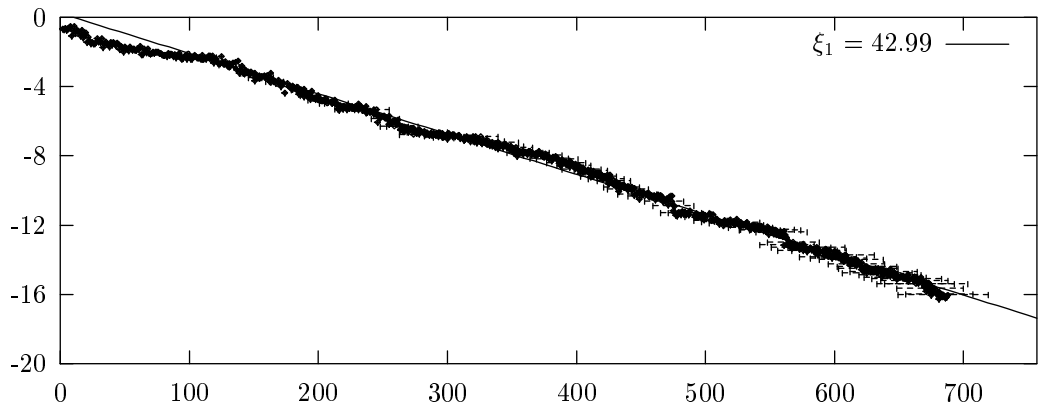


FIGURE 53. $\langle \log t_N \rangle_E$ vs. $N$ in 1D, $W = 1$, $E \in [-1.5, -0.5]$

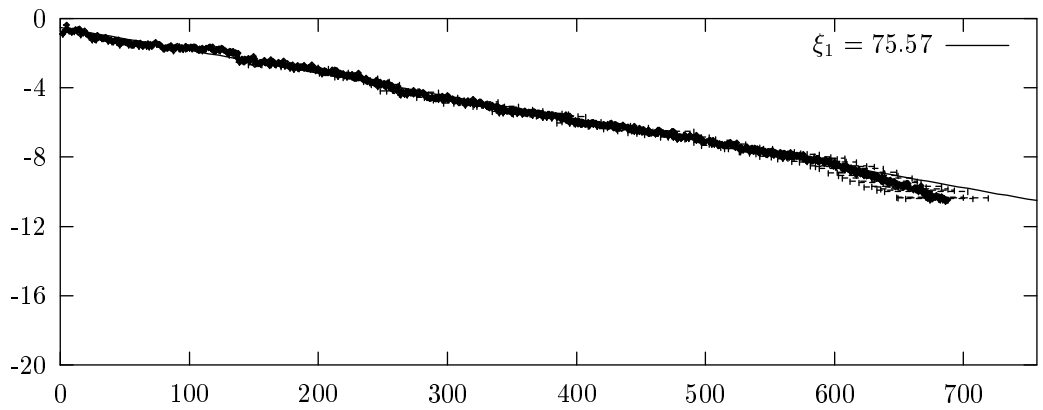


FIGURE 54. $\langle \log t_N \rangle_E$ vs. $N$ in 1D, $W = 1$, $E \in [-0.5, 0.5]$

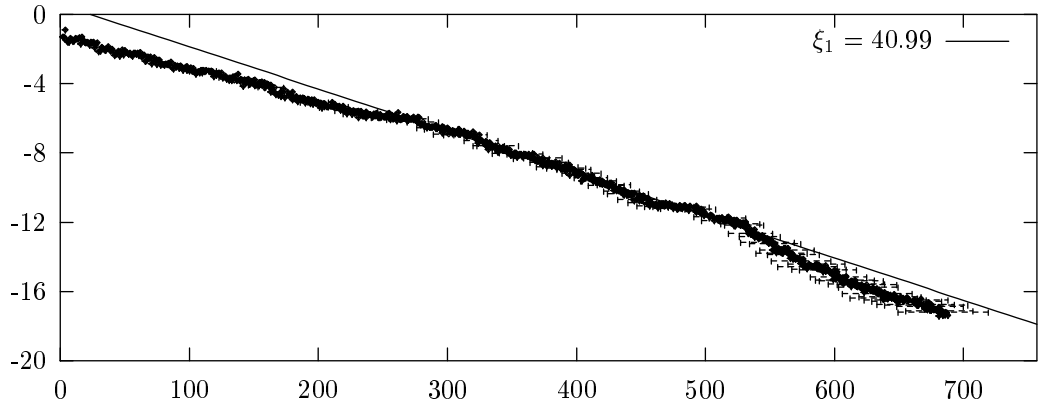


FIGURE 55. $\langle \log t_N \rangle_E$ vs. $N$ in 1D, $W = 1$, $E \in [0.5, 1.5]$

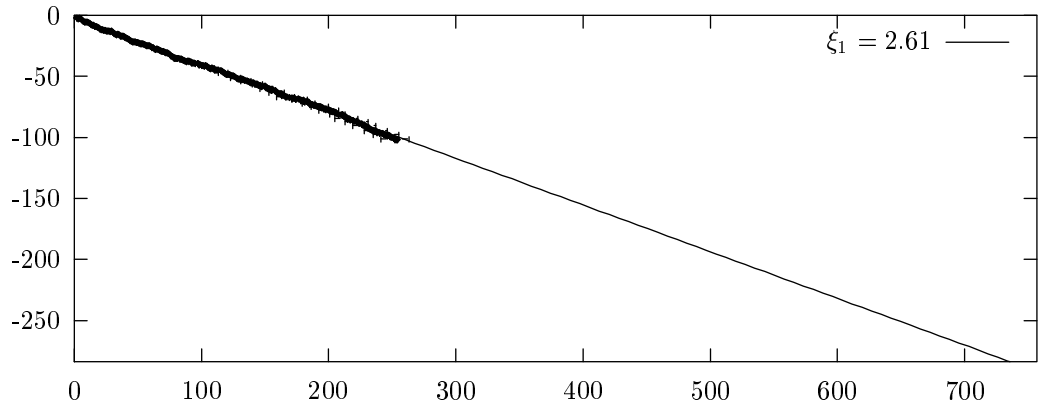


FIGURE 56. $\langle \log t_N \rangle_E$ vs. $N$ in 1D, $W = 1$, $E \in [1.5, 2.5]$

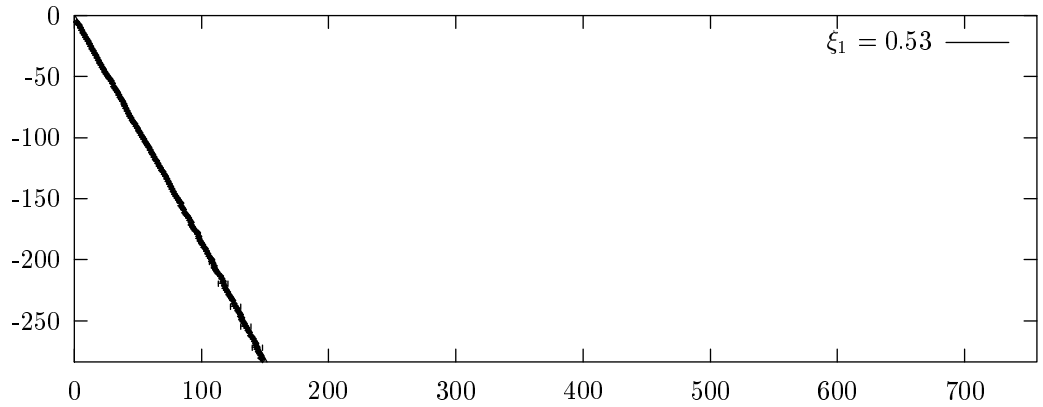


FIGURE 57. $\langle \log t_N \rangle_E$ vs. $N$ in 1D, $W = 1$, $E \in [2.5, 3.5]$

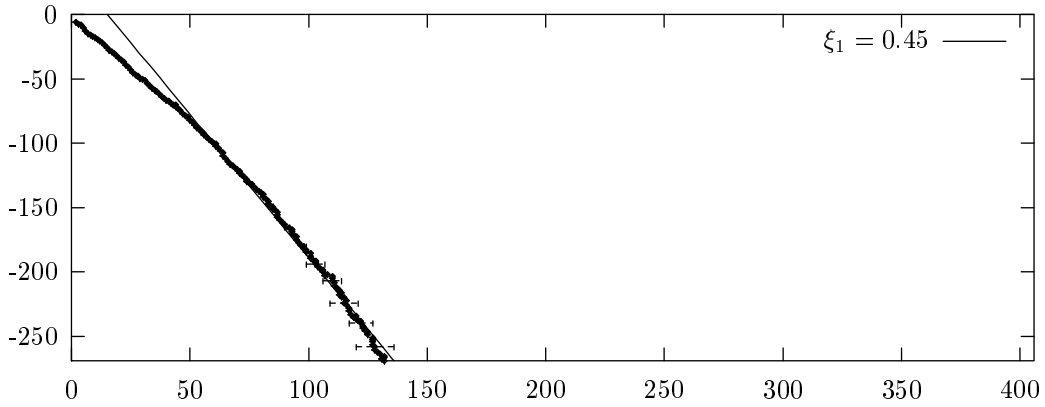


FIGURE 58. $\langle \log t_N \rangle_E$ vs. $N$ in 1D, $W = 2$, $E \in [-3.5, -2.5]$

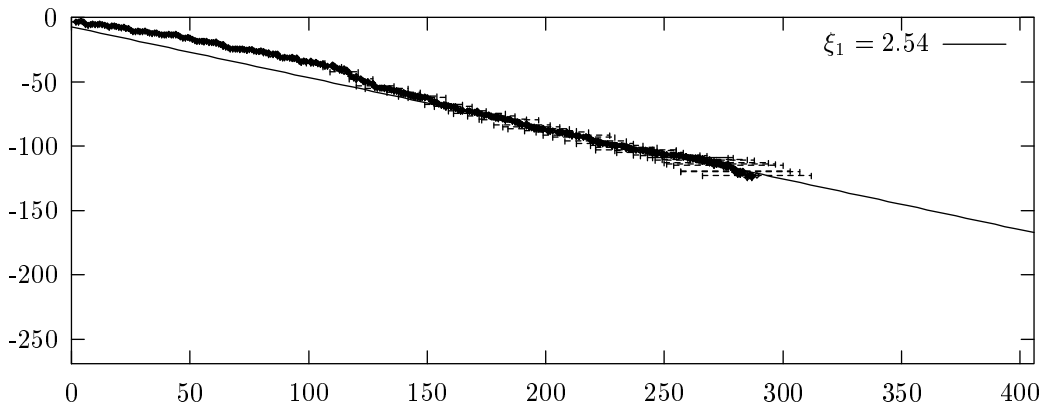


FIGURE 59. $\langle \log t_N \rangle_E$ vs. $N$ in 1D, $W = 2$, $E \in [-2.5, -1.5]$

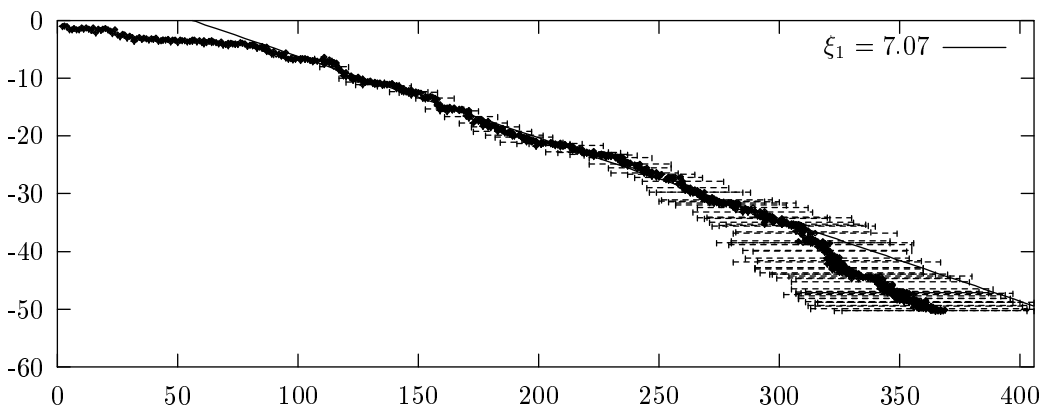


FIGURE 60. $\langle \log t_N \rangle_E$ vs. $N$ in 1D, $W = 2$, $E \in [-1.5, -0.5]$

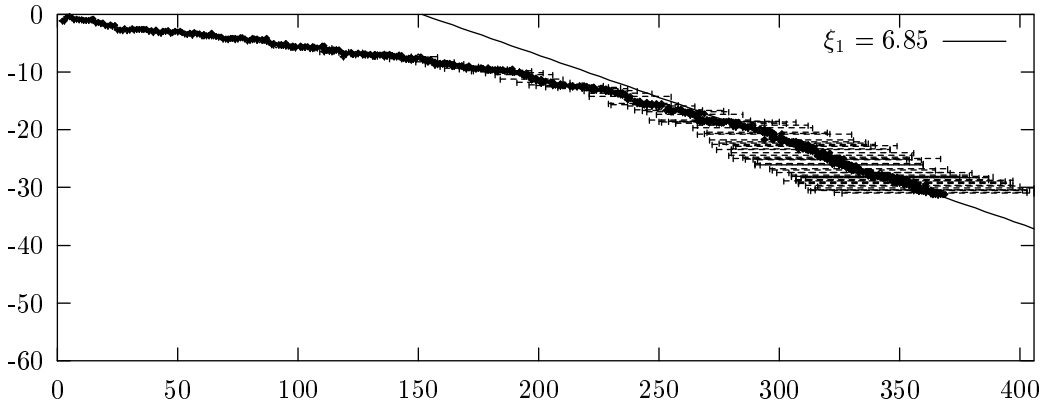


FIGURE 61. $\langle \log t_N \rangle_E$ vs. $N$ in 1D, $W = 2$, $E \in [-0.5, 0.5]$

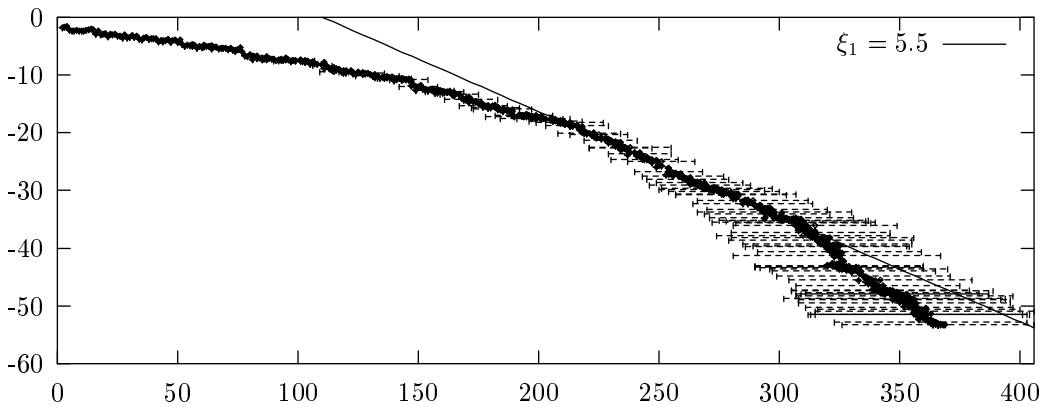


FIGURE 62. $\langle \log t_N \rangle_E$ vs. $N$ in 1D, $W = 2$, $E \in [0.5, 1.5]$

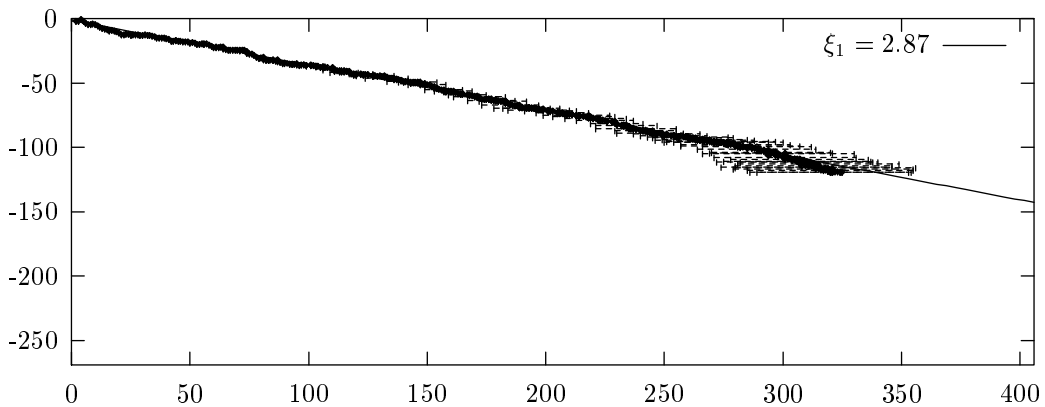


FIGURE 63. $\langle \log t_N \rangle_E$ vs. $N$ in 1D, $W = 2$, $E \in [1.5, 2.5]$

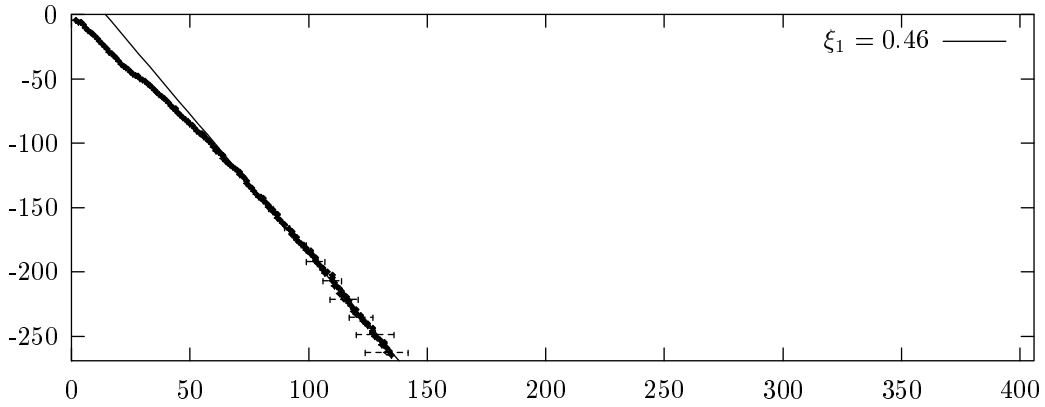


FIGURE 64. $\langle \log t_N \rangle_E$ vs. $N$ in 1D, $W = 2$, $E \in [2.5, 3.5]$

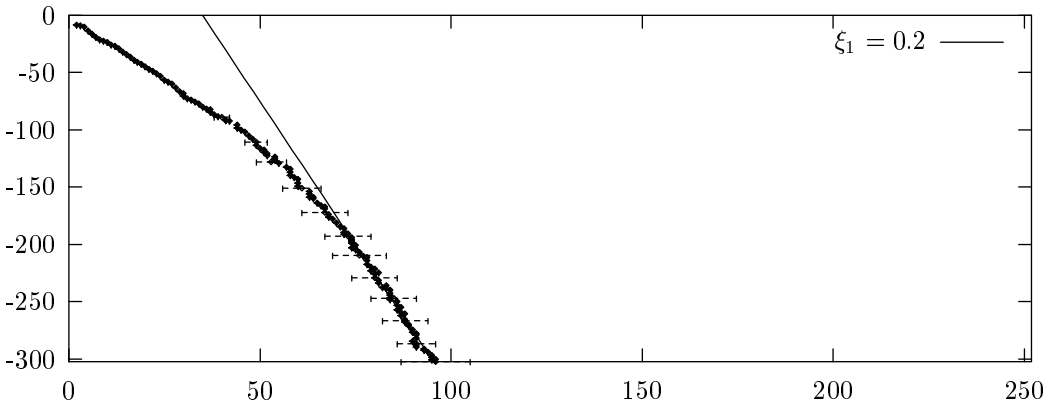


FIGURE 65. $\langle \log t_N \rangle_E$ vs. $N$ in 1D, $W = 4$, $E \in [-4.5, -3.5]$

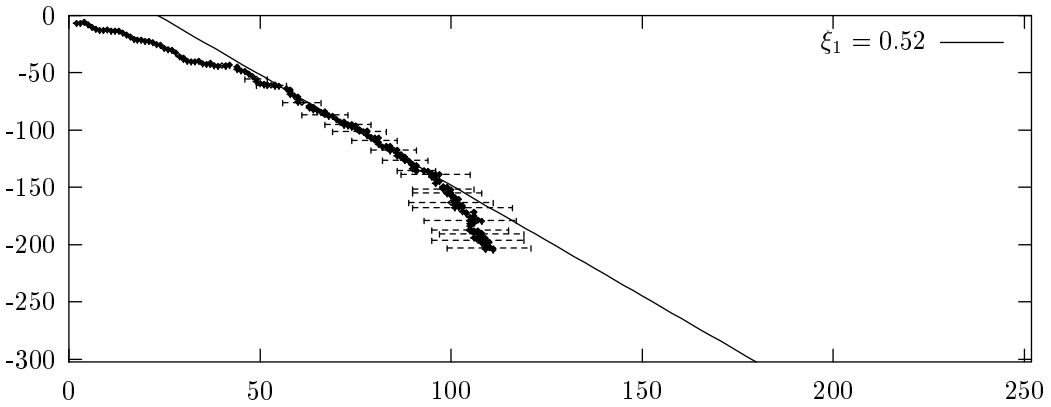


FIGURE 66. $\langle \log t_N \rangle_E$ vs. $N$ in 1D, $W = 4$, $E \in [-3.5, -2.5]$

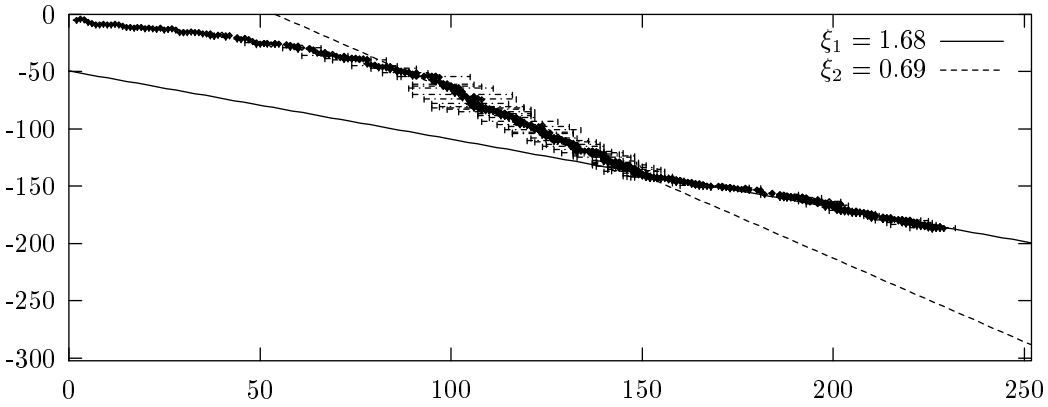


FIGURE 67. $\langle \log t_N \rangle_E$ vs. $N$ in 1D, $W = 4$, $E \in [-2.5, -1.5]$

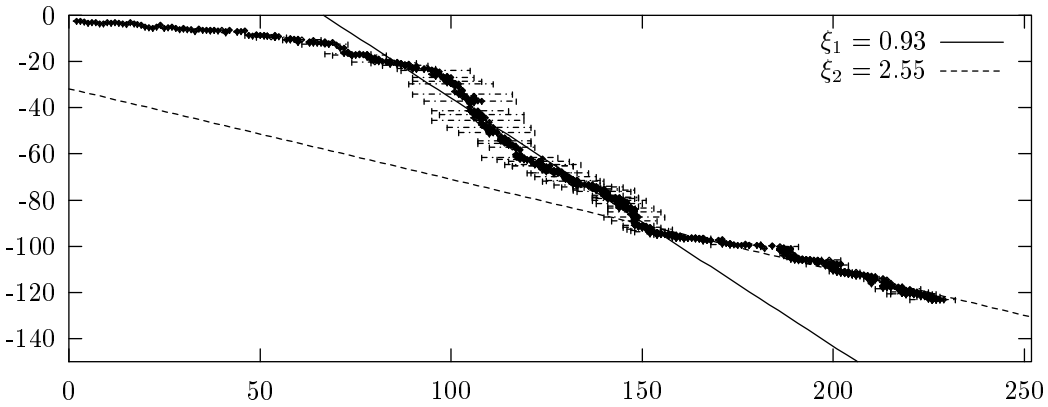


FIGURE 68. $\langle \log t_N \rangle_E$ vs. $N$ in 1D, $W = 4$, $E \in [-1.5, -0.5]$

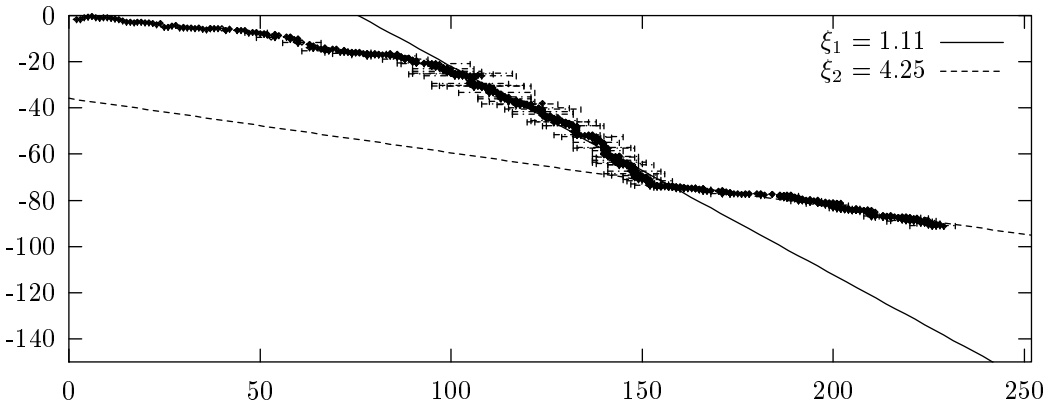


FIGURE 69. $\langle \log t_N \rangle_E$ vs. $N$ in 1D, $W = 4$, $E \in [-0.5, 0.5]$

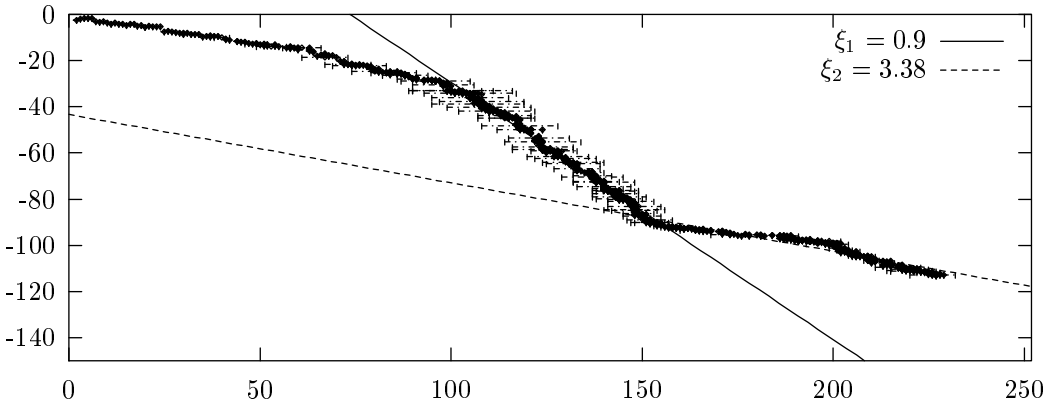


FIGURE 70. $\langle \log t_N \rangle_E$ vs. $N$ in 1D, $W = 4$, $E \in [0.5, 1.5]$

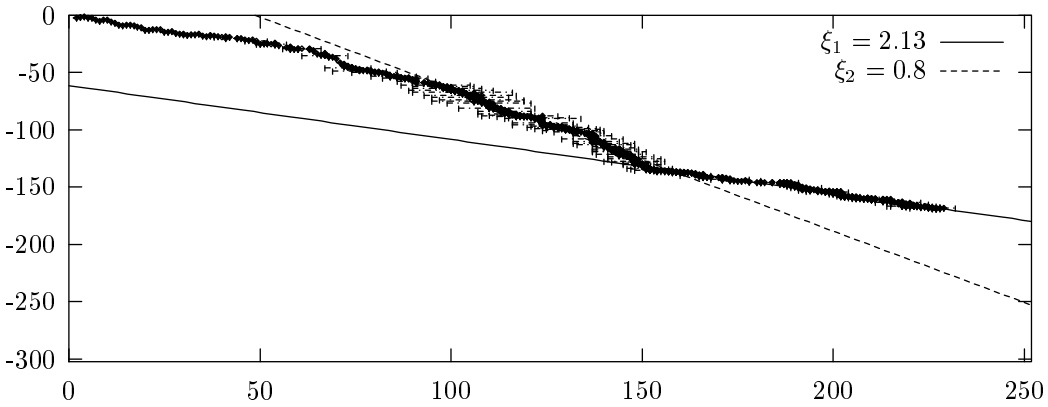


FIGURE 71. $\langle \log t_N \rangle_E$ vs. $N$ in 1D, $W = 4$, $E \in [1.5, 2.5]$

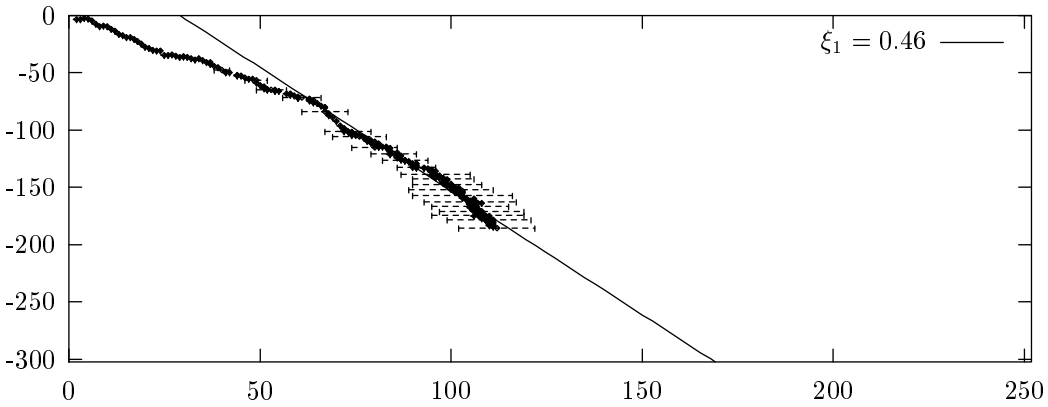


FIGURE 72. $\langle \log t_N \rangle_E$ vs. $N$ in 1D, $W = 4$, $E \in [2.5, 3.5]$

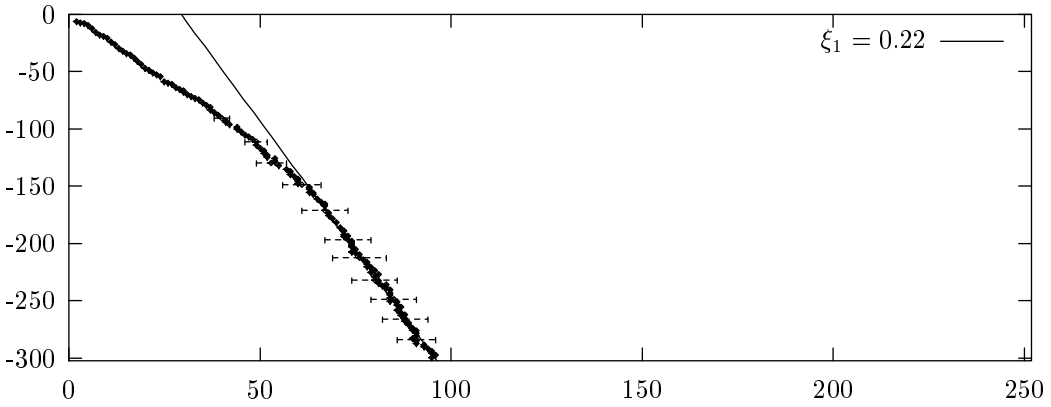


FIGURE 73. $\langle \log t_N \rangle_E$ vs. $N$ in 1D, $W = 4$, $E \in [3.5, 4.5]$

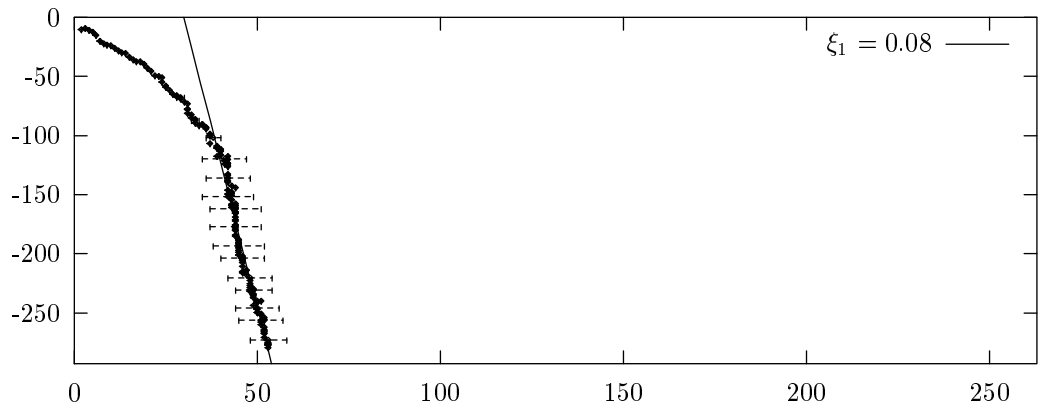


FIGURE 74. $\langle \log t_N \rangle_E$ vs. $N$ in 1D, $W = 8$, $E \in [-5.5, -4.5]$

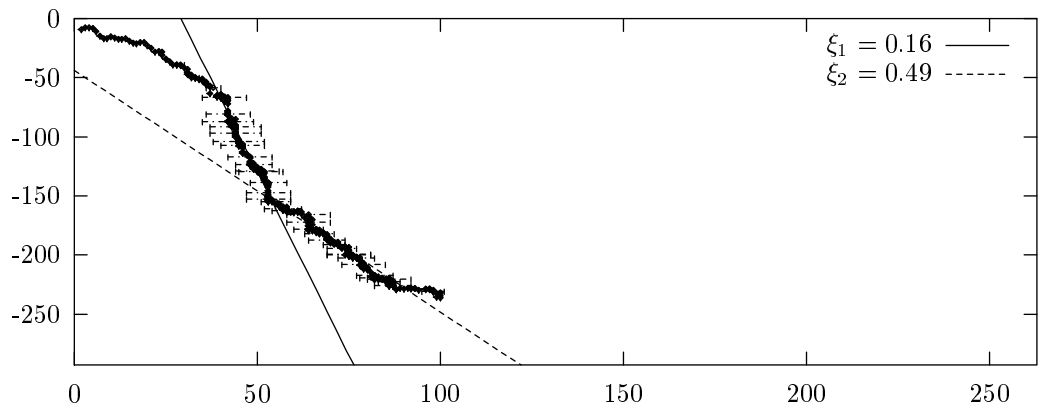


FIGURE 75. $\langle \log t_N \rangle_E$ vs. $N$ in 1D, $W = 8$, $E \in [-4.5, -3.5]$

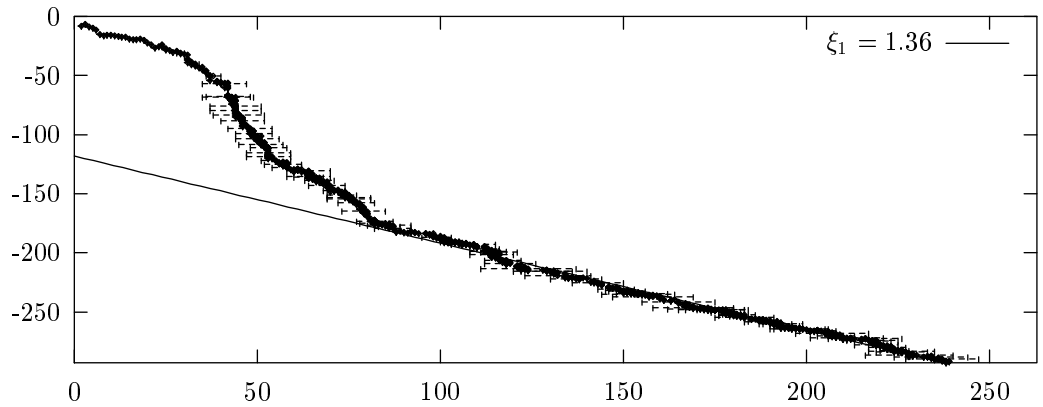


FIGURE 76. $\langle \log t_N \rangle_E$ vs. $N$ in 1D, $W = 8$, $E \in [-3.5, -2.5]$

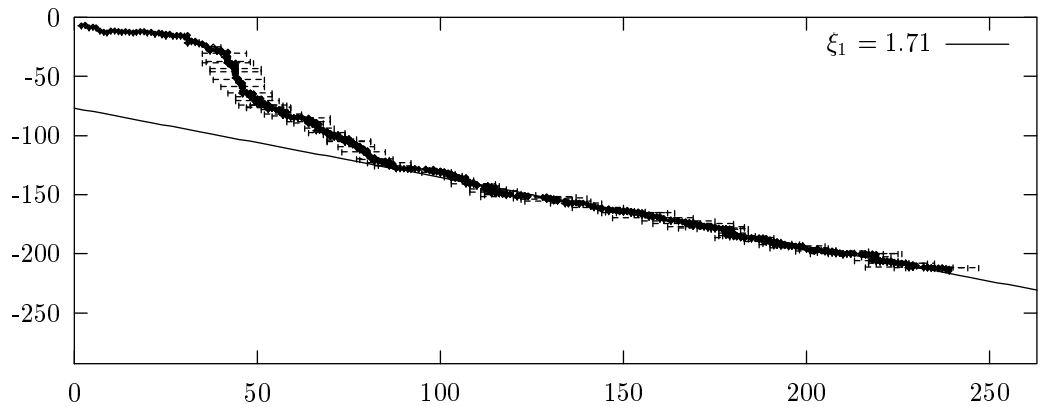


FIGURE 77. $\langle \log t_N \rangle_E$ vs. $N$ in 1D, $W = 8$, $E \in [-2.5, -1.5]$

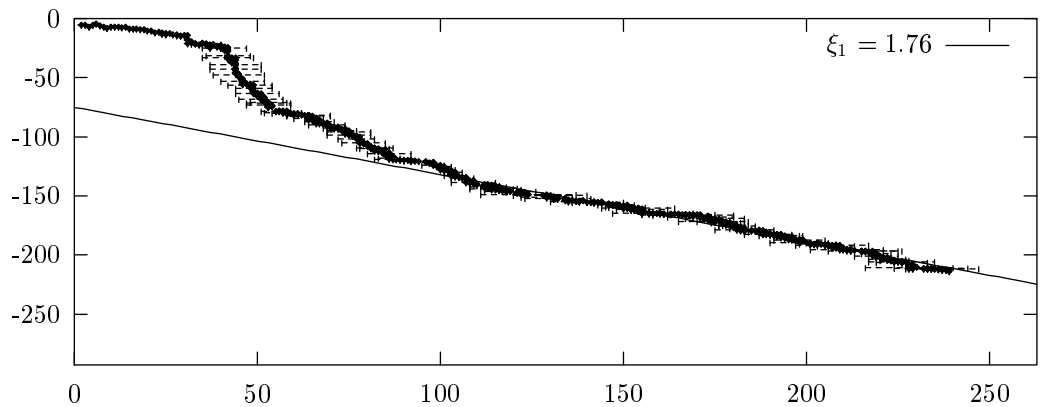


FIGURE 78. $\langle \log t_N \rangle_E$ vs. $N$ in 1D, $W = 8$, $E \in [-1.5, -0.5]$

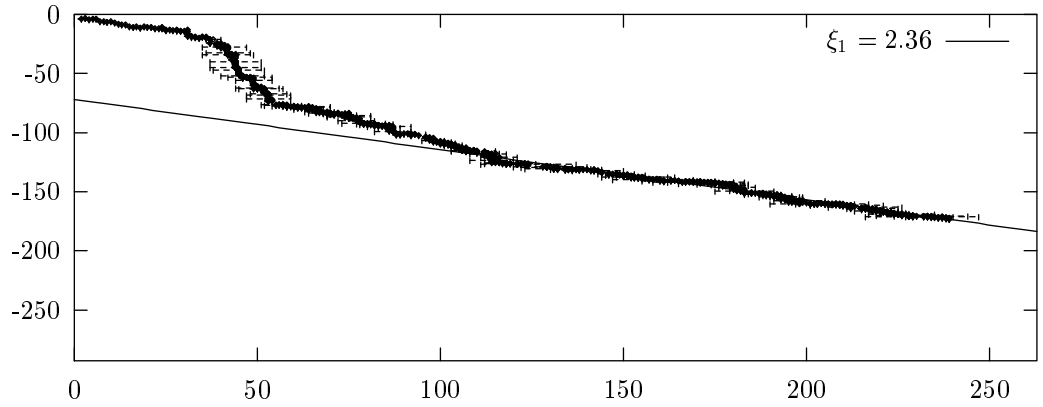


FIGURE 79. $\langle \log t_N \rangle_E$ vs. $N$ in 1D, $W = 8$, $E \in [-0.5, 0.5]$

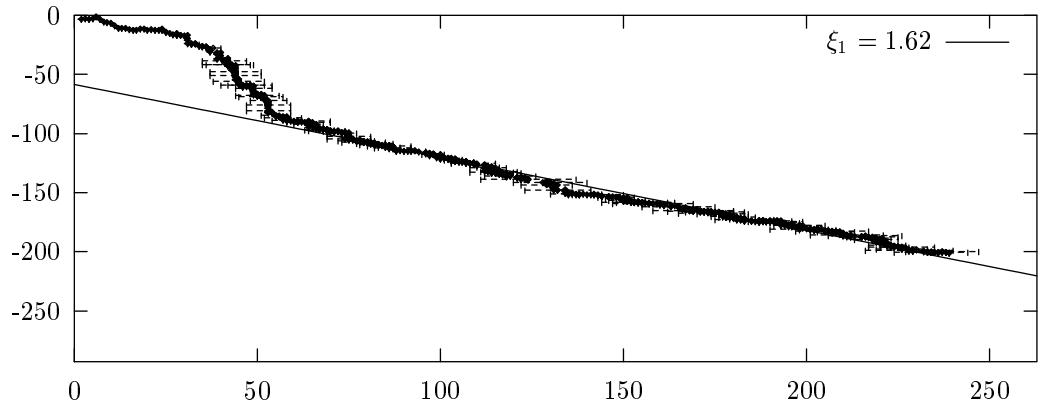


FIGURE 80. $\langle \log t_N \rangle_E$ vs. $N$ in 1D, $W = 8$, $E \in [0.5, 1.5]$

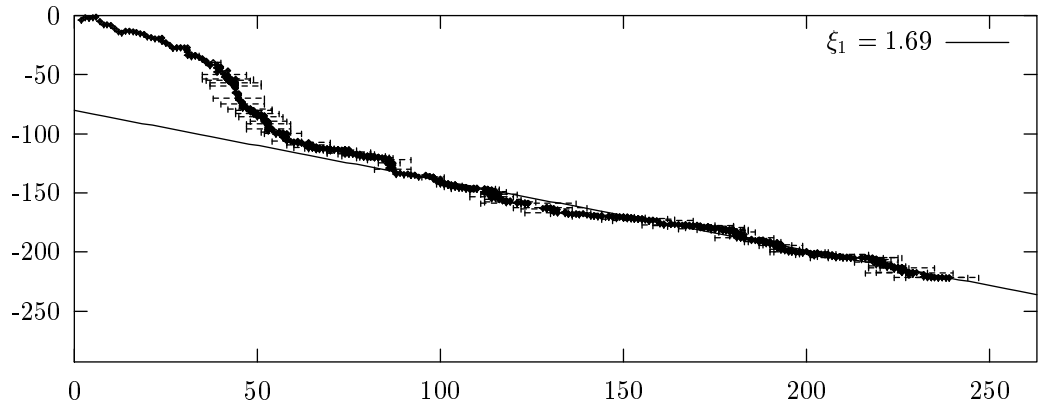


FIGURE 81. $\langle \log t_N \rangle_E$ vs. $N$ in 1D, $W = 8$, $E \in [1.5, 2.5]$

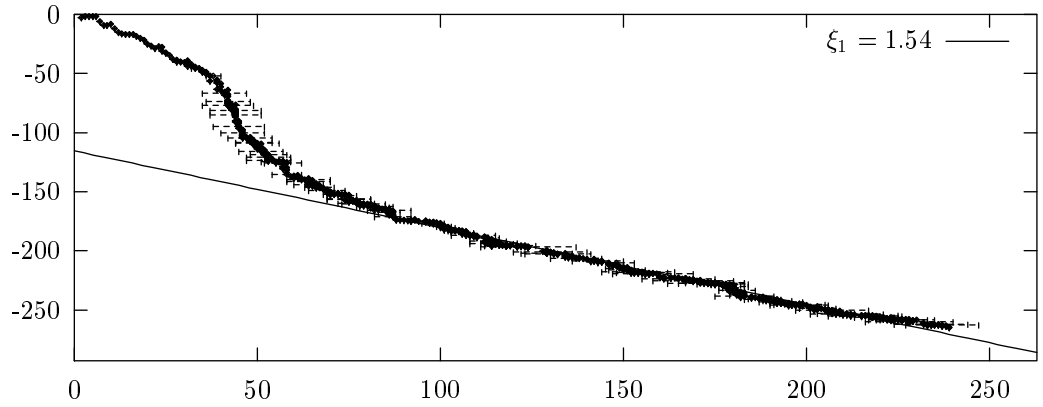


FIGURE 82. $\langle \log t_N \rangle_E$ vs. $N$ in 1D, $W = 8$, $E \in [2.5, 3.5]$

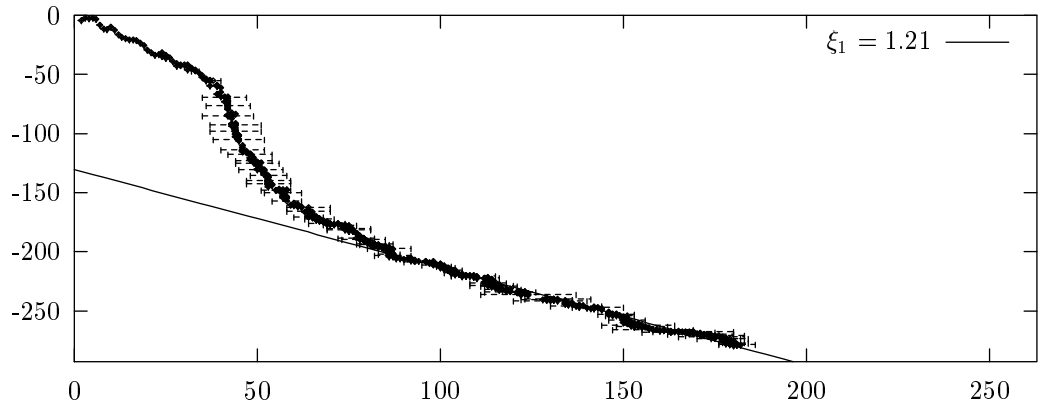


FIGURE 83. $\langle \log t_N \rangle_E$ vs. $N$ in 1D, $W = 8$, $E \in [3.5, 4.5]$

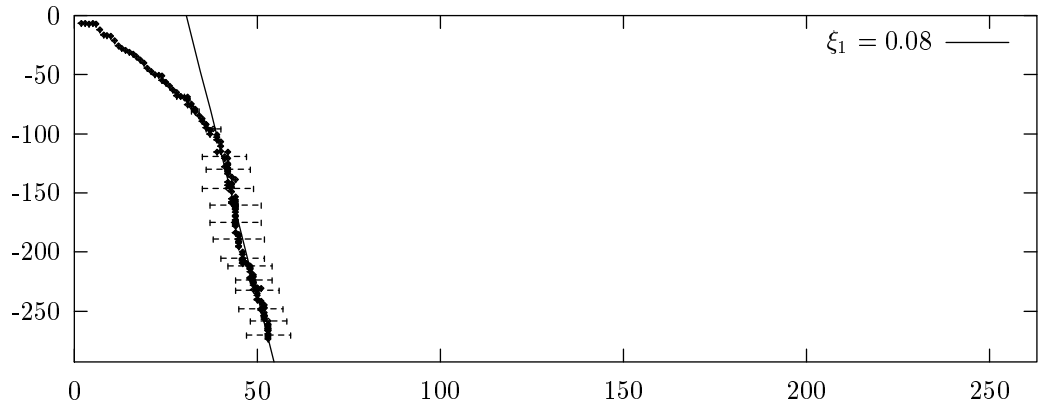


FIGURE 84. $\langle \log t_N \rangle_E$ vs. $N$ in 1D, $W = 8$, $E \in [4.5, 5.5]$

# APPENDIX B

## TRANSMITTANCE PLOTS FOR DISORDERED 2D SYSTEM

This Appendix contains data plots of transmittance calculations in two-dimensional disordered systems at various disorder strengths, averaged at 1000 sample points over energy intervals across the entire band, as described in Sec. 4.5.

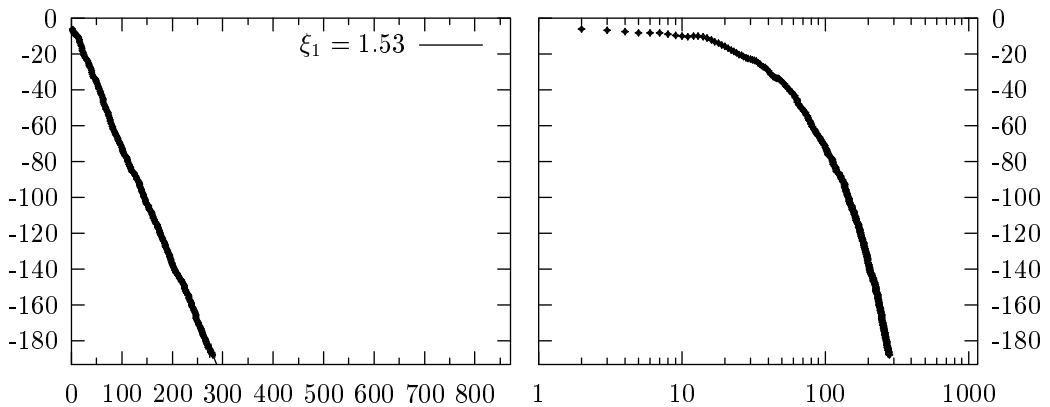


FIGURE 85. $\langle \log t_N \rangle_E$ vs. $N$ in 2D, $W = 4$, $E \in [-5.5, -4.5]$

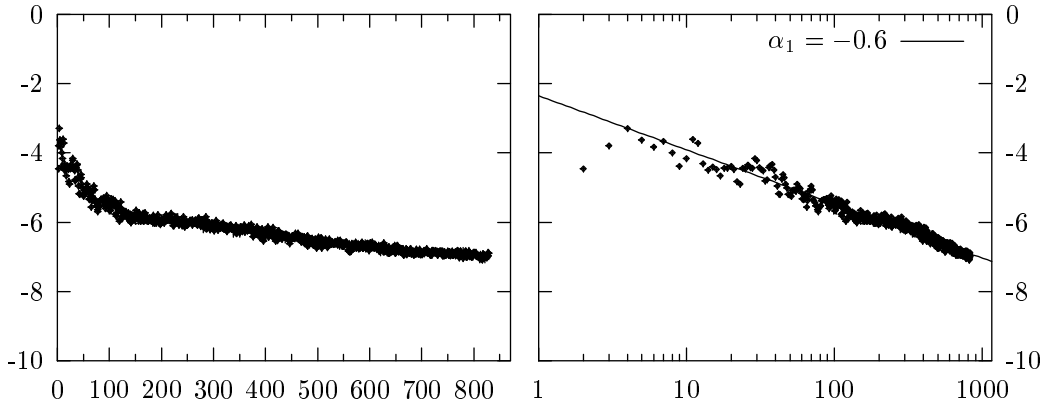


FIGURE 86. $\langle \log t_N \rangle_E$ vs. $N$ in 2D, $W = 4$, $E \in [-4.5, -3.5]$

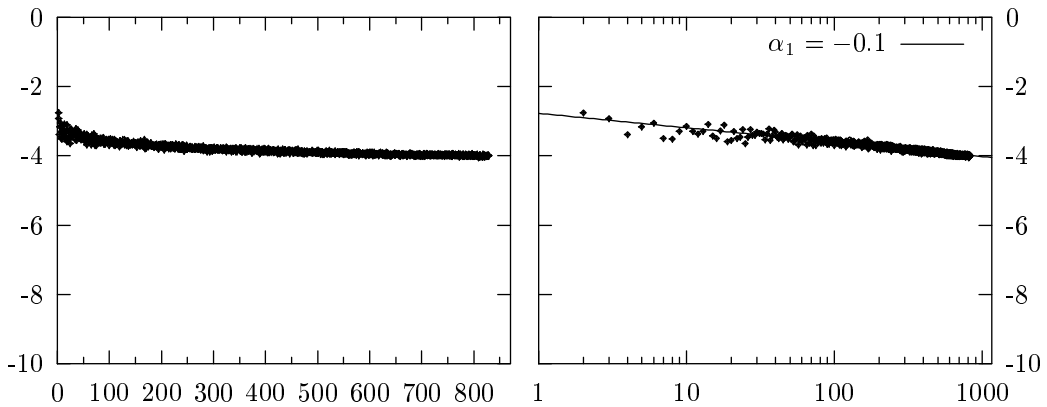


FIGURE 87. $\langle \log t_N \rangle_E$ vs. $N$ in 2D, $W = 4$, $E \in [-3.5, -2.5]$

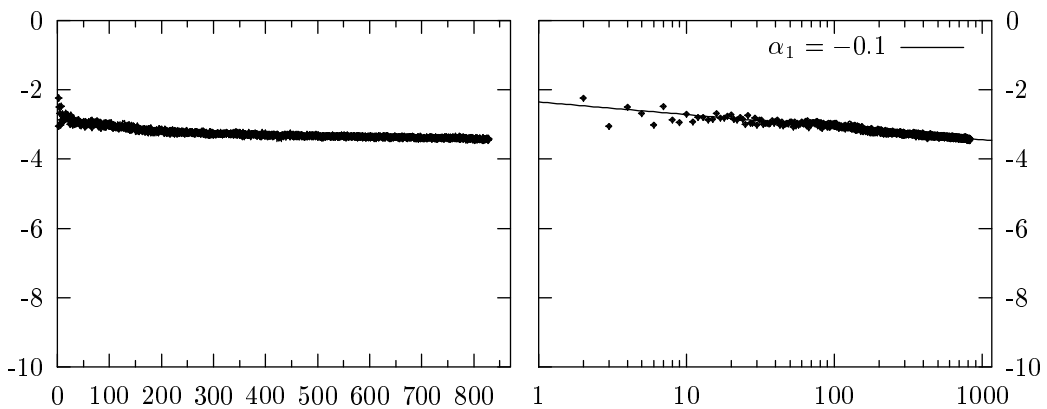


FIGURE 88. $\langle \log t_N \rangle_E$ vs. $N$ in 2D, $W = 4$, $E \in [-2.5, -1.5]$

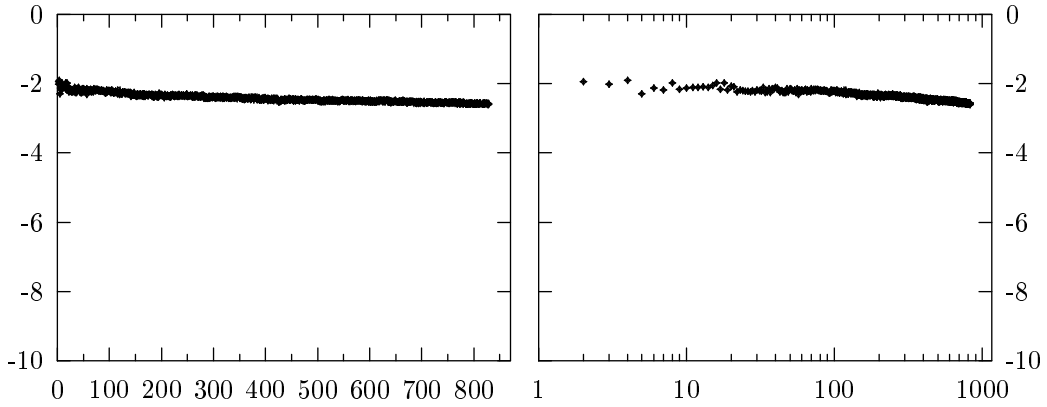


FIGURE 89. $\langle \log t_N \rangle_E$ vs. $N$ in 2D, $W = 4$, $E \in [-1.5, -0.5]$

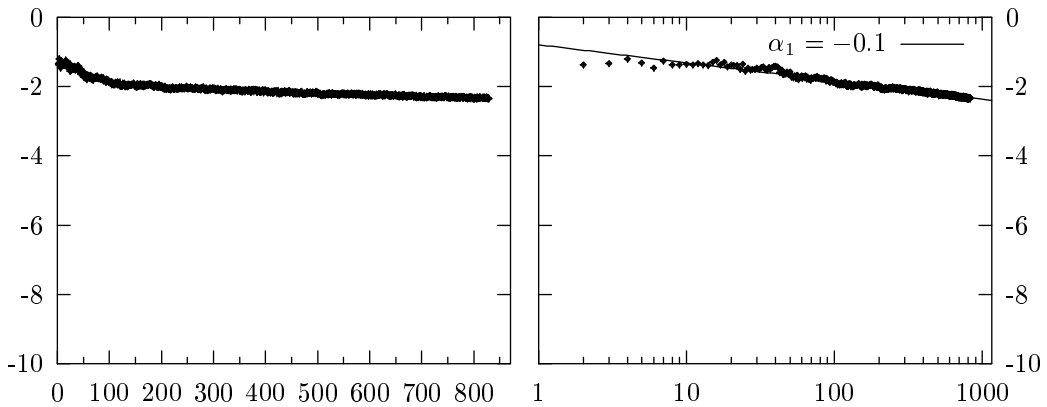


FIGURE 90. $\langle \log t_N \rangle_E$ vs. $N$ in 2D, $W = 4$, $E \in [-0.5, 0.5]$

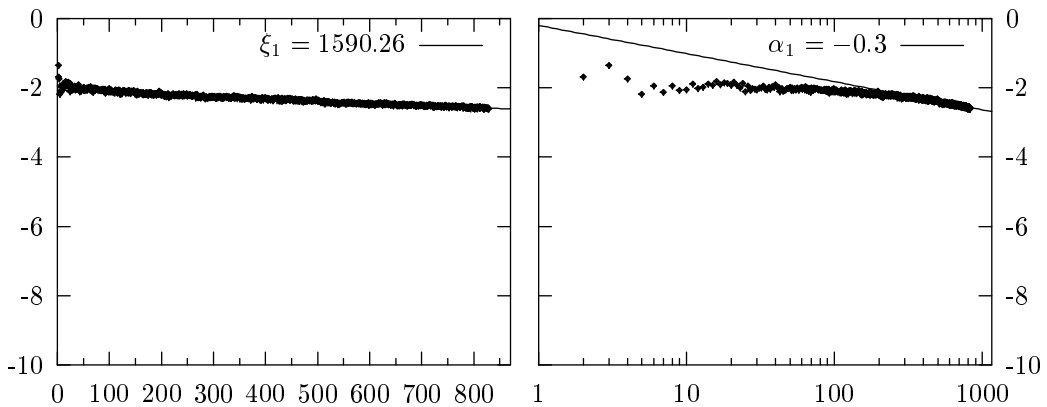


FIGURE 91. $\langle \log t_N \rangle_E$ vs. $N$ in 2D, $W = 4$, $E \in [0.5, 1.5]$

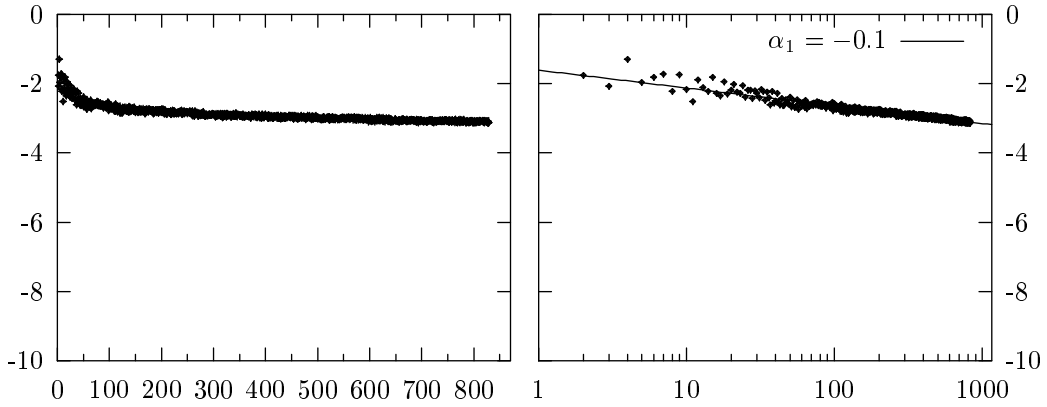


FIGURE 92. $\langle \log t_N \rangle_E$ vs. $N$ in 2D, $W = 4$, $E \in [1.5, 2.5]$

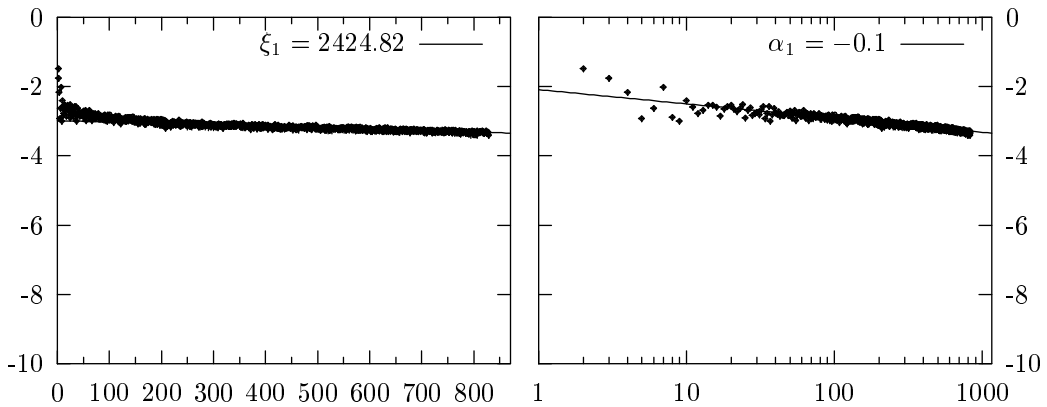


FIGURE 93. $\langle \log t_N \rangle_E$ vs. $N$ in 2D, $W = 4$, $E \in [2.5, 3.5]$

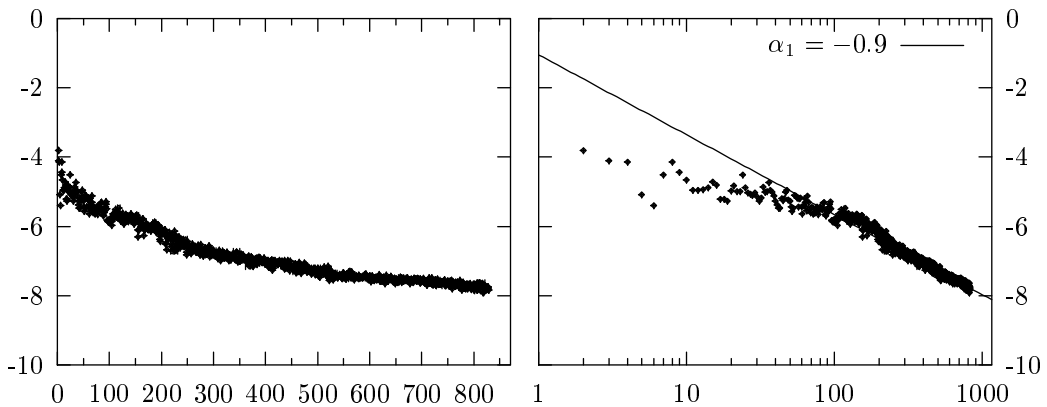


FIGURE 94. $\langle \log t_N \rangle_E$ vs. $N$ in 2D, $W = 4$, $E \in [3.5, 4.5]$

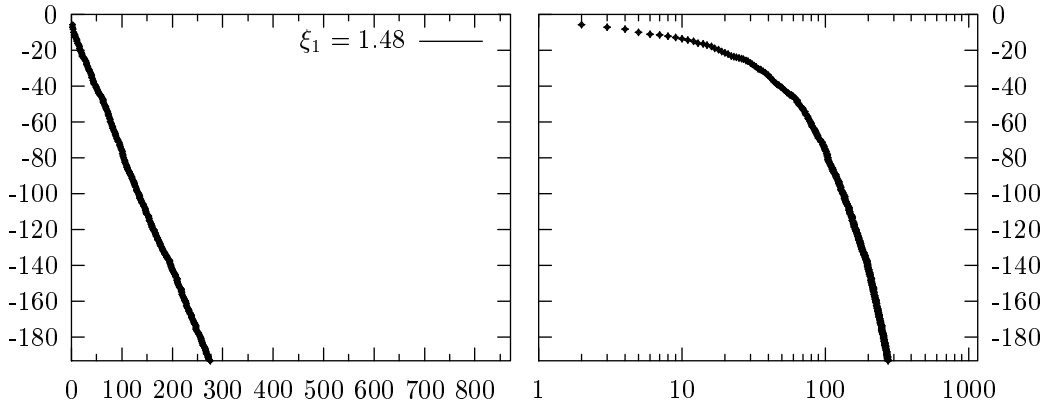


FIGURE 95. $\langle \log t_N \rangle_E$ vs. $N$ in 2D, $W = 4$, $E \in [4.5, 5.5]$

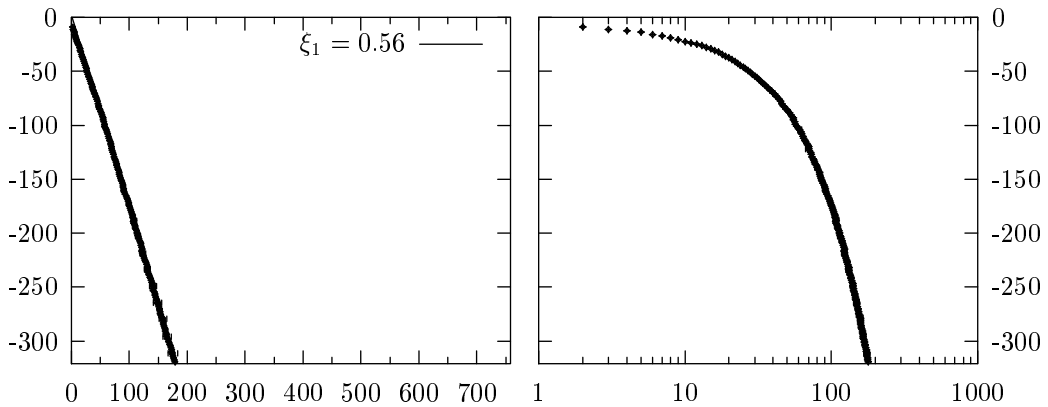


FIGURE 96. $\langle \log t_N \rangle_E$ vs. $N$ in 2D, $W = 8$, $E \in [-8.5, -7.5]$

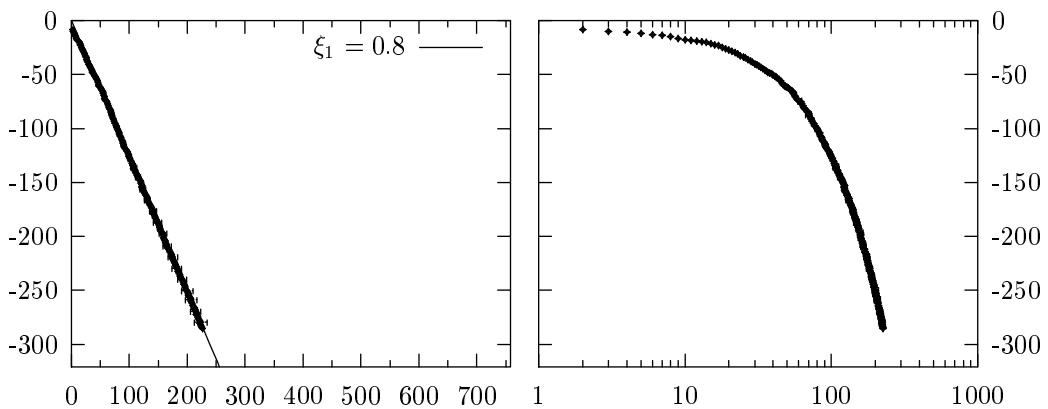


FIGURE 97. $\langle \log t_N \rangle_E$ vs. $N$ in 2D, $W = 8$, $E \in [-7.5, -6.5]$

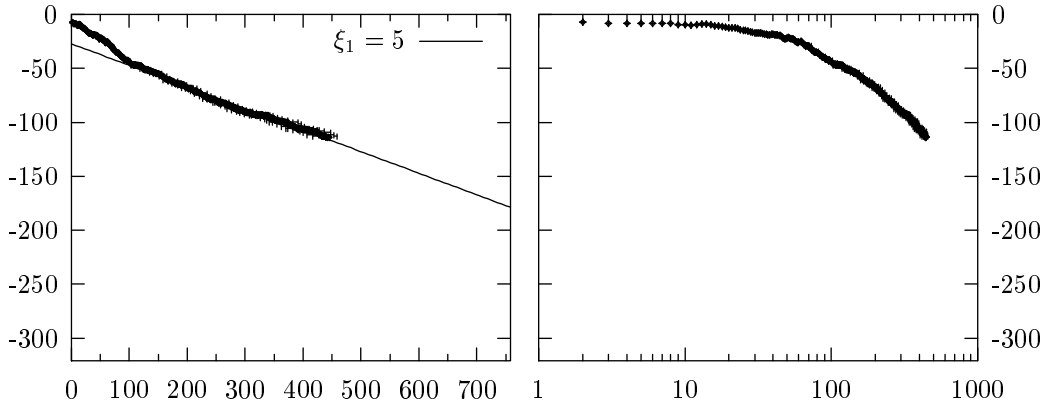


FIGURE 98. $\langle \log t_N \rangle_E$ vs. $N$ in 2D, $W = 8$, $E \in [-6.5, -5.5]$

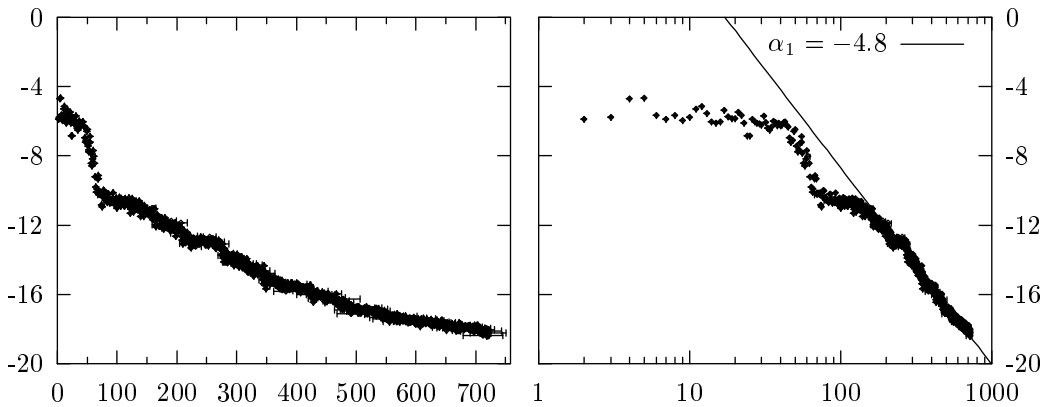


FIGURE 99. $\langle \log t_N \rangle_E$ vs. $N$ in 2D, $W = 8$, $E \in [-5.5, -4.5]$

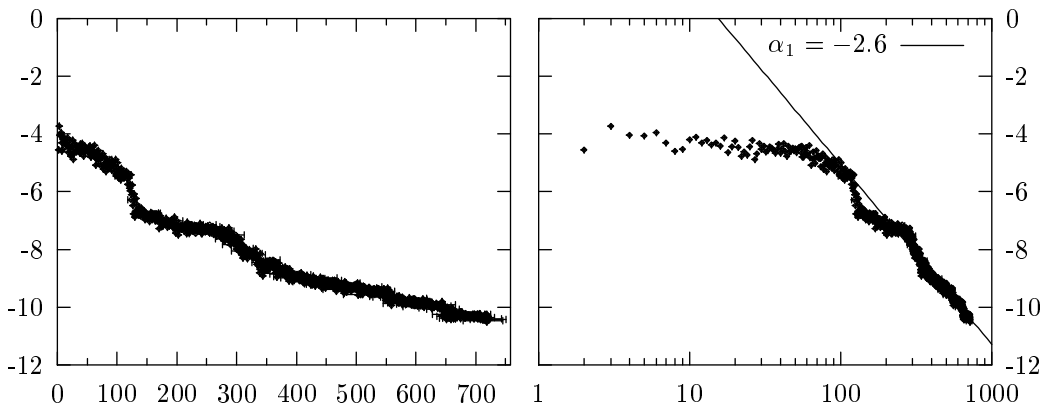


FIGURE 100. $\langle \log t_N \rangle_E$ vs. $N$ in 2D, $W = 8$, $E \in [-4.5, -3.5]$

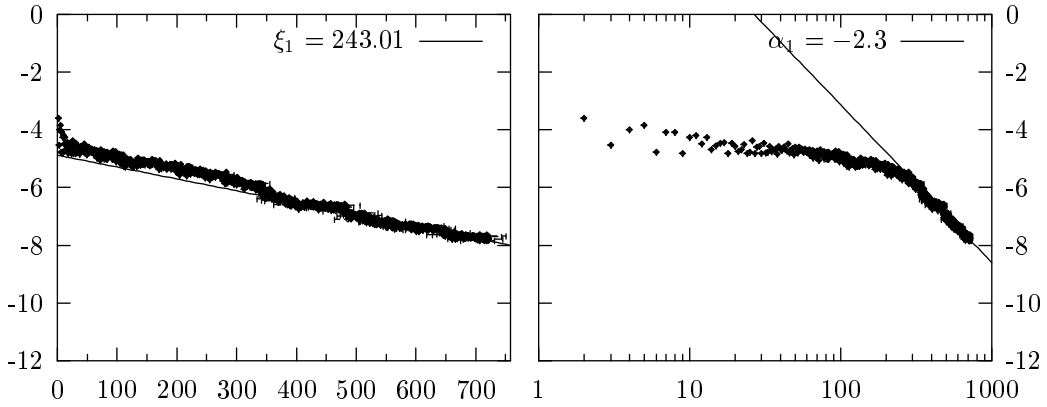


FIGURE 101. $\langle \log t_N \rangle_E$ vs. $N$ in 2D, $W = 8$, $E \in [-3.5, -2.5]$

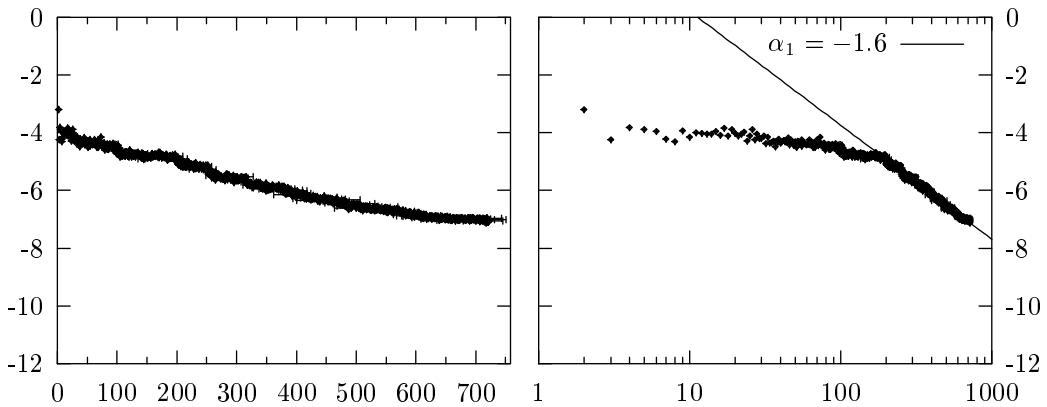


FIGURE 102. $\langle \log t_N \rangle_E$ vs. $N$ in 2D, $W = 8$, $E \in [-2.5, -1.5]$

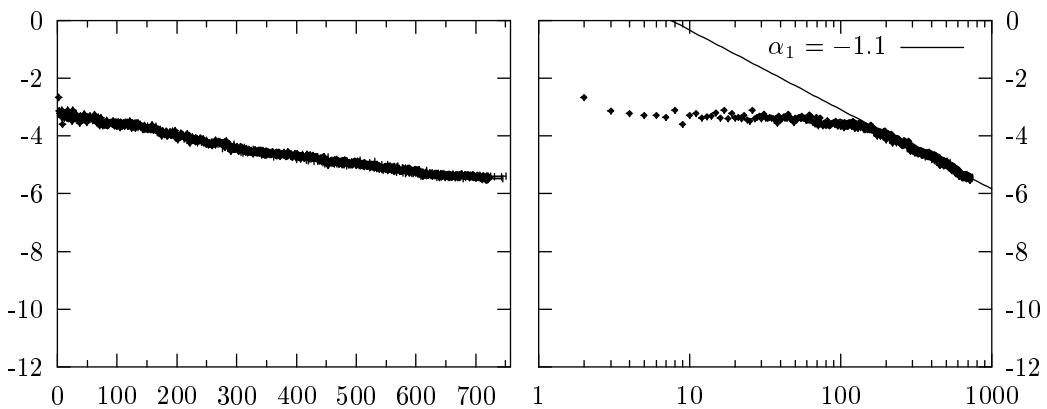


FIGURE 103. $\langle \log t_N \rangle_E$ vs. $N$ in 2D, $W = 8$, $E \in [-1.5, -0.5]$

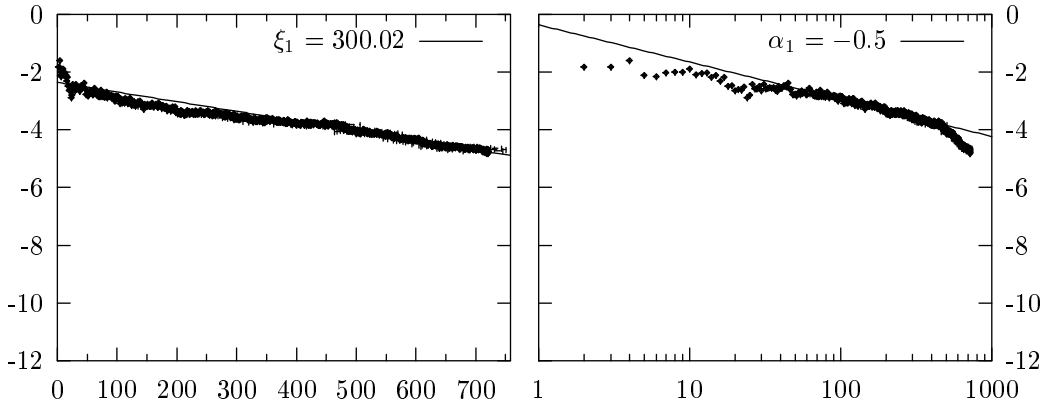


FIGURE 104. $\langle \log t_N \rangle_E$ vs. $N$ in 2D, $W = 8$, $E \in [-0.5, 0.5]$

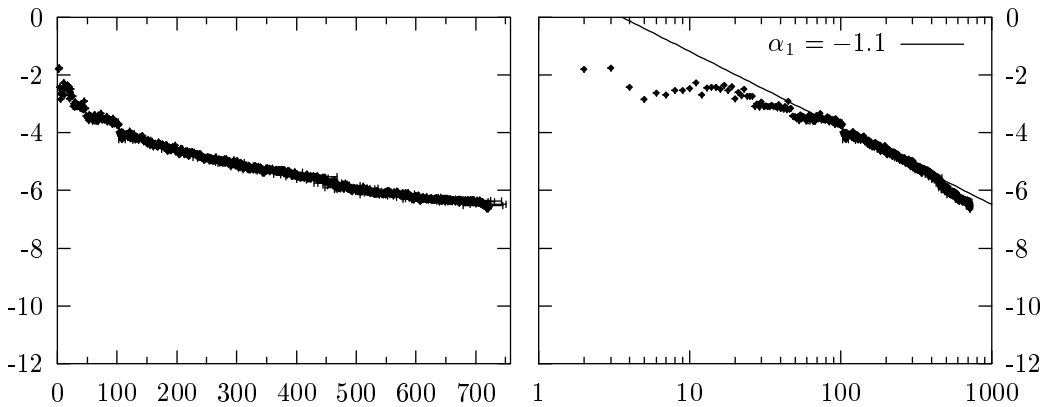


FIGURE 105. $\langle \log t_N \rangle_E$ vs. $N$ in 2D, $W = 8$, $E \in [0.5, 1.5]$

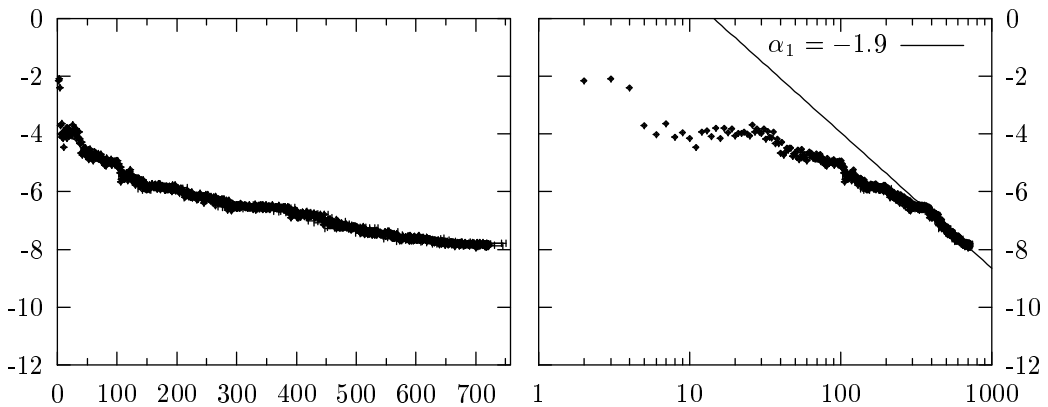


FIGURE 106. $\langle \log t_N \rangle_E$ vs. $N$ in 2D, $W = 8$, $E \in [1.5, 2.5]$

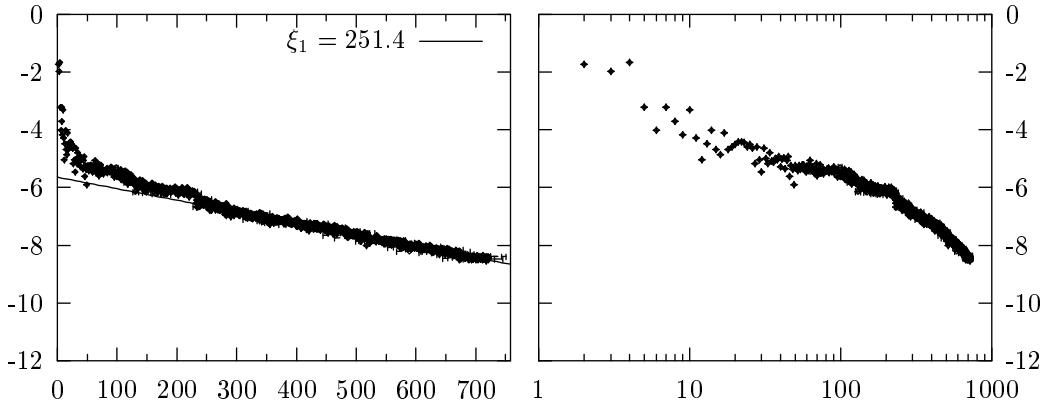


FIGURE 107. $\langle \log t_N \rangle_E$ vs. $N$ in 2D, $W = 8$, $E \in [2.5, 3.5]$

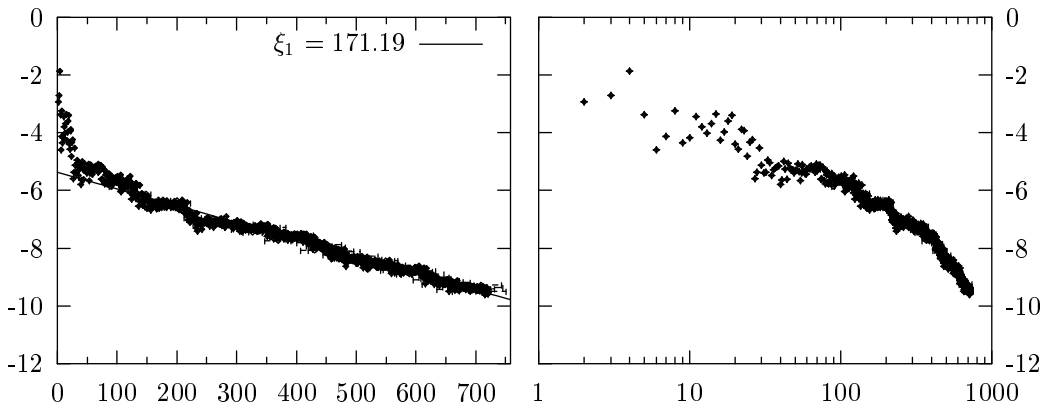


FIGURE 108. $\langle \log t_N \rangle_E$ vs. $N$ in 2D, $W = 8$, $E \in [3.5, 4.5]$

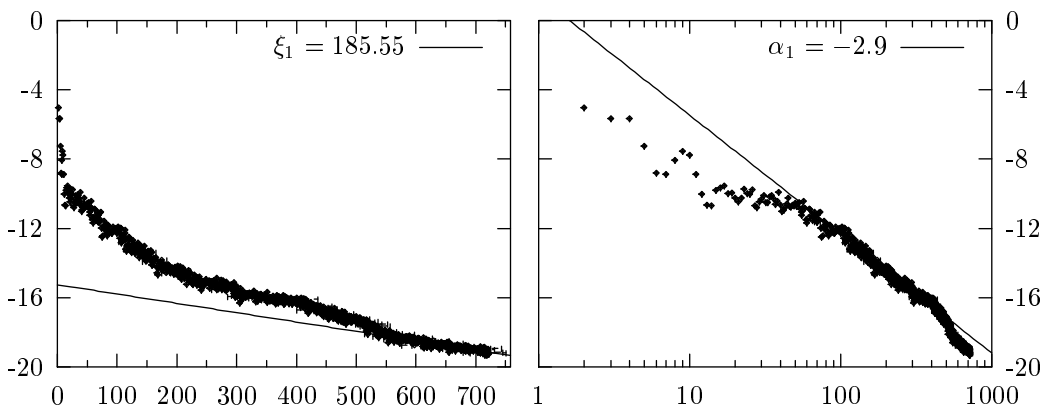


FIGURE 109. $\langle \log t_N \rangle_E$ vs. $N$ in 2D, $W = 8$, $E \in [4.5, 5.5]$

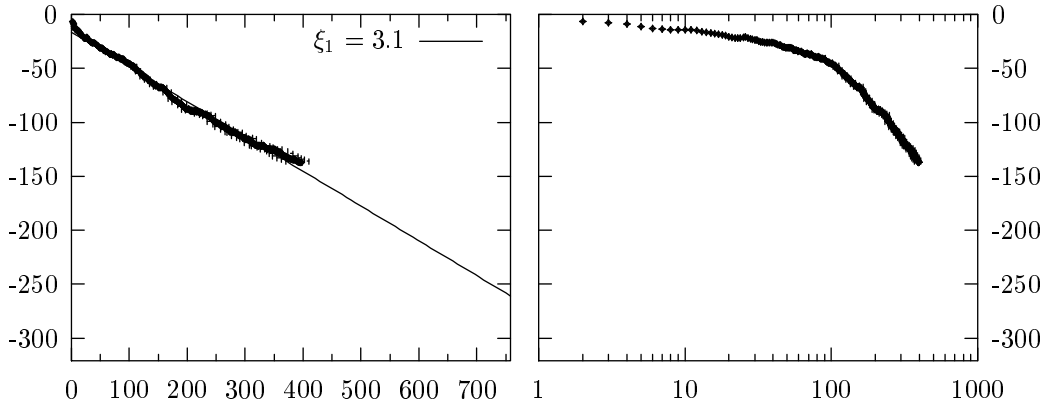


FIGURE 110. $\langle \log t_N \rangle_E$ vs. $N$ in 2D, $W = 8$, $E \in [5.5, 6.5]$

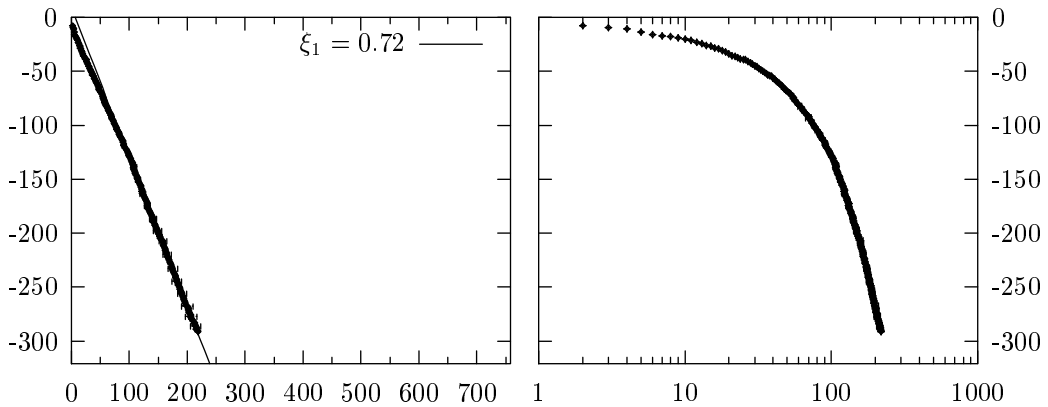


FIGURE 111. $\langle \log t_N \rangle_E$ vs. $N$ in 2D, $W = 8$, $E \in [6.5, 7.5]$

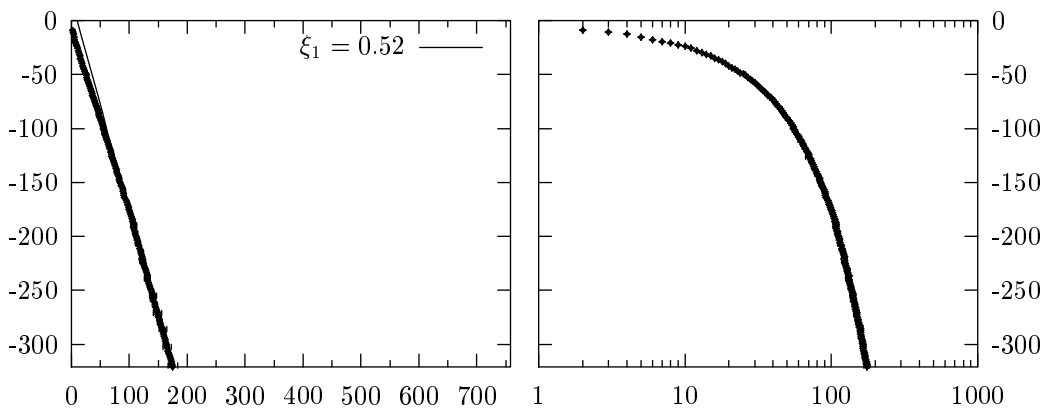


FIGURE 112. $\langle \log t_N \rangle_E$ vs. $N$ in 2D, $W = 8$, $E \in [7.5, 8.5]$

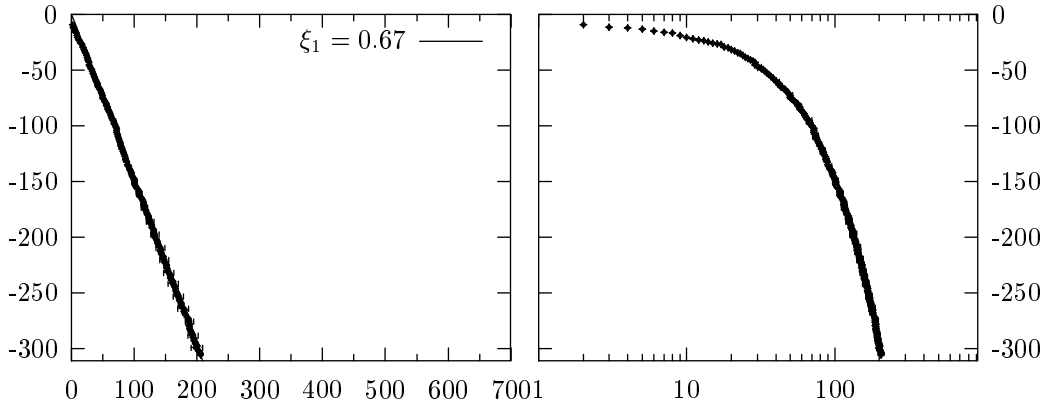


FIGURE 113. $\langle \log t_N \rangle_E$ vs. $N$ in 2D, $W = 12$, $E \in [-9.5, -8.5]$

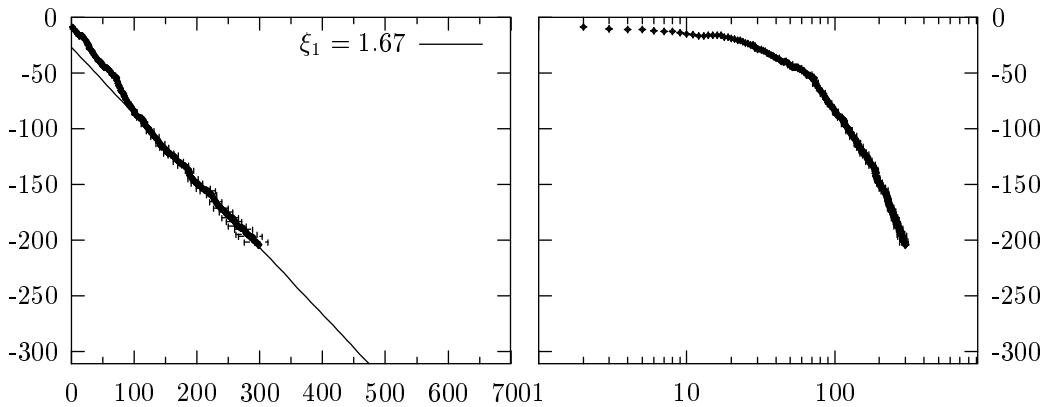


FIGURE 114. $\langle \log t_N \rangle_E$ vs. $N$ in 2D, $W = 12$, $E \in [-8.5, -7.5]$

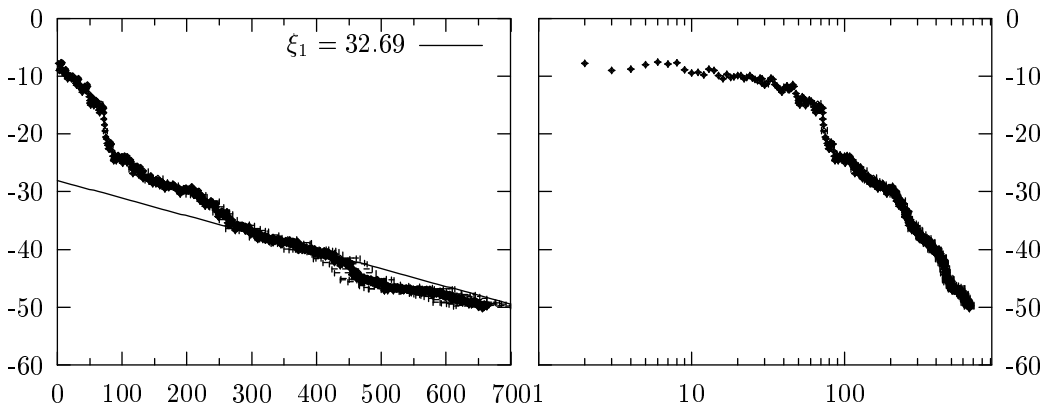


FIGURE 115. $\langle \log t_N \rangle_E$ vs. $N$ in 2D, $W = 12$, $E \in [-7.5, -6.5]$

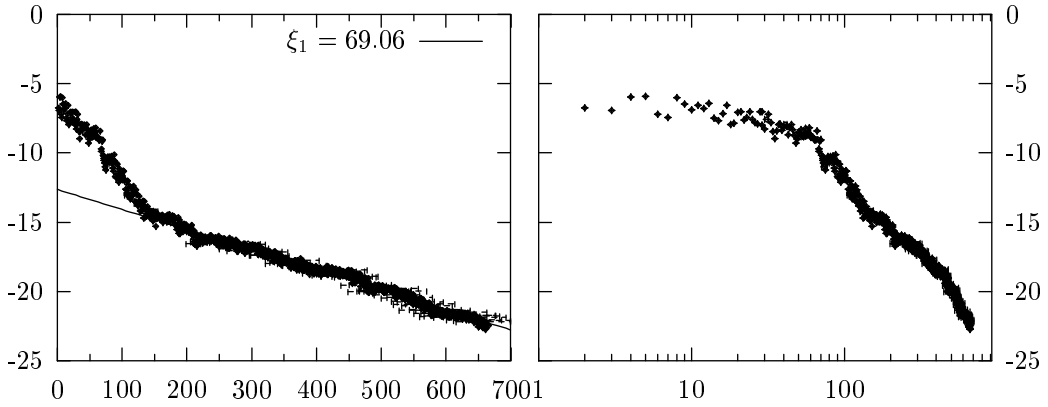


FIGURE 116. $\langle \log t_N \rangle_E$ vs. $N$ in 2D, $W = 12$, $E \in [-6.5, -5.5]$

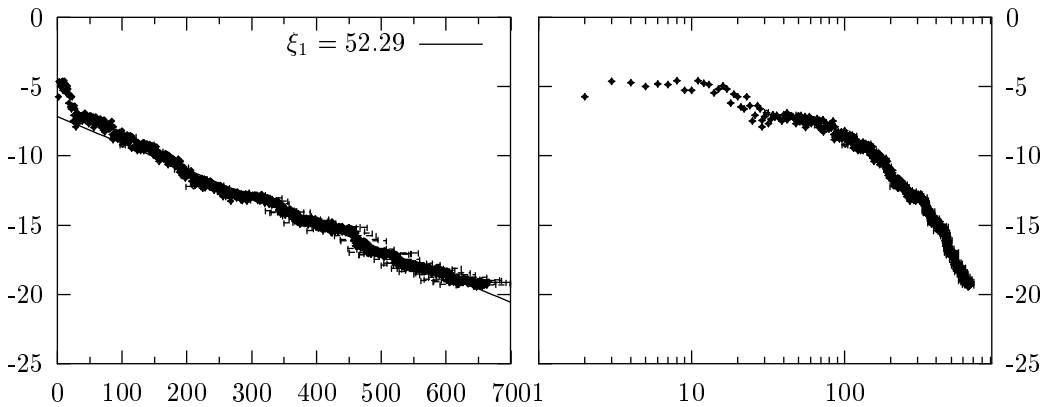


FIGURE 117. $\langle \log t_N \rangle_E$ vs. $N$ in 2D, $W = 12$, $E \in [-5.5, -4.5]$

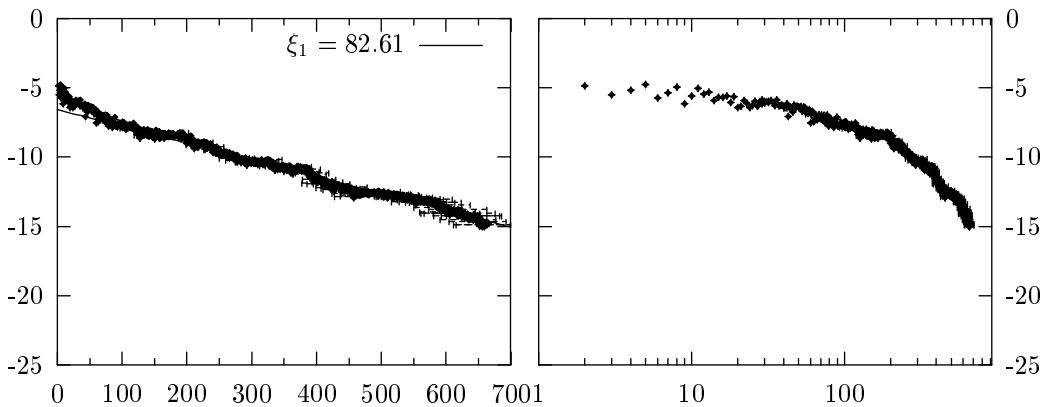


FIGURE 118. $\langle \log t_N \rangle_E$ vs. $N$ in 2D, $W = 12$, $E \in [-4.5, -3.5]$

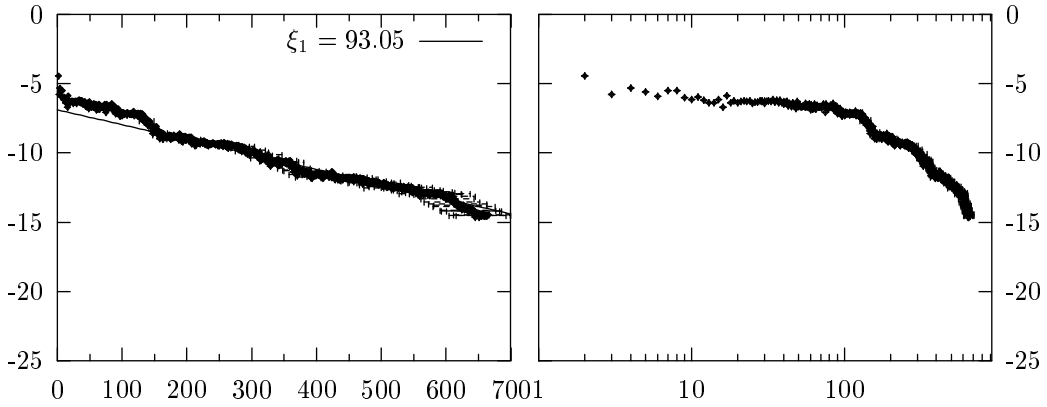


FIGURE 119. $\langle \log t_N \rangle_E$ vs. $N$ in 2D, $W = 12$, $E \in [-3.5, -2.5]$

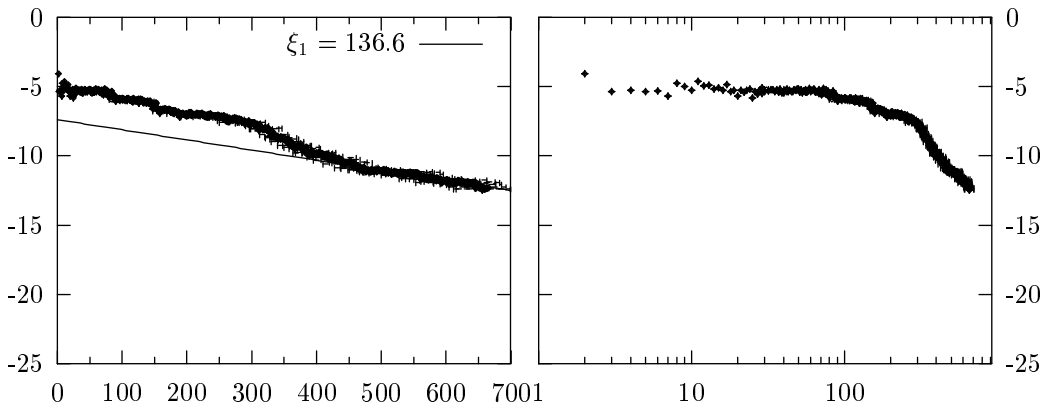


FIGURE 120. $\langle \log t_N \rangle_E$ vs. $N$ in 2D, $W = 12$, $E \in [-2.5, -1.5]$

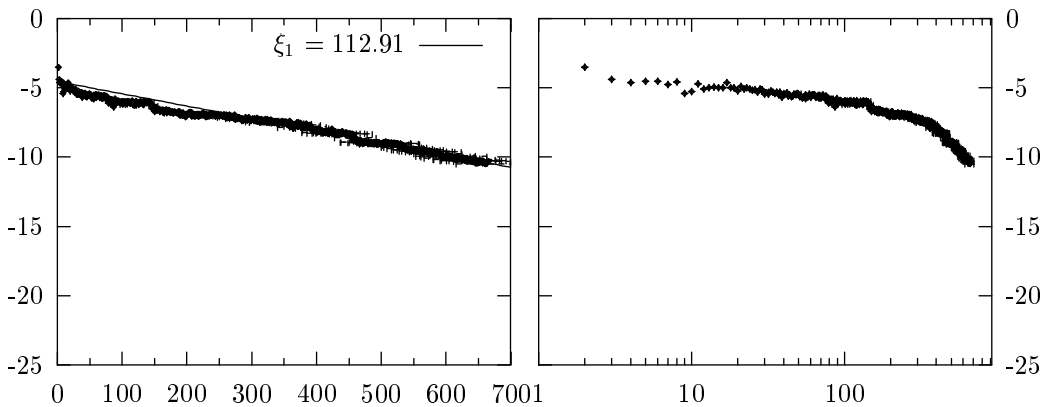


FIGURE 121. $\langle \log t_N \rangle_E$ vs. $N$ in 2D, $W = 12$, $E \in [-1.5, -0.5]$

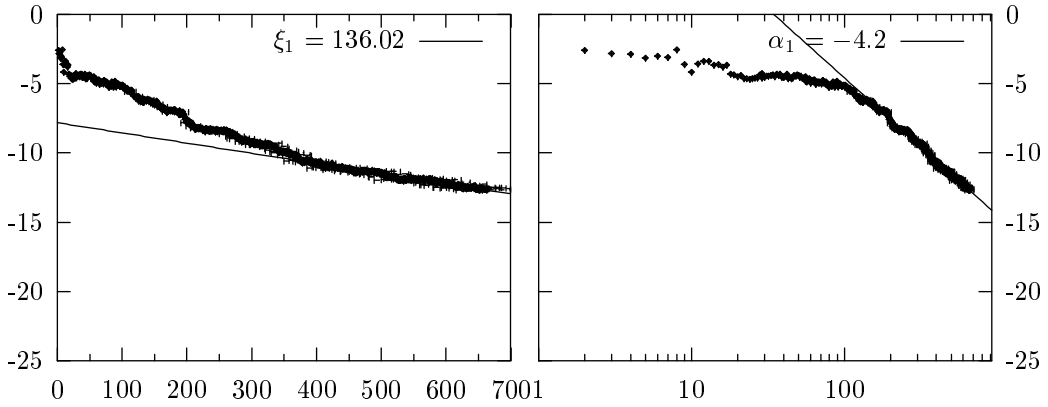


FIGURE 122. $\langle \log t_N \rangle_E$ vs. $N$ in 2D, $W = 12$, $E \in [-0.5, 0.5]$

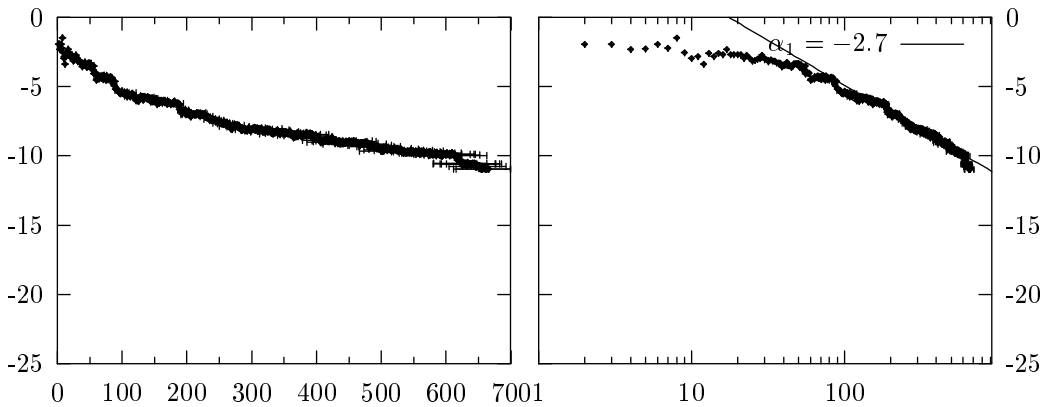


FIGURE 123. $\langle \log t_N \rangle_E$ vs. $N$ in 2D, $W = 12$, $E \in [0.5, 1.5]$

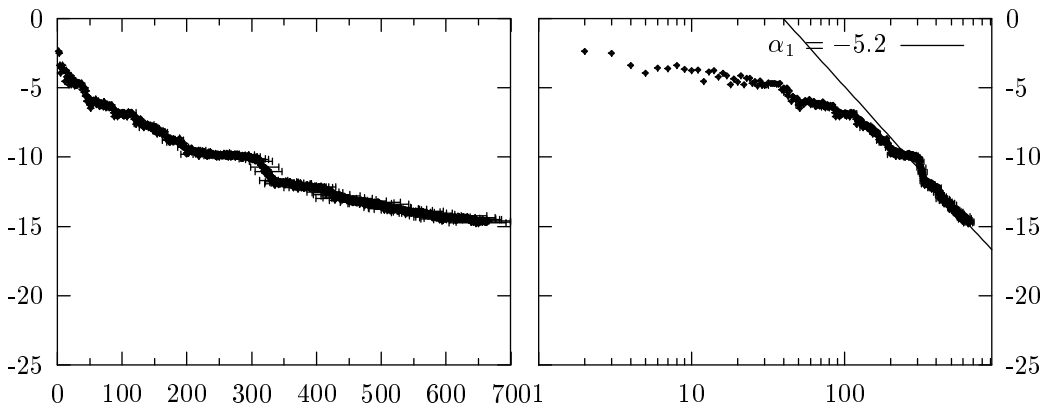


FIGURE 124. $\langle \log t_N \rangle_E$ vs. $N$ in 2D, $W = 12$, $E \in [1.5, 2.5]$

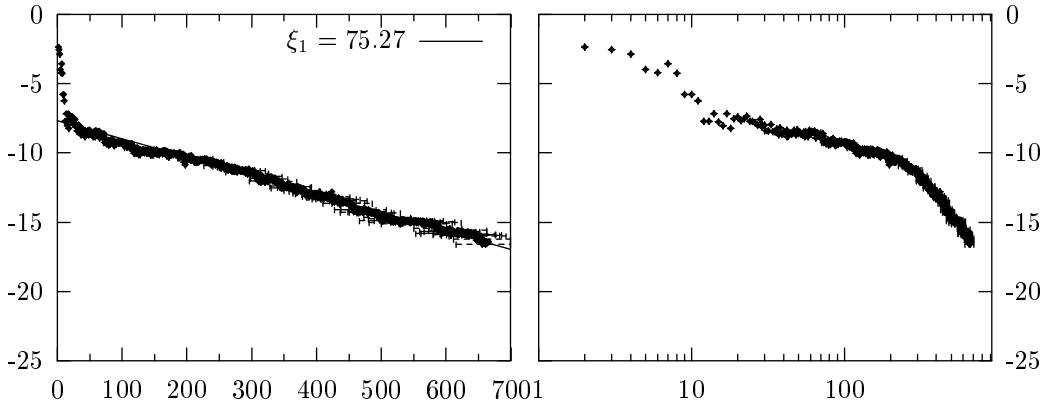


FIGURE 125. $\langle \log t_N \rangle_E$ vs. $N$ in 2D, $W = 12$, $E \in [2.5, 3.5]$

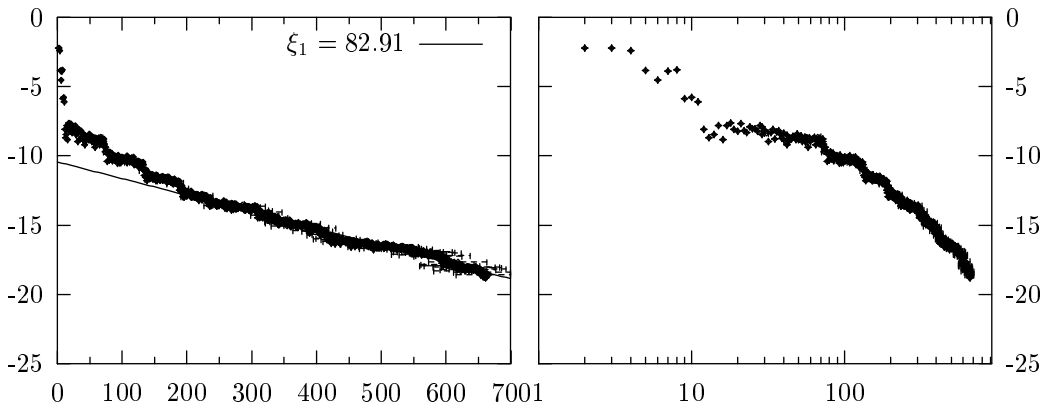


FIGURE 126. $\langle \log t_N \rangle_E$ vs. $N$ in 2D, $W = 12$, $E \in [3.5, 4.5]$

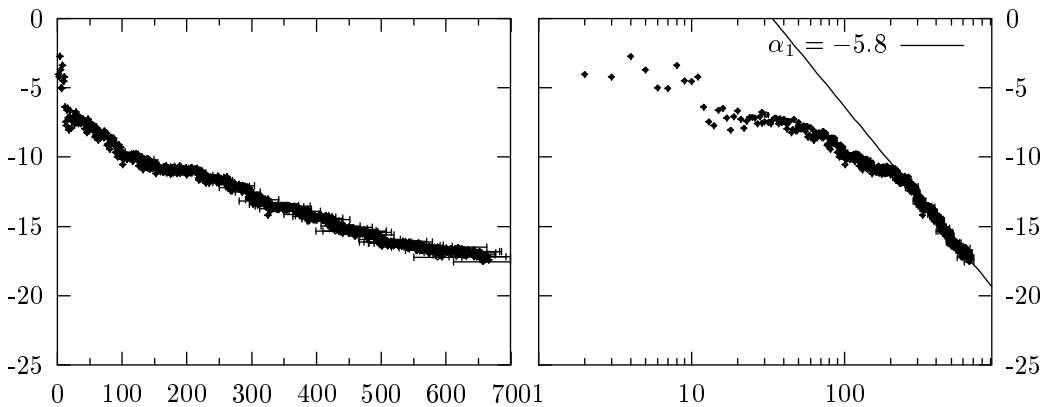


FIGURE 127. $\langle \log t_N \rangle_E$ vs. $N$ in 2D, $W = 12$, $E \in [4.5, 5.5]$

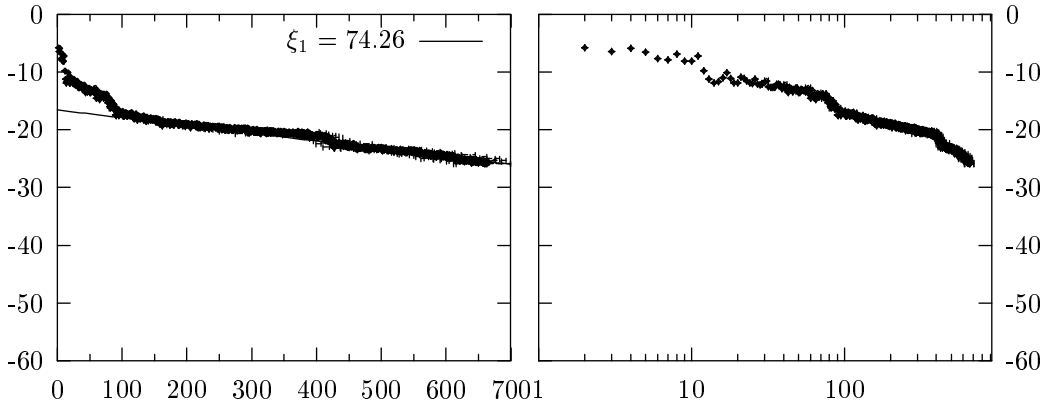


FIGURE 128. $\langle \log t_N \rangle_E$ vs. $N$ in 2D, $W = 12$, $E \in [5.5, 6.5]$

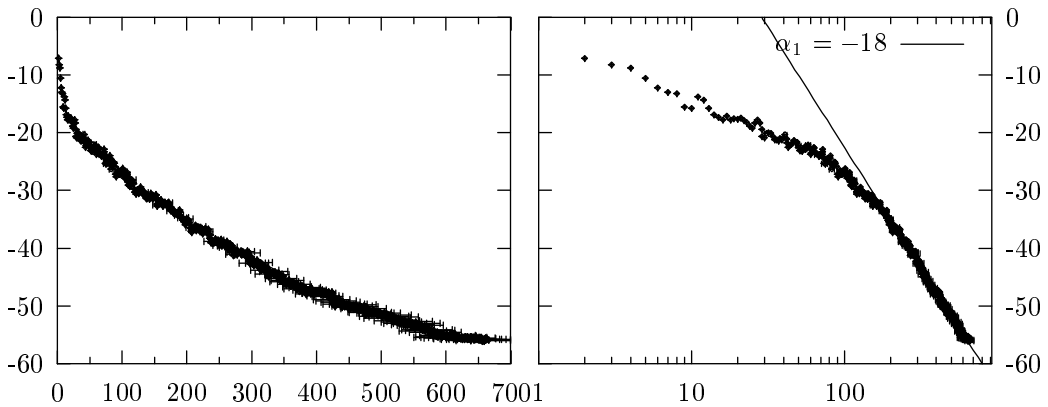


FIGURE 129. $\langle \log t_N \rangle_E$ vs. $N$ in 2D, $W = 12$, $E \in [6.5, 7.5]$

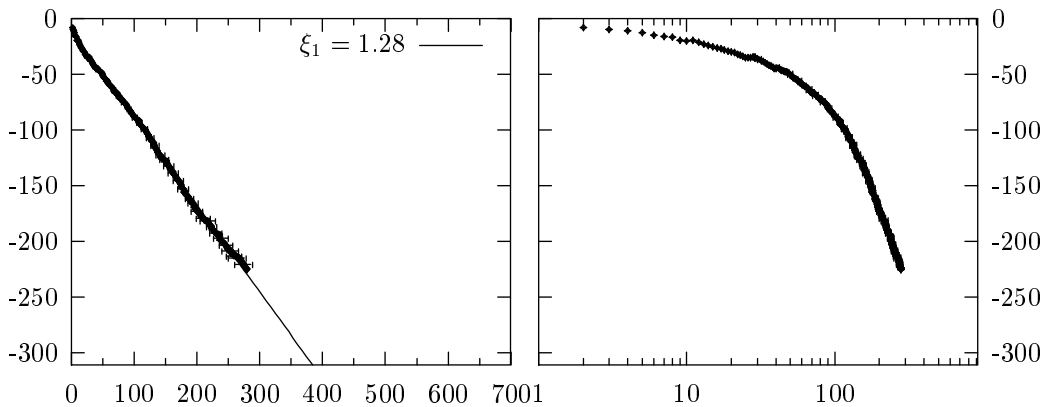


FIGURE 130. $\langle \log t_N \rangle_E$ vs. $N$ in 2D, $W = 12$, $E \in [7.5, 8.5]$

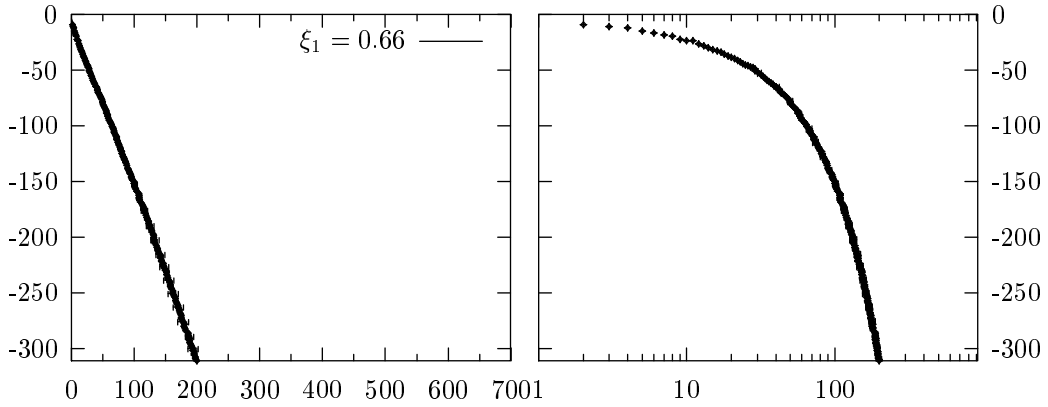


FIGURE 131. $\langle \log t_N \rangle_E$ vs. $N$ in 2D, $W = 12$, $E \in [8.5, 9.5]$

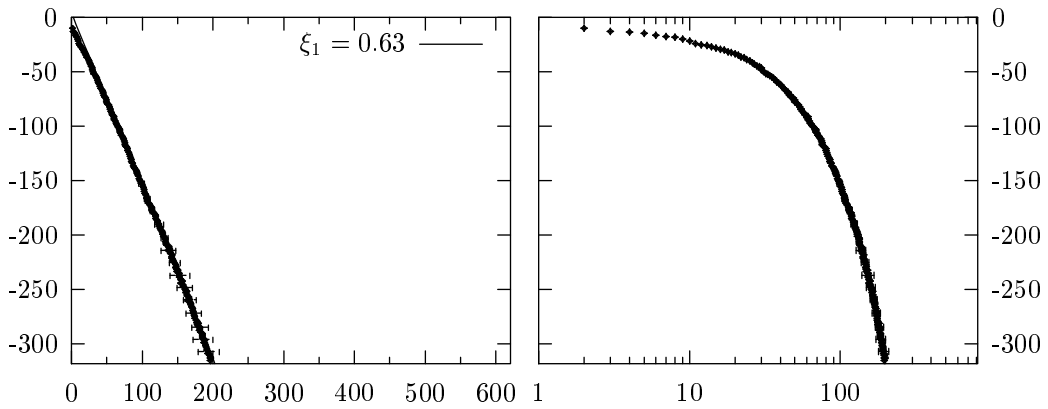


FIGURE 132. $\langle \log t_N \rangle_E$ vs. $N$ in 2D, $W = 16$, $E \in [-11.5, -10.5]$

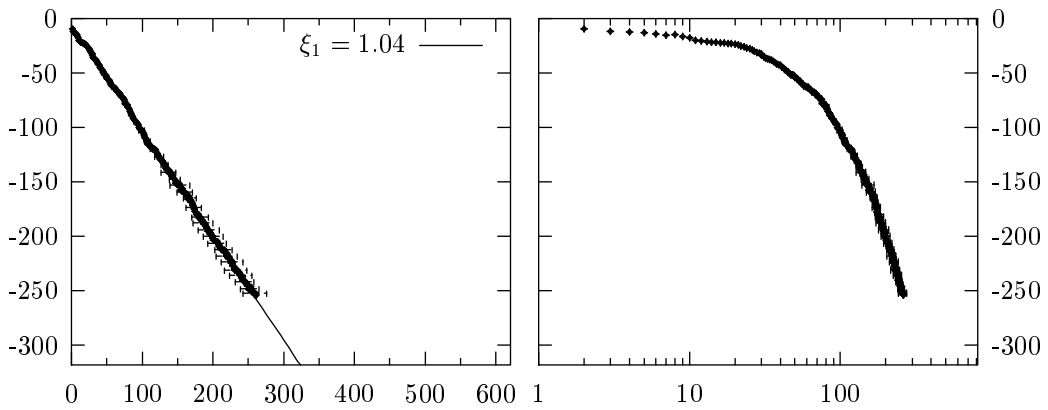


FIGURE 133. $\langle \log t_N \rangle_E$ vs. $N$ in 2D, $W = 16$, $E \in [-10.5, -9.5]$

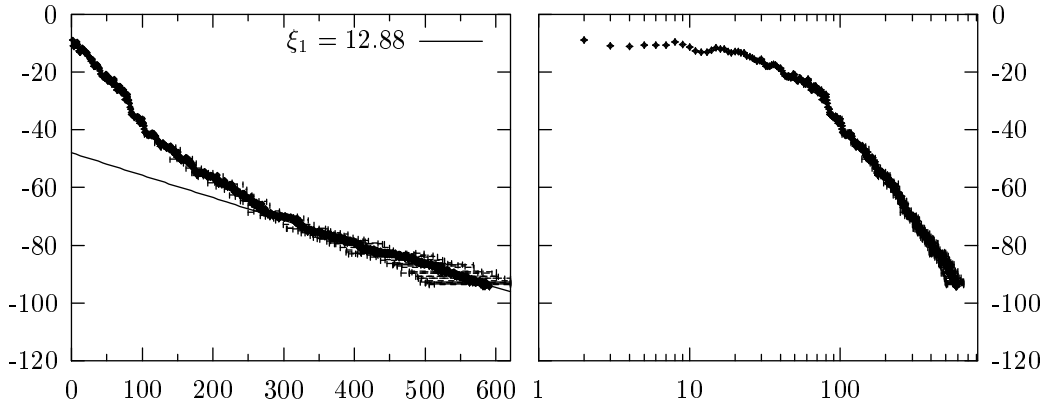


FIGURE 134. $\langle \log t_N \rangle_E$ vs. $N$ in 2D, $W = 16$, $E \in [-9.5, -8.5]$

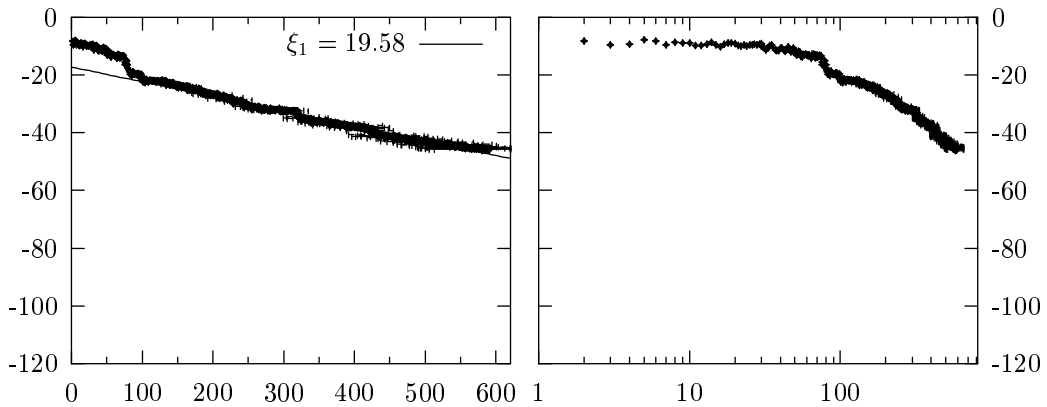


FIGURE 135. $\langle \log t_N \rangle_E$ vs. $N$ in 2D, $W = 16$, $E \in [-8.5, -7.5]$

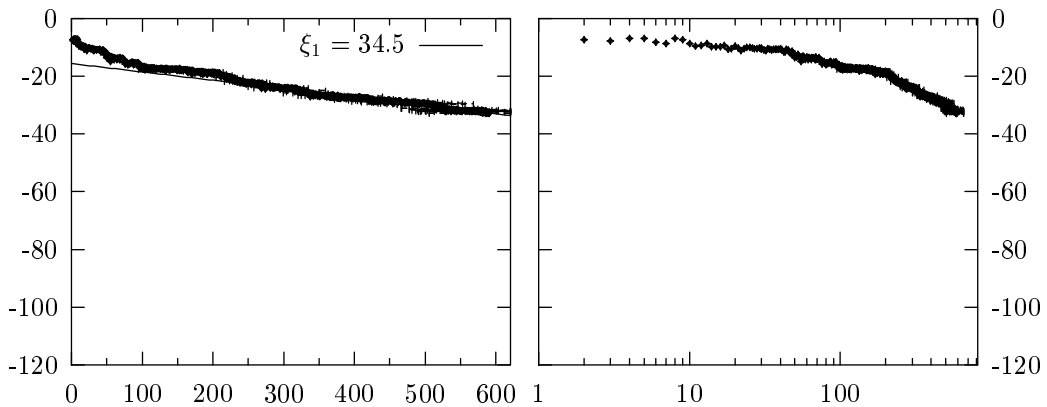


FIGURE 136. $\langle \log t_N \rangle_E$ vs. $N$ in 2D, $W = 16$, $E \in [-7.5, -6.5]$

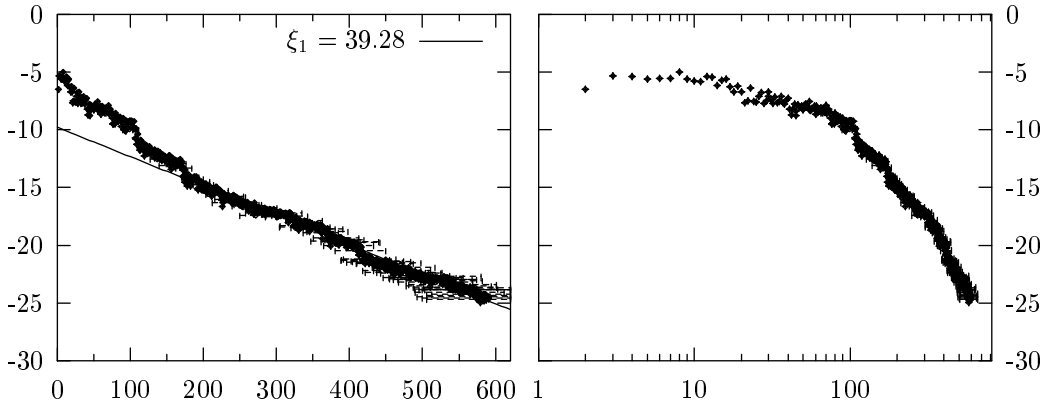


FIGURE 137. $\langle \log t_N \rangle_E$ vs. $N$ in 2D, $W = 16$, $E \in [-6.5, -5.5]$

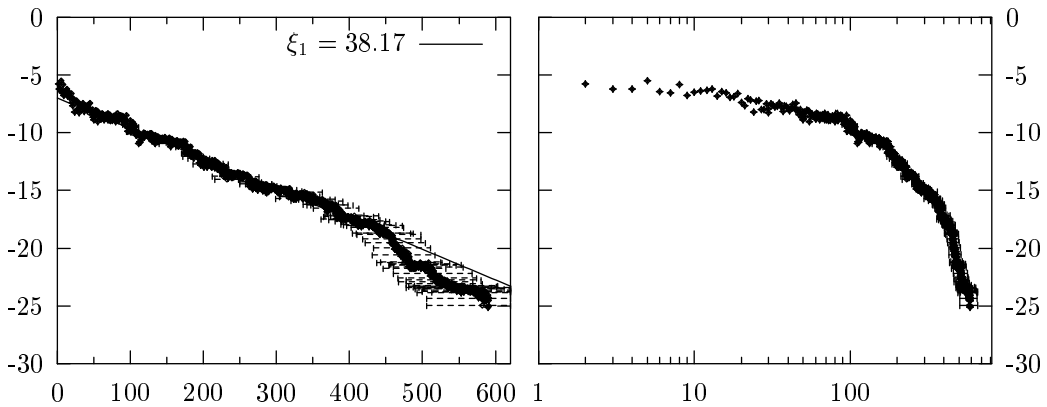


FIGURE 138. $\langle \log t_N \rangle_E$ vs. $N$ in 2D, $W = 16$, $E \in [-5.5, -4.5]$

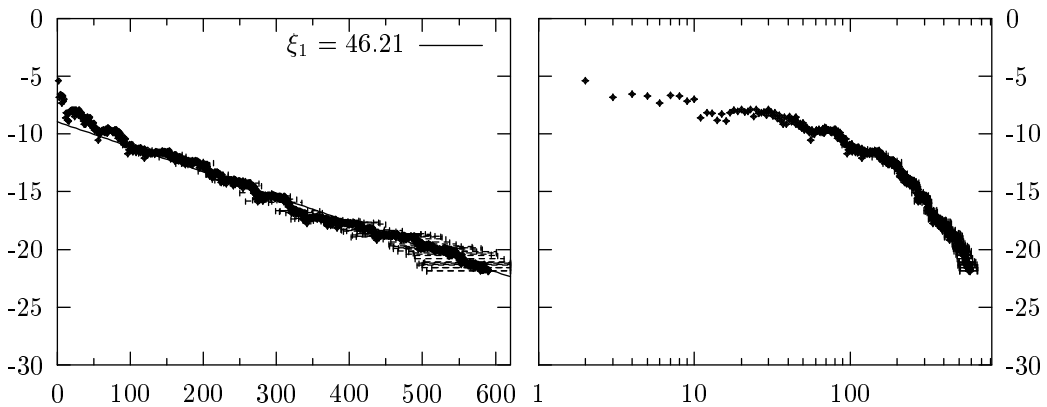


FIGURE 139. $\langle \log t_N \rangle_E$ vs. $N$ in 2D, $W = 16$, $E \in [-4.5, -3.5]$

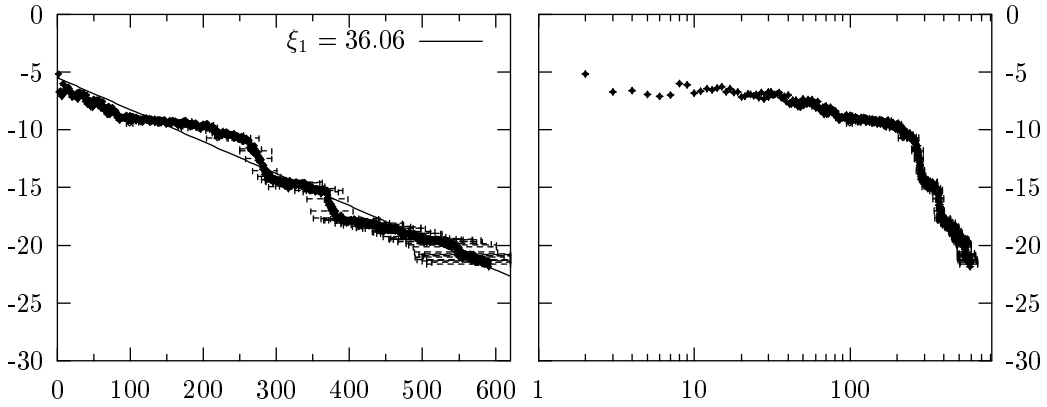


FIGURE 140. $\langle \log t_N \rangle_E$ vs. $N$ in 2D, $W = 16$, $E \in [-3.5, -2.5]$

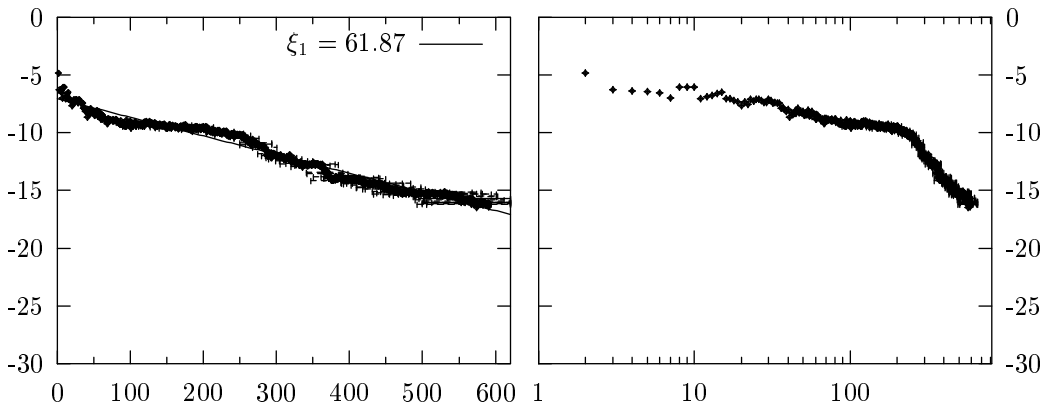


FIGURE 141. $\langle \log t_N \rangle_E$ vs. $N$ in 2D, $W = 16$, $E \in [-2.5, -1.5]$

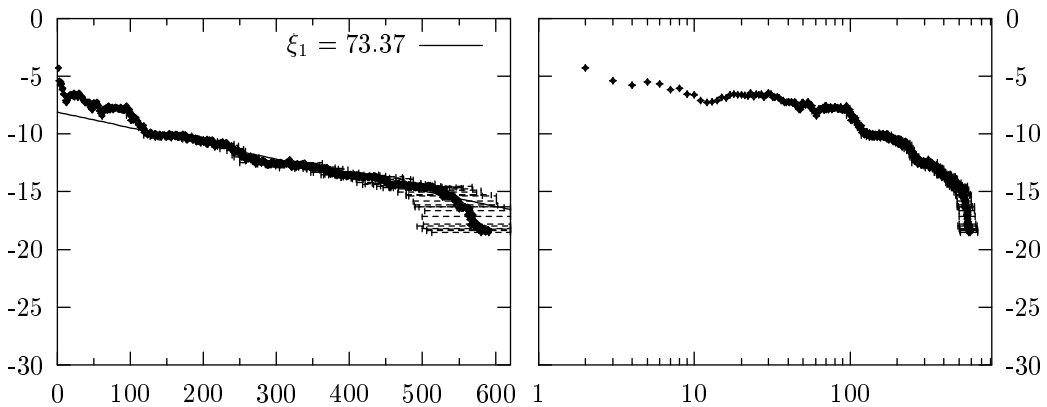


FIGURE 142. $\langle \log t_N \rangle_E$ vs. $N$ in 2D, $W = 16$, $E \in [-1.5, -0.5]$

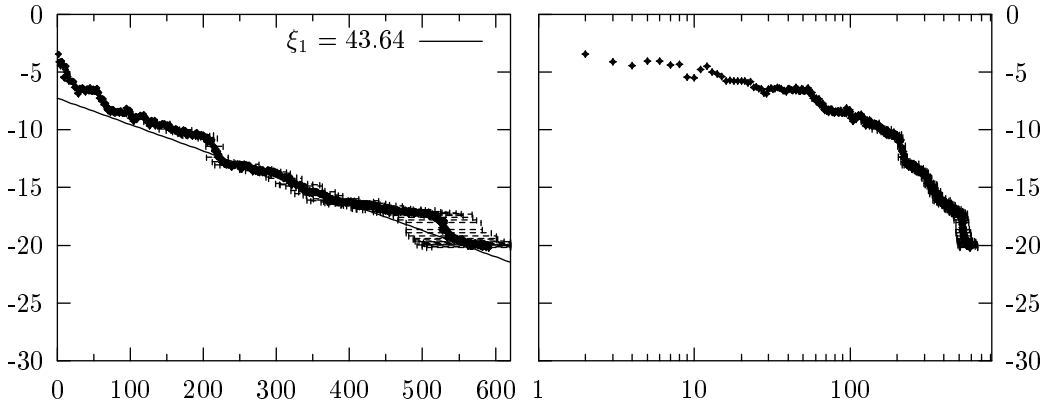


FIGURE 143. $\langle \log t_N \rangle_E$ vs. $N$ in 2D, $W = 16$, $E \in [-0.5, 0.5]$

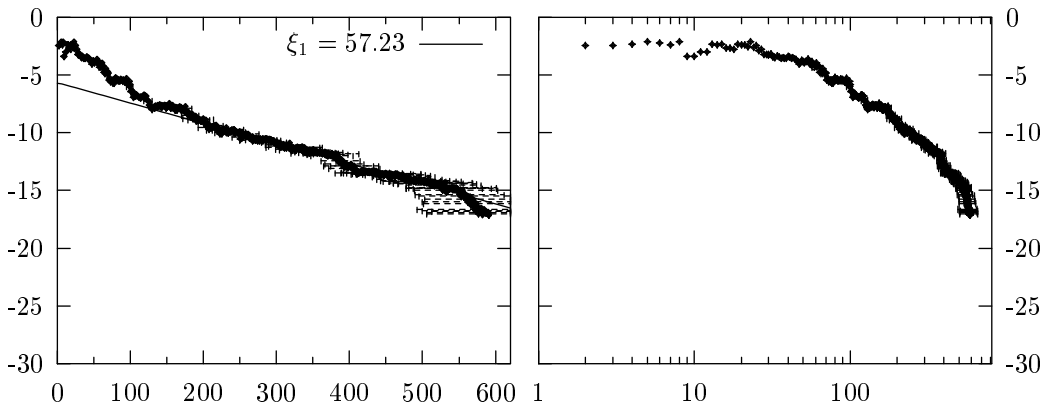


FIGURE 144. $\langle \log t_N \rangle_E$ vs. $N$ in 2D, $W = 16$, $E \in [0.5, 1.5]$

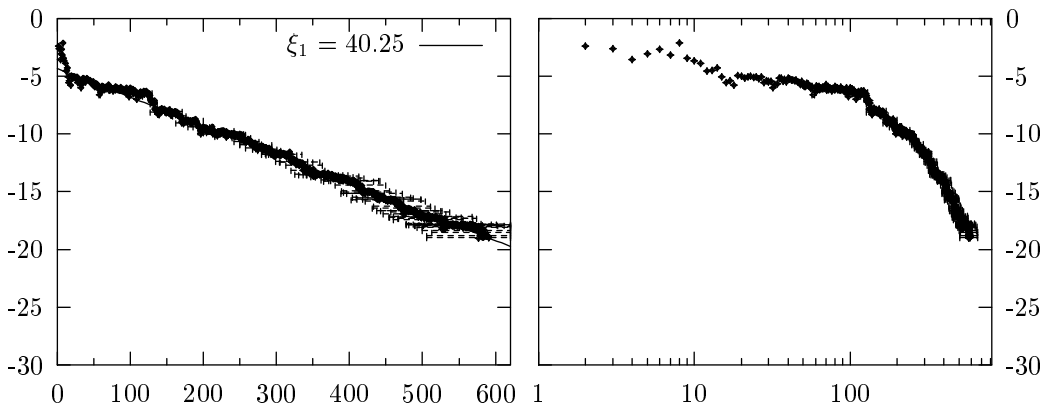


FIGURE 145. $\langle \log t_N \rangle_E$ vs. $N$ in 2D, $W = 16$, $E \in [1.5, 2.5]$

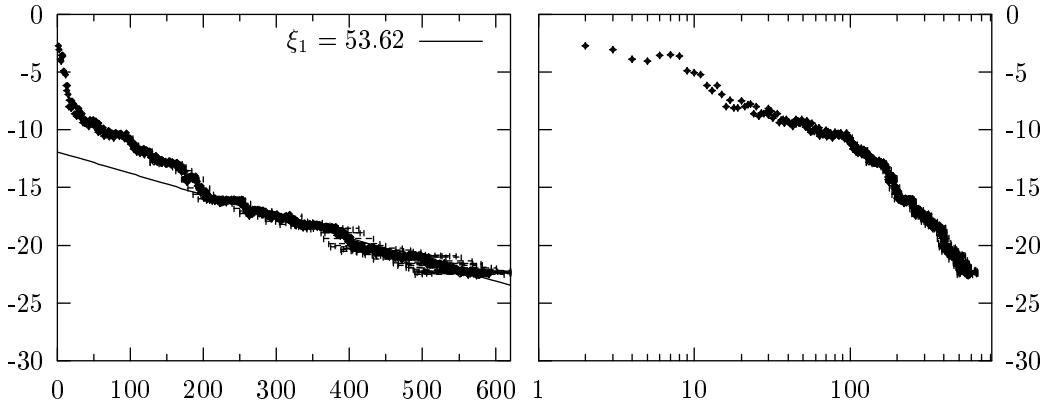


FIGURE 146. $\langle \log t_N \rangle_E$ vs. $N$ in 2D, $W = 16$, $E \in [2.5, 3.5]$

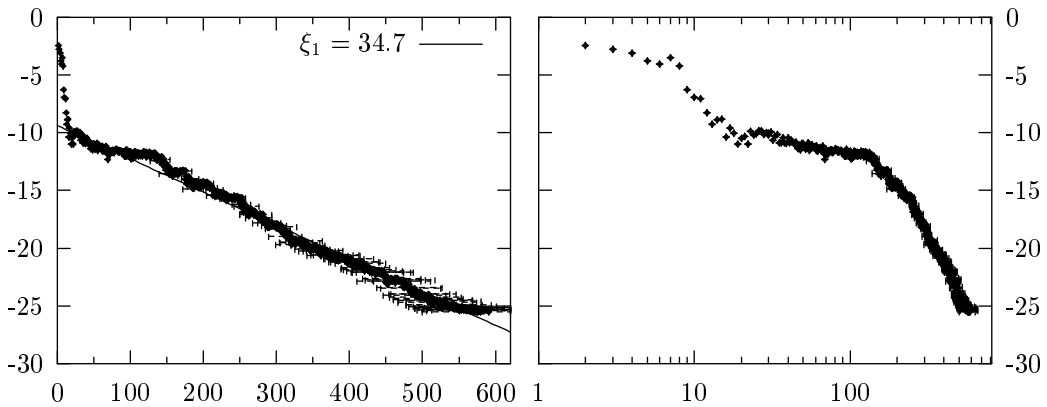


FIGURE 147. $\langle \log t_N \rangle_E$ vs. $N$ in 2D, $W = 16$, $E \in [3.5, 4.5]$

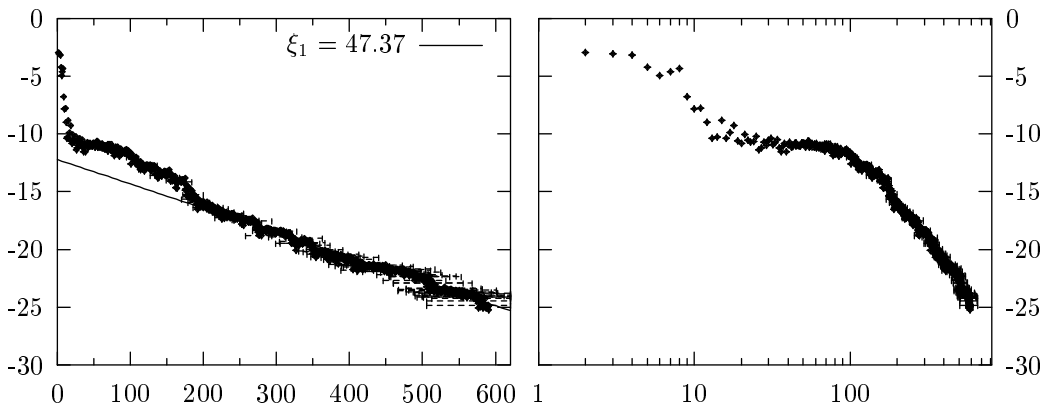


FIGURE 148. $\langle \log t_N \rangle_E$ vs. $N$ in 2D, $W = 16$, $E \in [4.5, 5.5]$

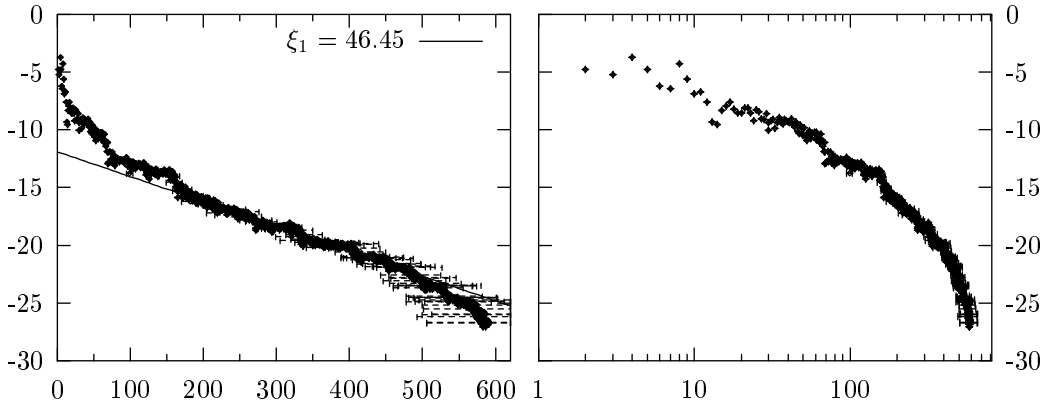


FIGURE 149. $\langle \log t_N \rangle_E$ vs. $N$ in 2D, $W = 16$, $E \in [5.5, 6.5]$

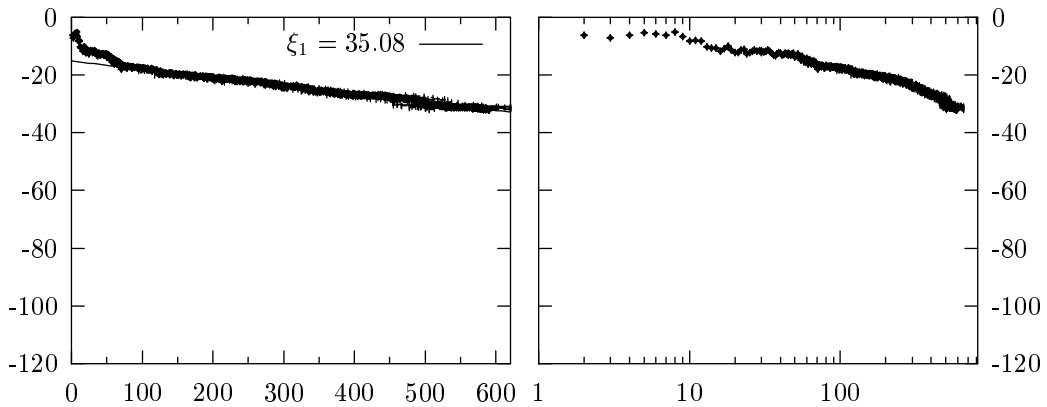


FIGURE 150. $\langle \log t_N \rangle_E$ vs. $N$ in 2D, $W = 16$, $E \in [6.5, 7.5]$

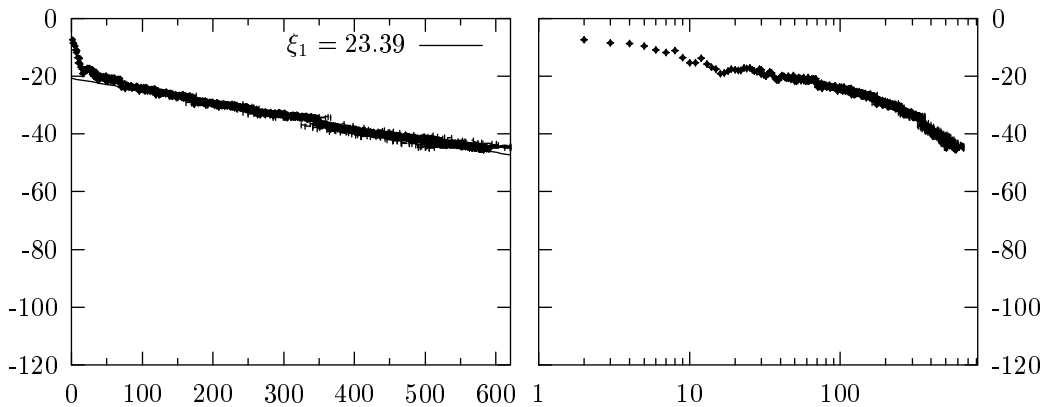


FIGURE 151. $\langle \log t_N \rangle_E$ vs. $N$ in 2D, $W = 16$, $E \in [7.5, 8.5]$

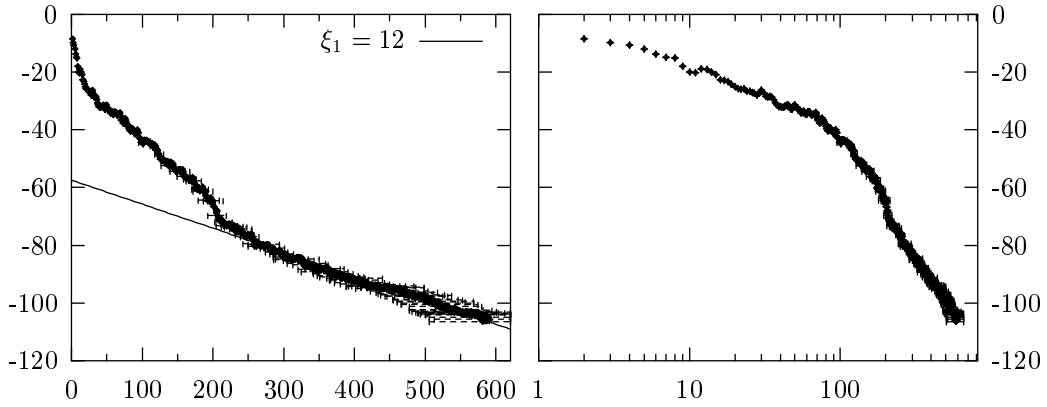


FIGURE 152. $\langle \log t_N \rangle_E$ vs. $N$ in 2D, $W = 16$, $E \in [8.5, 9.5]$

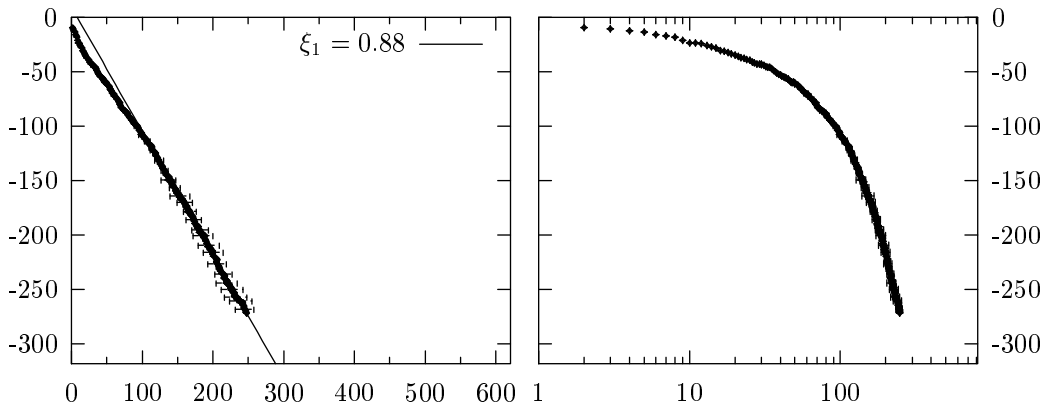


FIGURE 153. $\langle \log t_N \rangle_E$ vs. $N$ in 2D, $W = 16$, $E \in [9.5, 10.5]$

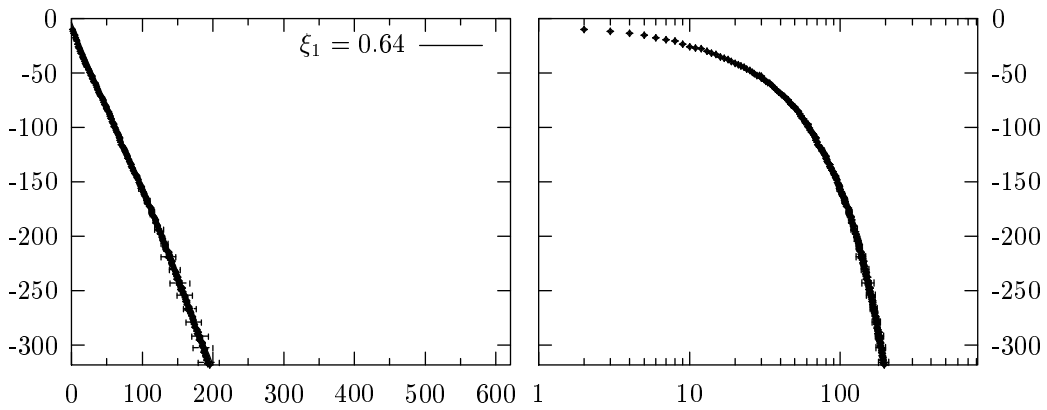


FIGURE 154. $\langle \log t_N \rangle_E$ vs. $N$ in 2D, $W = 16$, $E \in [10.5, 11.5]$

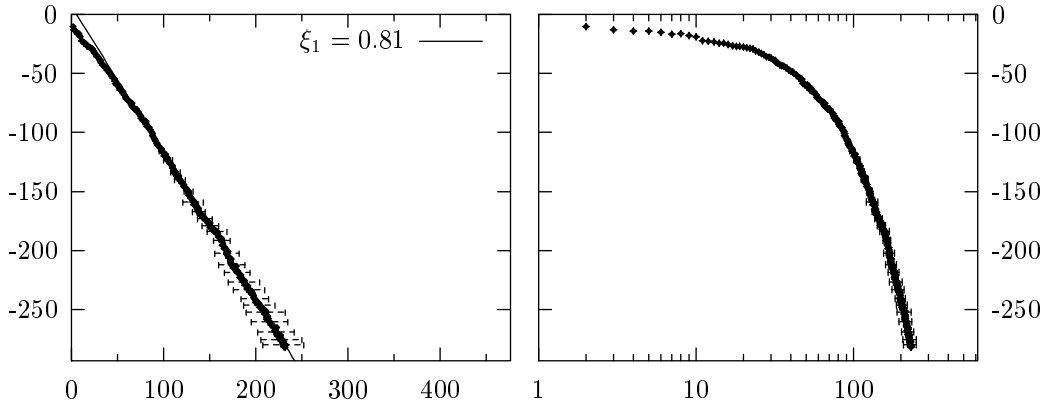


FIGURE 155. $\langle \log t_N \rangle_E$ vs. $N$ in 2D, $W = 20$, $E \in [-12.5, -11.5]$

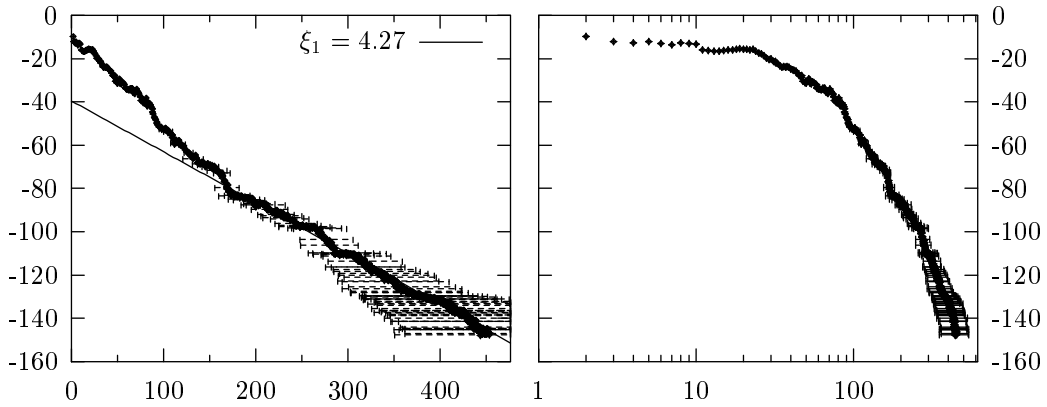


FIGURE 156. $\langle \log t_N \rangle_E$ vs. $N$ in 2D, $W = 20$, $E \in [-11.5, -10.5]$

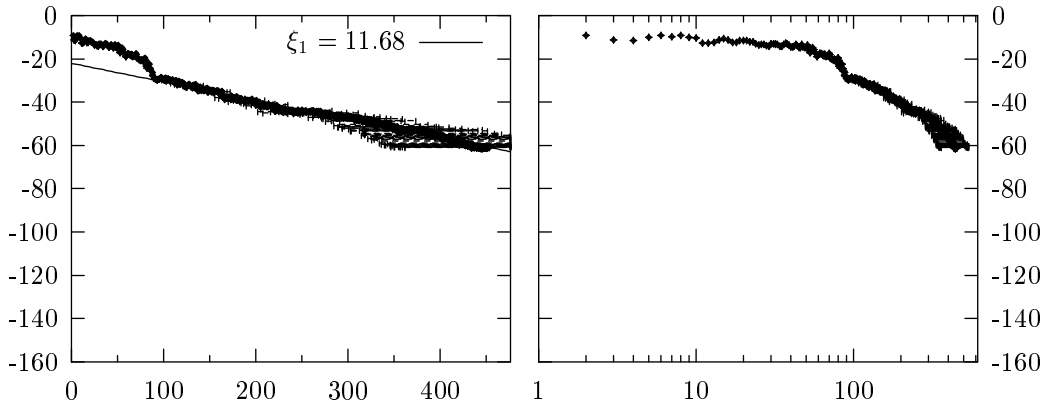


FIGURE 157. $\langle \log t_N \rangle_E$ vs. $N$ in 2D, $W = 20$, $E \in [-10.5, -9.5]$

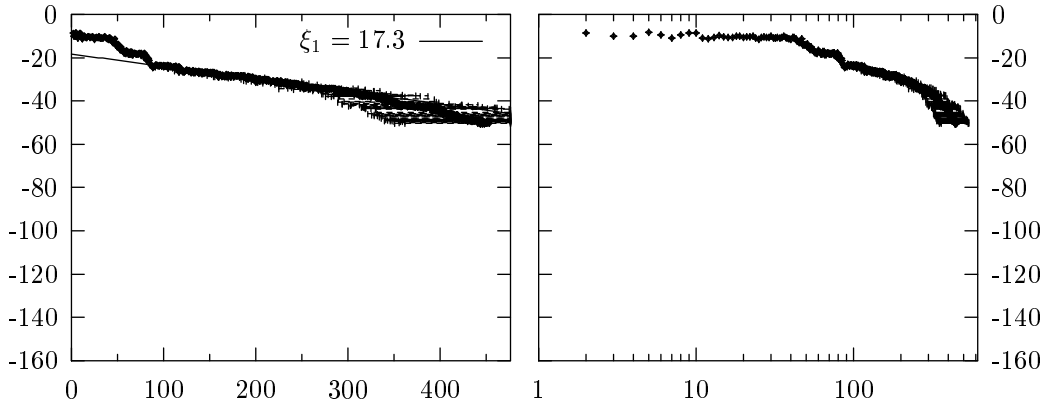


FIGURE 158. $\langle \log t_N \rangle_E$ vs. $N$ in 2D, $W = 20$, $E \in [-9.5, -8.5]$

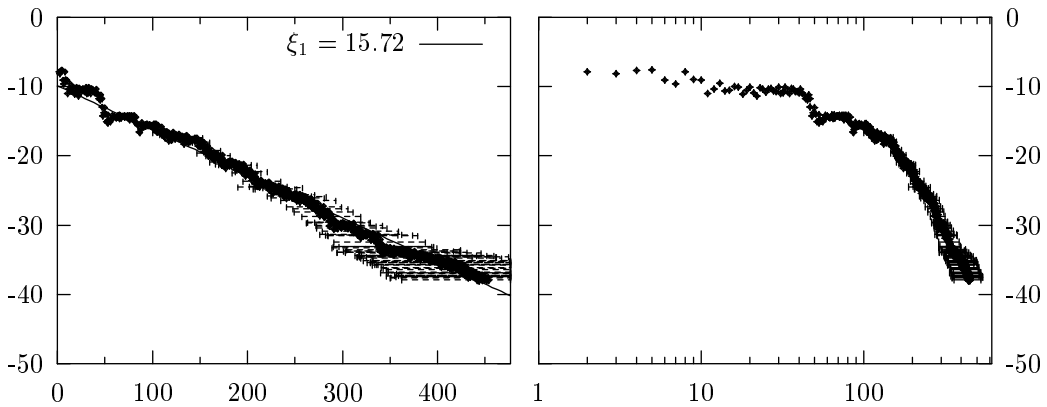


FIGURE 159. $\langle \log t_N \rangle_E$ vs. $N$ in 2D, $W = 20$, $E \in [-8.5, -7.5]$

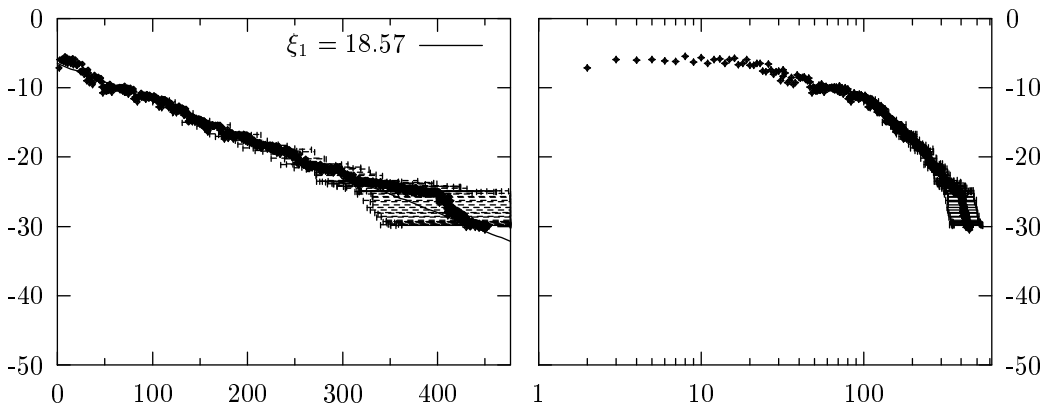


FIGURE 160. $\langle \log t_N \rangle_E$ vs. $N$ in 2D, $W = 20$, $E \in [-7.5, -6.5]$

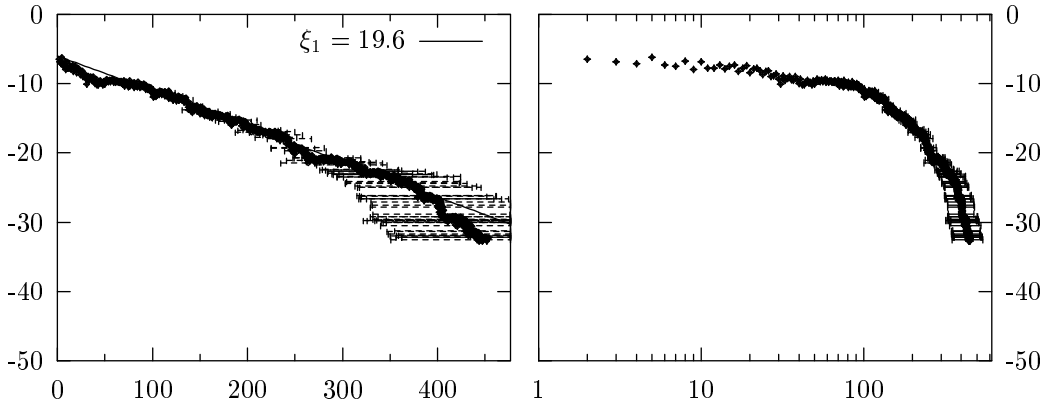


FIGURE 161. $\langle \log t_N \rangle_E$ vs. $N$ in 2D, $W = 20$, $E \in [-6.5, -5.5]$

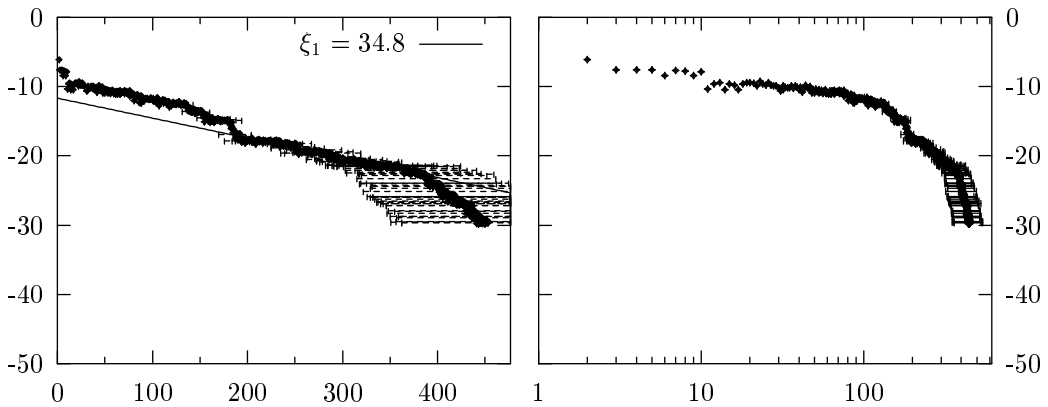


FIGURE 162. $\langle \log t_N \rangle_E$ vs. $N$ in 2D, $W = 20$, $E \in [-5.5, -4.5]$

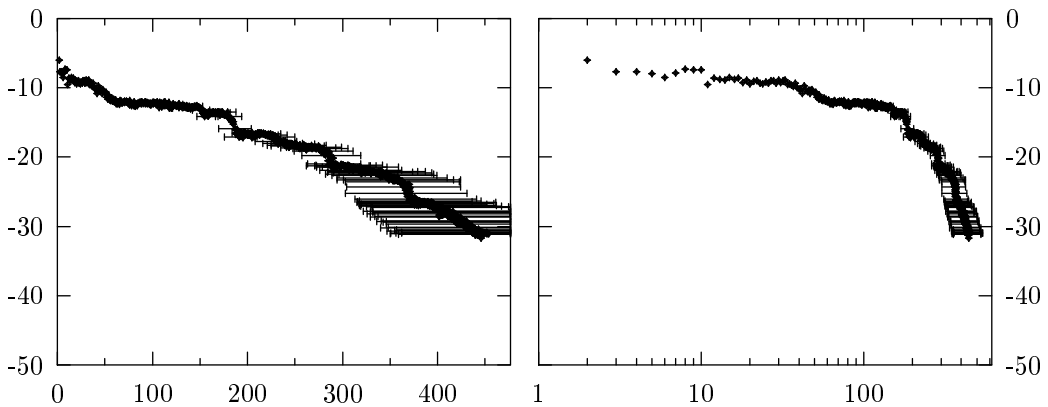


FIGURE 163. $\langle \log t_N \rangle_E$ vs. $N$ in 2D, $W = 20$, $E \in [-4.5, -3.5]$

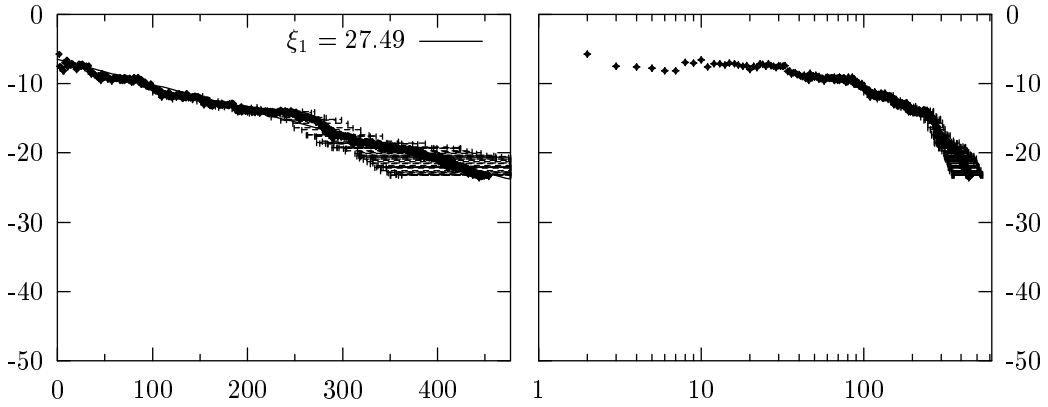


FIGURE 164. $\langle \log t_N \rangle_E$ vs. $N$ in 2D, $W = 20$, $E \in [-3.5, -2.5]$

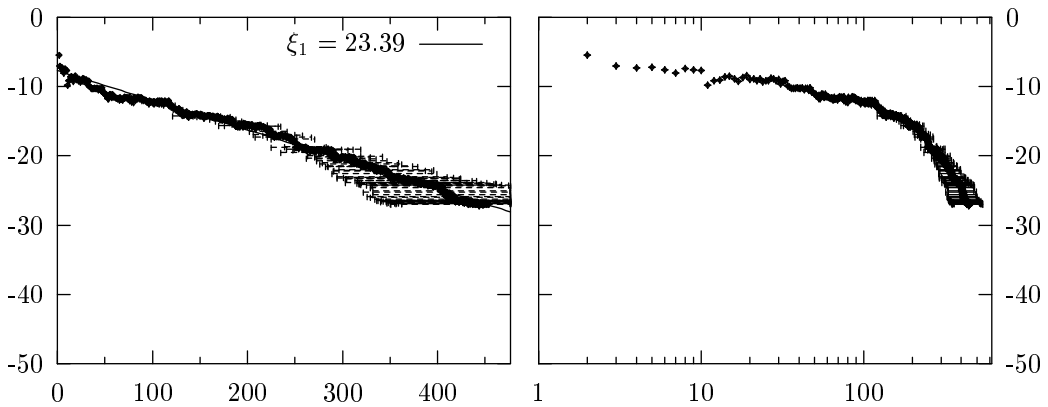


FIGURE 165. $\langle \log t_N \rangle_E$ vs. $N$ in 2D, $W = 20$, $E \in [-2.5, -1.5]$

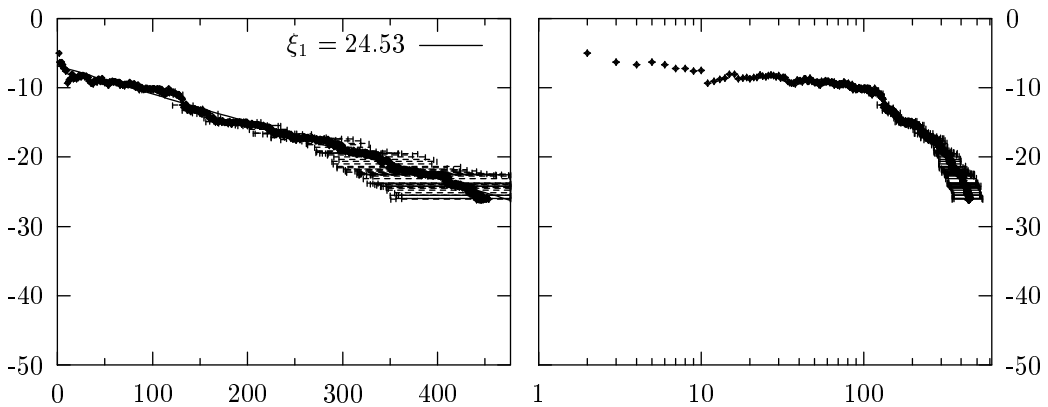


FIGURE 166. $\langle \log t_N \rangle_E$ vs. $N$ in 2D, $W = 20$, $E \in [-1.5, -0.5]$

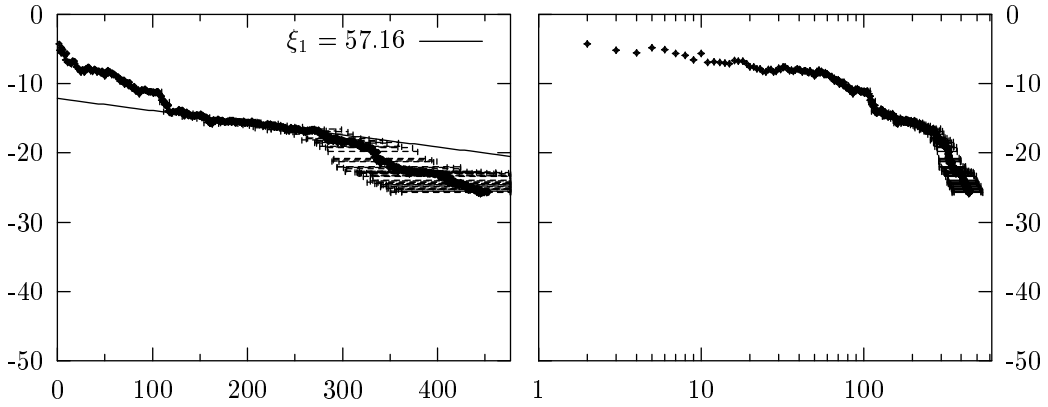


FIGURE 167. $\langle \log t_N \rangle_E$ vs. $N$ in 2D, $W = 20$, $E \in [-0.5, 0.5]$

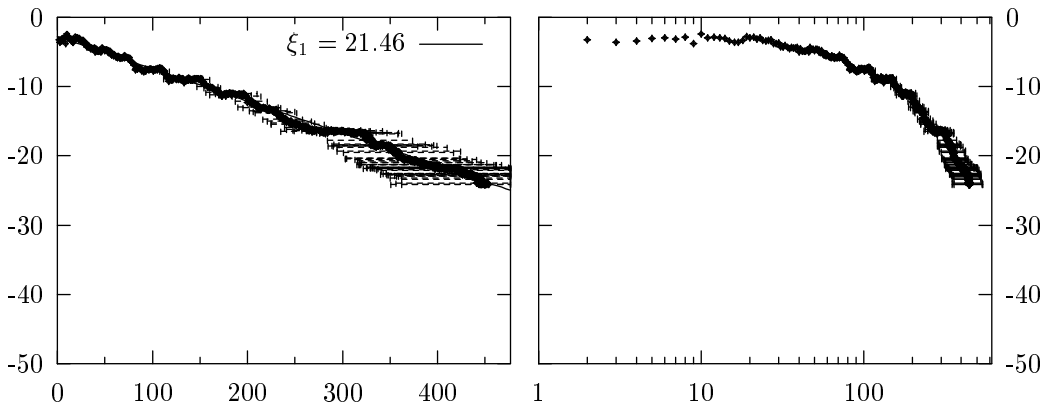


FIGURE 168. $\langle \log t_N \rangle_E$ vs. $N$ in 2D, $W = 20$, $E \in [0.5, 1.5]$

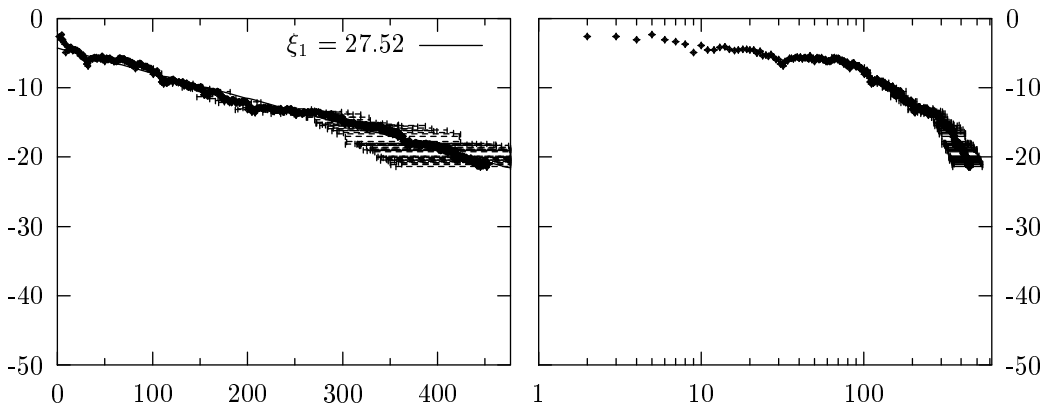


FIGURE 169. $\langle \log t_N \rangle_E$ vs. $N$ in 2D, $W = 20$, $E \in [1.5, 2.5]$

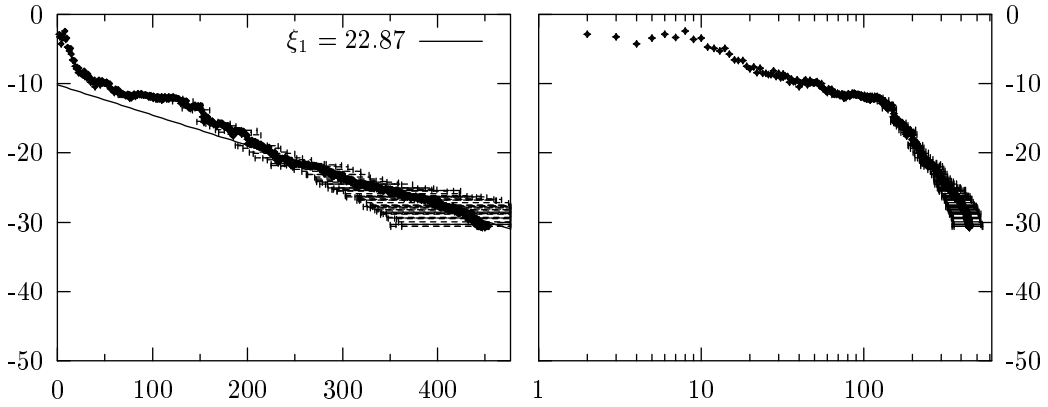


FIGURE 170. $\langle \log t_N \rangle_E$ vs. $N$ in 2D, $W = 20$, $E \in [2.5, 3.5]$

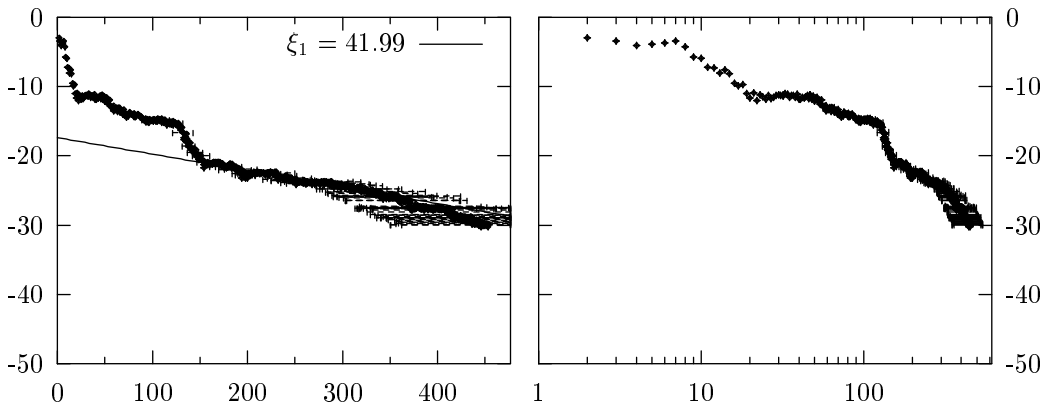


FIGURE 171. $\langle \log t_N \rangle_E$ vs. $N$ in 2D, $W = 20$, $E \in [3.5, 4.5]$

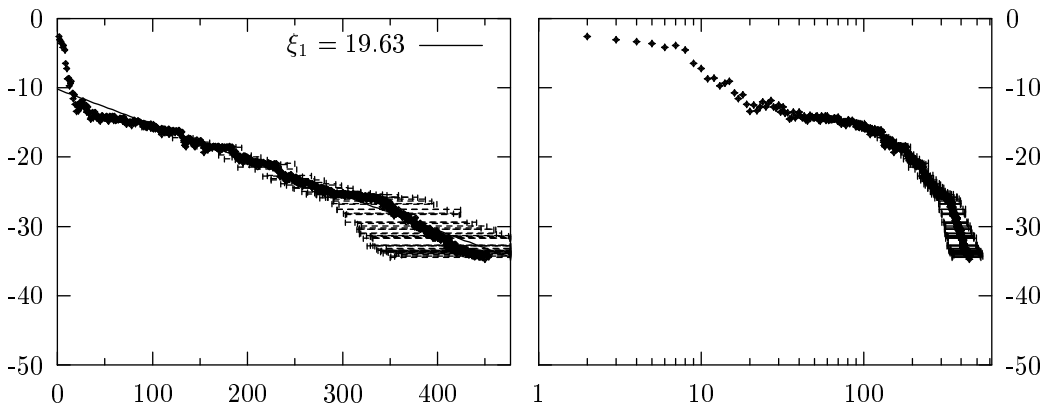


FIGURE 172. $\langle \log t_N \rangle_E$ vs. $N$ in 2D, $W = 20$, $E \in [4.5, 5.5]$

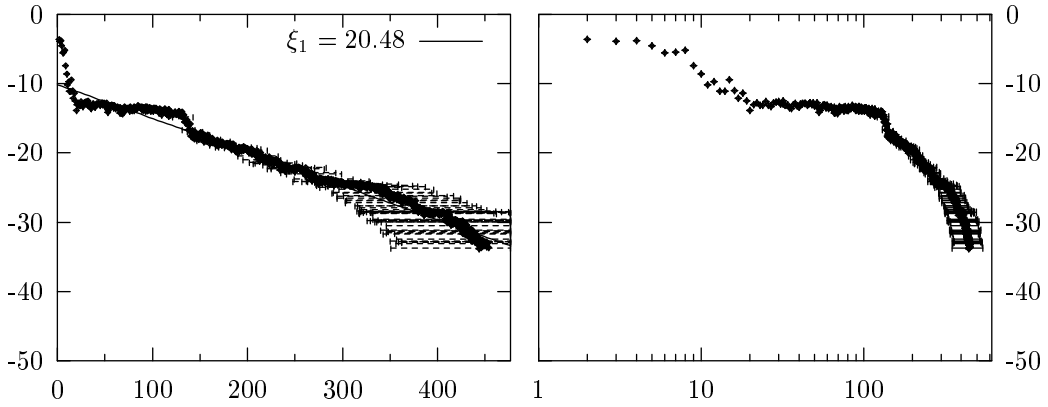


FIGURE 173. $\langle \log t_N \rangle_E$ vs. $N$ in 2D, $W = 20$, $E \in [5.5, 6.5]$

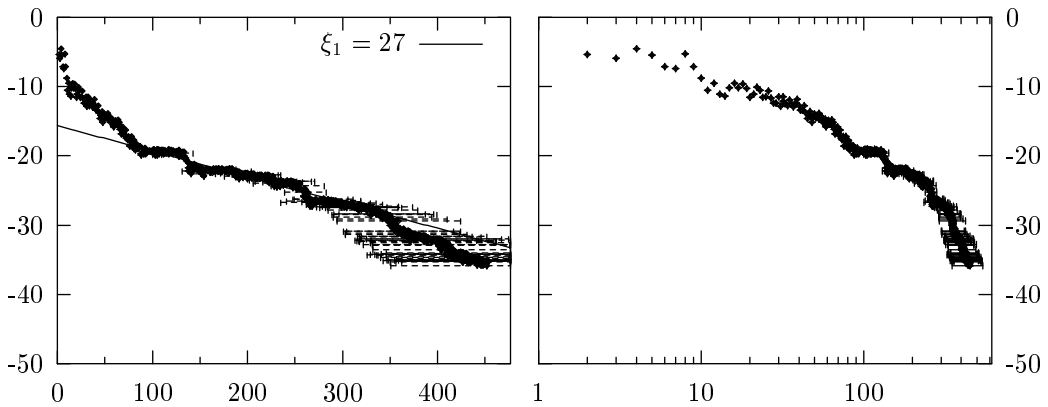


FIGURE 174. $\langle \log t_N \rangle_E$ vs. $N$ in 2D, $W = 20$, $E \in [6.5, 7.5]$

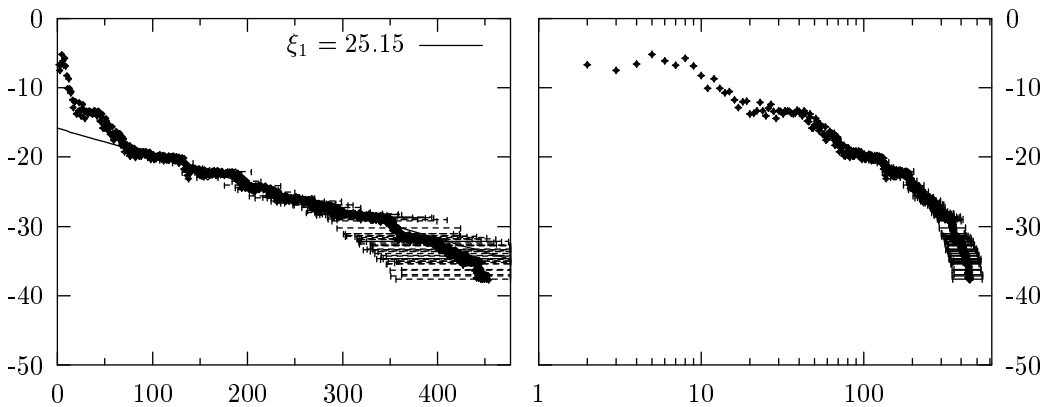


FIGURE 175. $\langle \log t_N \rangle_E$ vs. $N$ in 2D, $W = 20$, $E \in [7.5, 8.5]$

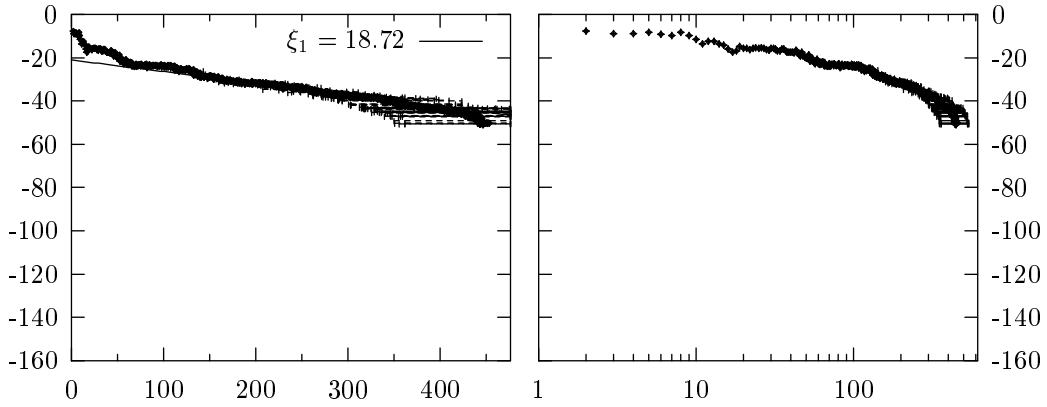


FIGURE 176. $\langle \log t_N \rangle_E$ vs. $N$ in 2D, $W = 20$, $E \in [8.5, 9.5]$

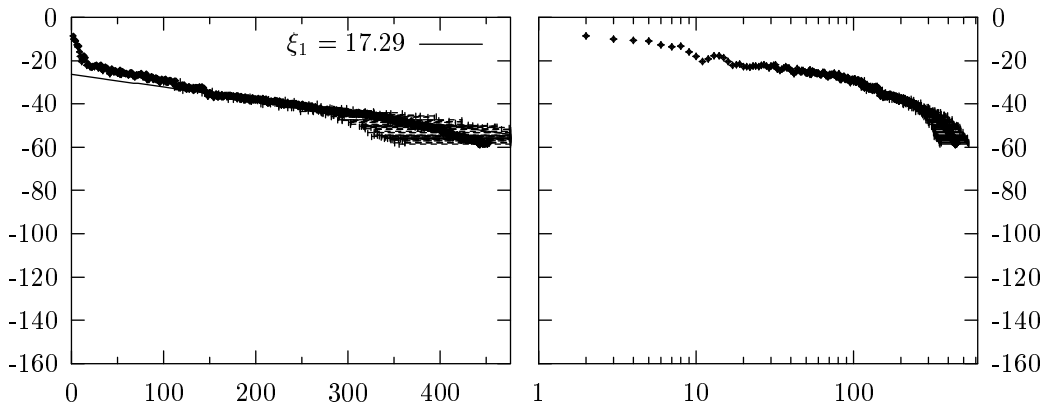


FIGURE 177. $\langle \log t_N \rangle_E$ vs. $N$ in 2D, $W = 20$, $E \in [9.5, 10.5]$

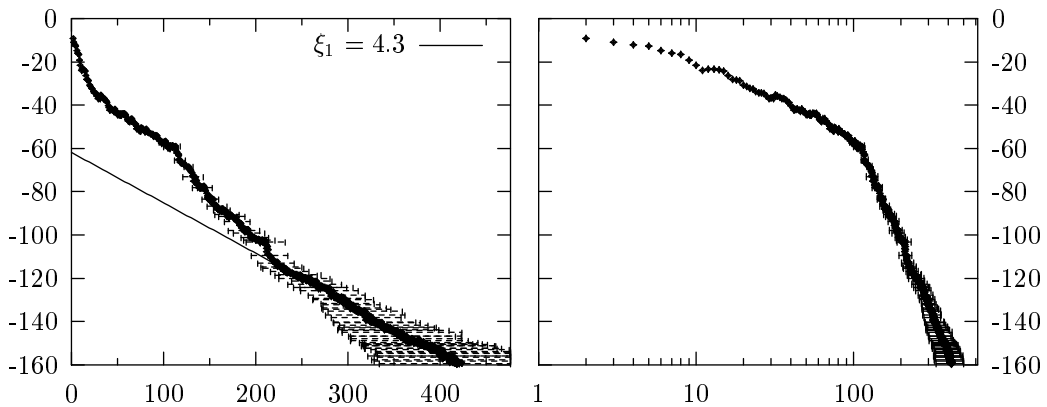


FIGURE 178. $\langle \log t_N \rangle_E$ vs. $N$ in 2D, $W = 20$, $E \in [10.5, 11.5]$

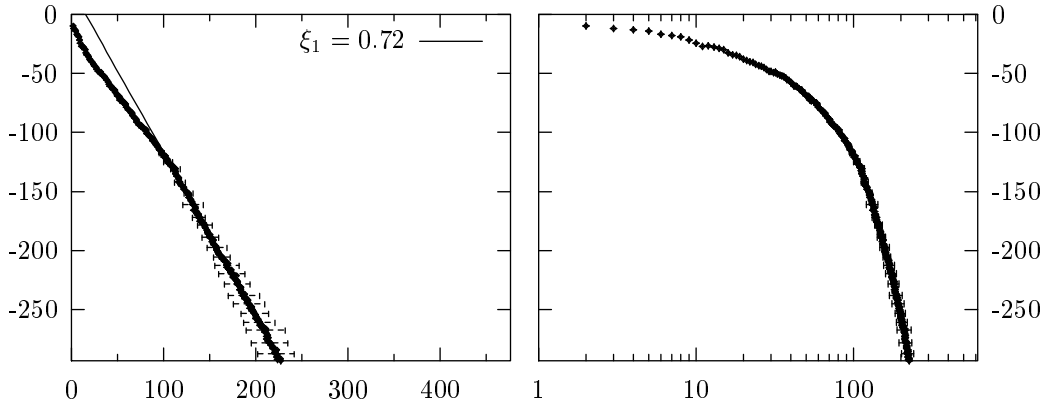


FIGURE 179. $\langle \log t_N \rangle_E$ vs. $N$ in 2D, $W = 20$, $E \in [11.5, 12.5]$

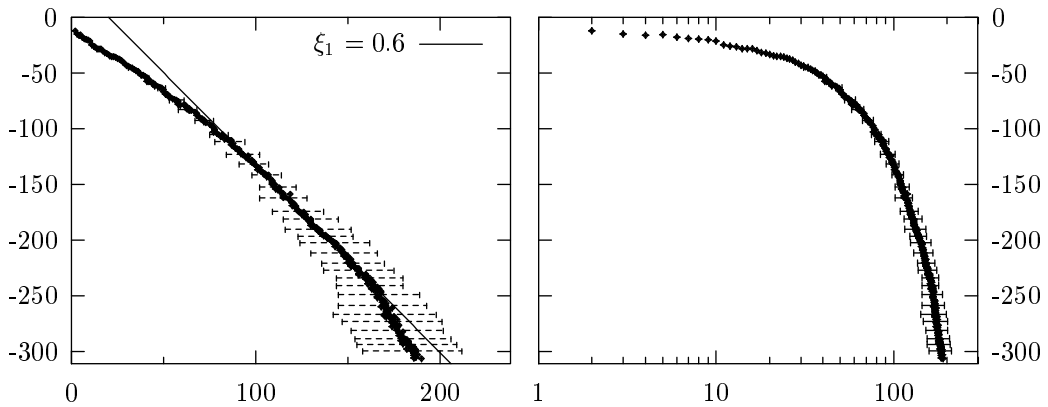


FIGURE 180. $\langle \log t_N \rangle_E$ vs. $N$ in 2D, $W = 30$, $E \in [-17.5, -16.5]$

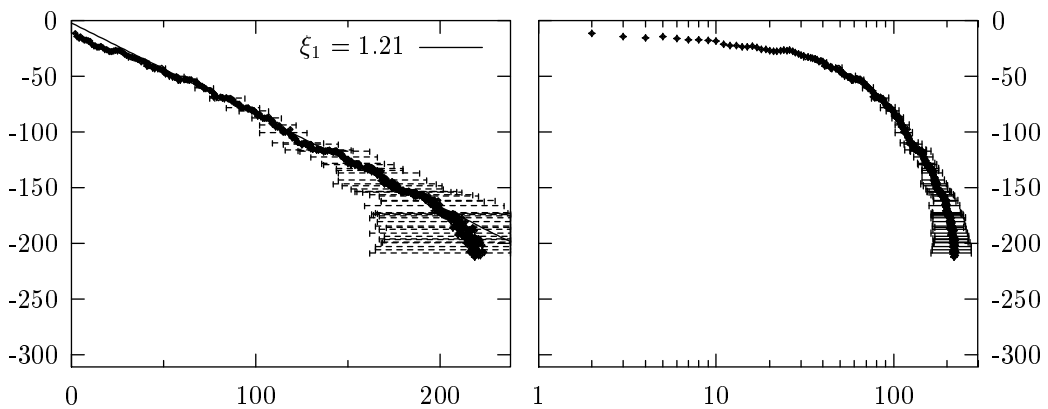


FIGURE 181. $\langle \log t_N \rangle_E$ vs. $N$ in 2D, $W = 30$, $E \in [-16.5, -15.5]$

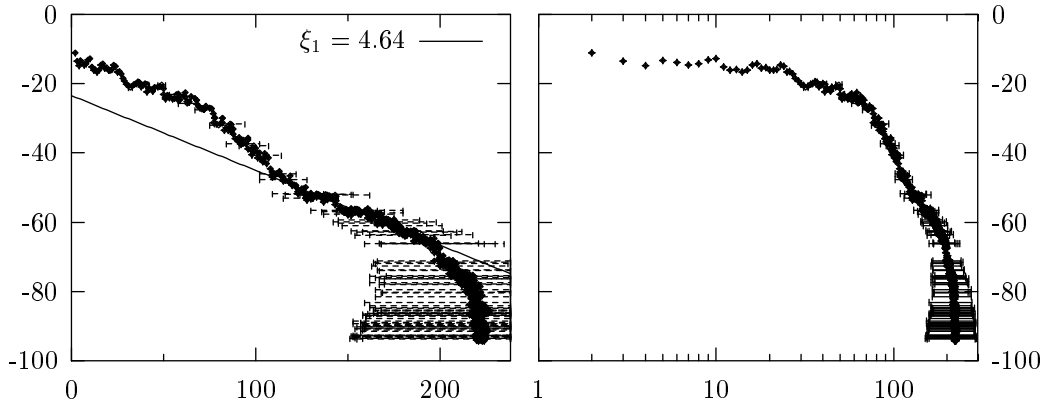


FIGURE 182. $\langle \log t_N \rangle_E$ vs. $N$ in 2D, $W = 30$, $E \in [-15.5, -14.5]$

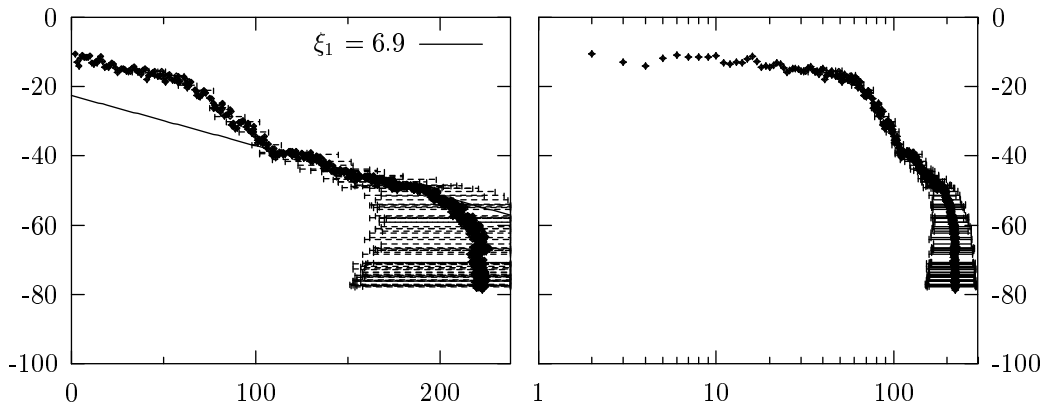


FIGURE 183. $\langle \log t_N \rangle_E$ vs. $N$ in 2D, $W = 30$, $E \in [-14.5, -13.5]$

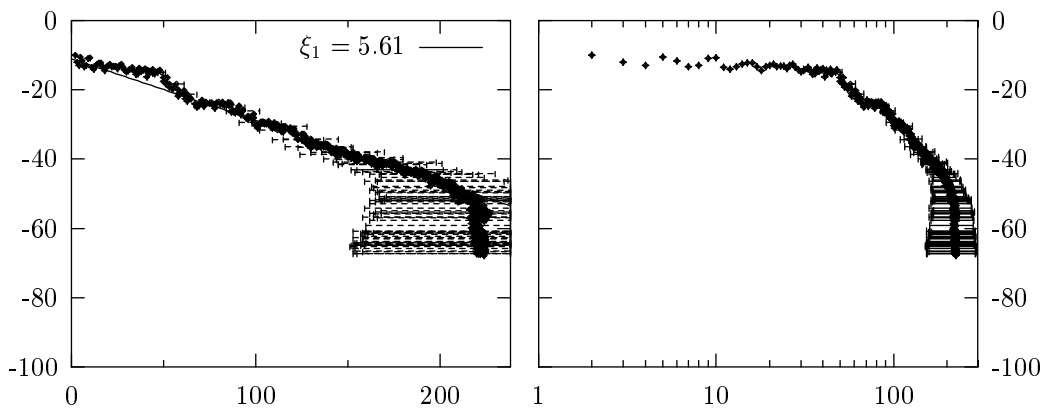


FIGURE 184. $\langle \log t_N \rangle_E$ vs. $N$ in 2D, $W = 30$, $E \in [-13.5, -12.5]$

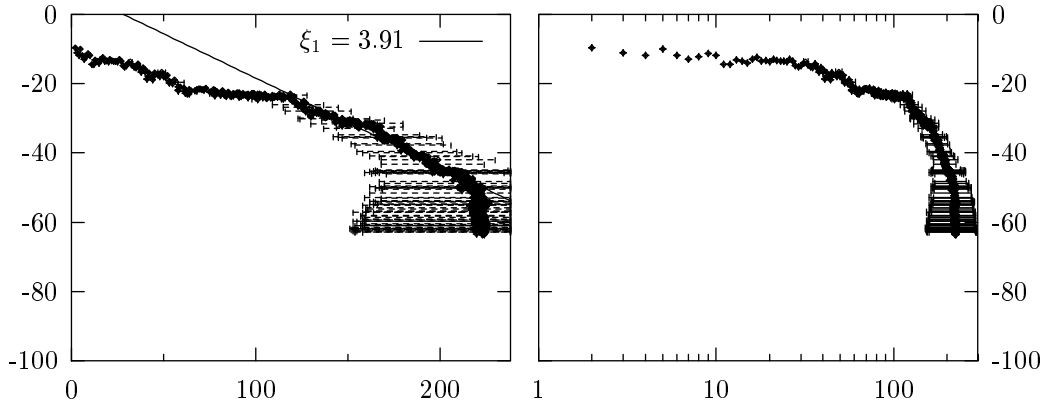


FIGURE 185. $\langle \log t_N \rangle_E$ vs. $N$ in 2D, $W = 30$, $E \in [-12.5, -11.5]$

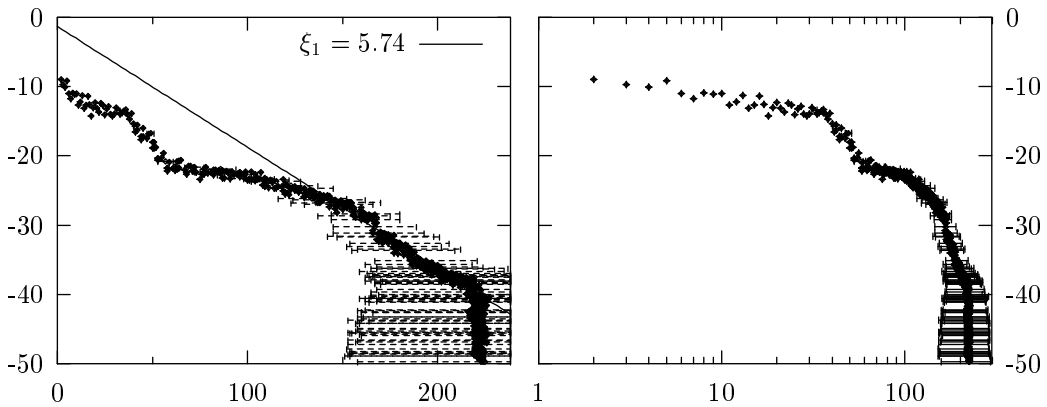


FIGURE 186. $\langle \log t_N \rangle_E$ vs. $N$ in 2D, $W = 30$, $E \in [-11.5, -10.5]$

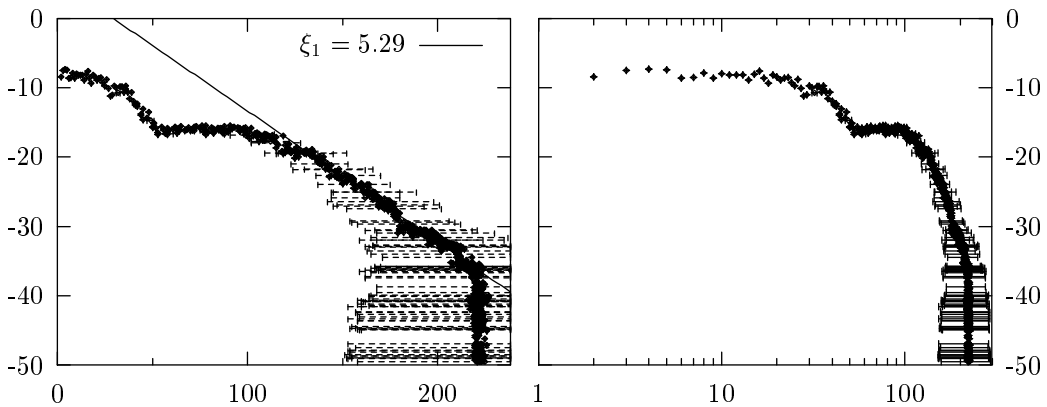


FIGURE 187. $\langle \log t_N \rangle_E$ vs. $N$ in 2D, $W = 30$, $E \in [-10.5, -9.5]$

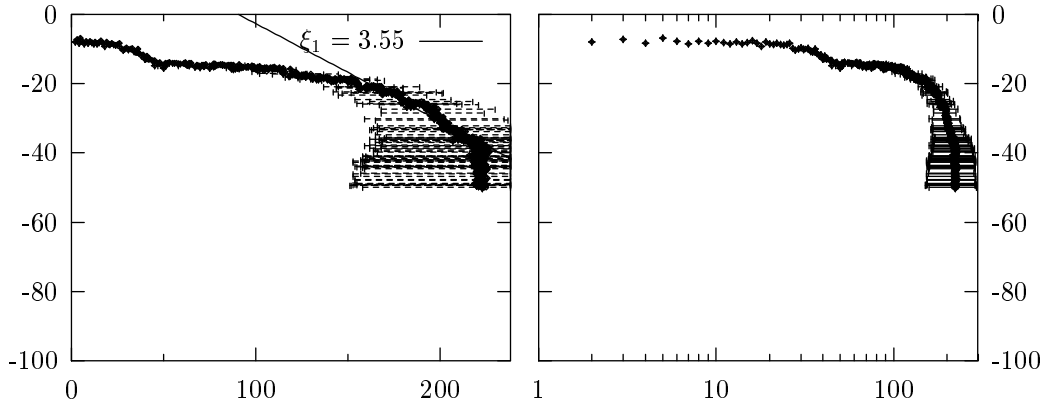


FIGURE 188. $\langle \log t_N \rangle_E$ vs. $N$ in 2D, $W = 30$, $E \in [-9.5, -8.5]$

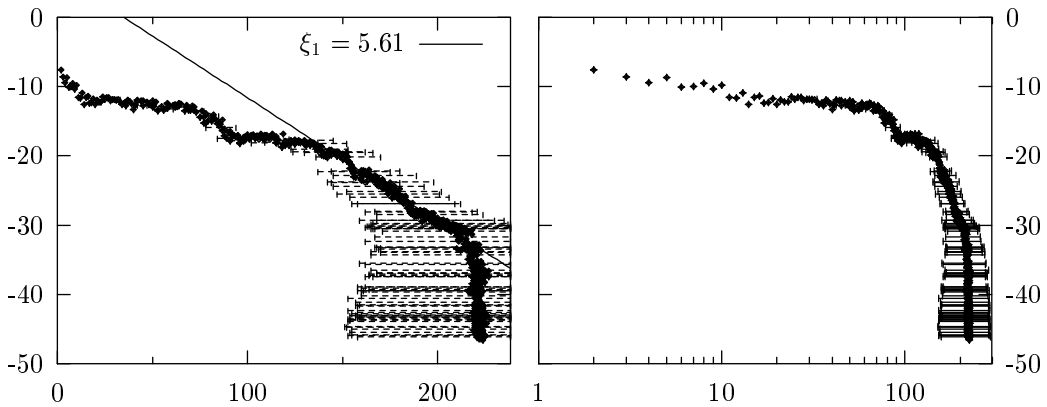


FIGURE 189. $\langle \log t_N \rangle_E$ vs. $N$ in 2D, $W = 30$, $E \in [-8.5, -7.5]$

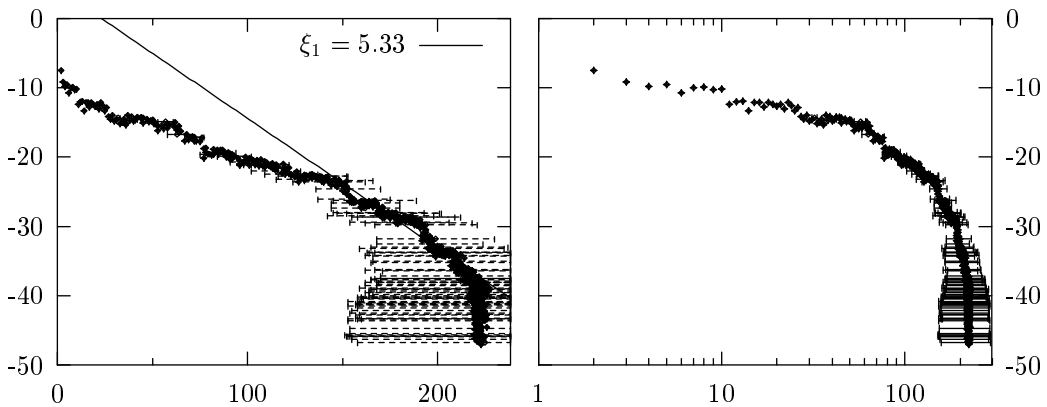


FIGURE 190. $\langle \log t_N \rangle_E$ vs. $N$ in 2D, $W = 30$, $E \in [-7.5, -6.5]$

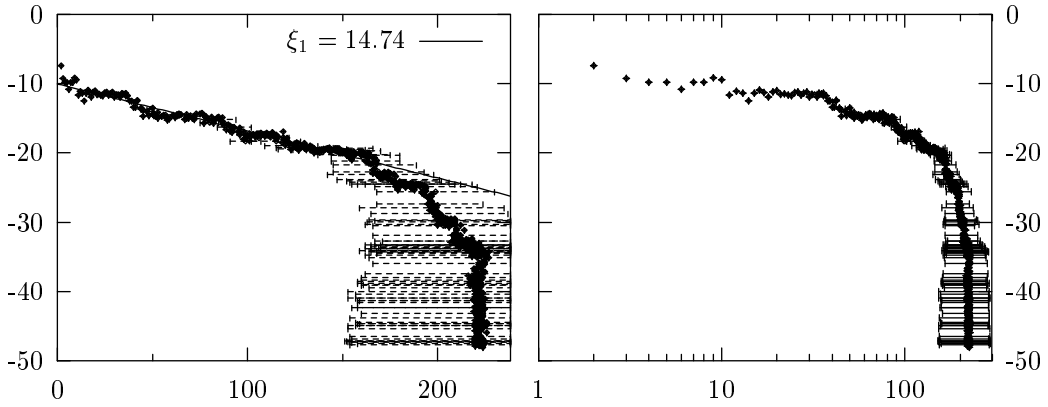


FIGURE 191. $\langle \log t_N \rangle_E$ vs. $N$ in 2D, $W = 30$, $E \in [-6.5, -5.5]$

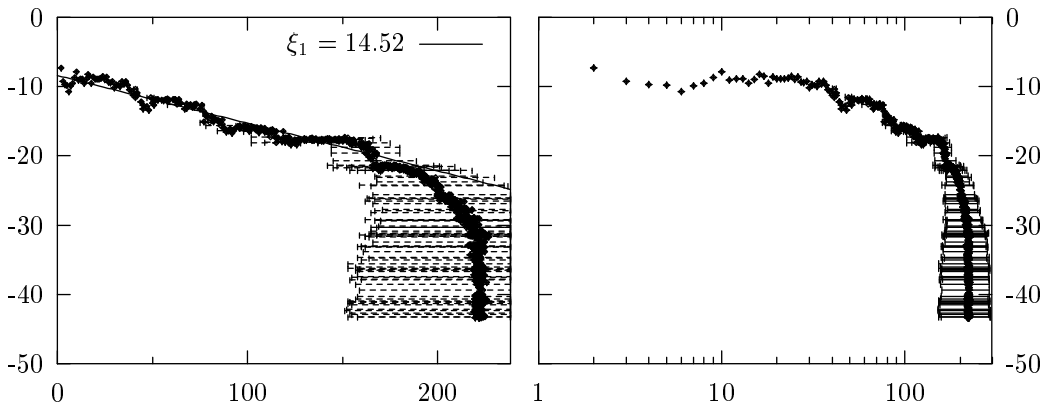


FIGURE 192. $\langle \log t_N \rangle_E$ vs. $N$ in 2D, $W = 30$, $E \in [-5.5, -4.5]$

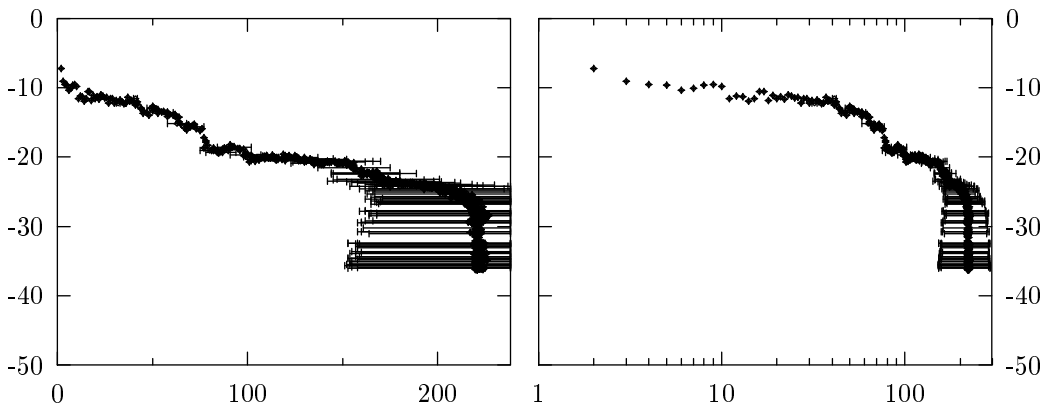


FIGURE 193. $\langle \log t_N \rangle_E$ vs. $N$ in 2D, $W = 30$, $E \in [-4.5, -3.5]$

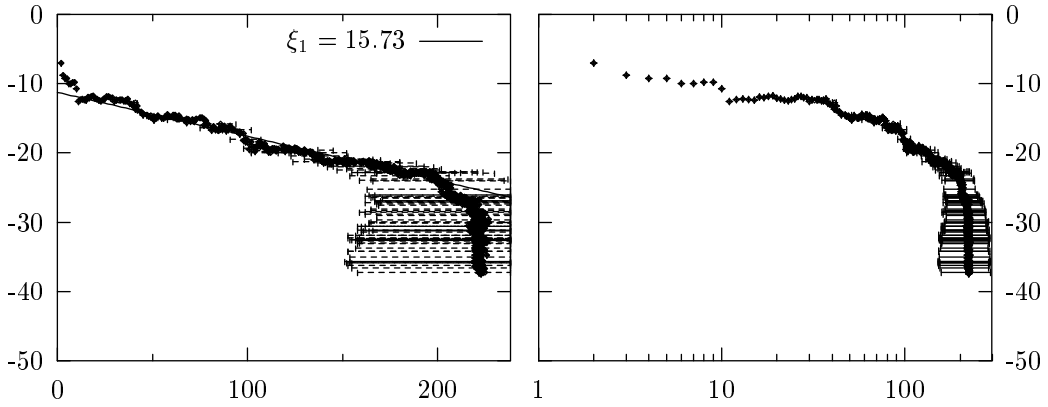


FIGURE 194. $\langle \log t_N \rangle_E$ vs. $N$ in 2D, $W = 30$, $E \in [-3.5, -2.5]$

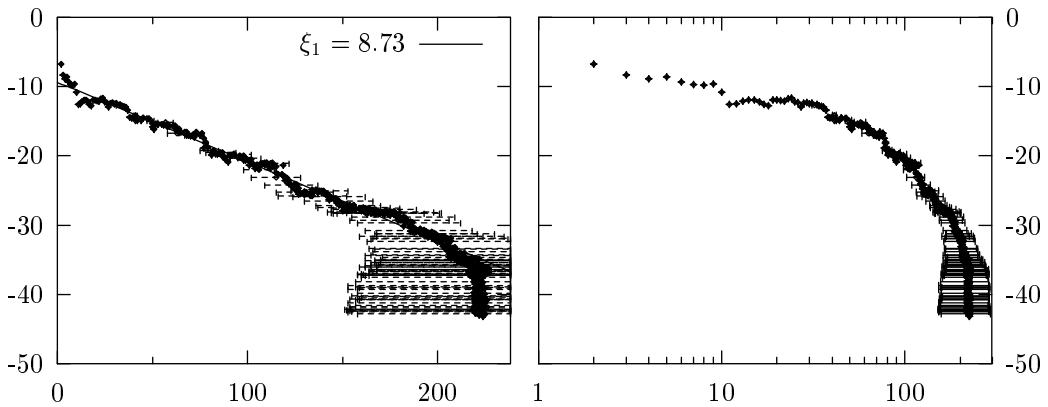


FIGURE 195. $\langle \log t_N \rangle_E$ vs. $N$ in 2D, $W = 30$, $E \in [-2.5, -1.5]$

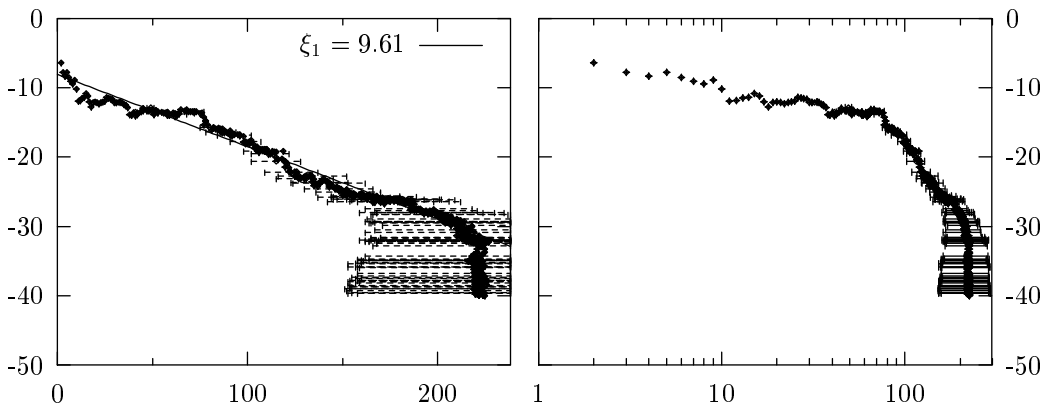


FIGURE 196. $\langle \log t_N \rangle_E$ vs. $N$ in 2D, $W = 30$, $E \in [-1.5, -0.5]$

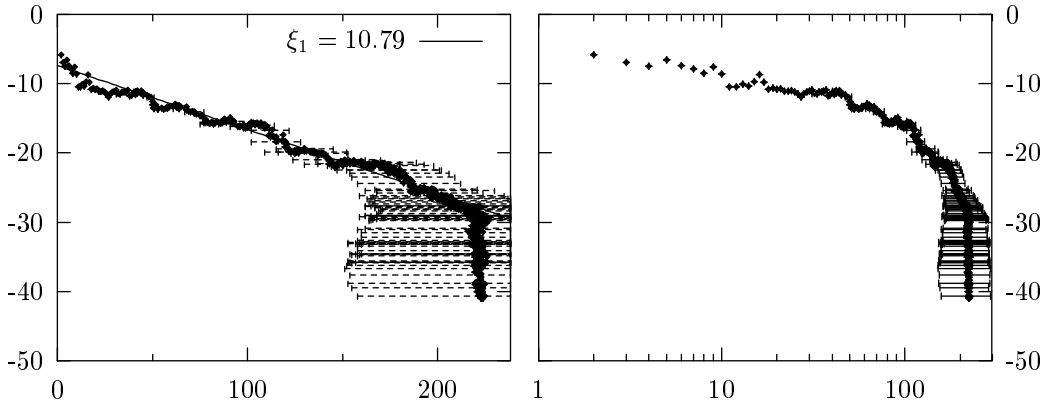


FIGURE 197. $\langle \log t_N \rangle_E$ vs. $N$ in 2D, $W = 30$, $E \in [-0.5, 0.5]$

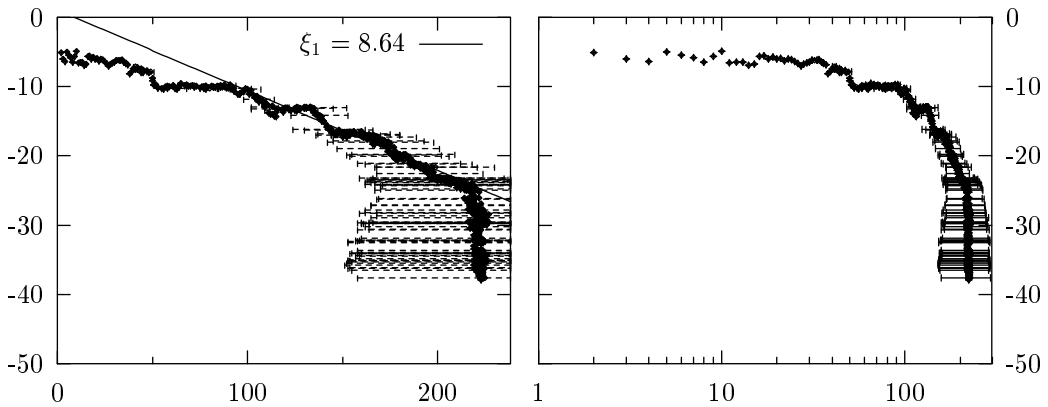


FIGURE 198. $\langle \log t_N \rangle_E$ vs. $N$ in 2D, $W = 30$, $E \in [0.5, 1.5]$

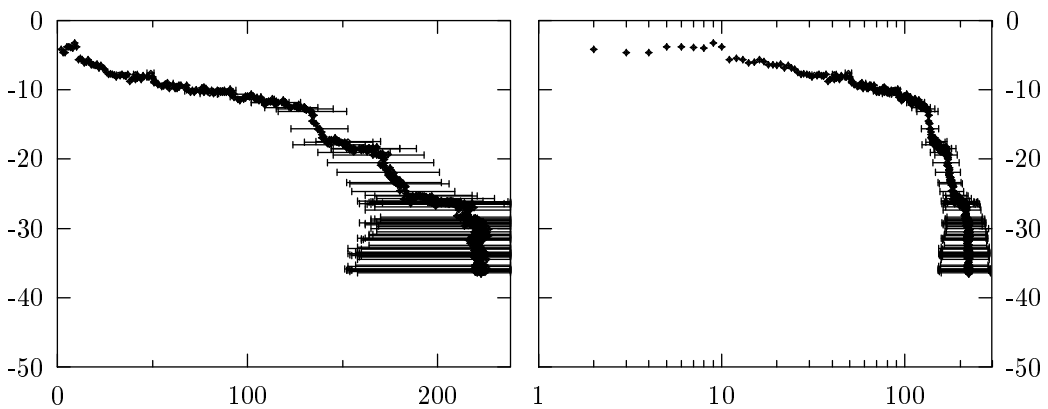


FIGURE 199. $\langle \log t_N \rangle_E$ vs. $N$ in 2D, $W = 30$, $E \in [1.5, 2.5]$

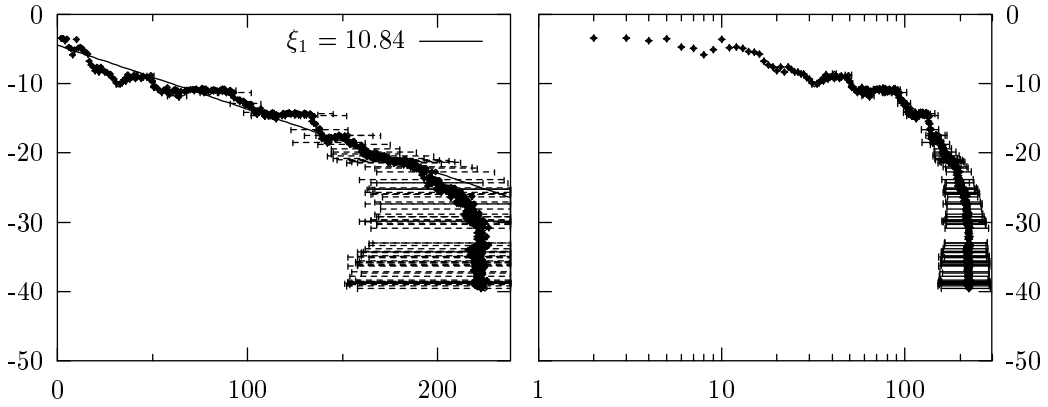


FIGURE 200. $\langle \log t_N \rangle_E$ vs. $N$ in 2D, $W = 30$, $E \in [2.5, 3.5]$

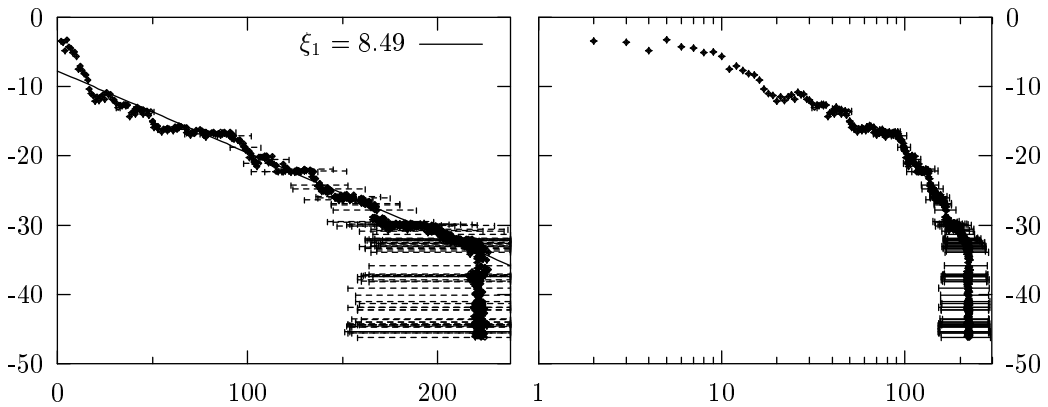


FIGURE 201. $\langle \log t_N \rangle_E$ vs. $N$ in 2D, $W = 30$, $E \in [3.5, 4.5]$

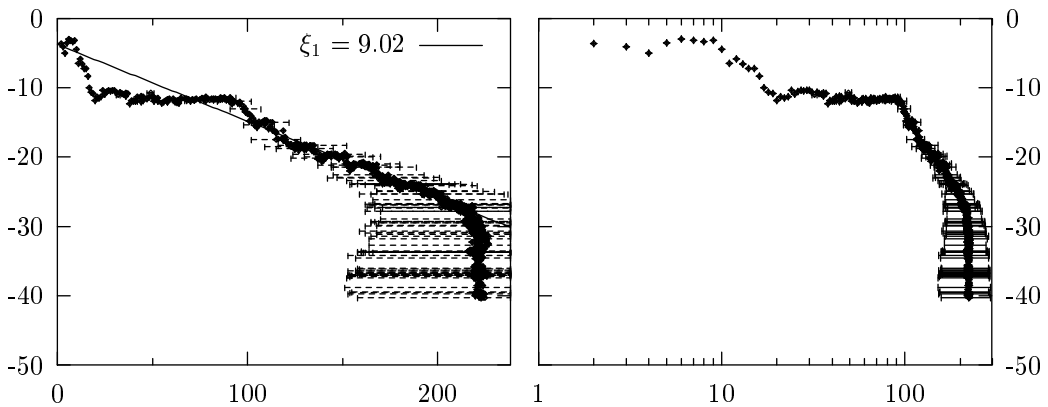


FIGURE 202. $\langle \log t_N \rangle_E$ vs. $N$ in 2D, $W = 30$, $E \in [4.5, 5.5]$

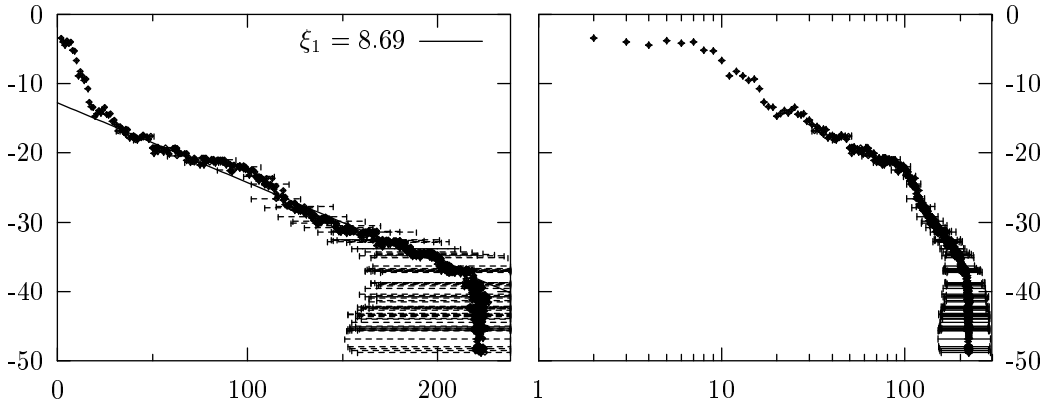


FIGURE 203. $\langle \log t_N \rangle_E$ vs. $N$ in 2D, $W = 30$, $E \in [5.5, 6.5]$

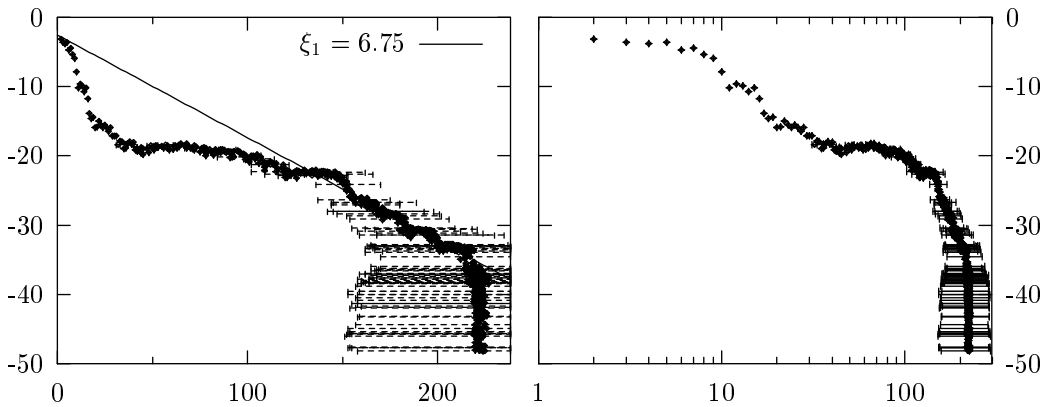


FIGURE 204. $\langle \log t_N \rangle_E$ vs. $N$ in 2D, $W = 30$, $E \in [6.5, 7.5]$

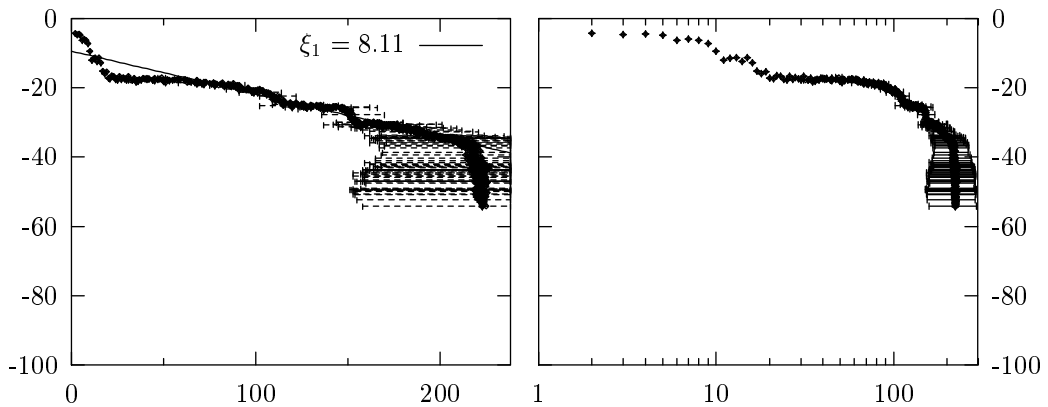


FIGURE 205. $\langle \log t_N \rangle_E$ vs. $N$ in 2D, $W = 30$, $E \in [7.5, 8.5]$

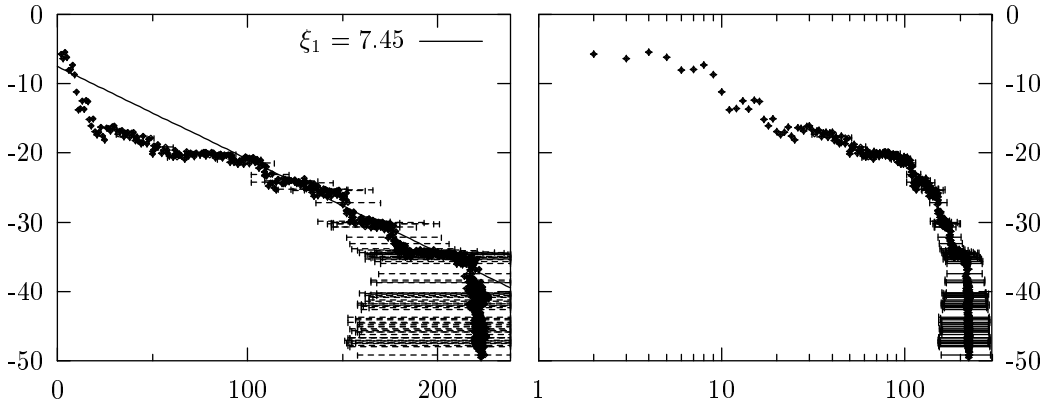


FIGURE 206. $\langle \log t_N \rangle_E$ vs. $N$ in 2D, $W = 30$, $E \in [8.5, 9.5]$

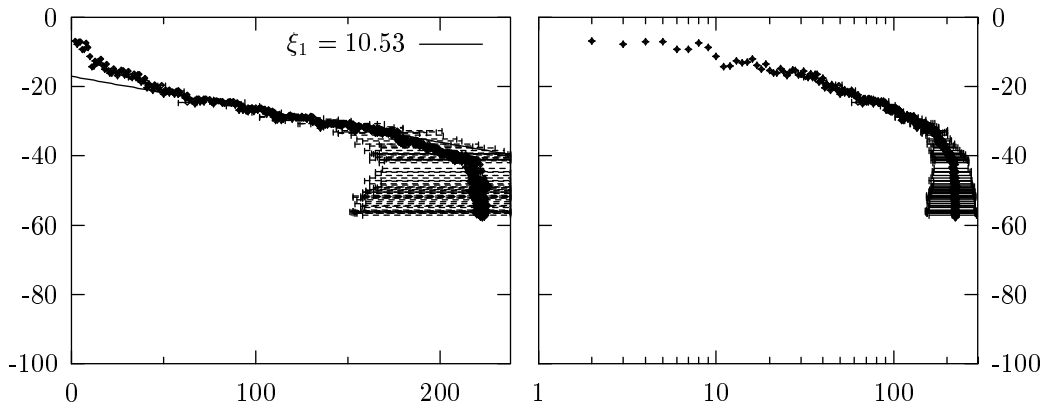


FIGURE 207. $\langle \log t_N \rangle_E$ vs. $N$ in 2D, $W = 30$, $E \in [9.5, 10.5]$

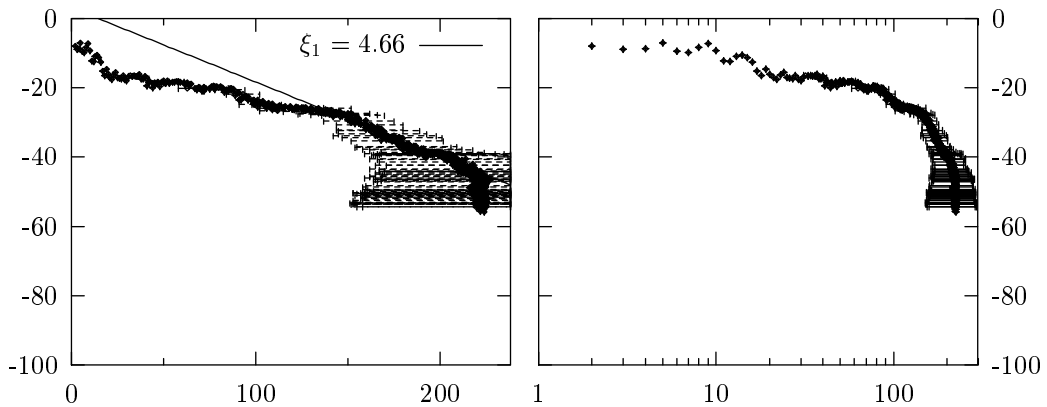


FIGURE 208. $\langle \log t_N \rangle_E$ vs. $N$ in 2D, $W = 30$, $E \in [10.5, 11.5]$

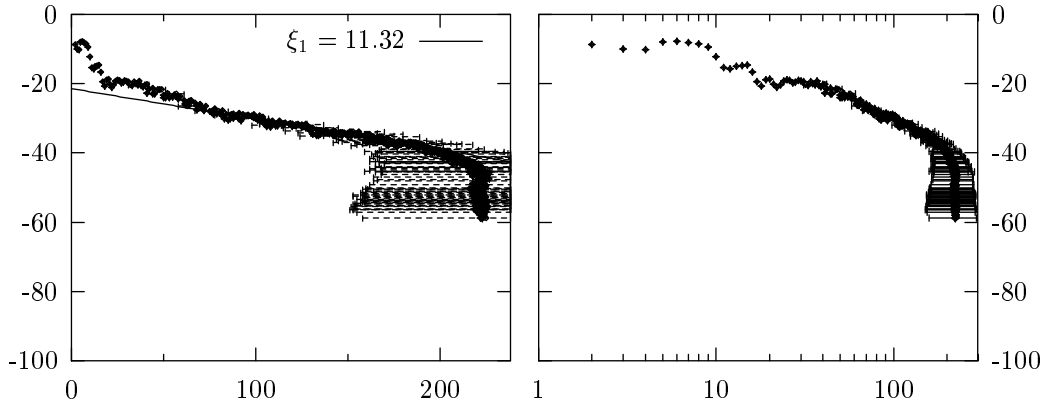


FIGURE 209. $\langle \log t_N \rangle_E$ vs. $N$ in 2D, $W = 30$, $E \in [11.5, 12.5]$

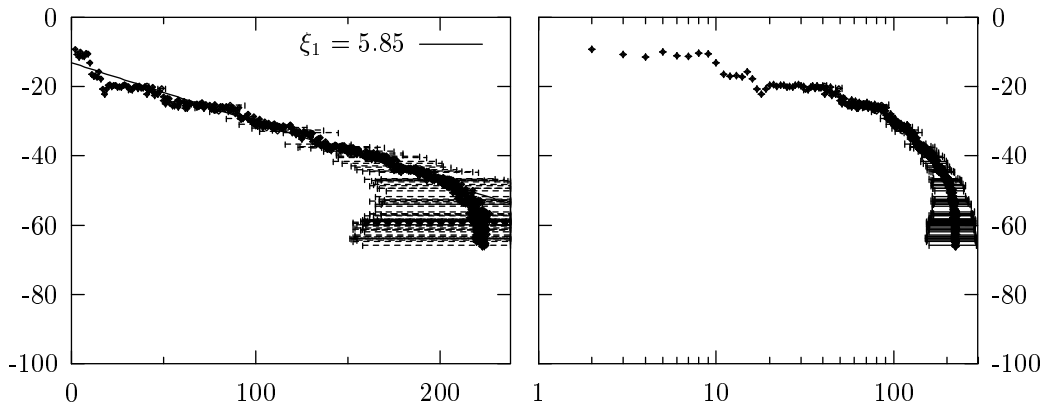


FIGURE 210. $\langle \log t_N \rangle_E$ vs. $N$ in 2D, $W = 30$, $E \in [12.5, 13.5]$

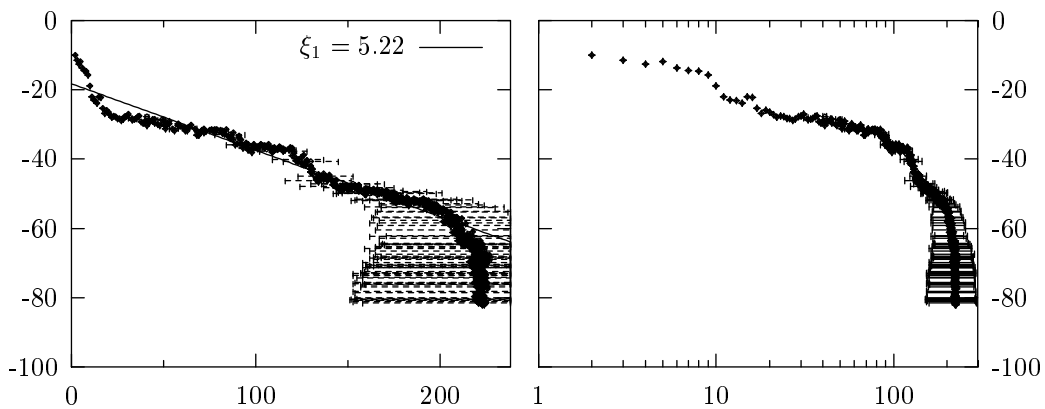


FIGURE 211. $\langle \log t_N \rangle_E$ vs. $N$ in 2D, $W = 30$, $E \in [13.5, 14.5]$

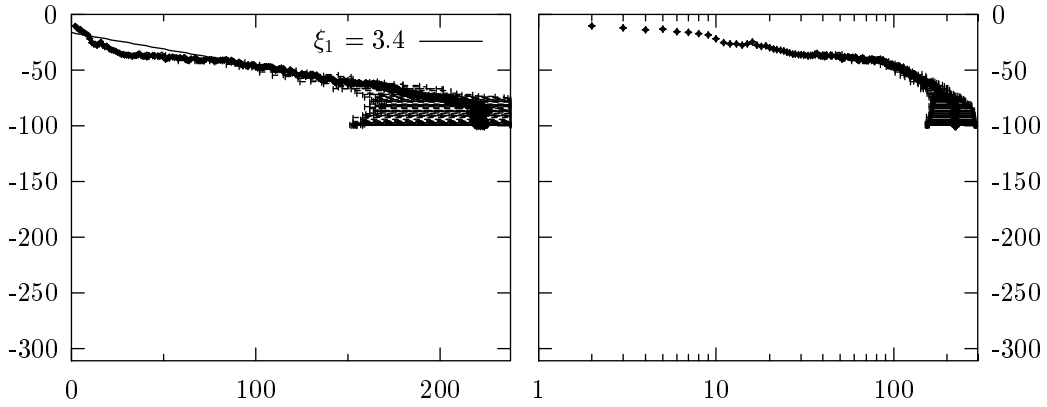


FIGURE 212. $\langle \log t_N \rangle_E$ vs. $N$ in 2D, $W = 30$, $E \in [14.5, 15.5]$

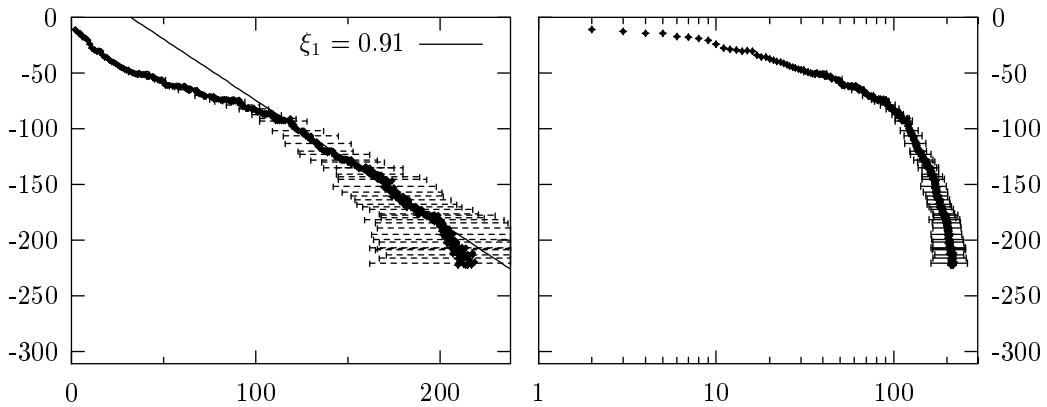


FIGURE 213. $\langle \log t_N \rangle_E$ vs. $N$ in 2D, $W = 30$, $E \in [15.5, 16.5]$

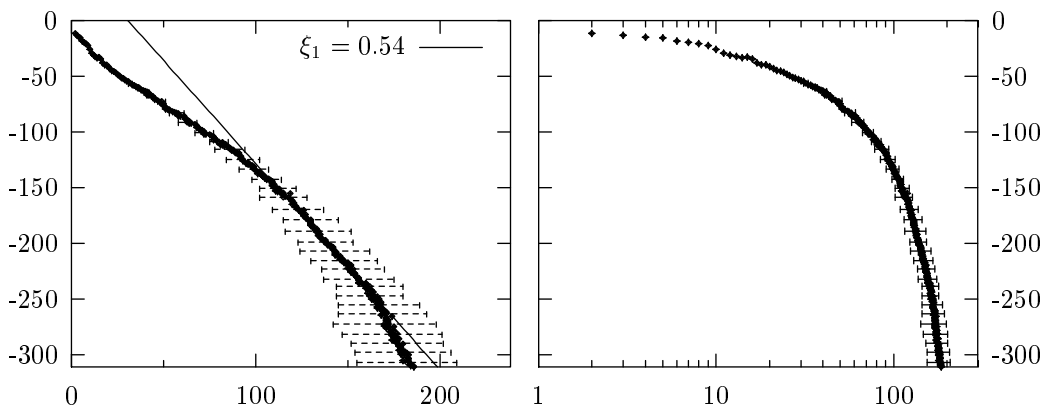


FIGURE 214. $\langle \log t_N \rangle_E$ vs. $N$ in 2D, $W = 30$, $E \in [16.5, 17.5]$

# APPENDIX C

## TRANSMITTANCE PLOTS FOR DISORDERED 3D SYSTEM

This Appendix contains data plots of transmittance calculations in three-dimensional disordered systems at various disorder strengths, averaged at 1000 sample points over energy intervals across the entire band, as described in Sec. 4.6.

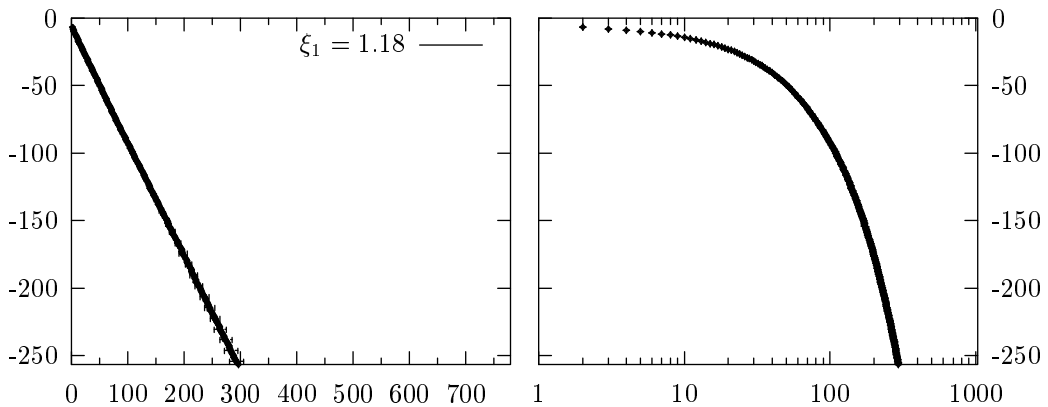


FIGURE 215. $\langle \log t_N \rangle_E$ vs. $N$ in 3D, $W = 4$, $E \in [-7.5, -6.5]$

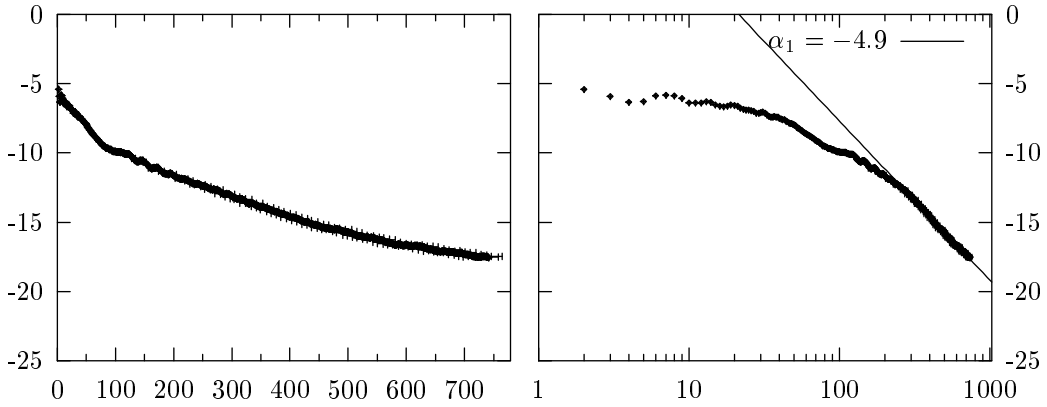


FIGURE 216. $\langle \log t_N \rangle_E$ vs. $N$ in 3D, $W = 4$, $E \in [-6.5, -5.5]$

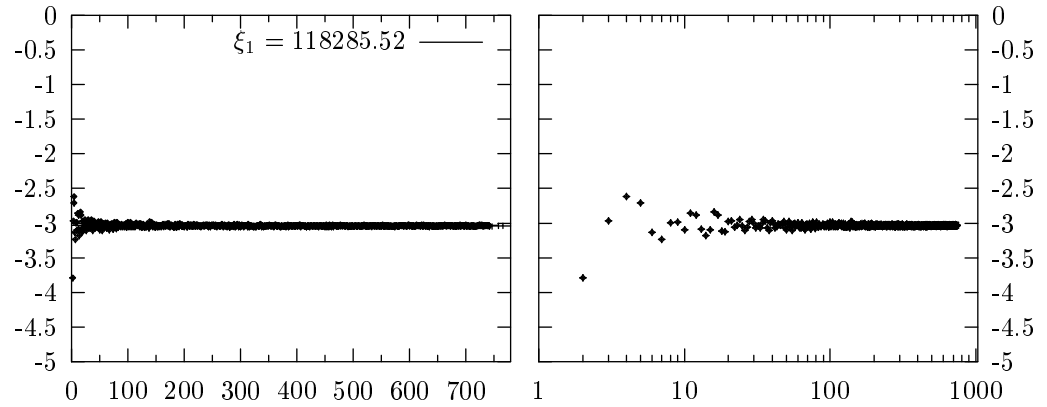


FIGURE 217. $\langle \log t_N \rangle_E$ vs. $N$ in 3D, $W = 4$, $E \in [-5.5, -4.5]$

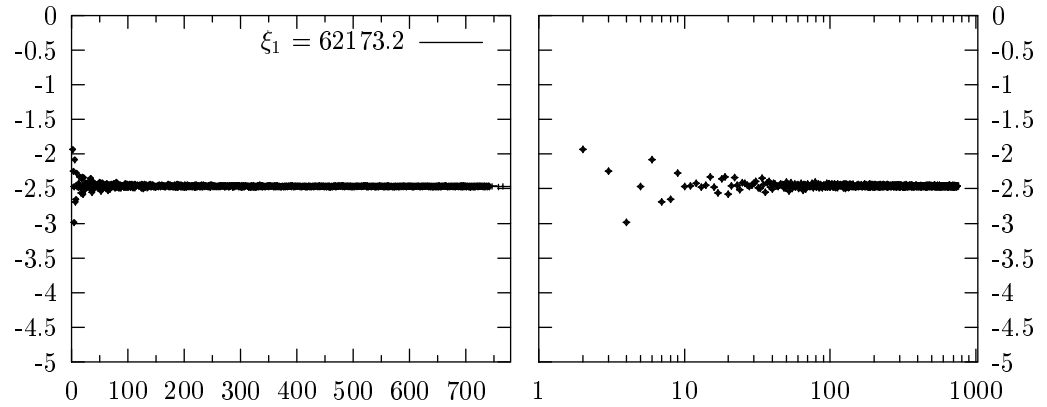


FIGURE 218. $\langle \log t_N \rangle_E$ vs. $N$ in 3D, $W = 4$, $E \in [-4.5, -3.5]$

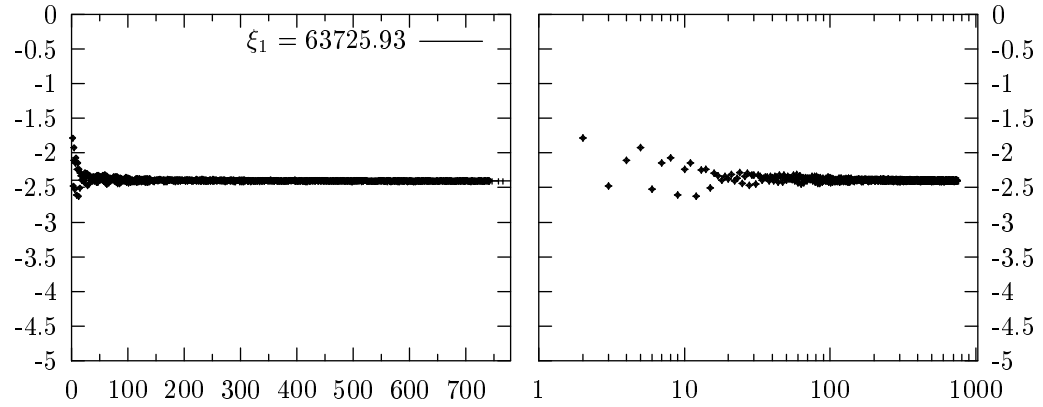


FIGURE 219. $\langle \log t_N \rangle_E$ vs. $N$ in 3D, $W = 4$, $E \in [-3.5, -2.5]$

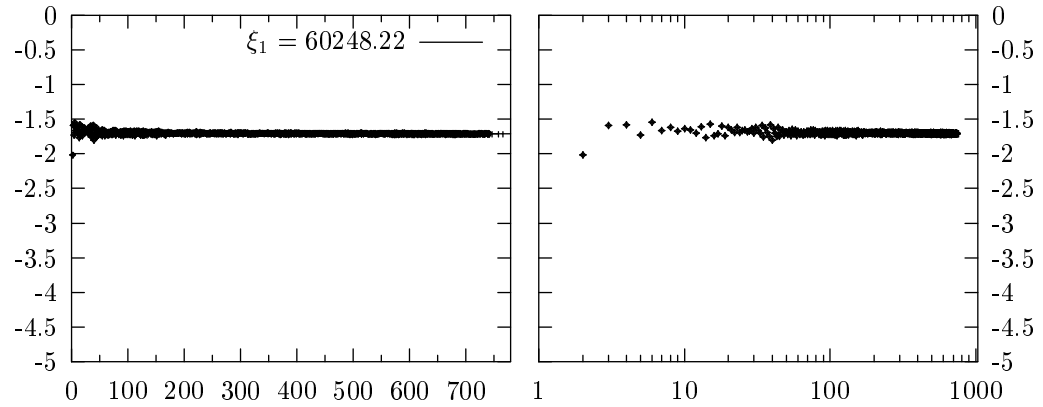


FIGURE 220. $\langle \log t_N \rangle_E$ vs. $N$ in 3D, $W = 4$, $E \in [-2.5, -1.5]$

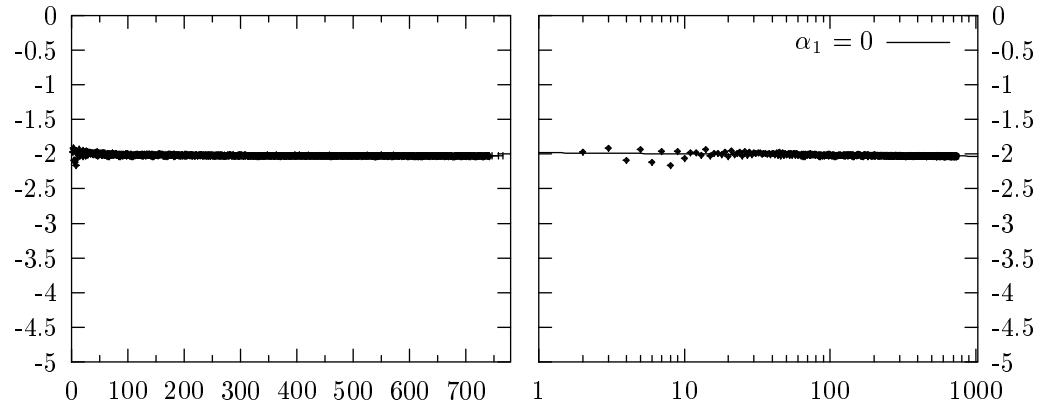


FIGURE 221. $\langle \log t_N \rangle_E$ vs. $N$ in 3D, $W = 4$, $E \in [-1.5, -0.5]$

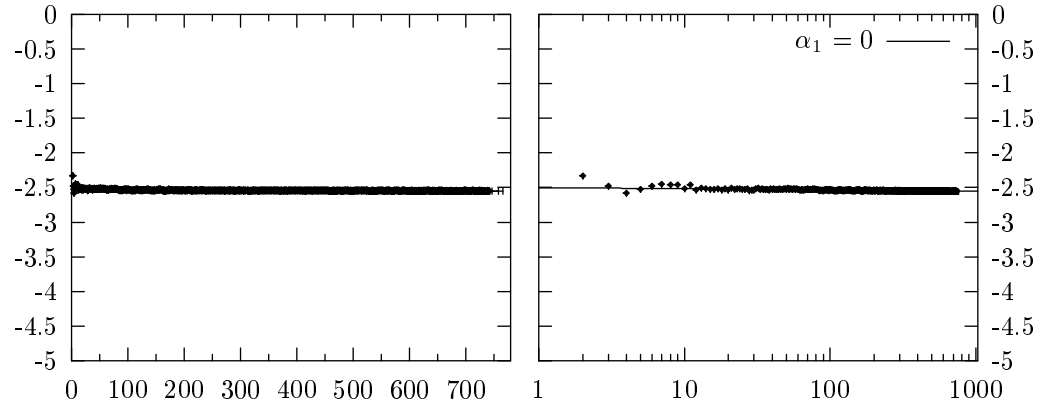


FIGURE 222. $\langle \log t_N \rangle_E$ vs. $N$ in 3D, $W = 4$, $E \in [-0.5, 0.5]$

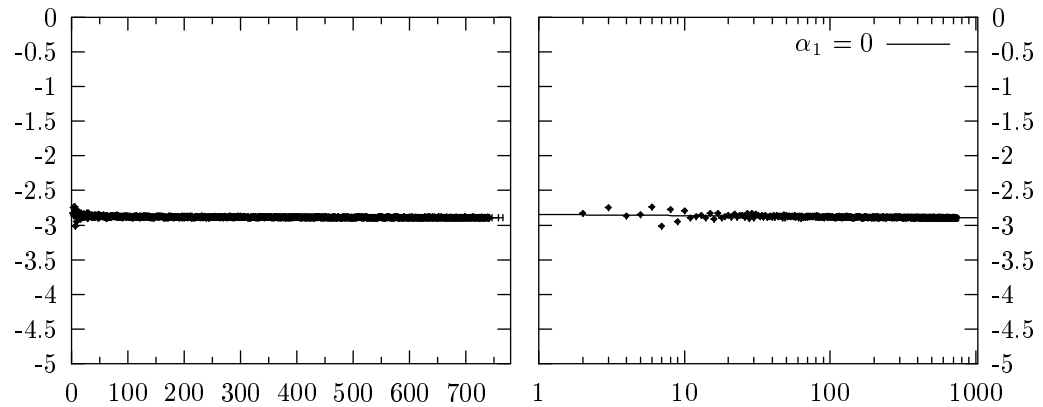


FIGURE 223. $\langle \log t_N \rangle_E$ vs. $N$ in 3D, $W = 4$, $E \in [0.5, 1.5]$

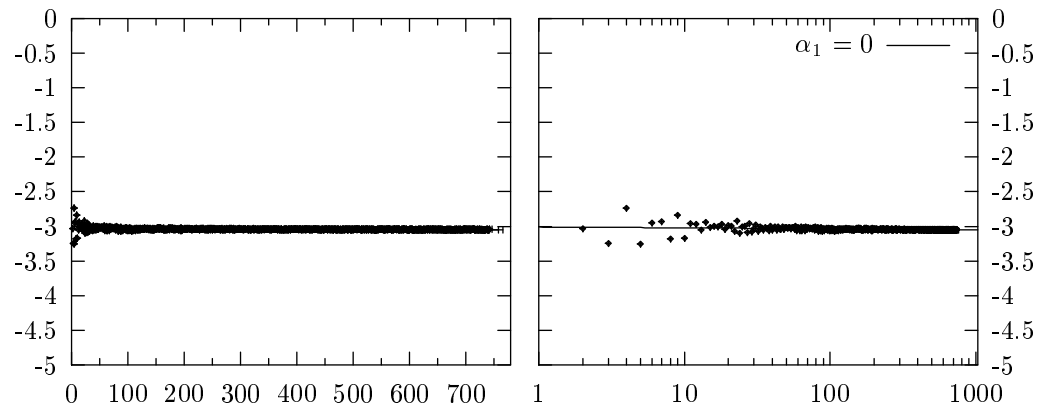


FIGURE 224. $\langle \log t_N \rangle_E$ vs. $N$ in 3D, $W = 4$, $E \in [1.5, 2.5]$

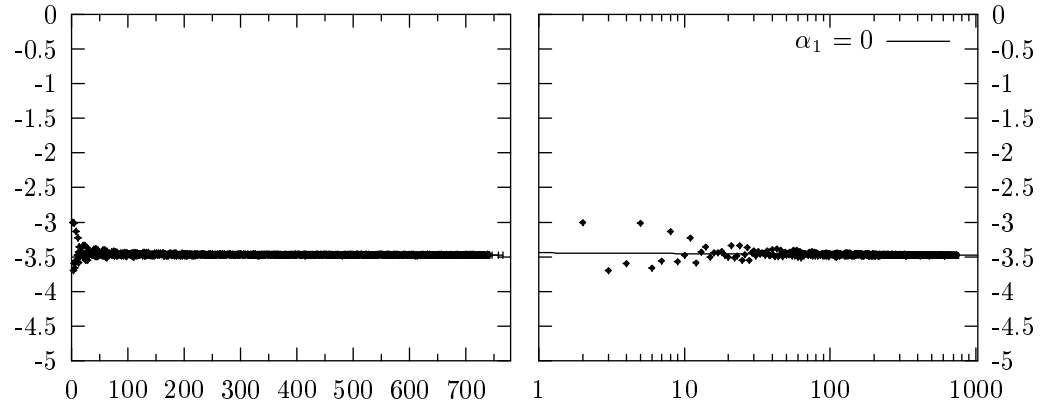


FIGURE 225. $\langle \log t_N \rangle_E$ vs. $N$ in 3D, $W = 4$, $E \in [2.5, 3.5]$

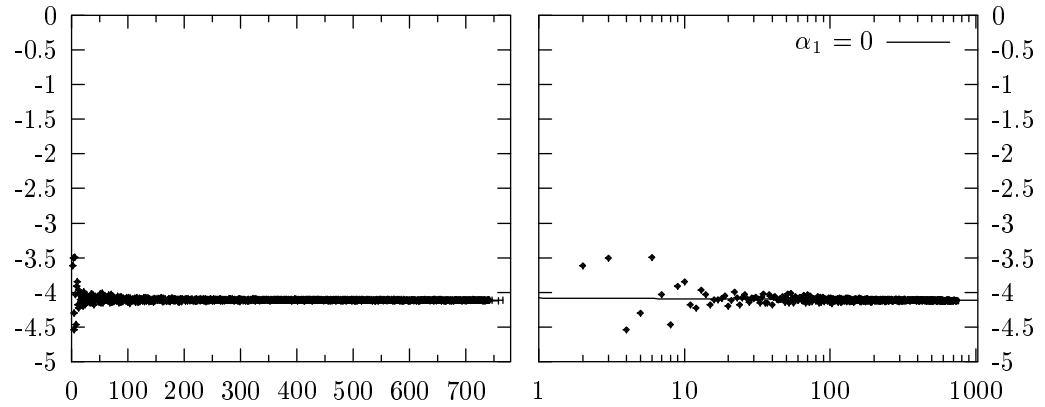


FIGURE 226. $\langle \log t_N \rangle_E$ vs. $N$ in 3D, $W = 4$, $E \in [3.5, 4.5]$

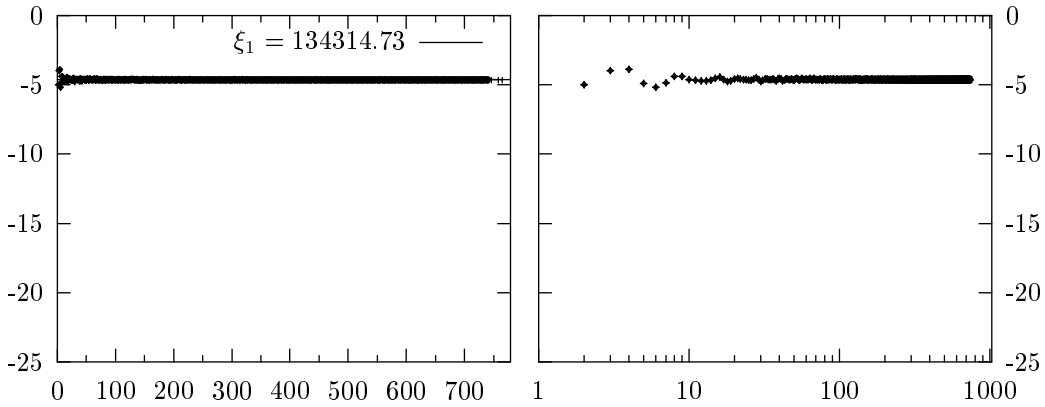


FIGURE 227. $\langle \log t_N \rangle_E$ vs. $N$ in 3D, $W = 4$, $E \in [4.5, 5.5]$

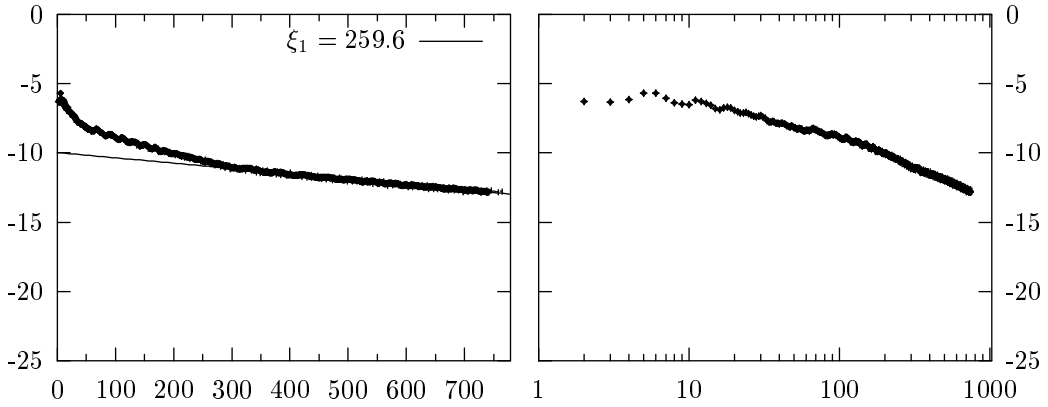


FIGURE 228. $\langle \log t_N \rangle_E$ vs. $N$ in 3D, $W = 4$, $E \in [5.5, 6.5]$

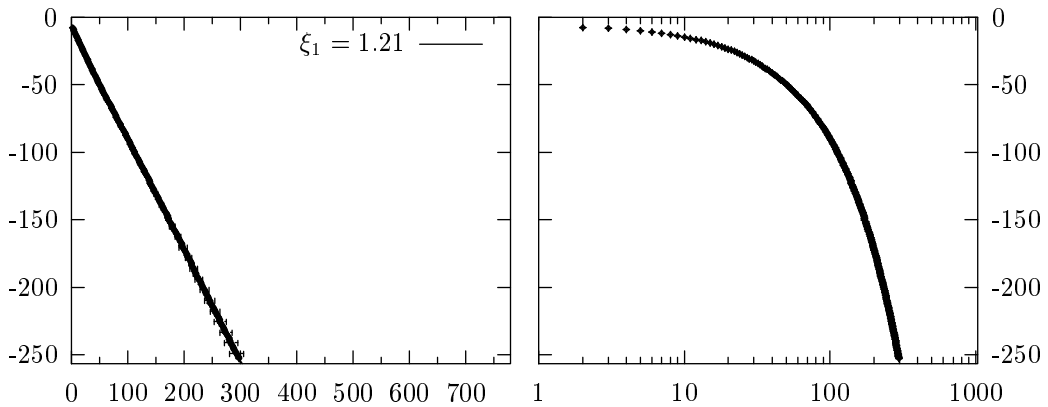


FIGURE 229. $\langle \log t_N \rangle_E$ vs. $N$ in 3D, $W = 4$, $E \in [6.5, 7.5]$

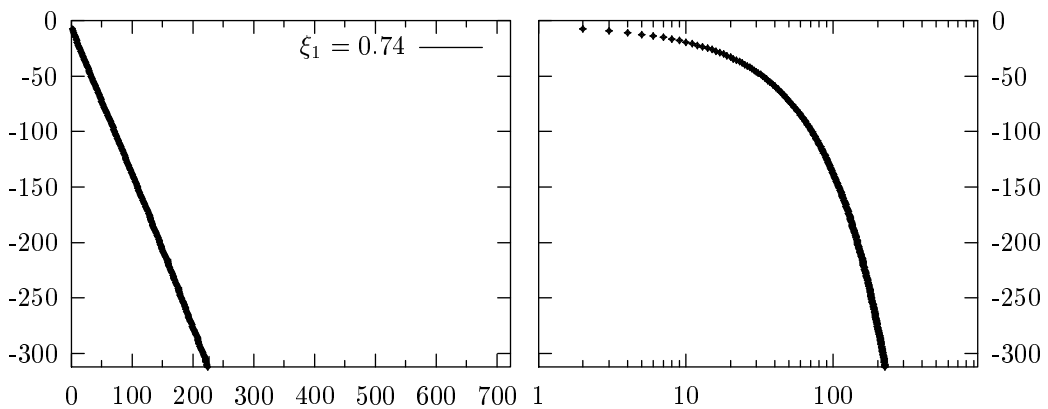


FIGURE 230. $\langle \log t_N \rangle_E$ vs. $N$ in 3D, $W = 8$, $E \in [-9.5, -8.5]$

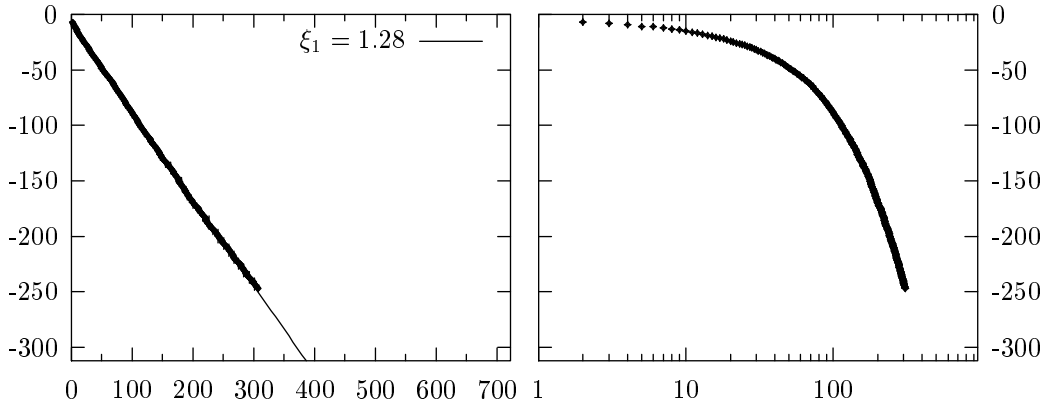


FIGURE 231. $\langle \log t_N \rangle_E$ vs. $N$ in 3D, $W = 8$, $E \in [-8.5, -7.5]$

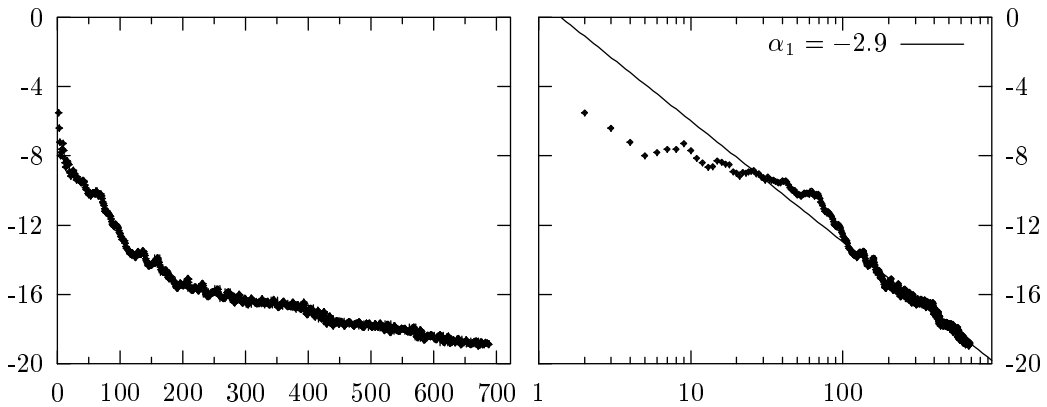


FIGURE 232. $\langle \log t_N \rangle_E$ vs. $N$ in 3D, $W = 8$, $E \in [-7.5, -6.5]$

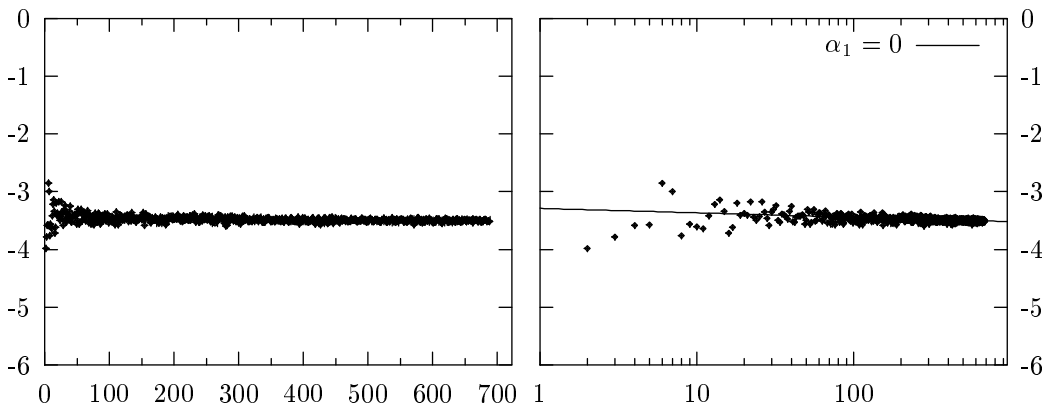


FIGURE 233. $\langle \log t_N \rangle_E$ vs. $N$ in 3D, $W = 8$, $E \in [-6.5, -5.5]$

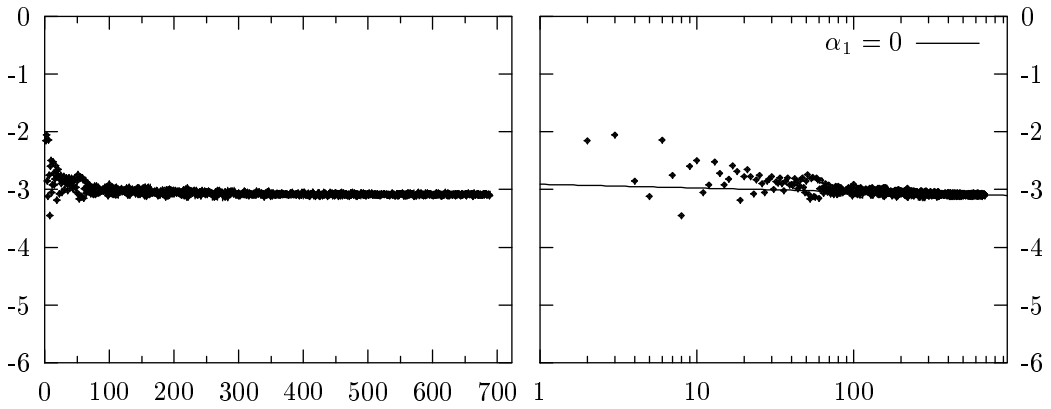


FIGURE 234. $\langle \log t_N \rangle_E$ vs. $N$ in 3D, $W = 8$, $E \in [-5.5, -4.5]$

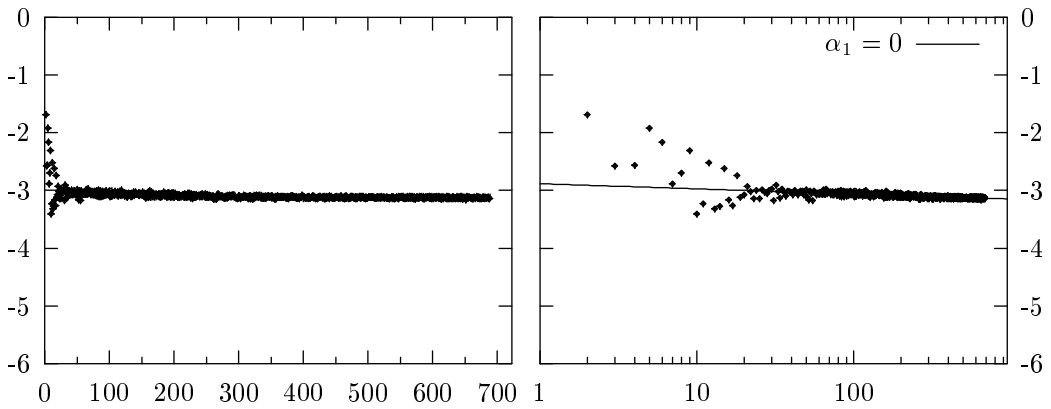


FIGURE 235. $\langle \log t_N \rangle_E$ vs. $N$ in 3D, $W = 8$, $E \in [-4.5, -3.5]$

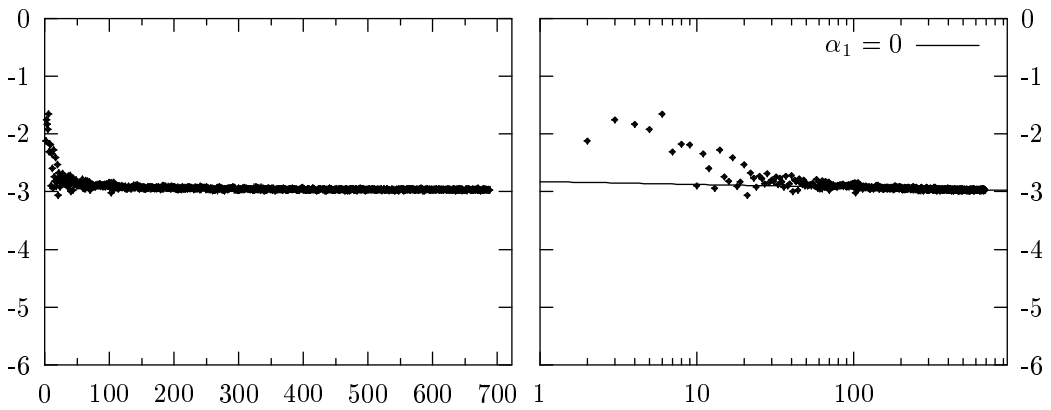


FIGURE 236. $\langle \log t_N \rangle_E$ vs. $N$ in 3D, $W = 8$, $E \in [-3.5, -2.5]$

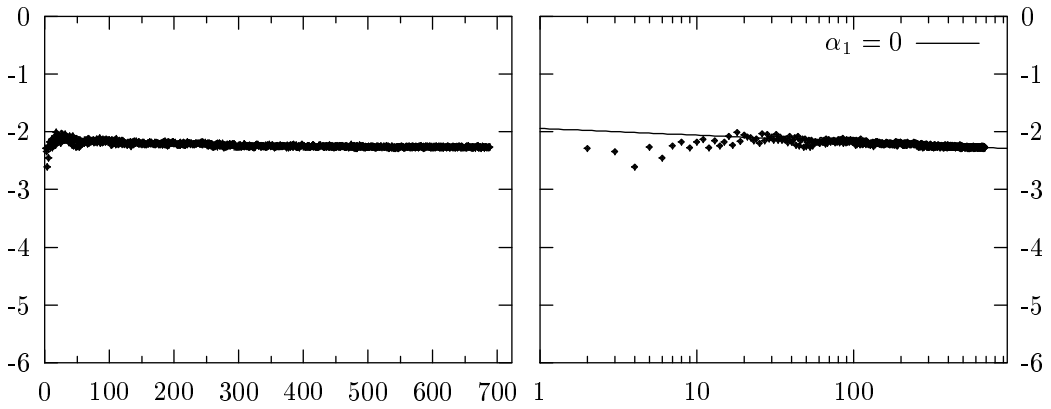


FIGURE 237. $\langle \log t_N \rangle_E$ vs. $N$ in 3D, $W = 8$, $E \in [-2.5, -1.5]$

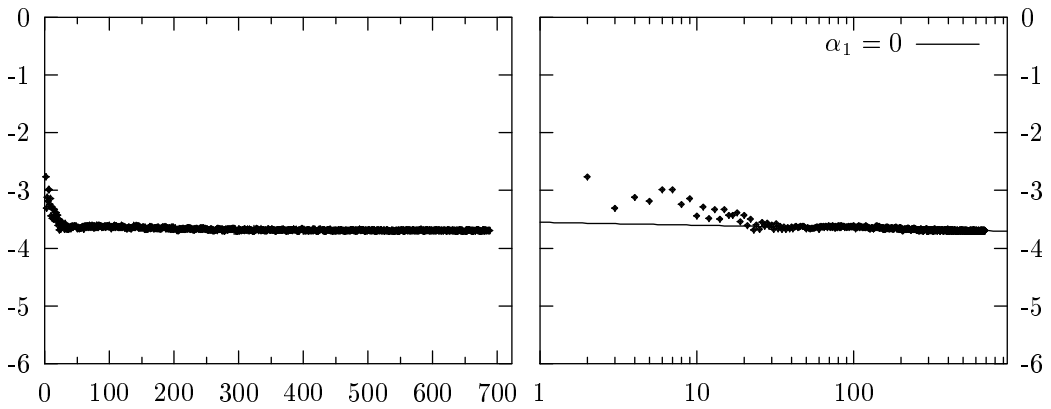


FIGURE 238. $\langle \log t_N \rangle_E$ vs. $N$ in 3D, $W = 8$, $E \in [-1.5, -0.5]$

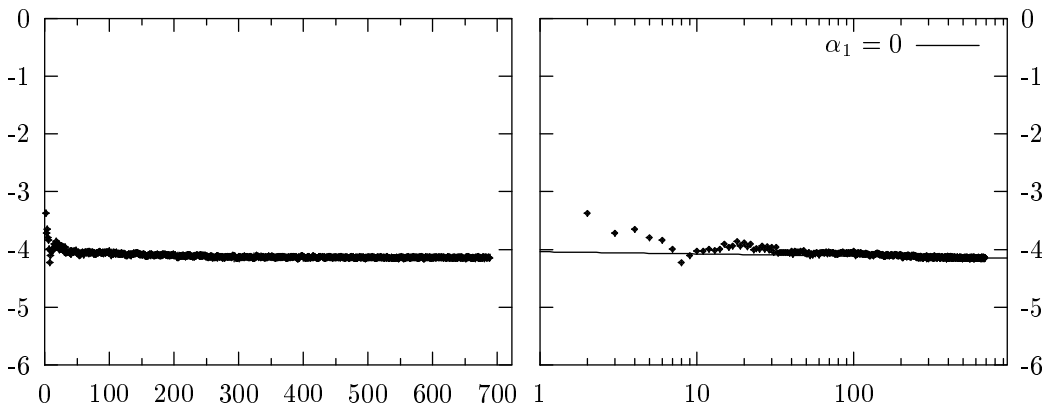


FIGURE 239. $\langle \log t_N \rangle_E$ vs. $N$ in 3D, $W = 8$, $E \in [-0.5, 0.5]$

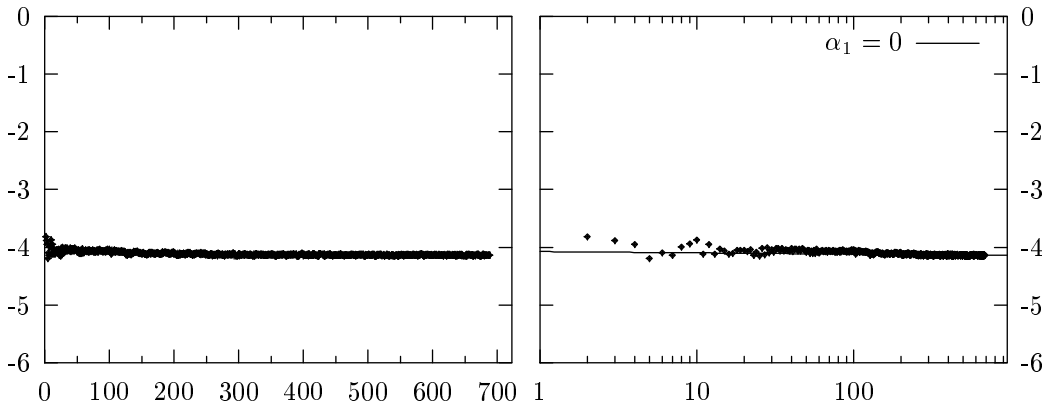


FIGURE 240. $\langle \log t_N \rangle_E$ vs. $N$ in 3D, $W = 8$, $E \in [0.5, 1.5]$

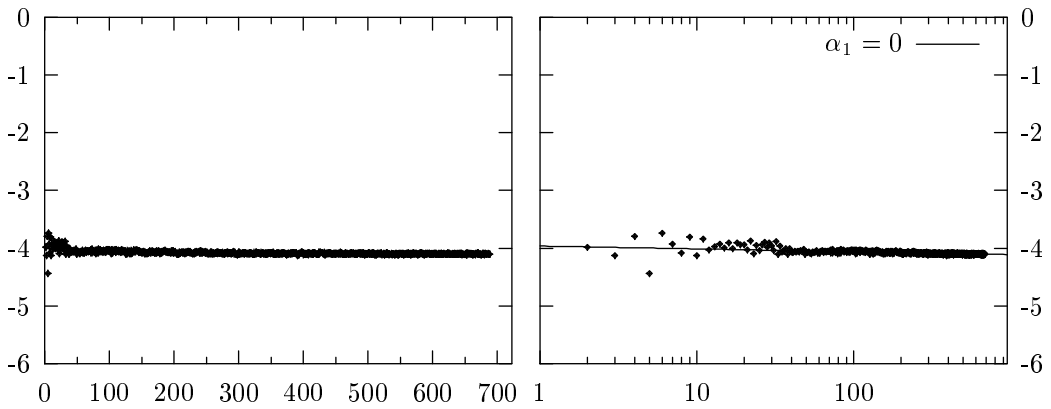


FIGURE 241. $\langle \log t_N \rangle_E$ vs. $N$ in 3D, $W = 8$, $E \in [1.5, 2.5]$

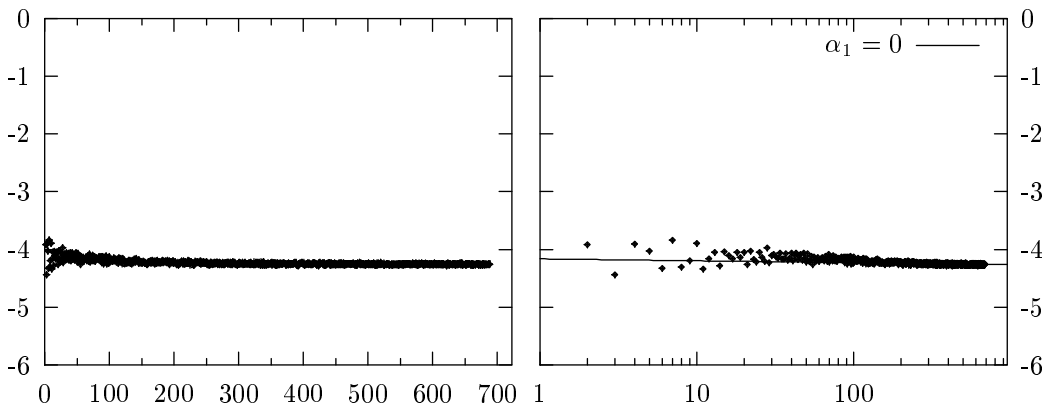


FIGURE 242. $\langle \log t_N \rangle_E$ vs. $N$ in 3D, $W = 8$, $E \in [2.5, 3.5]$

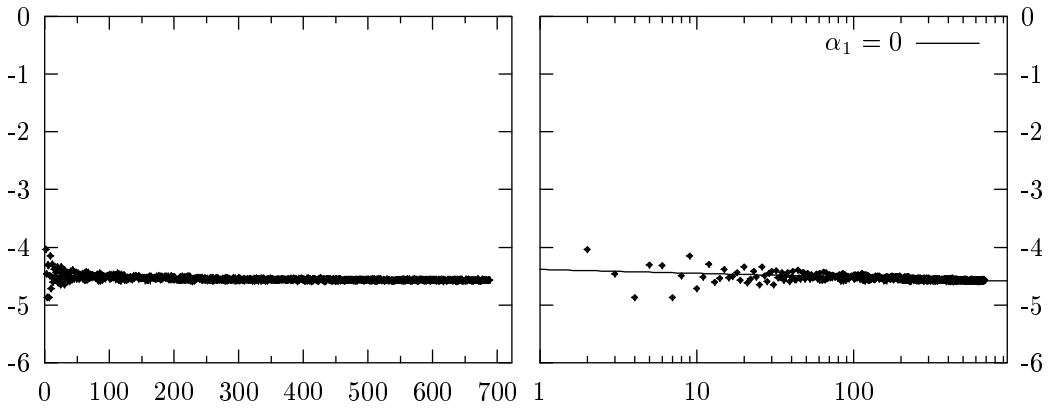


FIGURE 243. $\langle \log t_N \rangle_E$ vs. $N$ in 3D, $W = 8$, $E \in [3.5, 4.5]$

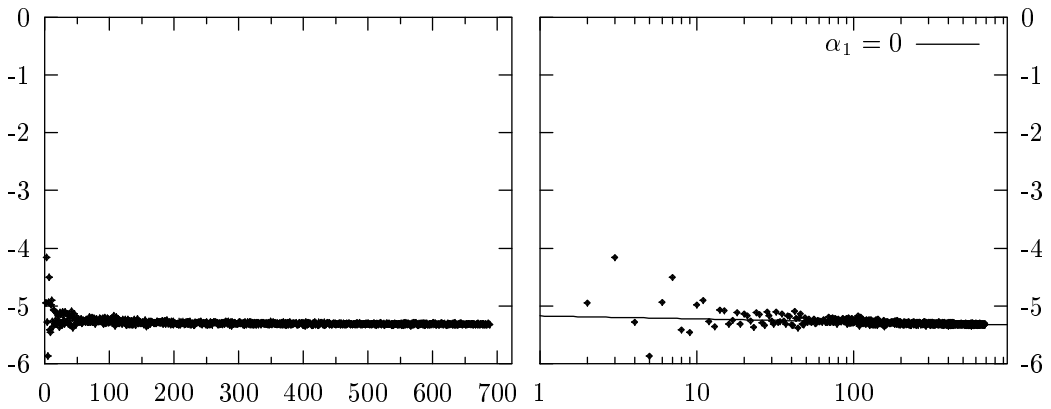


FIGURE 244. $\langle \log t_N \rangle_E$ vs. $N$ in 3D, $W = 8$, $E \in [4.5, 5.5]$

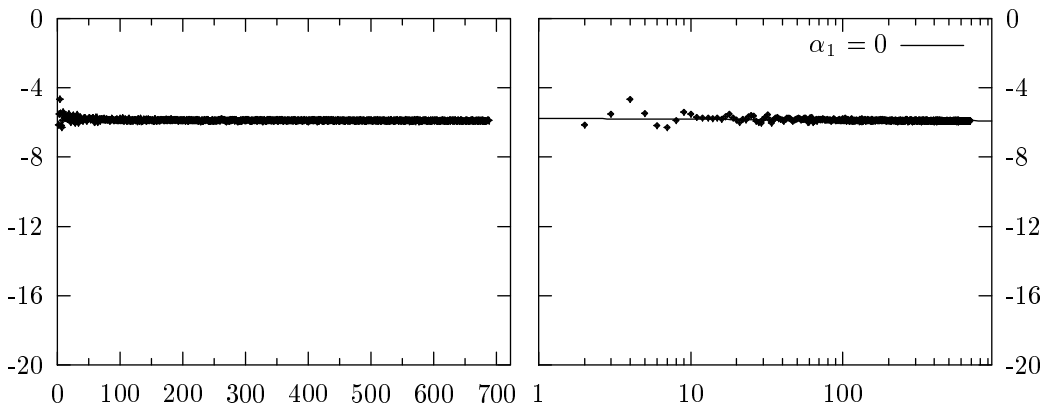


FIGURE 245. $\langle \log t_N \rangle_E$ vs. $N$ in 3D, $W = 8$, $E \in [5.5, 6.5]$

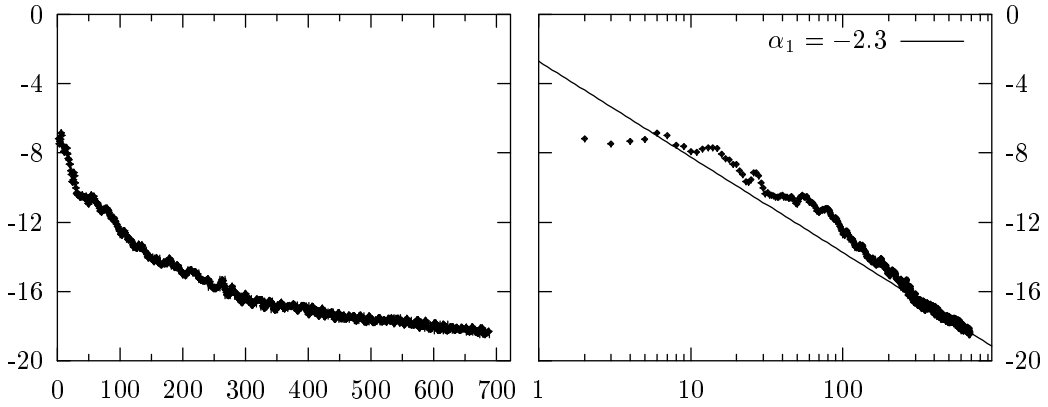


FIGURE 246. $\langle \log t_N \rangle_E$ vs. $N$ in 3D, $W = 8$, $E \in [6.5, 7.5]$

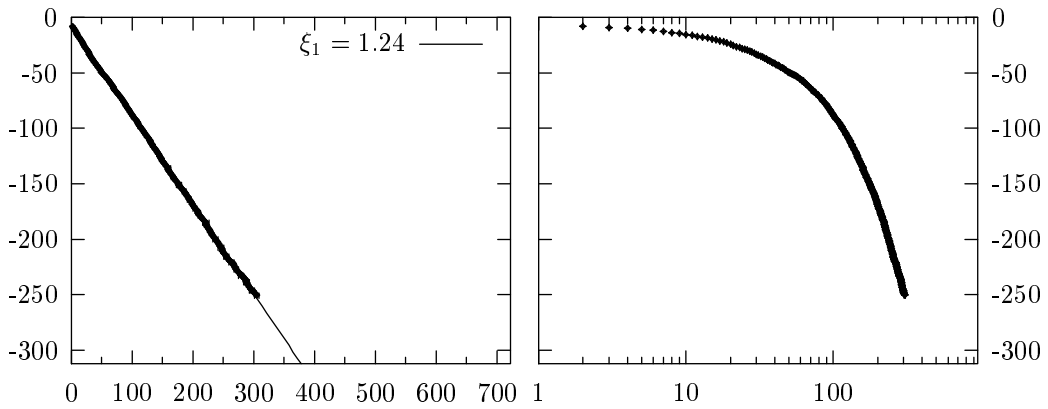


FIGURE 247. $\langle \log t_N \rangle_E$ vs. $N$ in 3D, $W = 8$, $E \in [7.5, 8.5]$

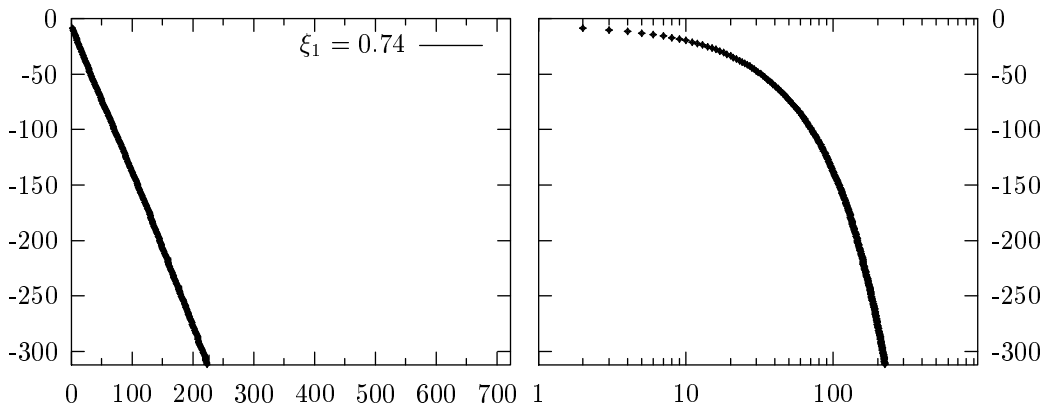


FIGURE 248. $\langle \log t_N \rangle_E$ vs. $N$ in 3D, $W = 8$, $E \in [8.5, 9.5]$

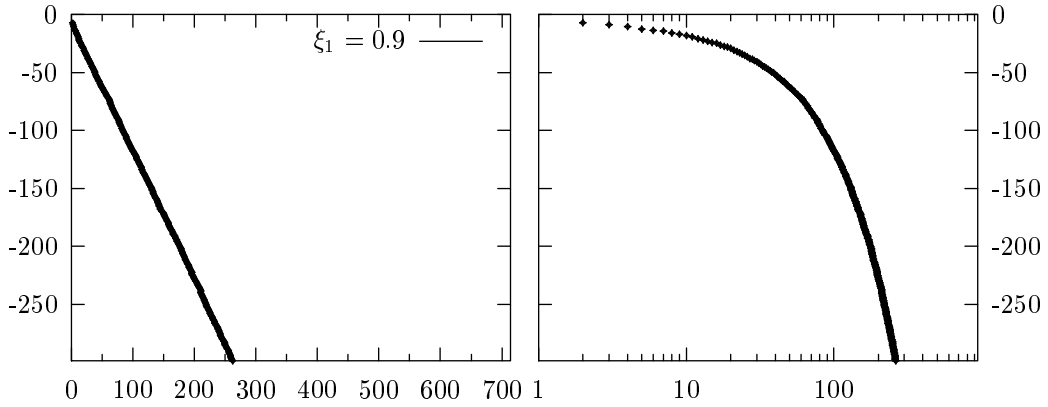


FIGURE 249. $\langle \log t_N \rangle_E$ vs. $N$ in 3D, $W = 12$, $E \in [-10.5, -9.5]$

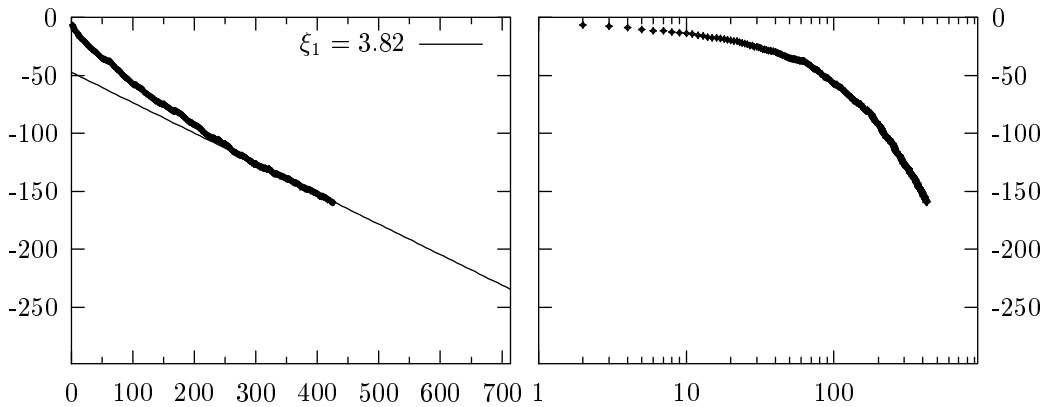


FIGURE 250. $\langle \log t_N \rangle_E$ vs. $N$ in 3D, $W = 12$, $E \in [-9.5, -8.5]$

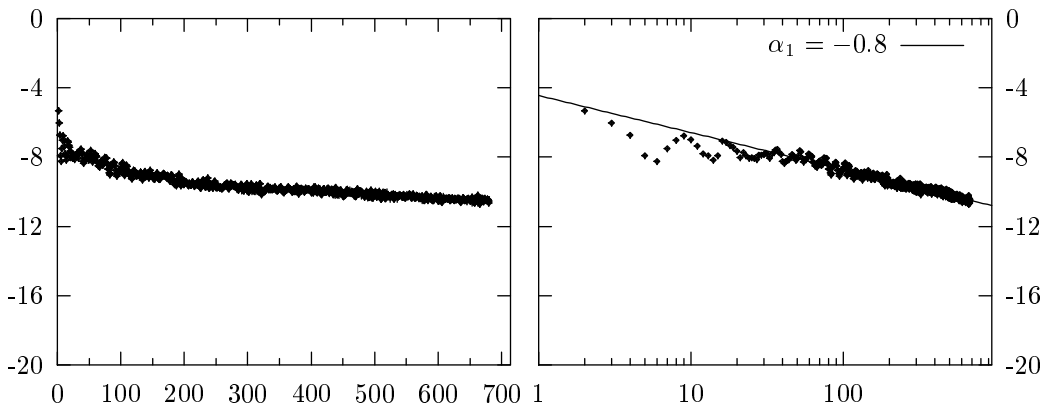


FIGURE 251. $\langle \log t_N \rangle_E$ vs. $N$ in 3D, $W = 12$, $E \in [-8.5, -7.5]$

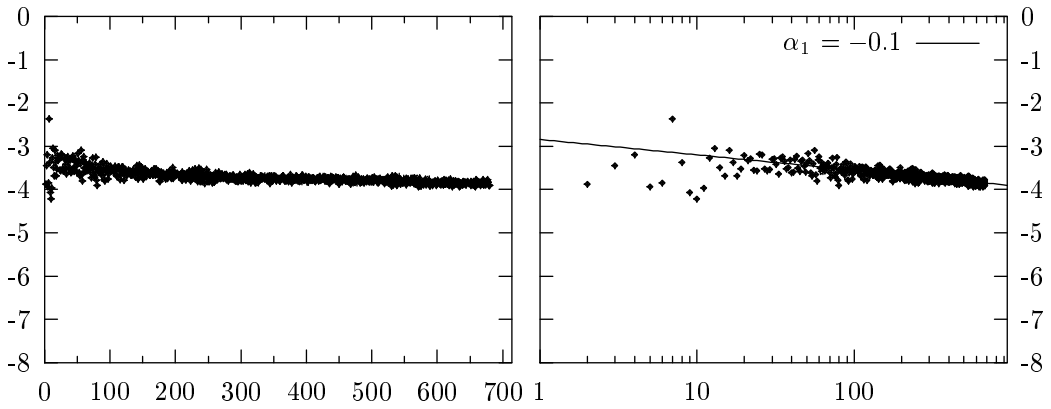


FIGURE 252. $\langle \log t_N \rangle_E$ vs. $N$ in 3D, $W = 12$, $E \in [-7.5, -6.5]$

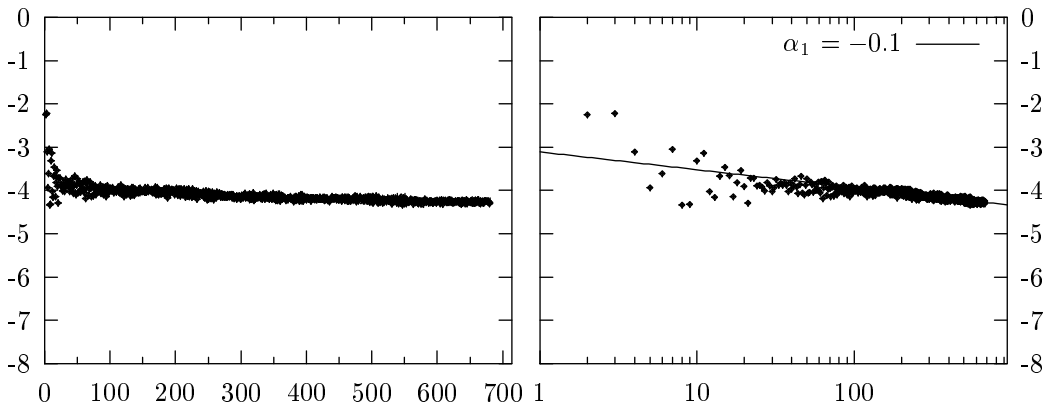


FIGURE 253. $\langle \log t_N \rangle_E$ vs. $N$ in 3D, $W = 12$, $E \in [-6.5, -5.5]$

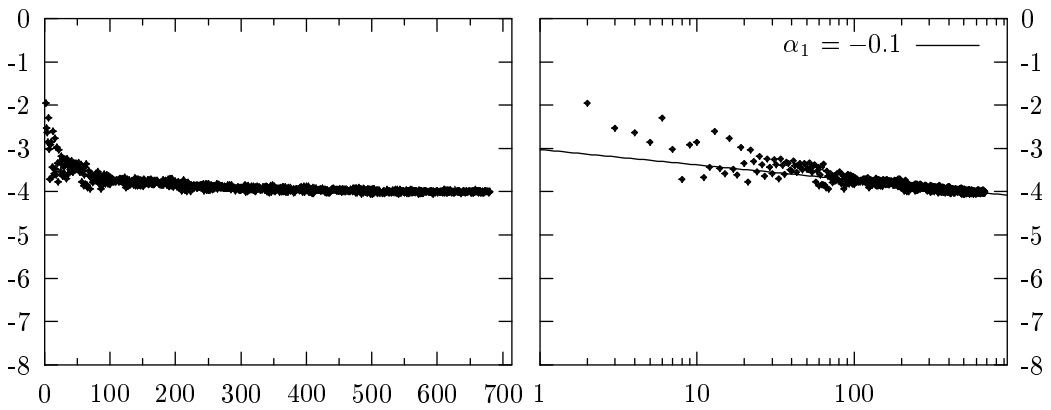


FIGURE 254. $\langle \log t_N \rangle_E$ vs. $N$ in 3D, $W = 12$, $E \in [-5.5, -4.5]$

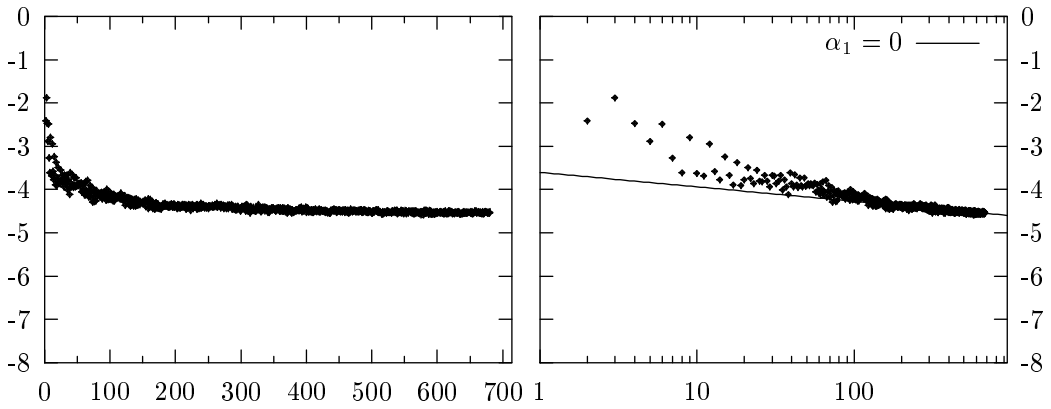


FIGURE 255. $\langle \log t_N \rangle_E$ vs. $N$ in 3D, $W = 12$, $E \in [-4.5, -3.5]$

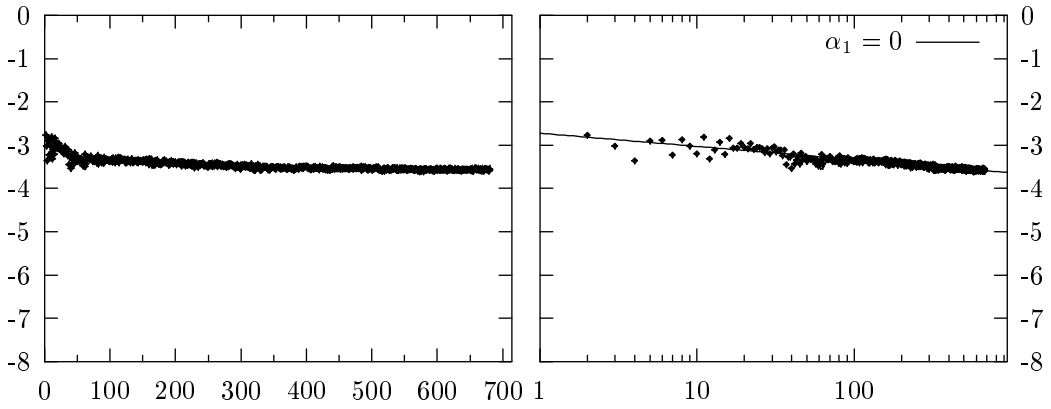


FIGURE 256. $\langle \log t_N \rangle_E$ vs. $N$ in 3D, $W = 12$, $E \in [-3.5, -2.5]$

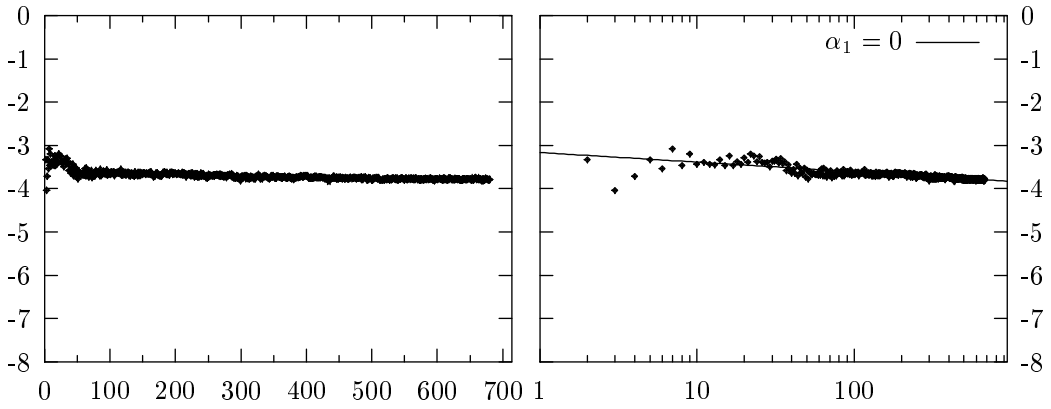


FIGURE 257. $\langle \log t_N \rangle_E$ vs. $N$ in 3D, $W = 12$, $E \in [-2.5, -1.5]$

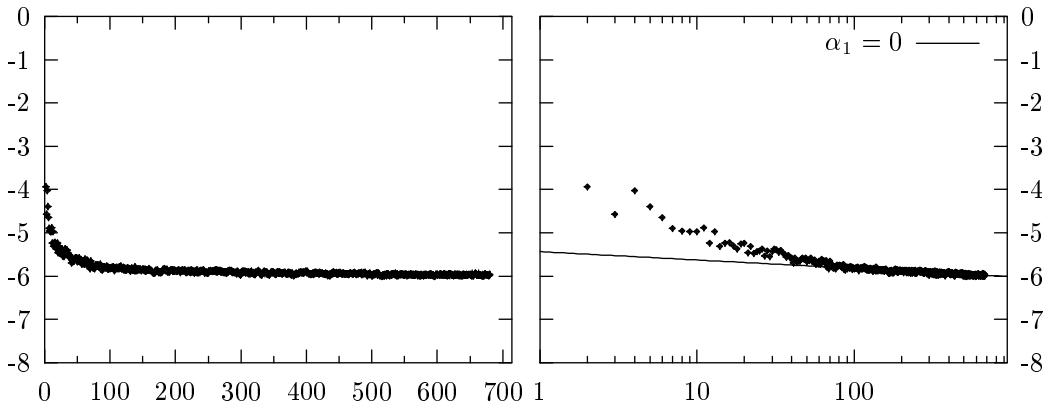


FIGURE 258. $\langle \log t_N \rangle_E$ vs. $N$ in 3D, $W = 12$, $E \in [-1.5, -0.5]$

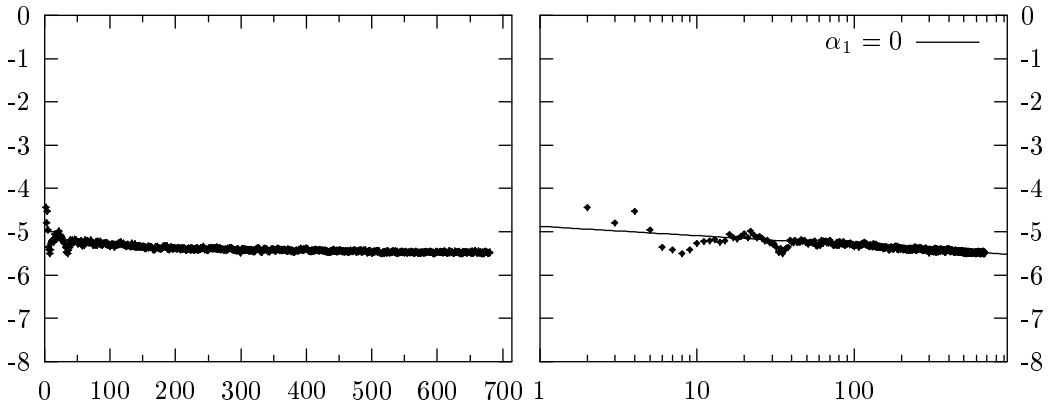


FIGURE 259. $\langle \log t_N \rangle_E$ vs. $N$ in 3D, $W = 12$, $E \in [-0.5, 0.5]$

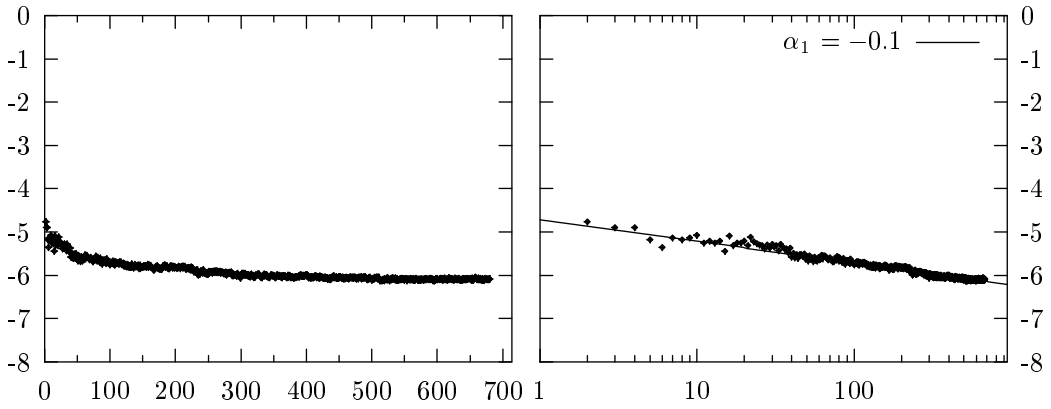


FIGURE 260. $\langle \log t_N \rangle_E$ vs. $N$ in 3D, $W = 12$, $E \in [0.5, 1.5]$

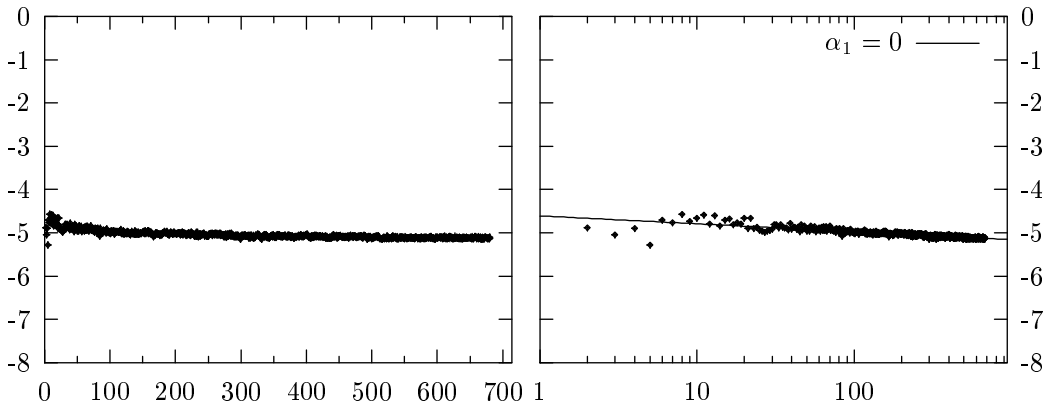


FIGURE 261. $\langle \log t_N \rangle_E$ vs. $N$ in 3D, $W = 12$, $E \in [1.5, 2.5]$

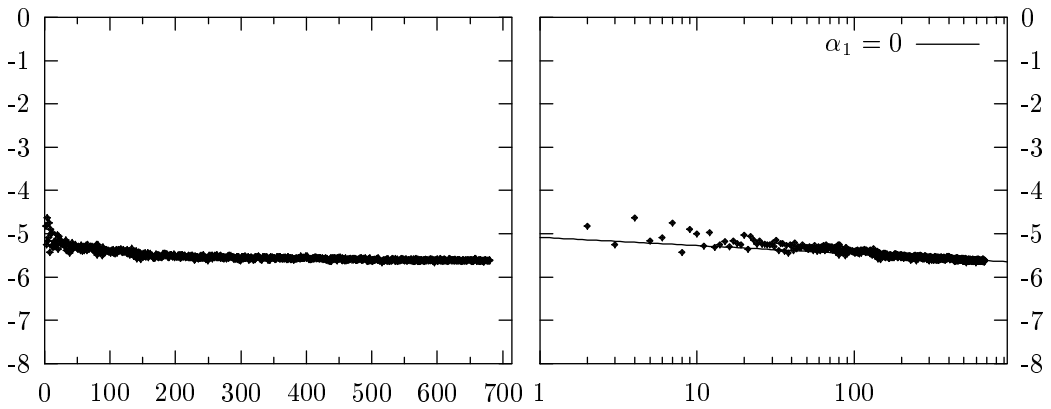


FIGURE 262. $\langle \log t_N \rangle_E$ vs. $N$ in 3D, $W = 12$, $E \in [2.5, 3.5]$

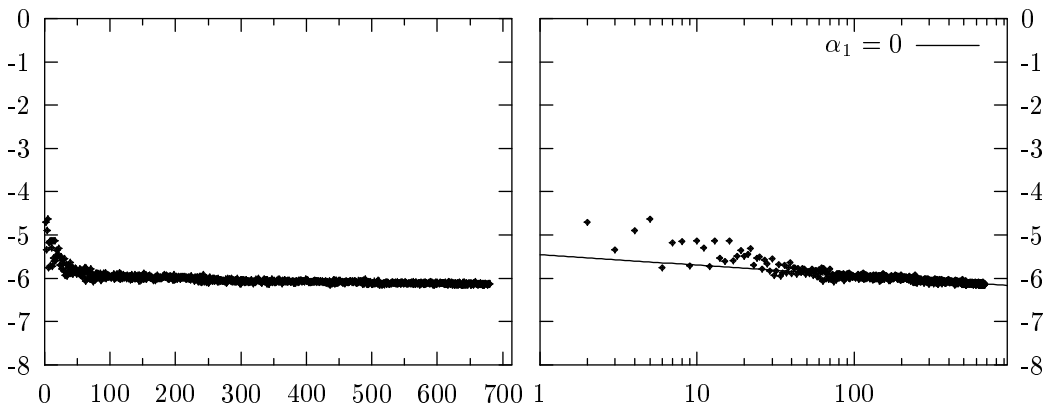


FIGURE 263. $\langle \log t_N \rangle_E$ vs. $N$ in 3D, $W = 12$, $E \in [3.5, 4.5]$

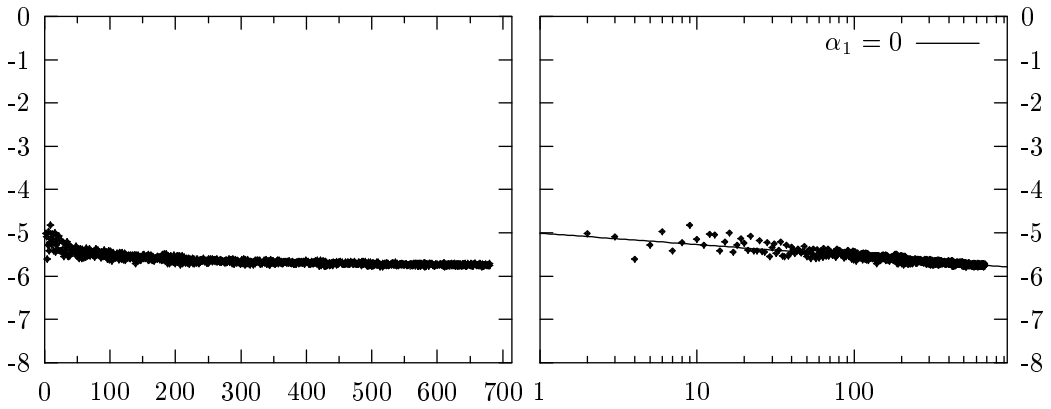


FIGURE 264. $\langle \log t_N \rangle_E$ vs. $N$ in 3D, $W = 12$, $E \in [4.5, 5.5]$

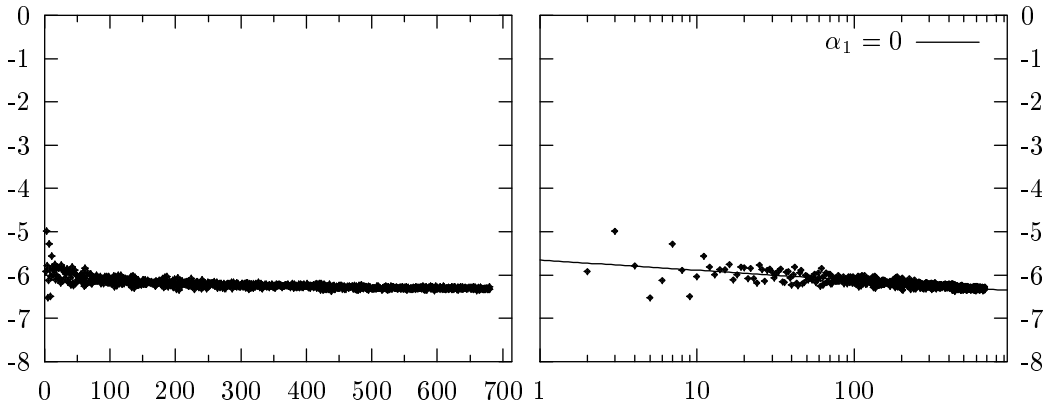


FIGURE 265. $\langle \log t_N \rangle_E$ vs. $N$ in 3D, $W = 12$, $E \in [5.5, 6.5]$

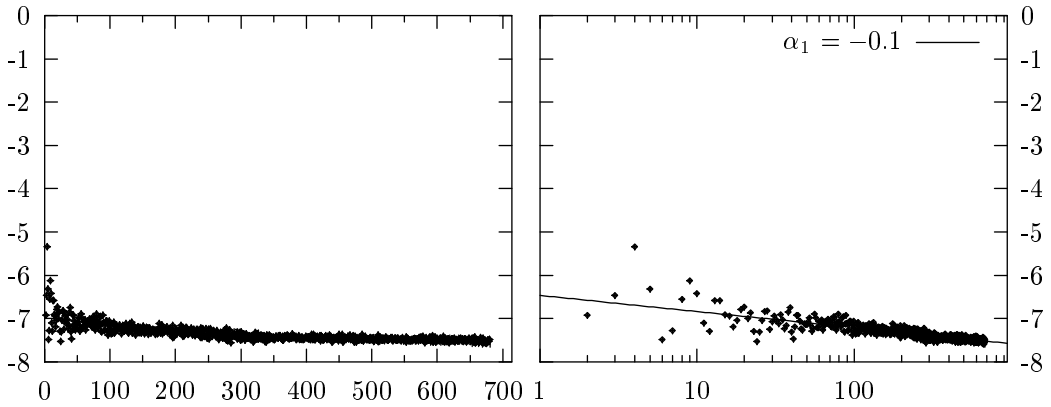


FIGURE 266. $\langle \log t_N \rangle_E$ vs. $N$ in 3D, $W = 12$, $E \in [6.5, 7.5]$

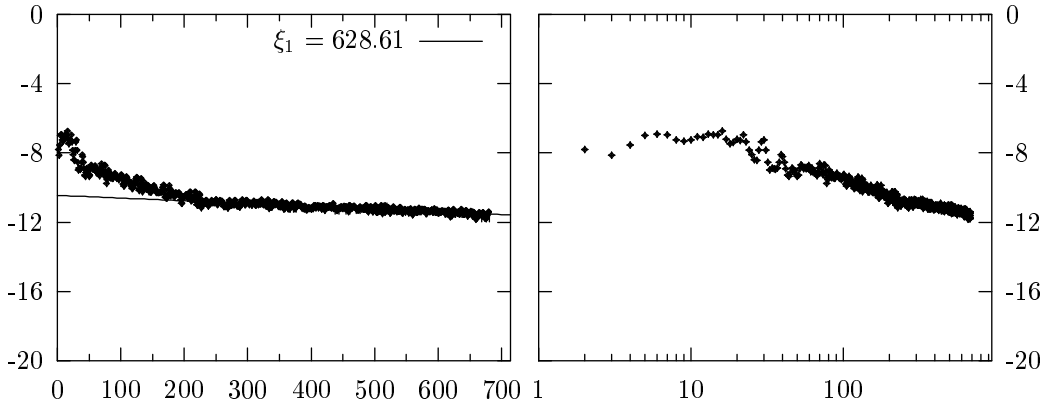


FIGURE 267. $\langle \log t_N \rangle_E$ vs. $N$ in 3D, $W = 12$, $E \in [7.5, 8.5]$

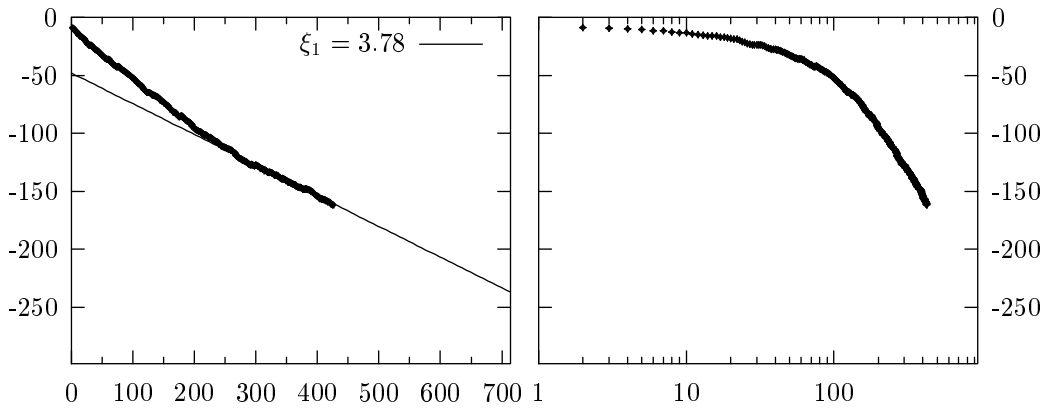


FIGURE 268. $\langle \log t_N \rangle_E$ vs. $N$ in 3D, $W = 12$, $E \in [8.5, 9.5]$

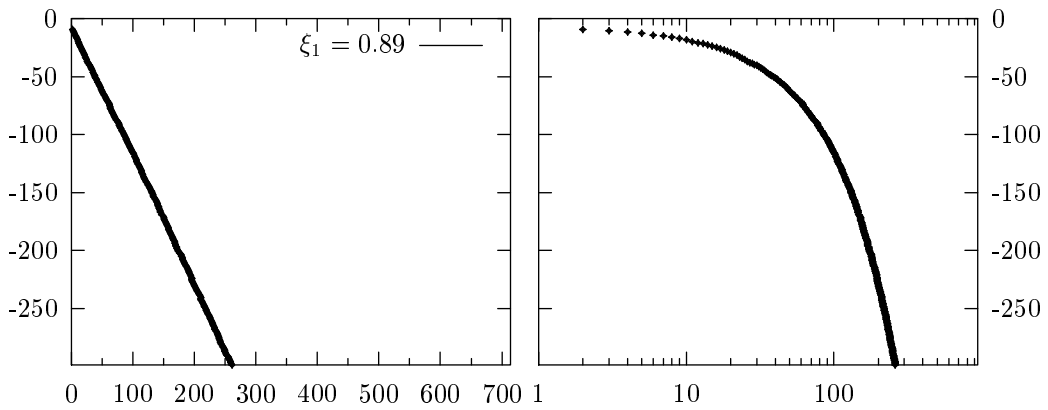


FIGURE 269. $\langle \log t_N \rangle_E$ vs. $N$ in 3D, $W = 12$, $E \in [9.5, 10.5]$

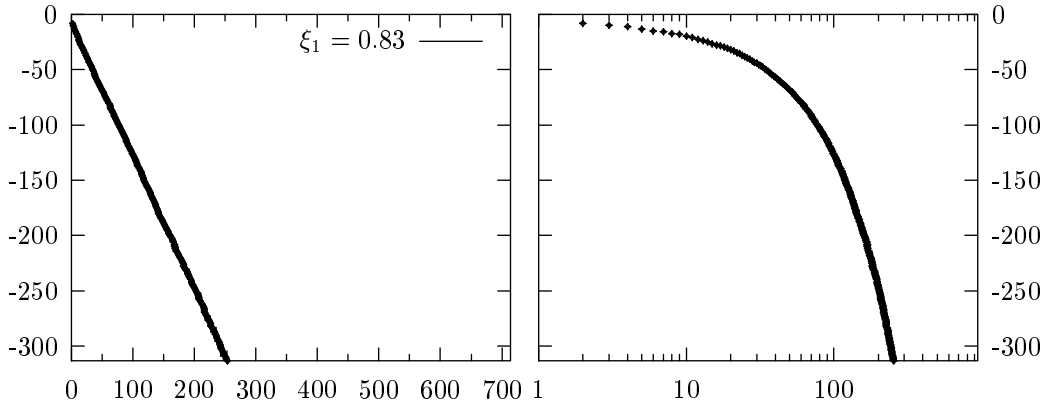


FIGURE 270. $\langle \log t_N \rangle_E$ vs. $N$ in 3D, $W = 16$, $E \in [-12.5, -11.5]$

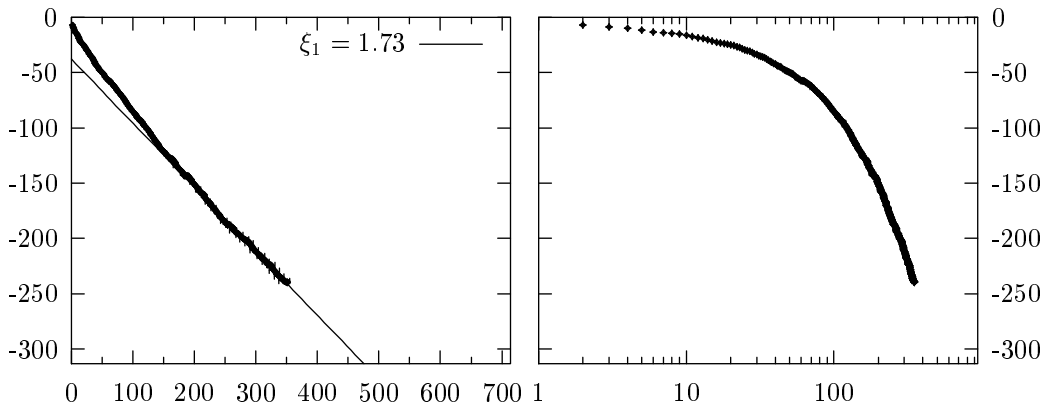


FIGURE 271. $\langle \log t_N \rangle_E$ vs. $N$ in 3D, $W = 16$, $E \in [-11.5, -10.5]$

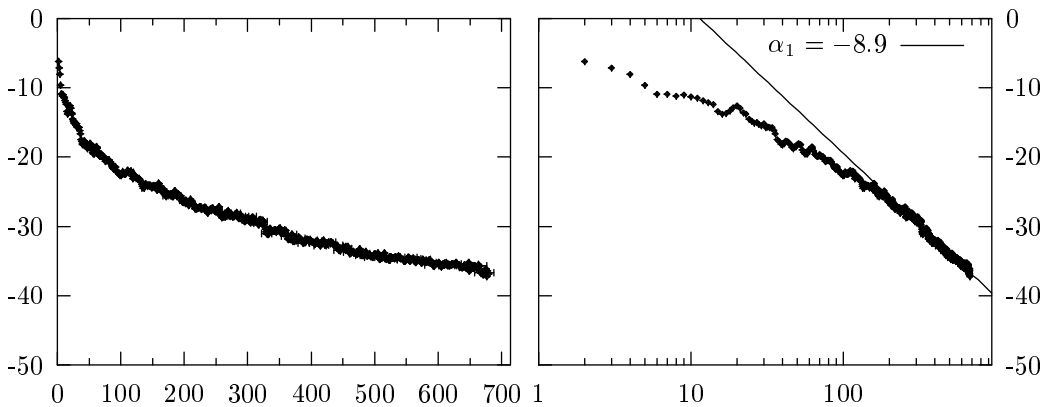


FIGURE 272. $\langle \log t_N \rangle_E$ vs. $N$ in 3D, $W = 16$, $E \in [-10.5, -9.5]$

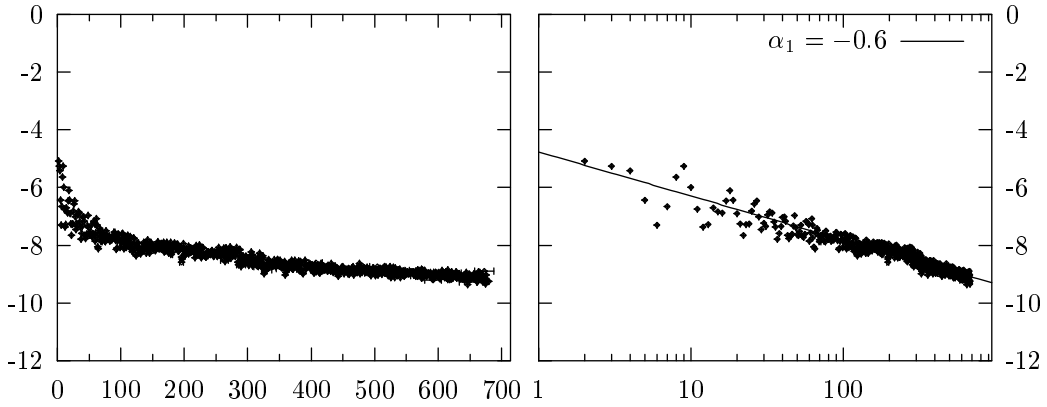


FIGURE 273. $\langle \log t_N \rangle_E$ vs. $N$ in 3D, $W = 16$, $E \in [-9.5, -8.5]$

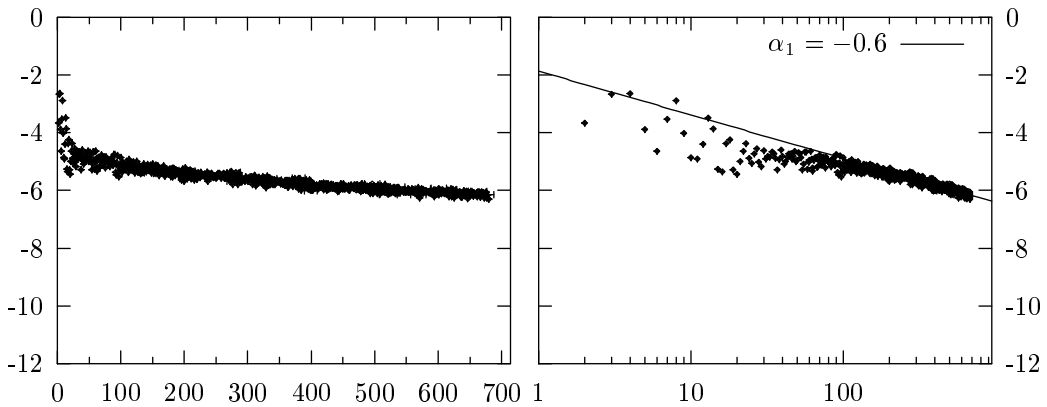


FIGURE 274. $\langle \log t_N \rangle_E$ vs. $N$ in 3D, $W = 16$, $E \in [-8.5, -7.5]$

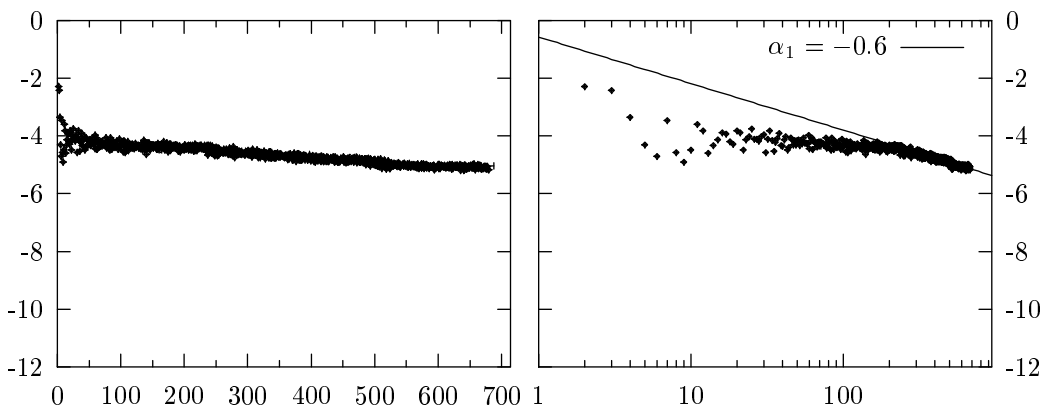


FIGURE 275. $\langle \log t_N \rangle_E$ vs. $N$ in 3D, $W = 16$, $E \in [-7.5, -6.5]$

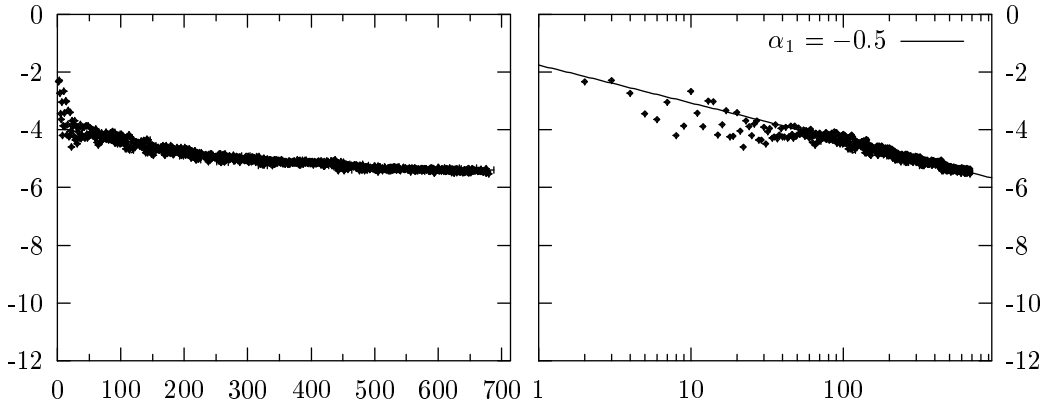


FIGURE 276. $\langle \log t_N \rangle_E$ vs. $N$ in 3D, $W = 16$, $E \in [-6.5, -5.5]$

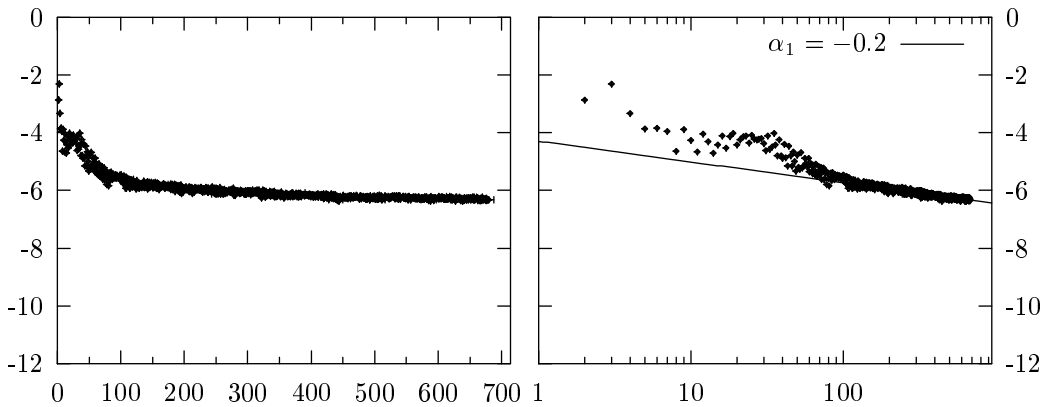


FIGURE 277. $\langle \log t_N \rangle_E$ vs. $N$ in 3D, $W = 16$, $E \in [-5.5, -4.5]$

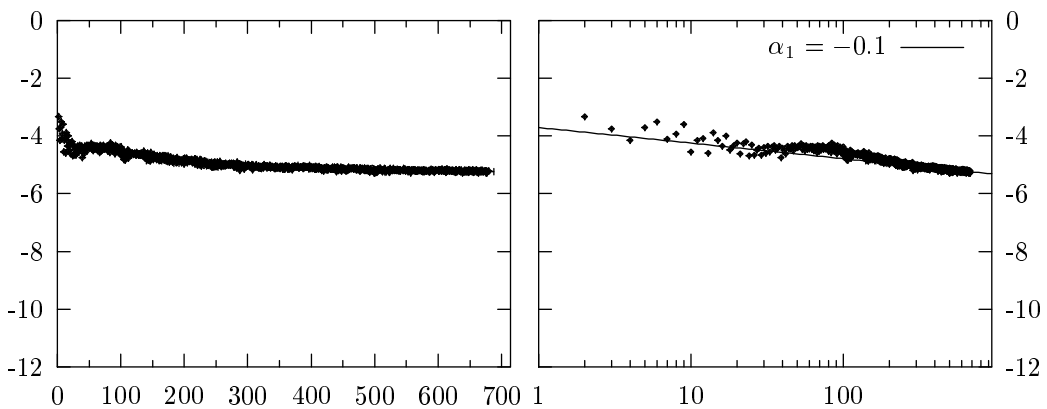


FIGURE 278. $\langle \log t_N \rangle_E$ vs. $N$ in 3D, $W = 16$, $E \in [-4.5, -3.5]$

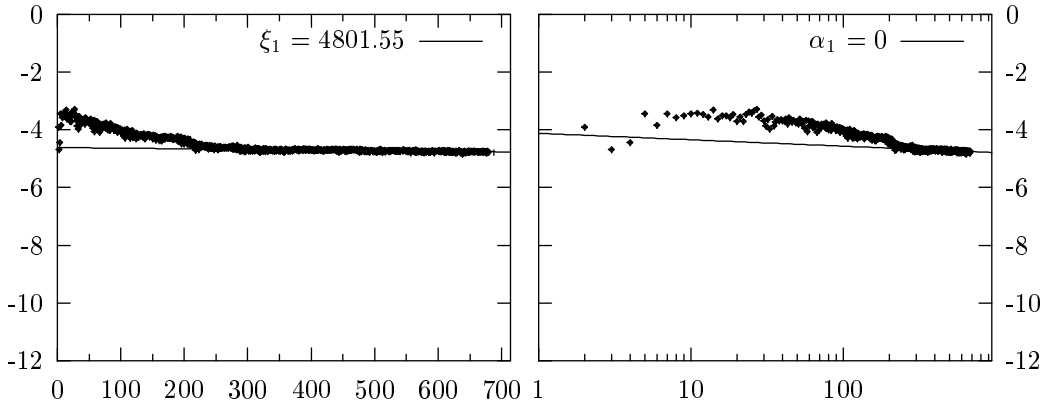


FIGURE 279. $\langle \log t_N \rangle_E$ vs. $N$ in 3D, $W = 16$, $E \in [-3.5, -2.5]$

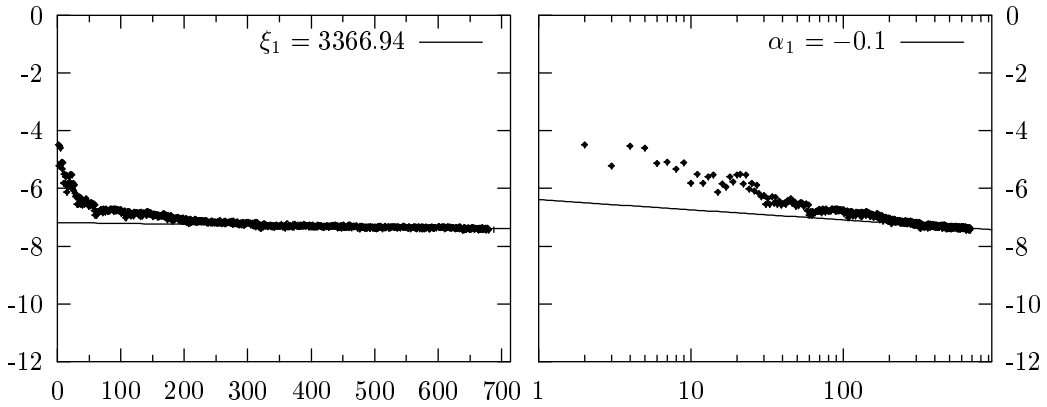


FIGURE 280. $\langle \log t_N \rangle_E$ vs. $N$ in 3D, $W = 16$, $E \in [-2.5, -1.5]$

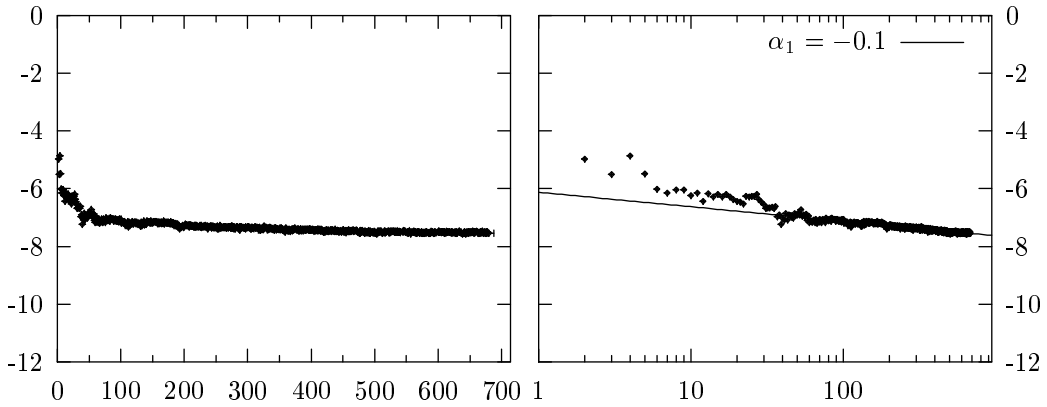


FIGURE 281. $\langle \log t_N \rangle_E$ vs. $N$ in 3D, $W = 16$, $E \in [-1.5, -0.5]$

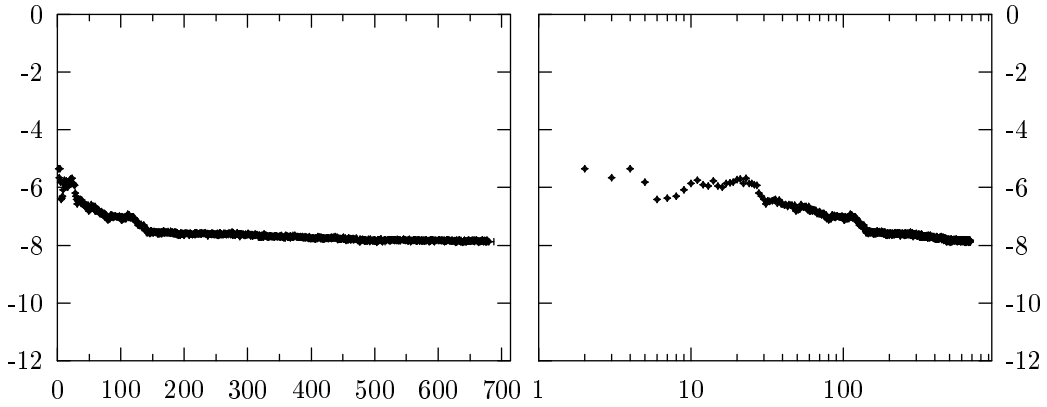


FIGURE 282. $\langle \log t_N \rangle_E$ vs. $N$ in 3D, $W = 16$, $E \in [-0.5, 0.5]$

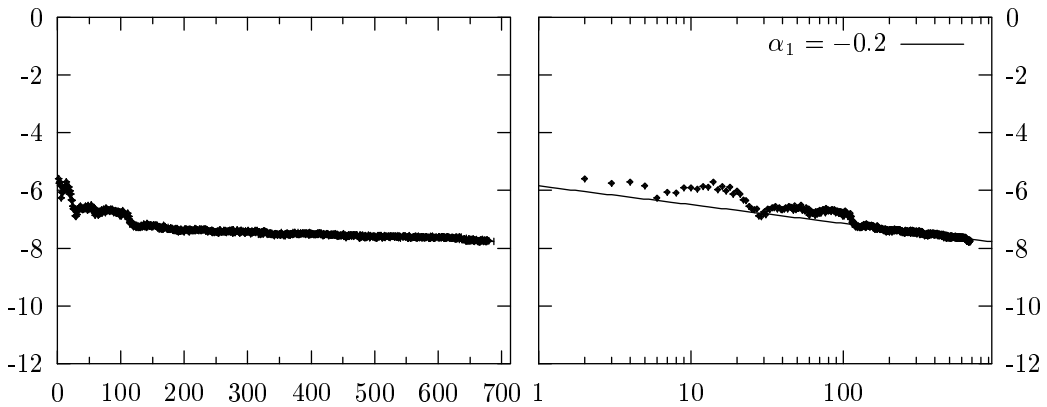


FIGURE 283. $\langle \log t_N \rangle_E$ vs. $N$ in 3D, $W = 16$, $E \in [0.5, 1.5]$

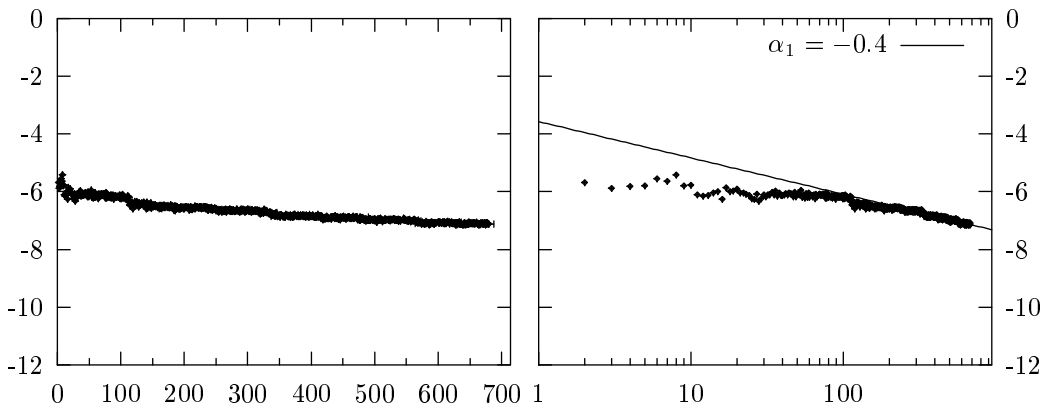


FIGURE 284. $\langle \log t_N \rangle_E$ vs. $N$ in 3D, $W = 16$, $E \in [1.5, 2.5]$

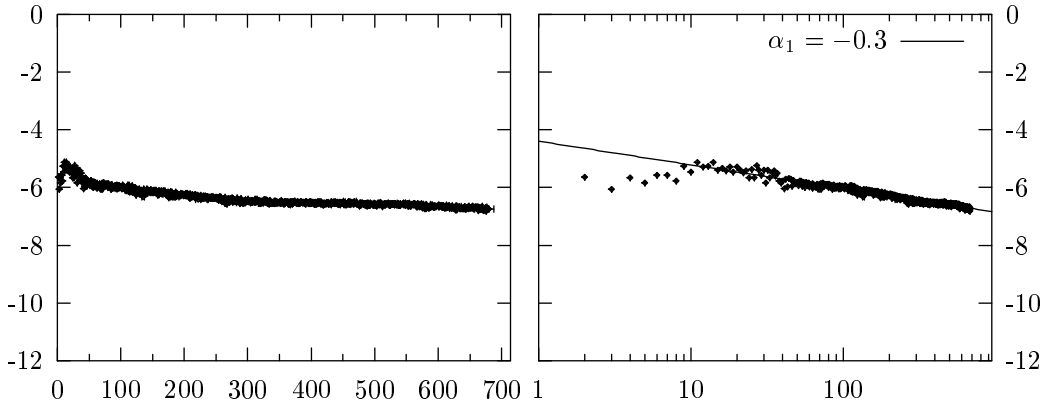


FIGURE 285. $\langle \log t_N \rangle_E$ vs. $N$ in 3D, $W = 16$, $E \in [2.5, 3.5]$

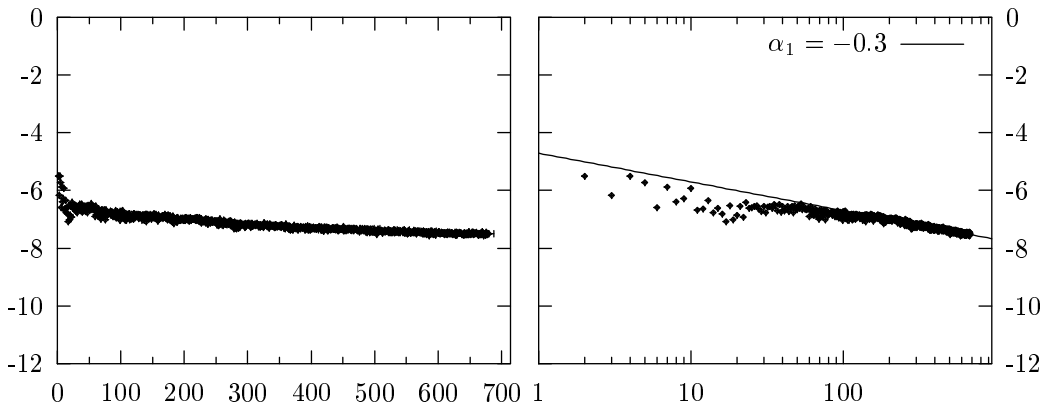


FIGURE 286. $\langle \log t_N \rangle_E$ vs. $N$ in 3D, $W = 16$, $E \in [3.5, 4.5]$

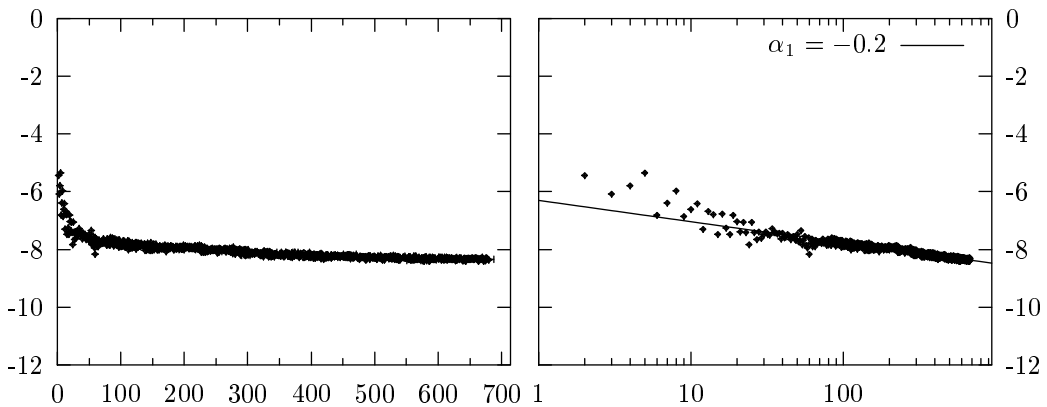


FIGURE 287. $\langle \log t_N \rangle_E$ vs. $N$ in 3D, $W = 16$, $E \in [4.5, 5.5]$

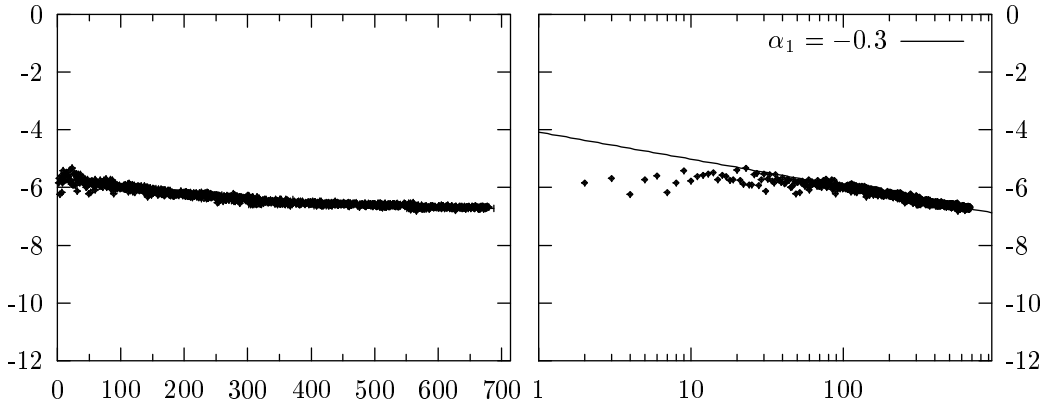


FIGURE 288. $\langle \log t_N \rangle_E$ vs. $N$ in 3D, $W = 16$, $E \in [5.5, 6.5]$

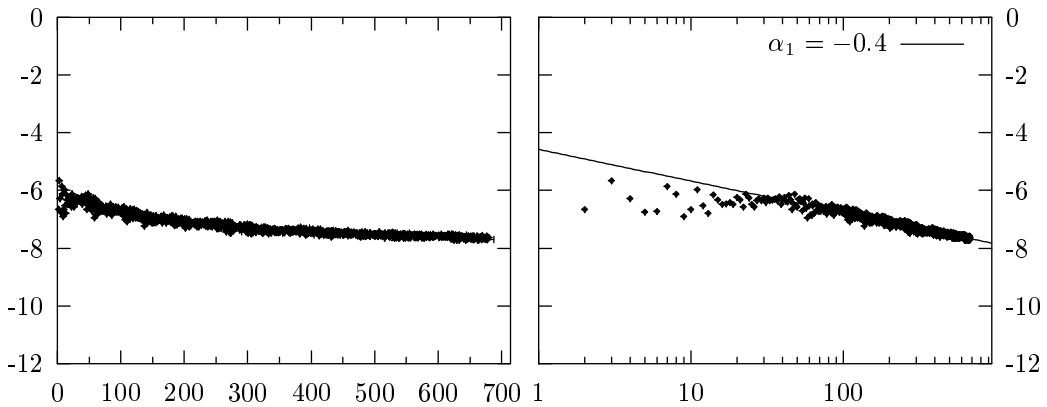


FIGURE 289. $\langle \log t_N \rangle_E$ vs. $N$ in 3D, $W = 16$, $E \in [6.5, 7.5]$

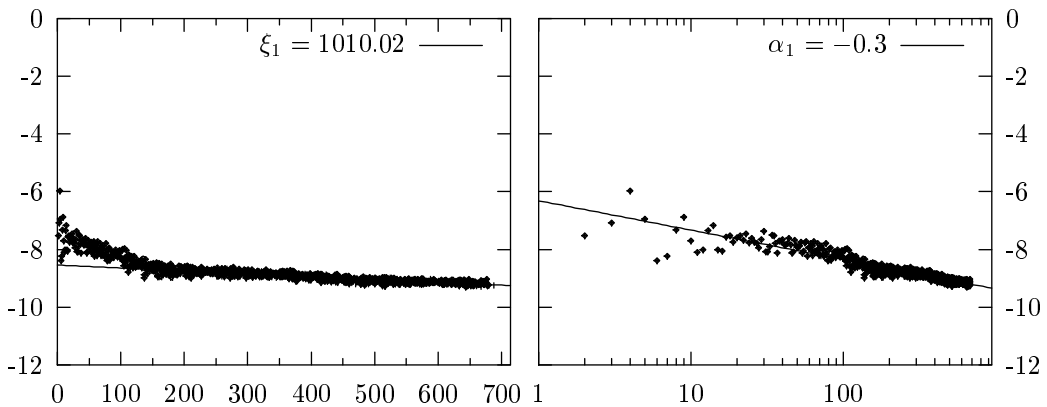


FIGURE 290. $\langle \log t_N \rangle_E$ vs. $N$ in 3D, $W = 16$, $E \in [7.5, 8.5]$

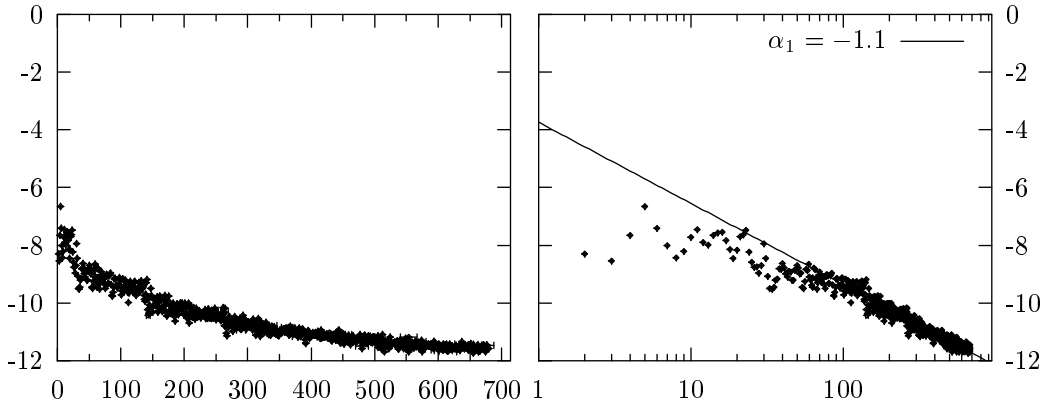


FIGURE 291. $\langle \log t_N \rangle_E$ vs. $N$ in 3D, $W = 16$, $E \in [8.5, 9.5]$

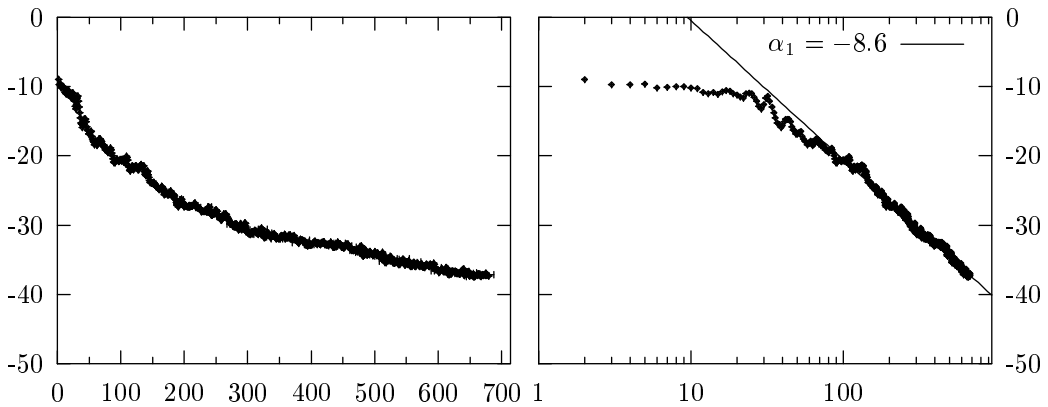


FIGURE 292. $\langle \log t_N \rangle_E$ vs. $N$ in 3D, $W = 16$, $E \in [9.5, 10.5]$

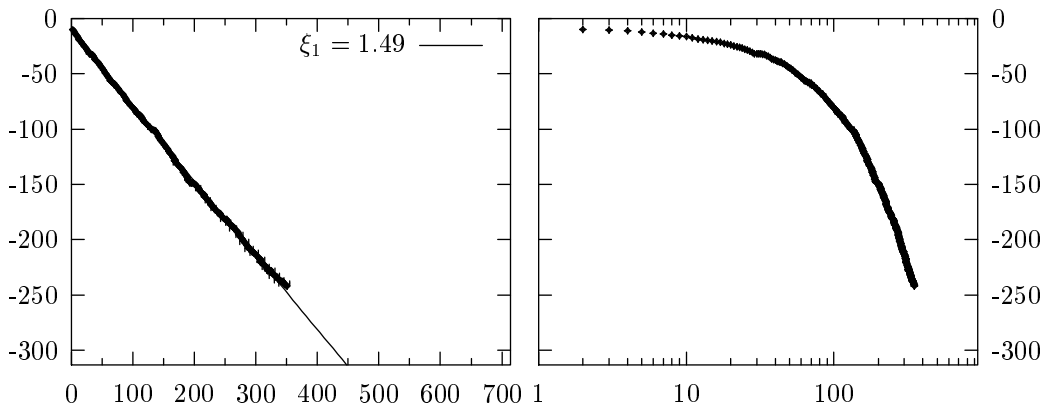


FIGURE 293. $\langle \log t_N \rangle_E$ vs. $N$ in 3D, $W = 16$, $E \in [10.5, 11.5]$

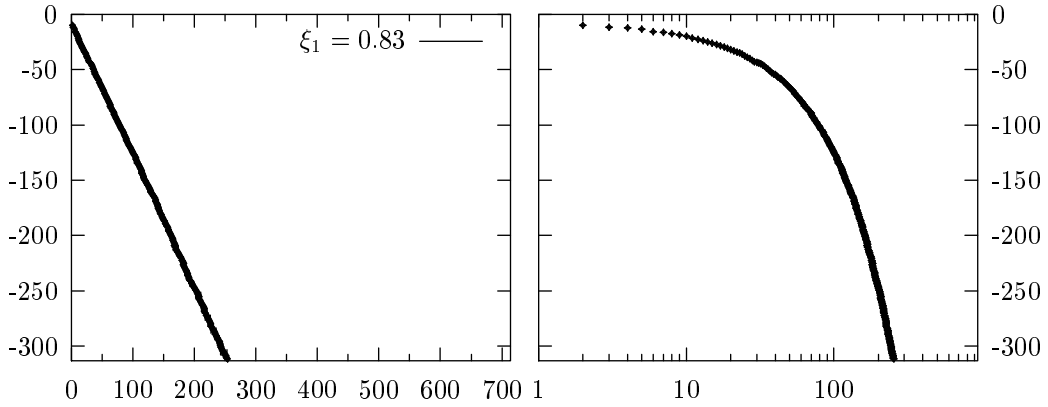


FIGURE 294. $\langle \log t_N \rangle_E$ vs. $N$ in 3D, $W = 16$, $E \in [11.5, 12.5]$

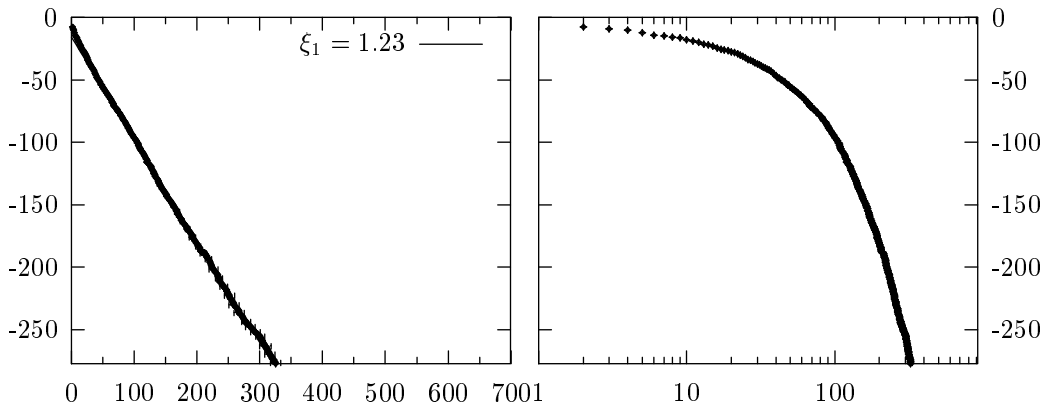


FIGURE 295. $\langle \log t_N \rangle_E$ vs. $N$ in 3D, $W = 20$, $E \in [-13.5, -12.5]$

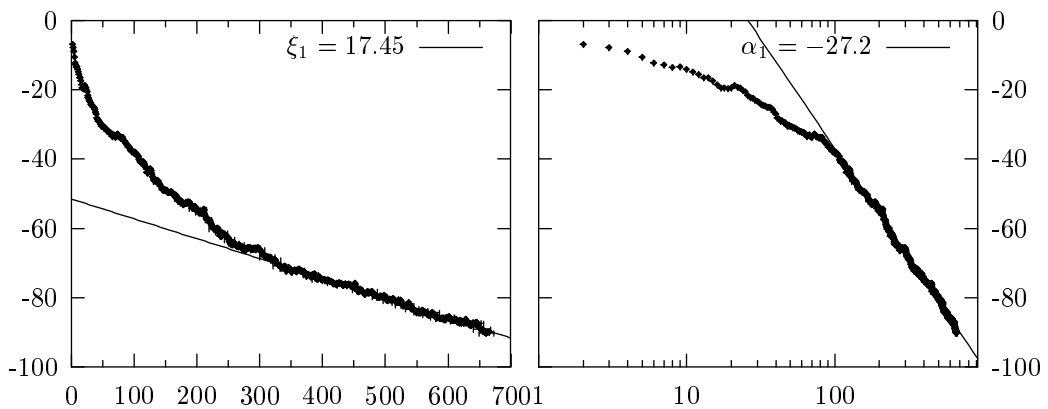


FIGURE 296. $\langle \log t_N \rangle_E$ vs. $N$ in 3D, $W = 20$, $E \in [-12.5, -11.5]$

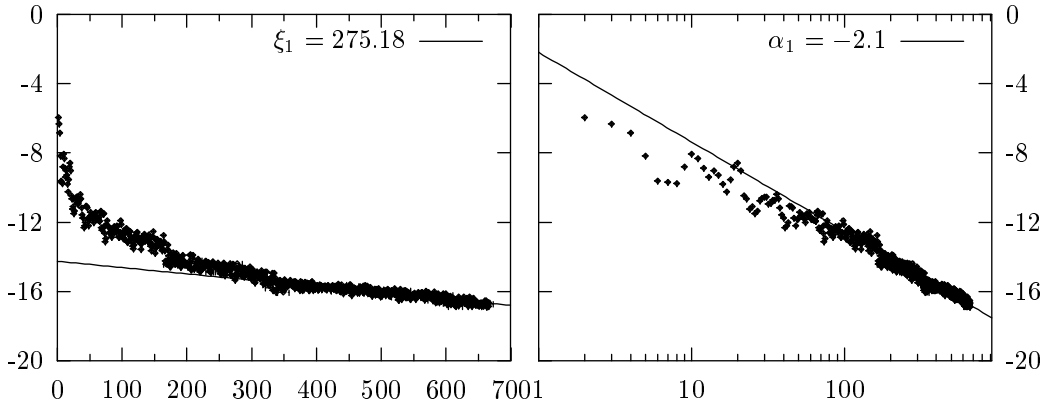


FIGURE 297. $\langle \log t_N \rangle_E$ vs. $N$ in 3D, $W = 20$, $E \in [-11.5, -10.5]$

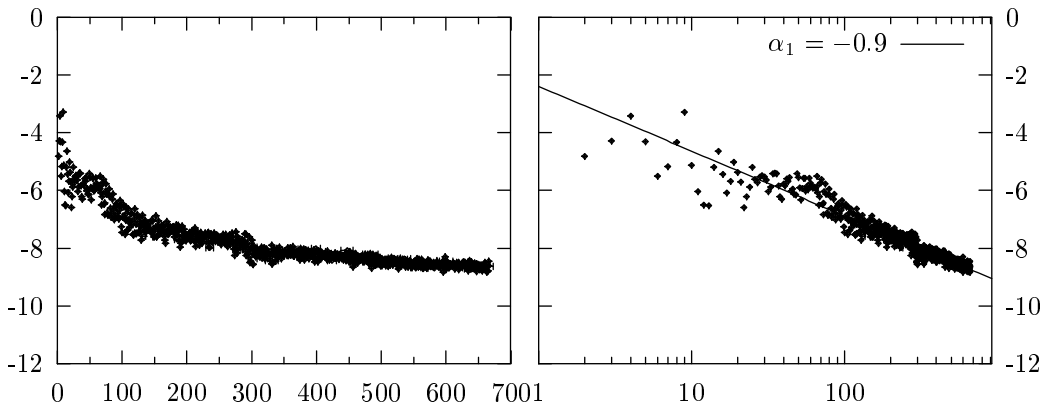


FIGURE 298. $\langle \log t_N \rangle_E$ vs. $N$ in 3D, $W = 20$, $E \in [-10.5, -9.5]$

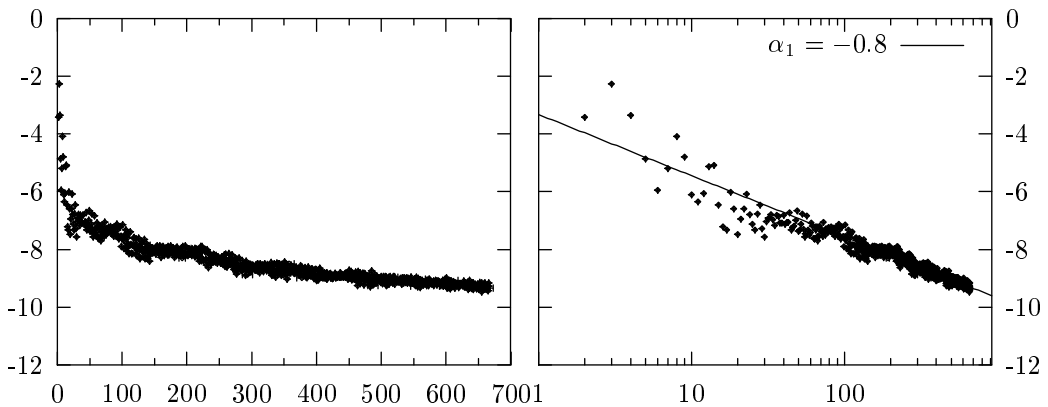


FIGURE 299. $\langle \log t_N \rangle_E$ vs. $N$ in 3D, $W = 20$, $E \in [-9.5, -8.5]$

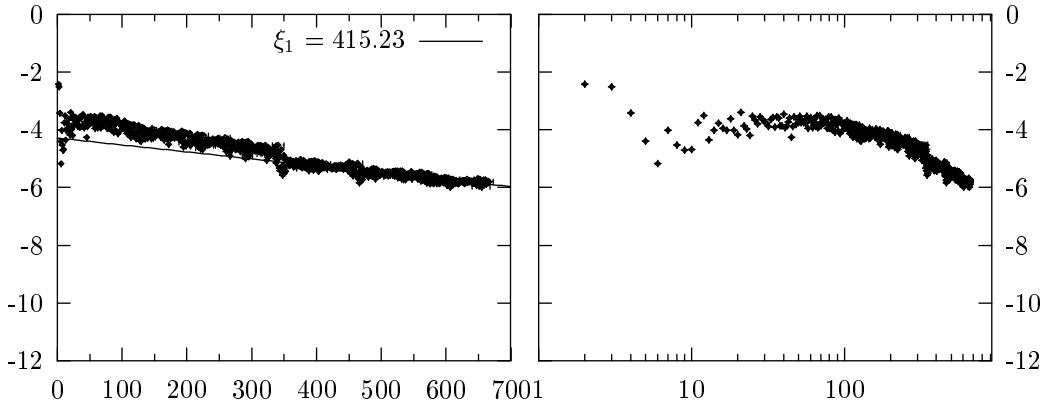


FIGURE 300. $\langle \log t_N \rangle_E$ vs. $N$ in 3D, $W = 20$, $E \in [-8.5, -7.5]$

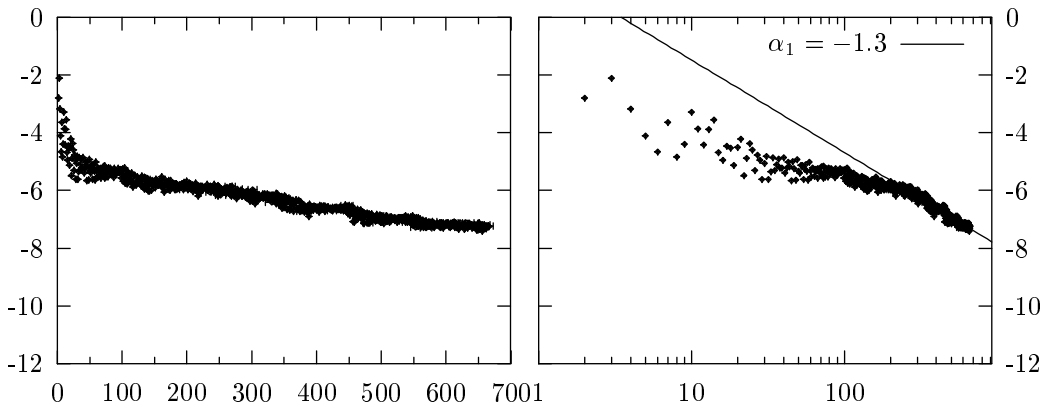


FIGURE 301. $\langle \log t_N \rangle_E$ vs. $N$ in 3D, $W = 20$, $E \in [-7.5, -6.5]$

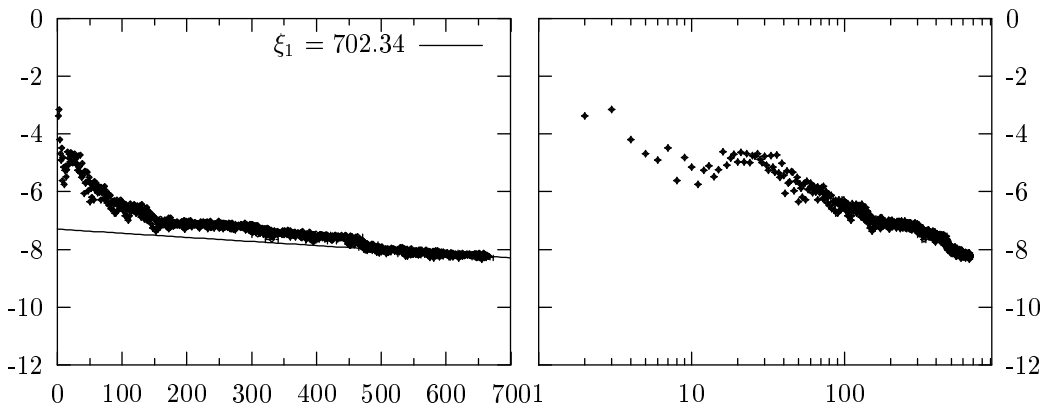


FIGURE 302. $\langle \log t_N \rangle_E$ vs. $N$ in 3D, $W = 20$, $E \in [-6.5, -5.5]$

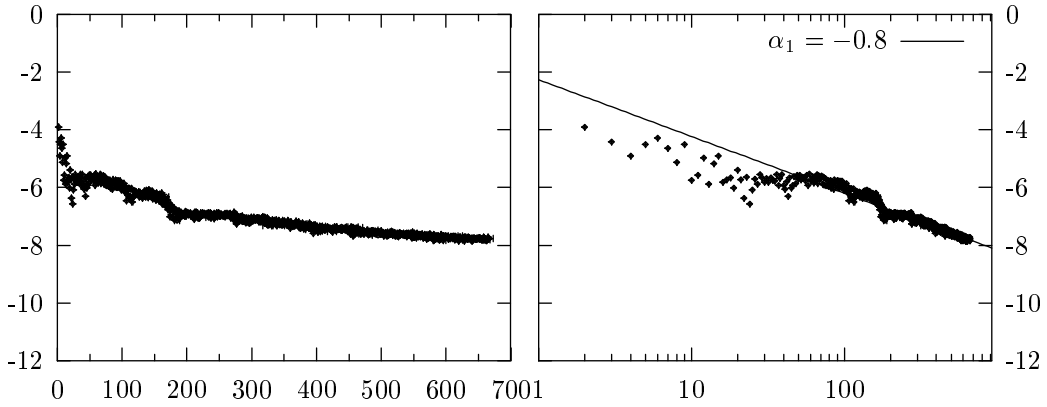


FIGURE 303. $\langle \log t_N \rangle_E$ vs. $N$ in 3D, $W = 20$, $E \in [-5.5, -4.5]$

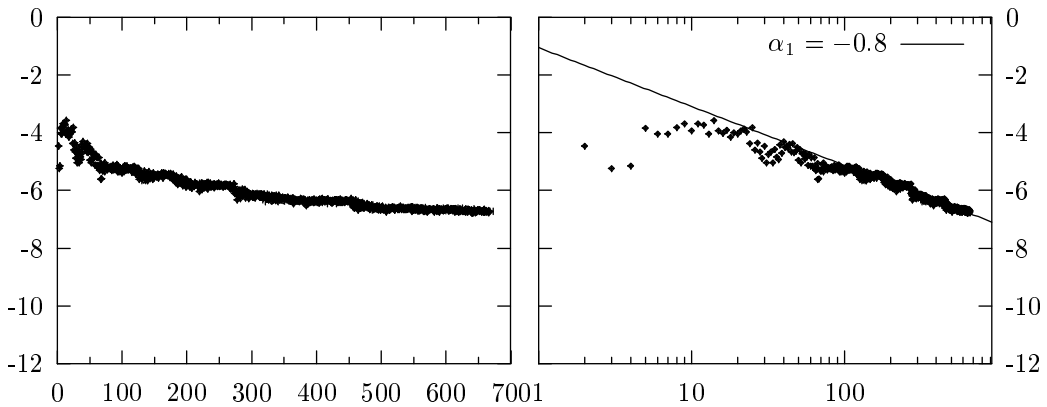


FIGURE 304. $\langle \log t_N \rangle_E$ vs. $N$ in 3D, $W = 20$, $E \in [-4.5, -3.5]$

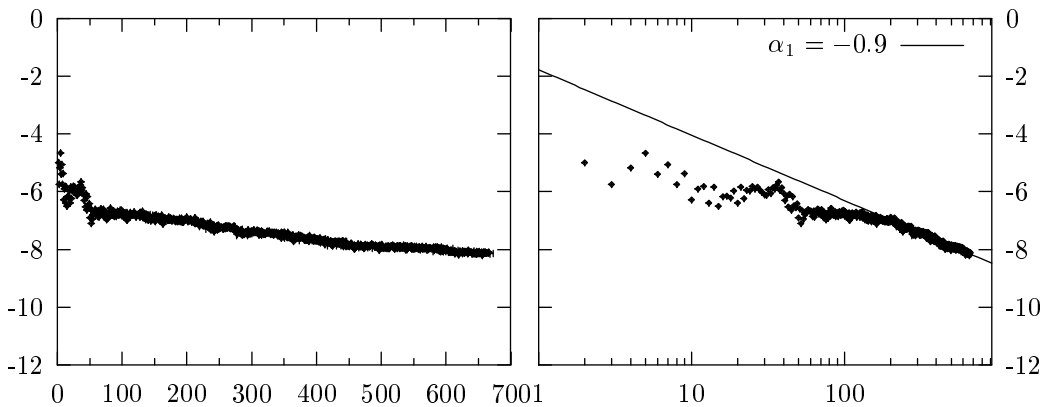


FIGURE 305. $\langle \log t_N \rangle_E$ vs. $N$ in 3D, $W = 20$, $E \in [-3.5, -2.5]$

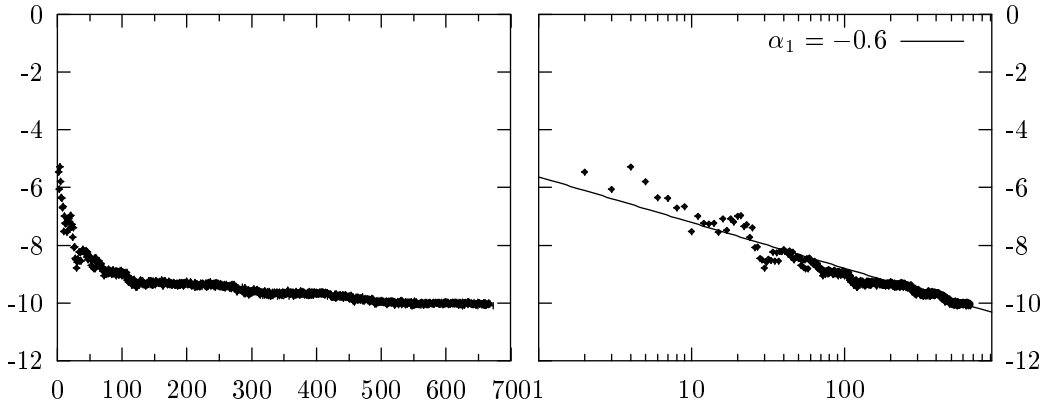


FIGURE 306. $\langle \log t_N \rangle_E$ vs. $N$ in 3D, $W = 20$, $E \in [-2.5, -1.5]$

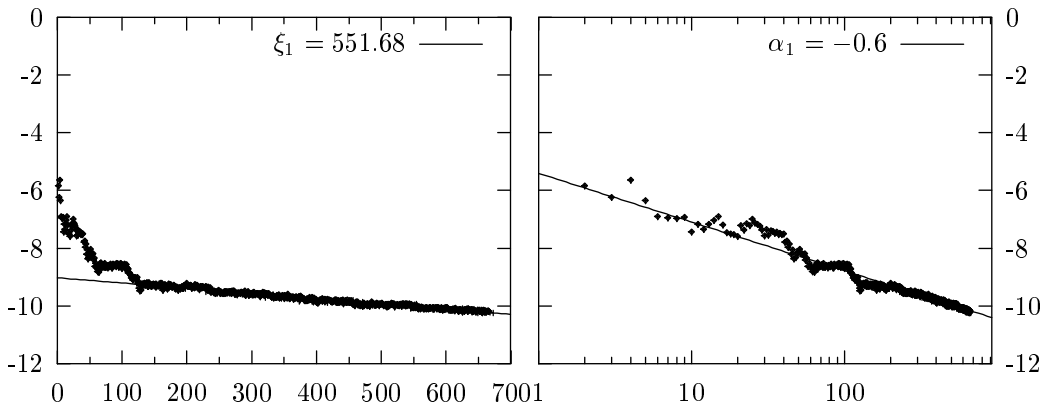


FIGURE 307. $\langle \log t_N \rangle_E$ vs. $N$ in 3D, $W = 20$, $E \in [-1.5, -0.5]$

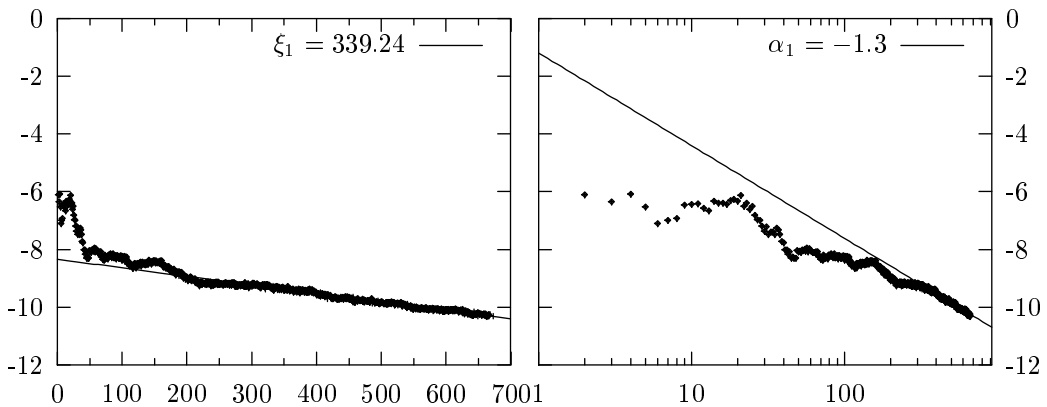


FIGURE 308. $\langle \log t_N \rangle_E$ vs. $N$ in 3D, $W = 20$, $E \in [-0.5, 0.5]$

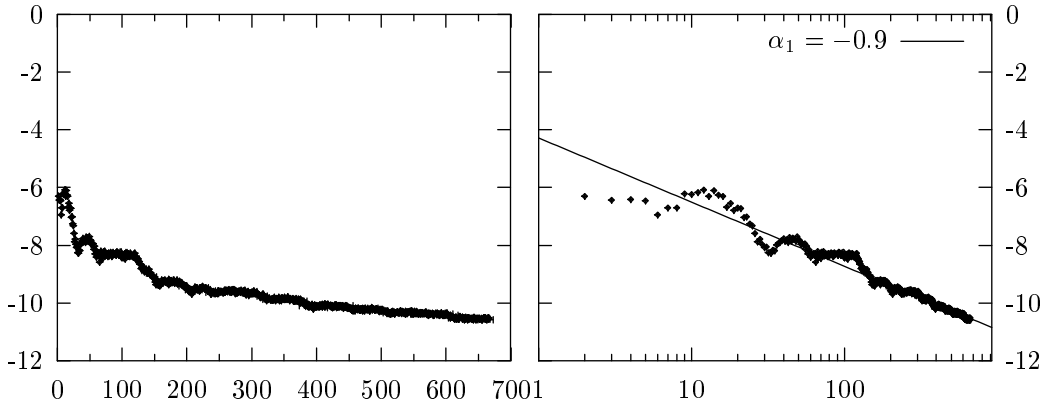


FIGURE 309. $\langle \log t_N \rangle_E$ vs. $N$ in 3D, $W = 20$, $E \in [0.5, 1.5]$

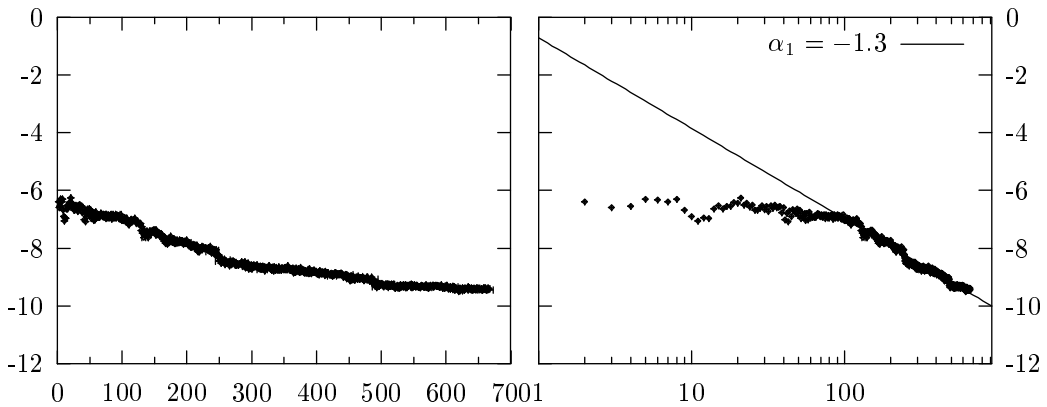


FIGURE 310. $\langle \log t_N \rangle_E$ vs. $N$ in 3D, $W = 20$, $E \in [1.5, 2.5]$

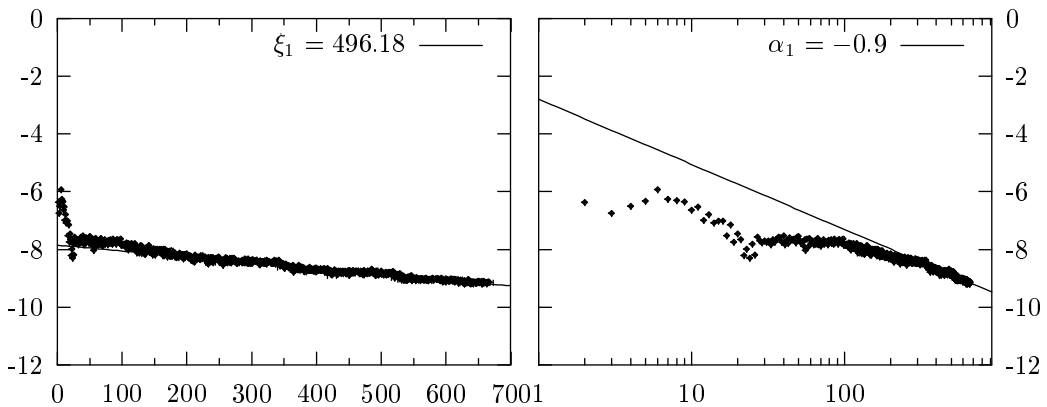


FIGURE 311. $\langle \log t_N \rangle_E$ vs. $N$ in 3D, $W = 20$, $E \in [2.5, 3.5]$

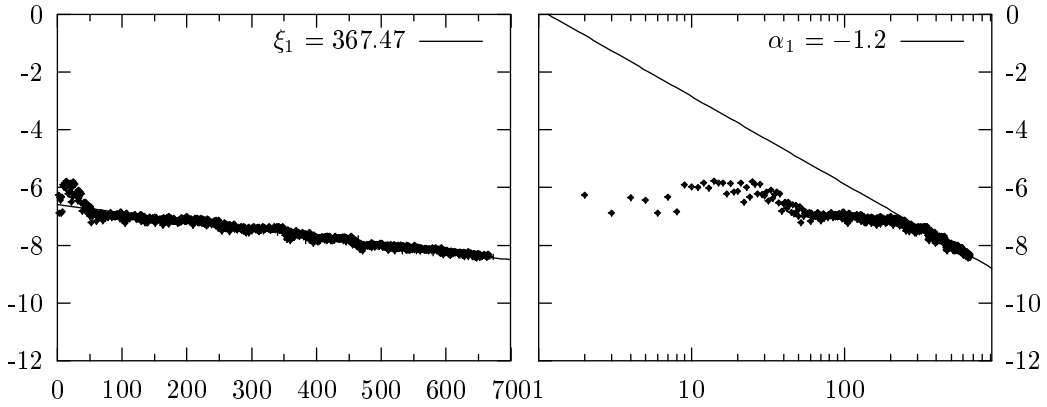


FIGURE 312. $\langle \log t_N \rangle_E$ vs. $N$ in 3D, $W = 20$, $E \in [3.5, 4.5]$

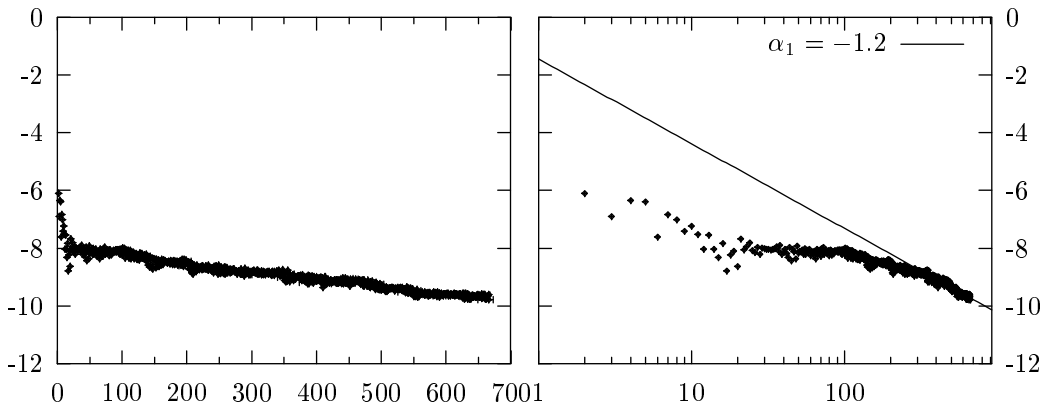


FIGURE 313. $\langle \log t_N \rangle_E$ vs. $N$ in 3D, $W = 20$, $E \in [4.5, 5.5]$

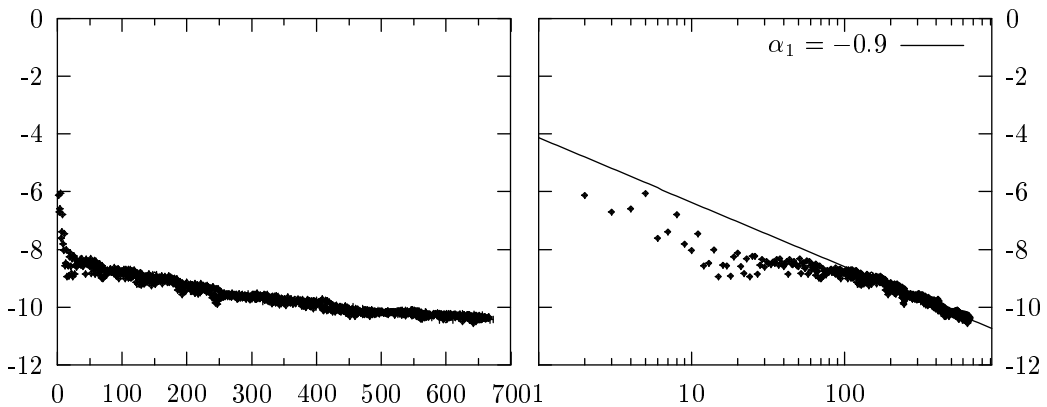


FIGURE 314. $\langle \log t_N \rangle_E$ vs. $N$ in 3D, $W = 20$, $E \in [5.5, 6.5]$

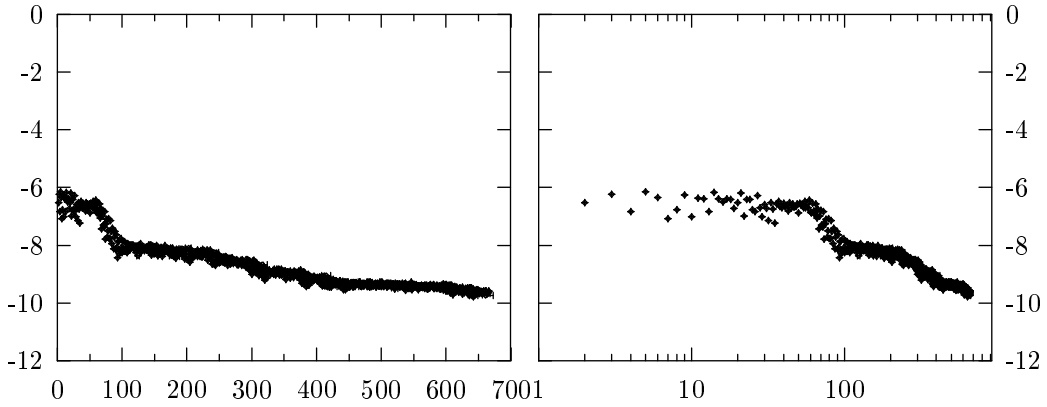


FIGURE 315. $\langle \log t_N \rangle_E$ vs. $N$ in 3D, $W = 20$, $E \in [6.5, 7.5]$

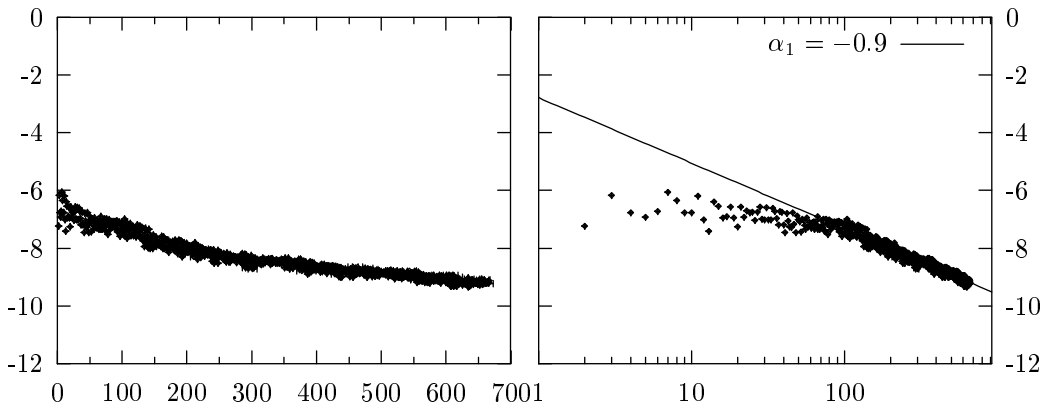


FIGURE 316. $\langle \log t_N \rangle_E$ vs. $N$ in 3D, $W = 20$, $E \in [7.5, 8.5]$

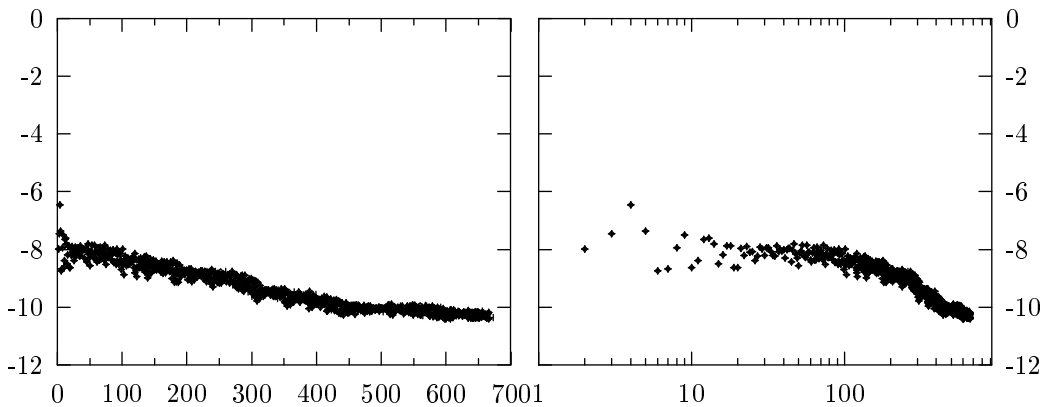


FIGURE 317. $\langle \log t_N \rangle_E$ vs. $N$ in 3D, $W = 20$, $E \in [8.5, 9.5]$

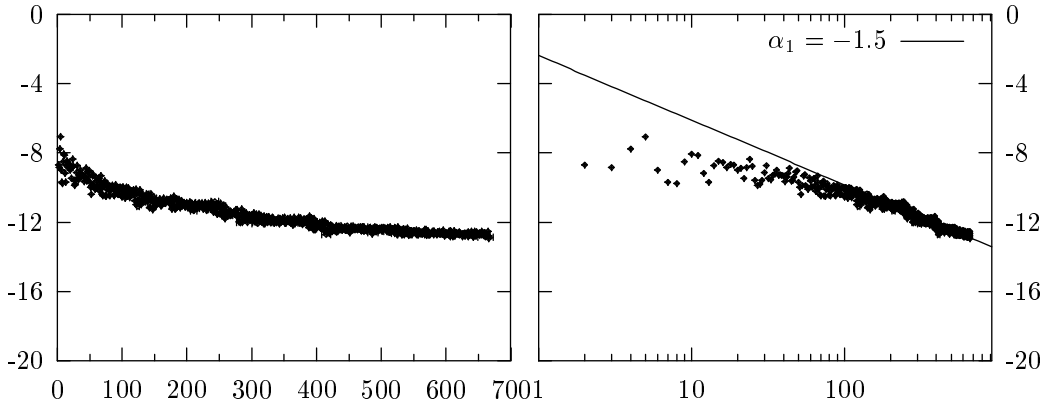


FIGURE 318. $\langle \log t_N \rangle_E$ vs. $N$ in 3D, $W = 20$, $E \in [9.5, 10.5]$

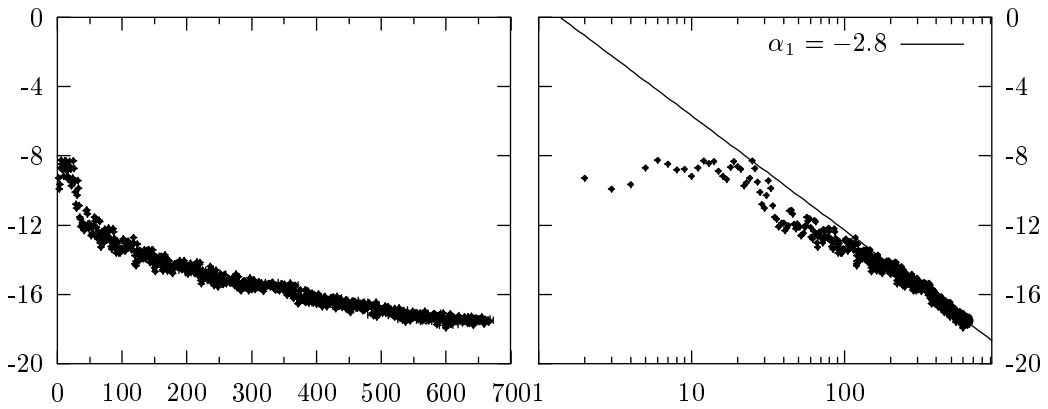


FIGURE 319. $\langle \log t_N \rangle_E$ vs. $N$ in 3D, $W = 20$, $E \in [10.5, 11.5]$

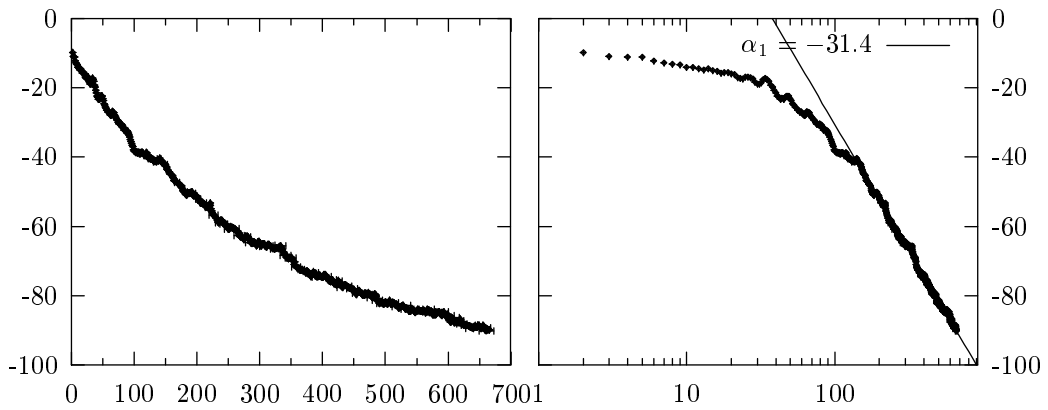


FIGURE 320. $\langle \log t_N \rangle_E$ vs. $N$ in 3D, $W = 20$, $E \in [11.5, 12.5]$

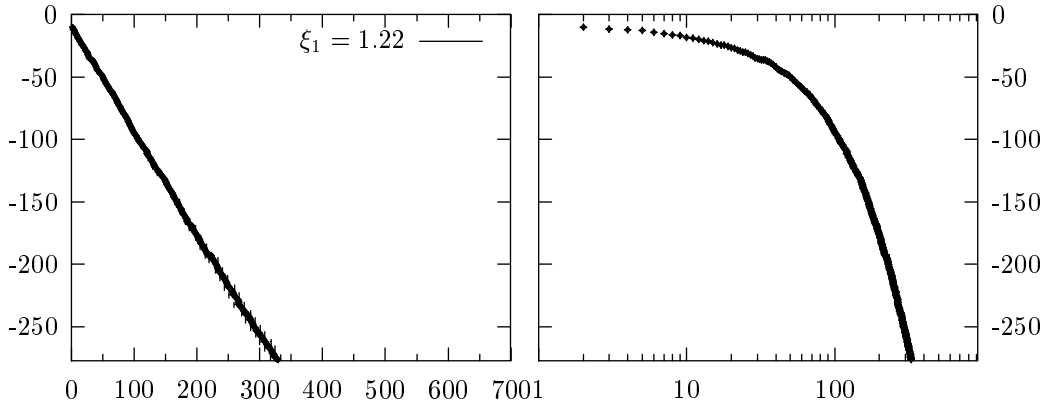


FIGURE 321. $\langle \log t_N \rangle_E$ vs. $N$ in 3D, $W = 20$, $E \in [12.5, 13.5]$

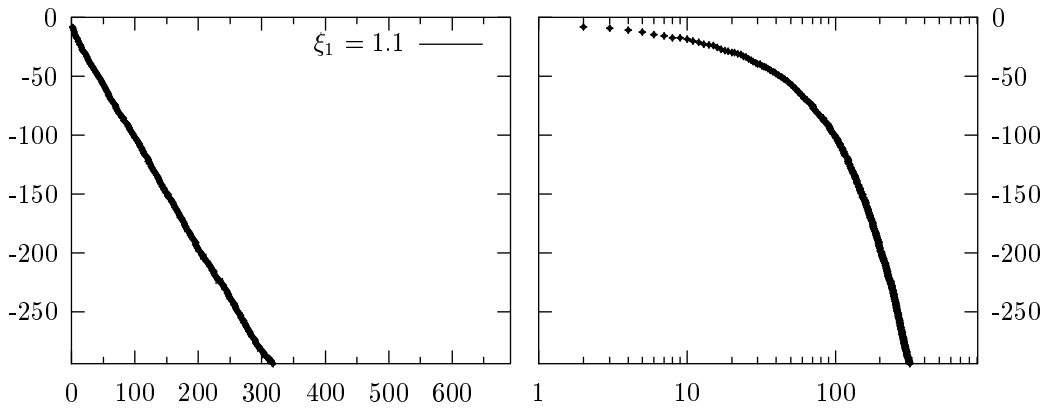


FIGURE 322. $\langle \log t_N \rangle_E$ vs. $N$ in 3D, $W = 24$, $E \in [-15.5, -14.5]$

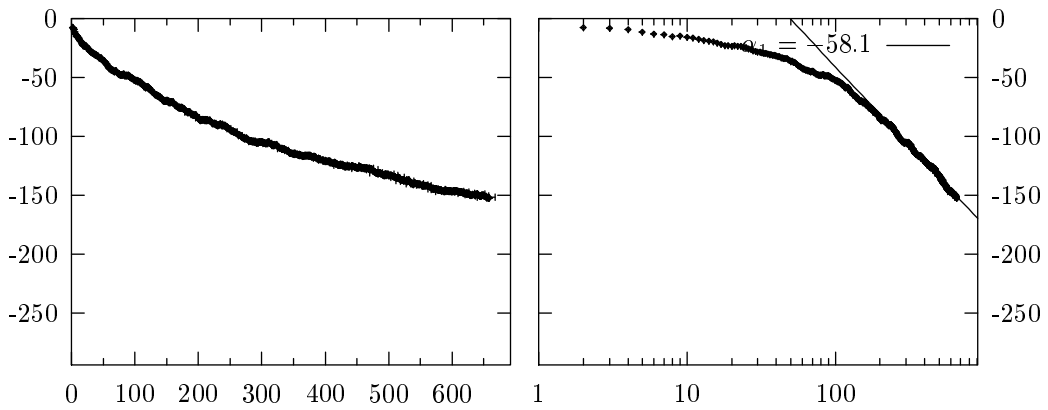


FIGURE 323. $\langle \log t_N \rangle_E$ vs. $N$ in 3D, $W = 24$, $E \in [-14.5, -13.5]$

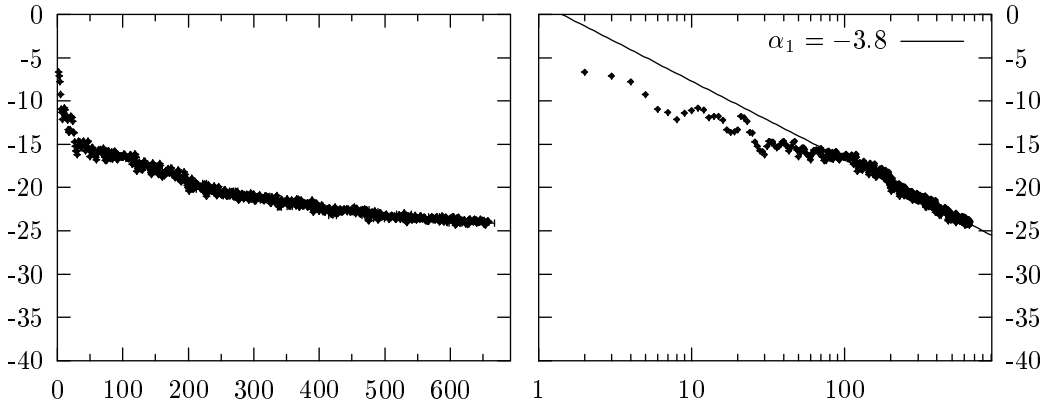


FIGURE 324. $\langle \log t_N \rangle_E$ vs. $N$ in 3D, $W = 24$, $E \in [-13.5, -12.5]$

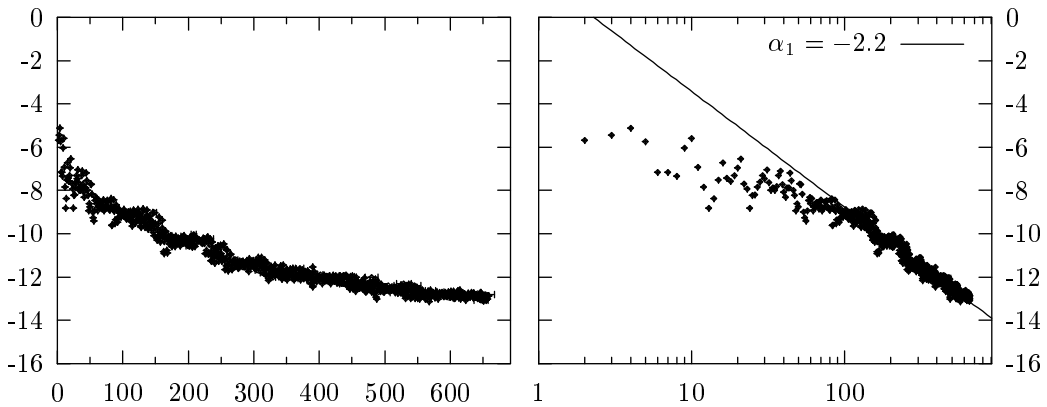


FIGURE 325. $\langle \log t_N \rangle_E$ vs. $N$ in 3D, $W = 24$, $E \in [-12.5, -11.5]$

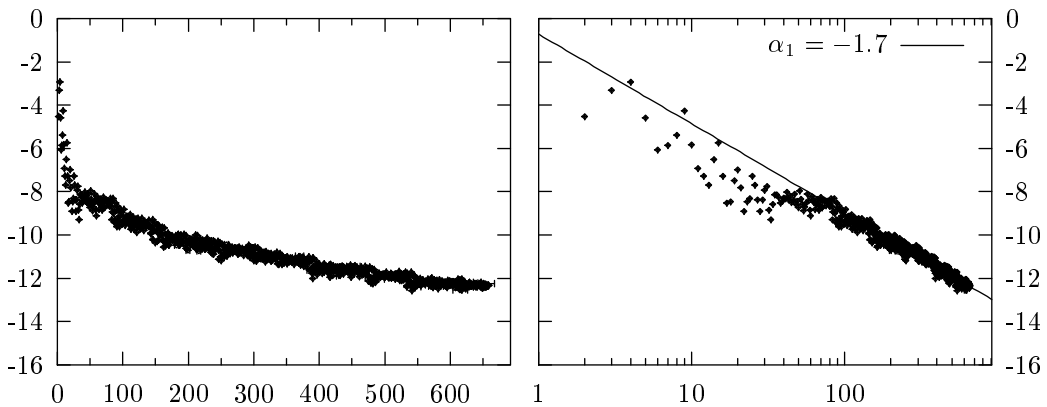


FIGURE 326. $\langle \log t_N \rangle_E$ vs. $N$ in 3D, $W = 24$, $E \in [-11.5, -10.5]$

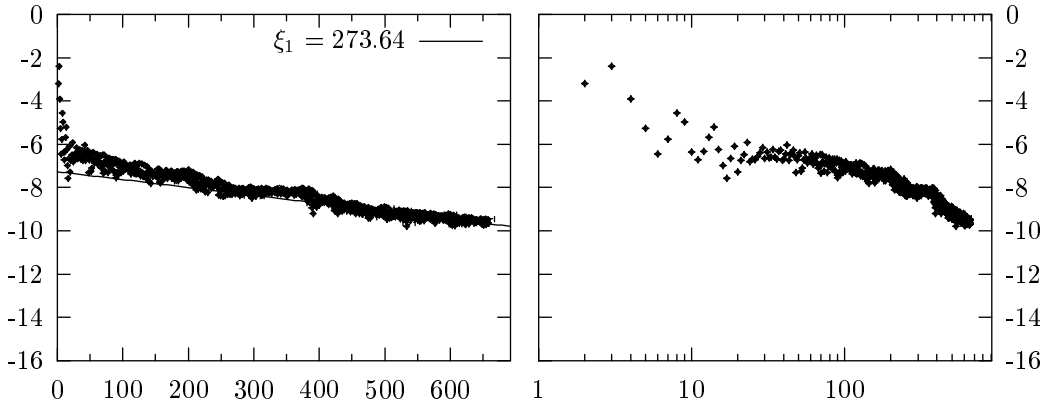


FIGURE 327. $\langle \log t_N \rangle_E$ vs. $N$ in 3D, $W = 24$, $E \in [-10.5, -9.5]$

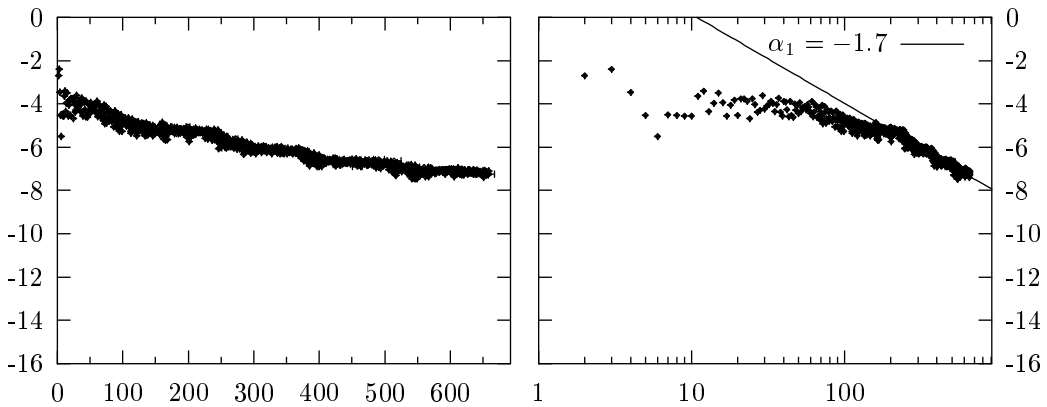


FIGURE 328. $\langle \log t_N \rangle_E$ vs. $N$ in 3D, $W = 24$, $E \in [-9.5, -8.5]$

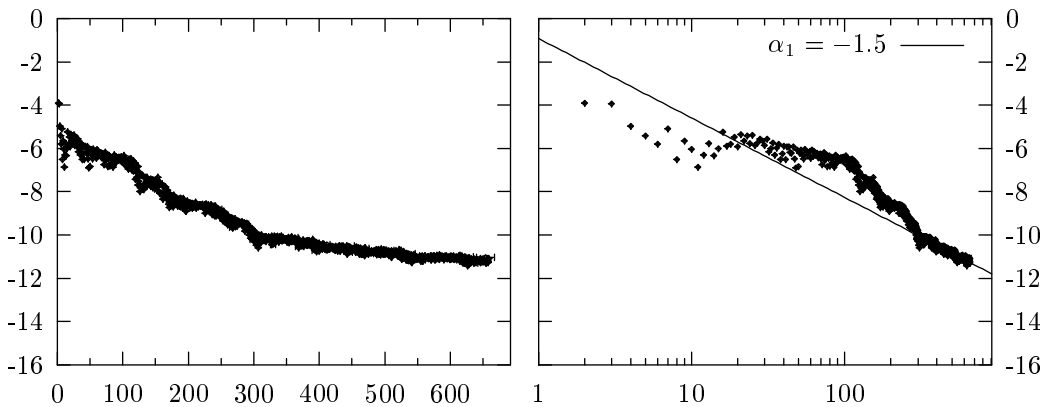


FIGURE 329. $\langle \log t_N \rangle_E$ vs. $N$ in 3D, $W = 24$, $E \in [-7.5, -6.5]$

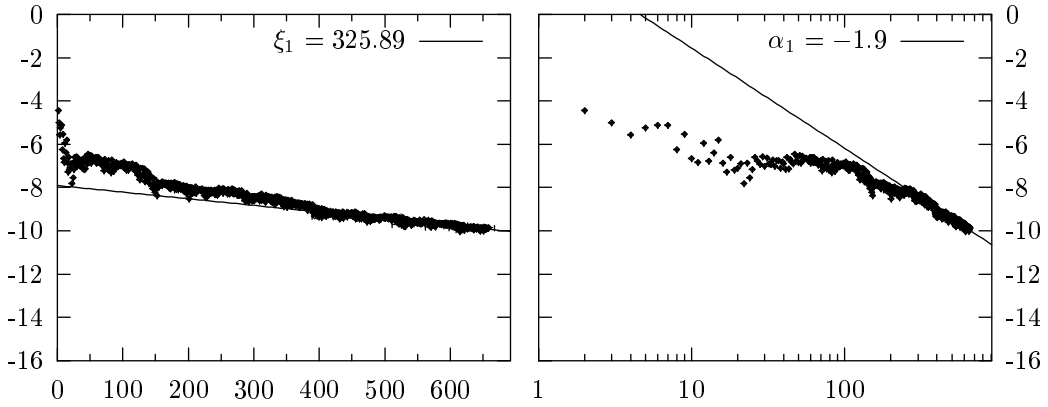


FIGURE 330. $\langle \log t_N \rangle_E$ vs. $N$ in 3D, $W = 24$, $E \in [-6.5, -5.5]$

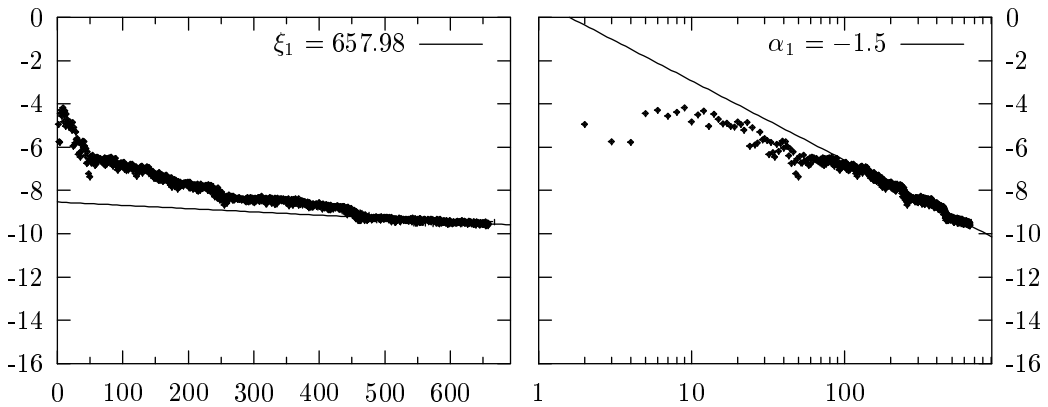


FIGURE 331. $\langle \log t_N \rangle_E$ vs. $N$ in 3D, $W = 24$, $E \in [-5.5, -4.5]$

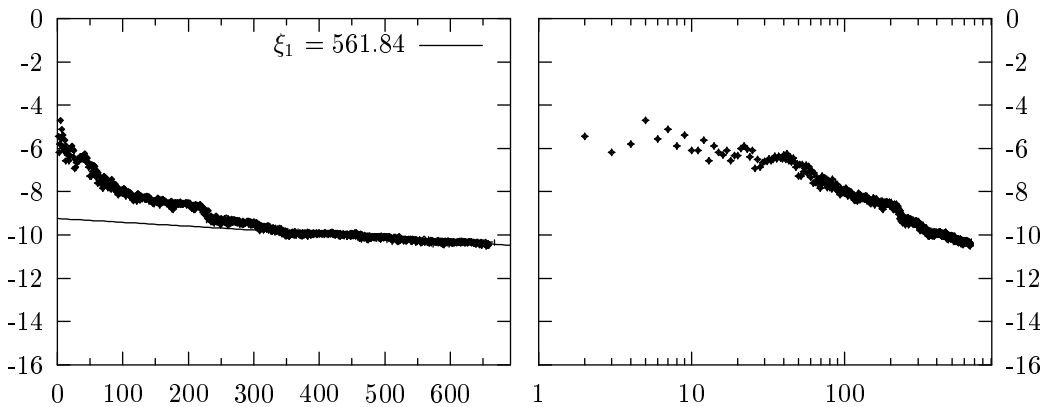


FIGURE 332. $\langle \log t_N \rangle_E$ vs. $N$ in 3D, $W = 24$, $E \in [-4.5, -3.5]$

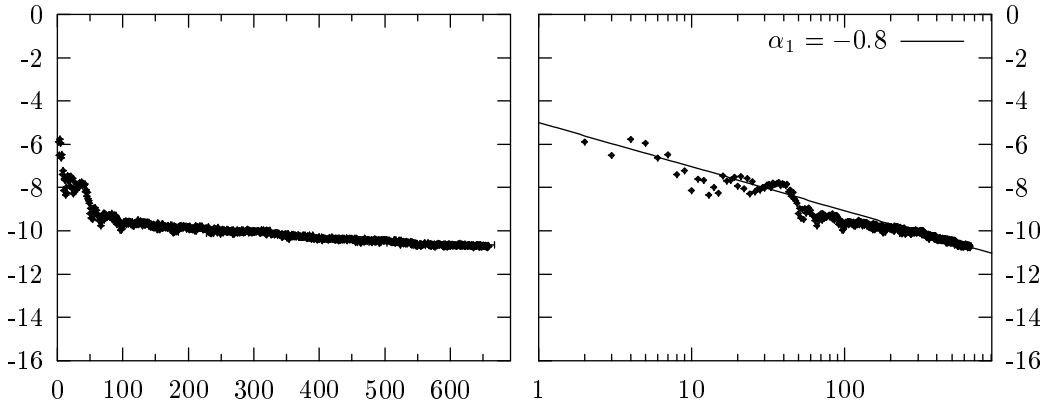


FIGURE 333. $\langle \log t_N \rangle_E$ vs. $N$ in 3D, $W = 24$, $E \in [-3.5, -2.5]$

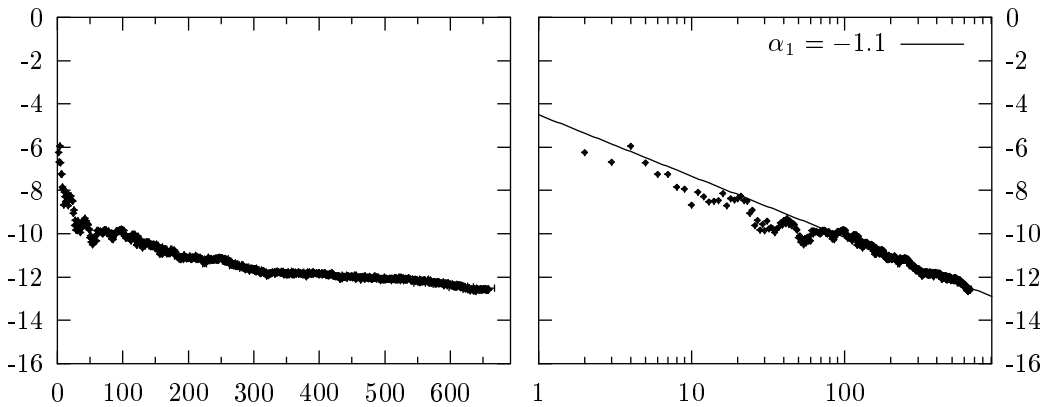


FIGURE 334. $\langle \log t_N \rangle_E$ vs. $N$ in 3D, $W = 24$, $E \in [-2.5, -1.5]$

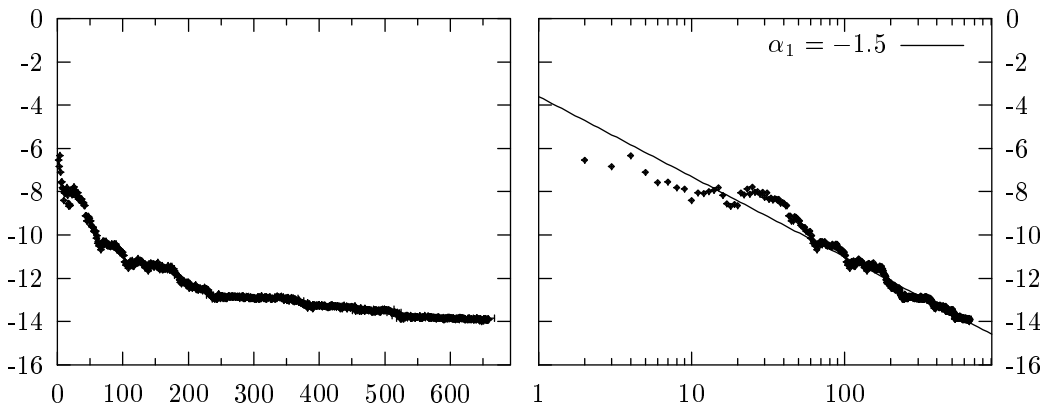


FIGURE 335. $\langle \log t_N \rangle_E$ vs. $N$ in 3D, $W = 24$, $E \in [-1.5, -0.5]$

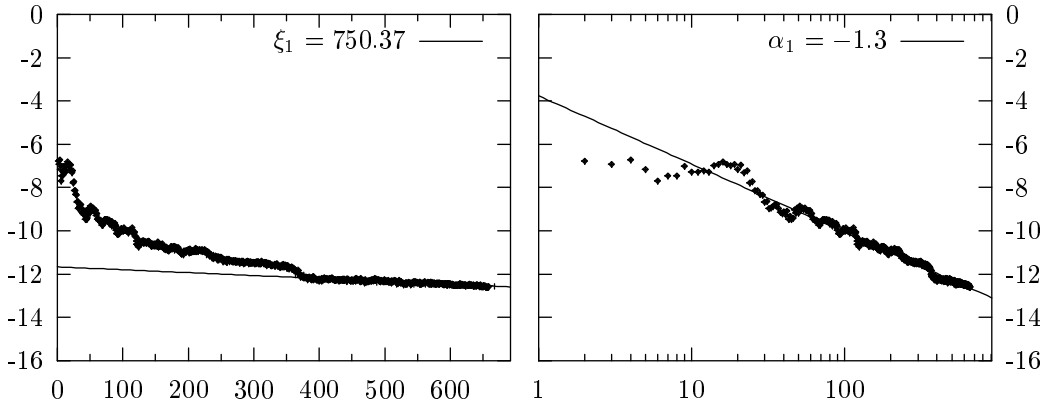


FIGURE 336. $\langle \log t_N \rangle_E$ vs. $N$ in 3D, $W = 24$, $E \in [-0.5, 0.5]$

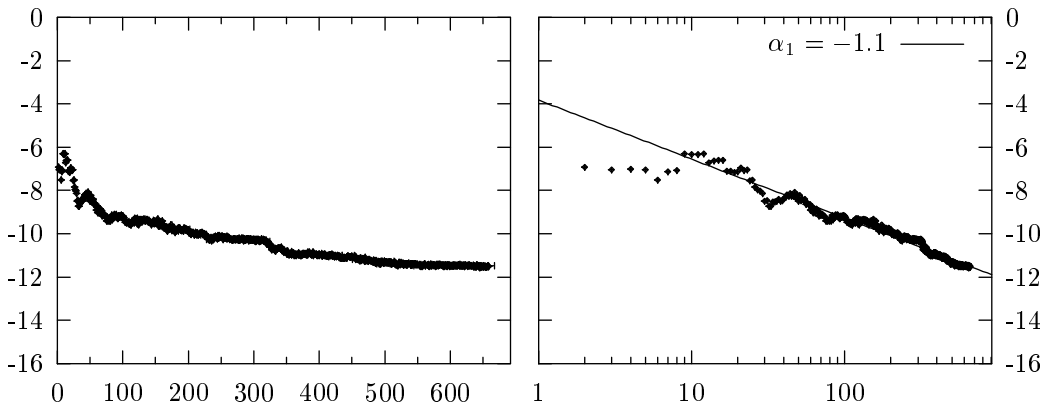


FIGURE 337. $\langle \log t_N \rangle_E$ vs. $N$ in 3D, $W = 24$, $E \in [0.5, 1.5]$

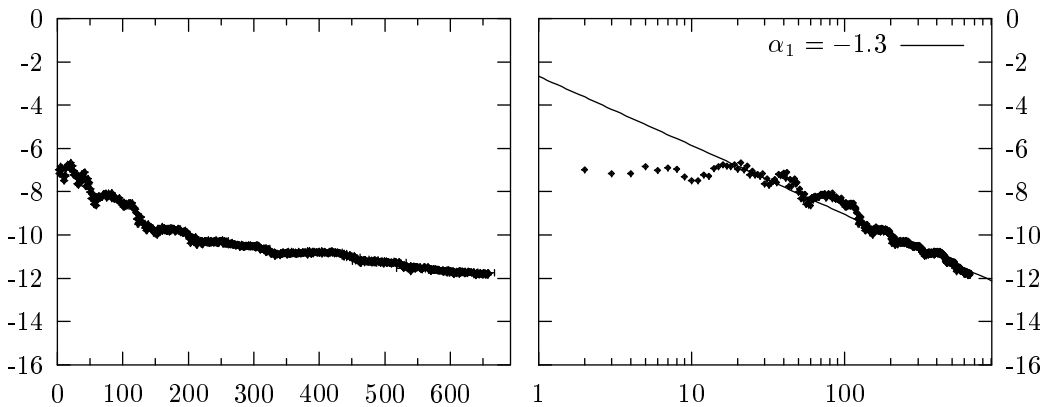


FIGURE 338. $\langle \log t_N \rangle_E$ vs. $N$ in 3D, $W = 24$, $E \in [1.5, 2.5]$

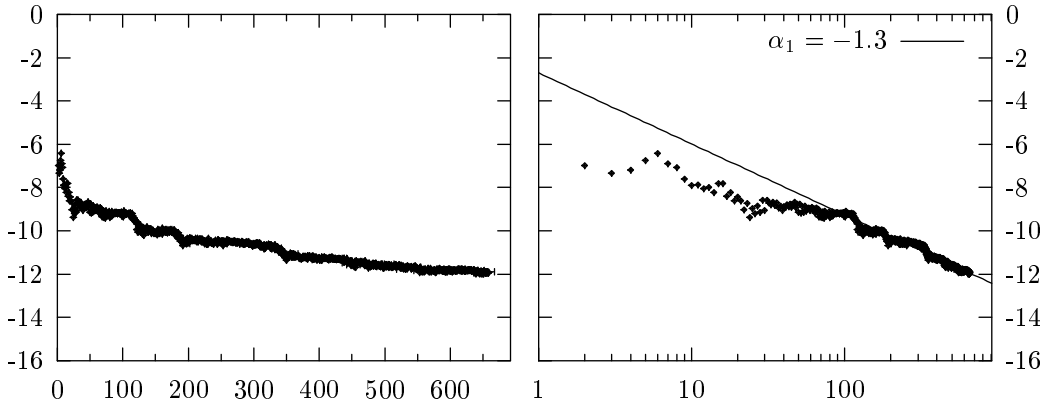


FIGURE 339. $\langle \log t_N \rangle_E$ vs. $N$ in 3D, $W = 24$, $E \in [2.5, 3.5]$

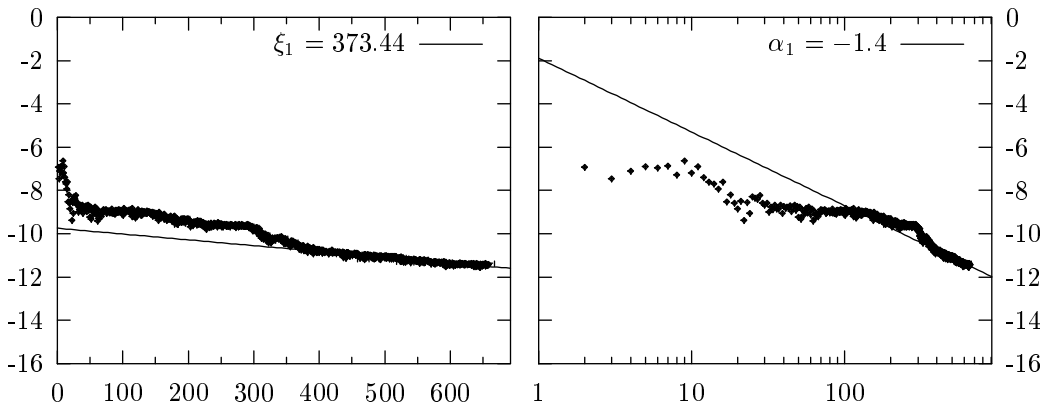


FIGURE 340. $\langle \log t_N \rangle_E$ vs. $N$ in 3D, $W = 24$, $E \in [3.5, 4.5]$

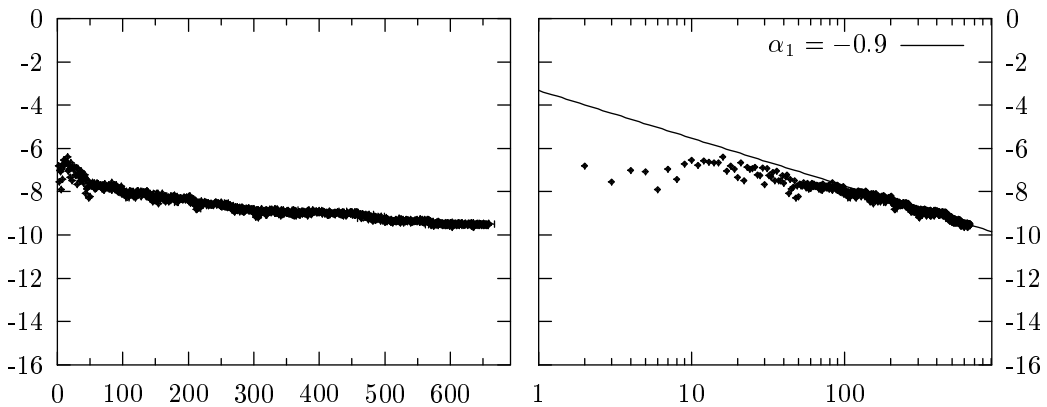


FIGURE 341. $\langle \log t_N \rangle_E$ vs. $N$ in 3D, $W = 24$, $E \in [4.5, 5.5]$

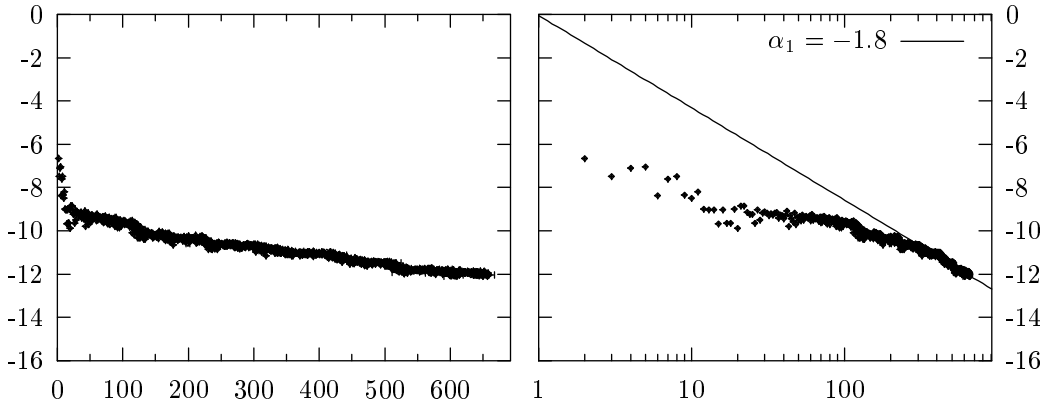


FIGURE 342. $\langle \log t_N \rangle_E$ vs. $N$ in 3D, $W = 24$, $E \in [5.5, 6.5]$

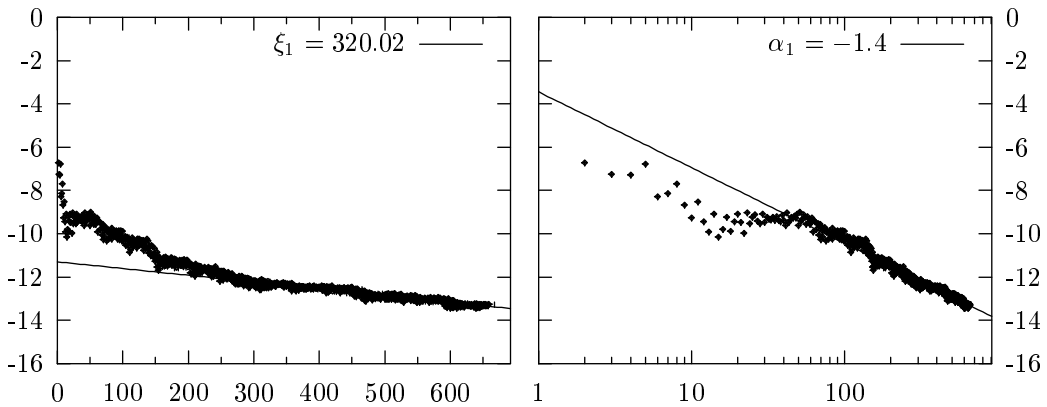


FIGURE 343. $\langle \log t_N \rangle_E$ vs. $N$ in 3D, $W = 24$, $E \in [6.5, 7.5]$

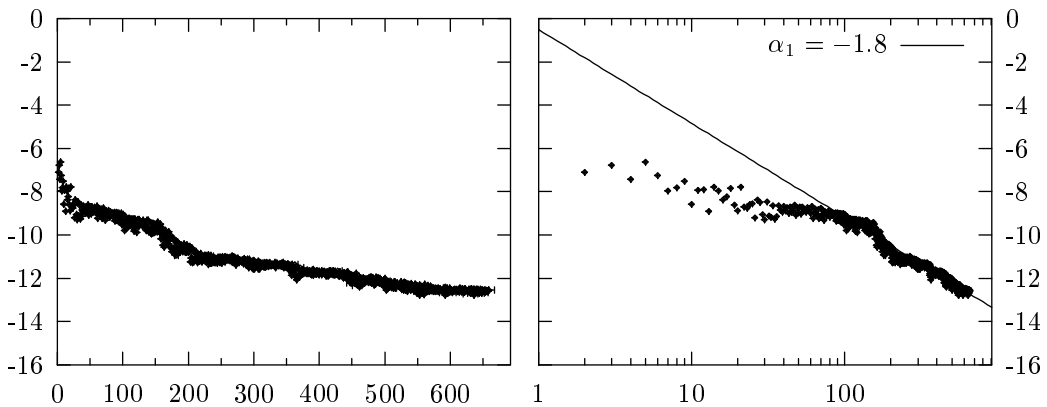


FIGURE 344. $\langle \log t_N \rangle_E$ vs. $N$ in 3D, $W = 24$, $E \in [7.5, 8.5]$

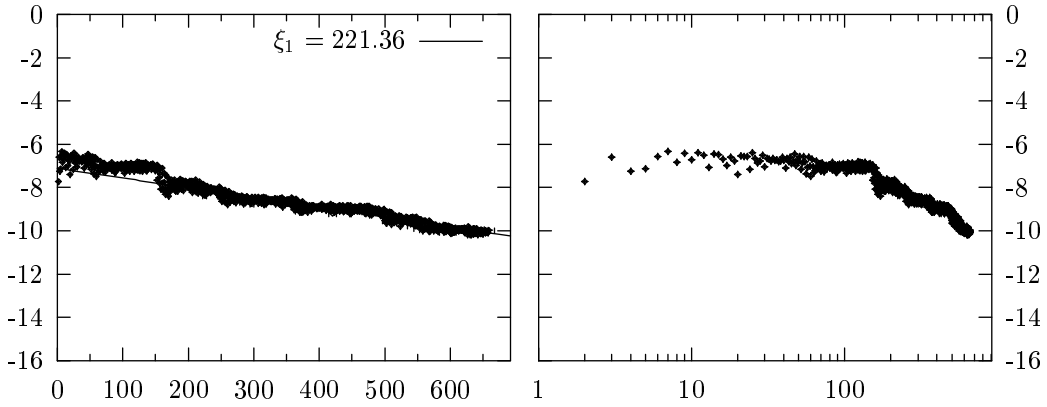


FIGURE 345. $\langle \log t_N \rangle_E$ vs. $N$ in 3D, $W = 24$, $E \in [8.5, 9.5]$

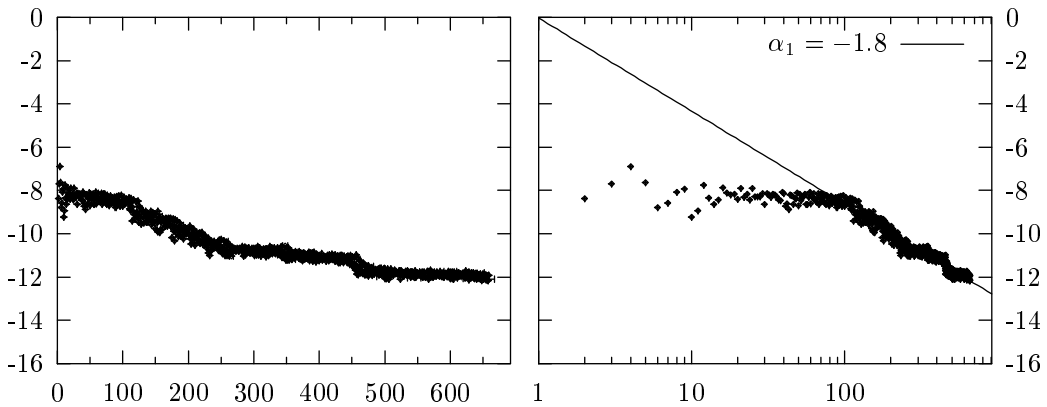


FIGURE 346. $\langle \log t_N \rangle_E$ vs. $N$ in 3D, $W = 24$, $E \in [9.5, 10.5]$

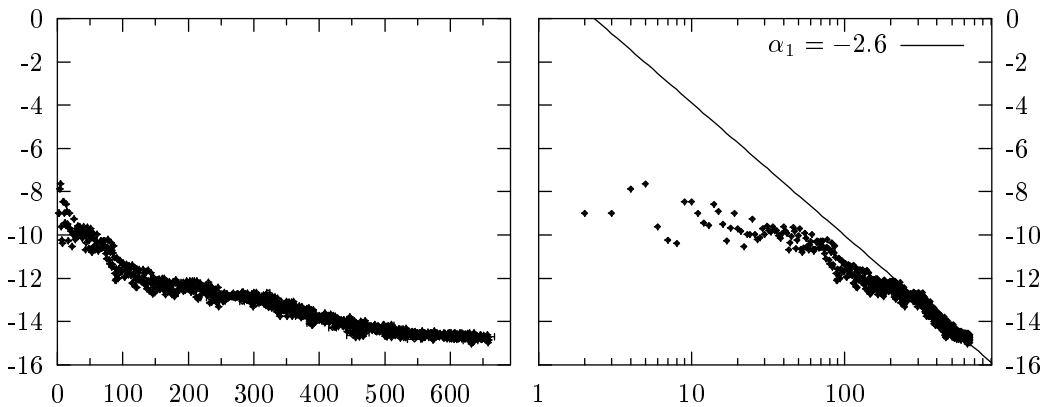


FIGURE 347. $\langle \log t_N \rangle_E$ vs. $N$ in 3D, $W = 24$, $E \in [10.5, 11.5]$

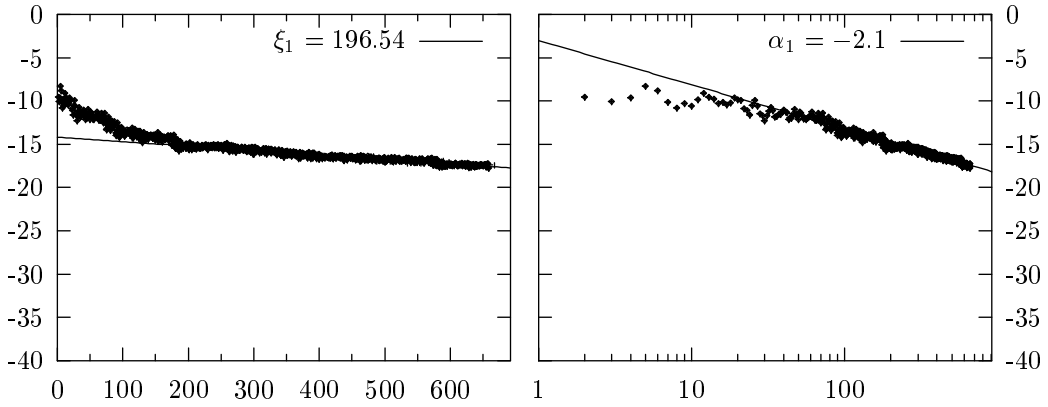


FIGURE 348. $\langle \log t_N \rangle_E$ vs. $N$ in 3D, $W = 24$, $E \in [11.5, 12.5]$

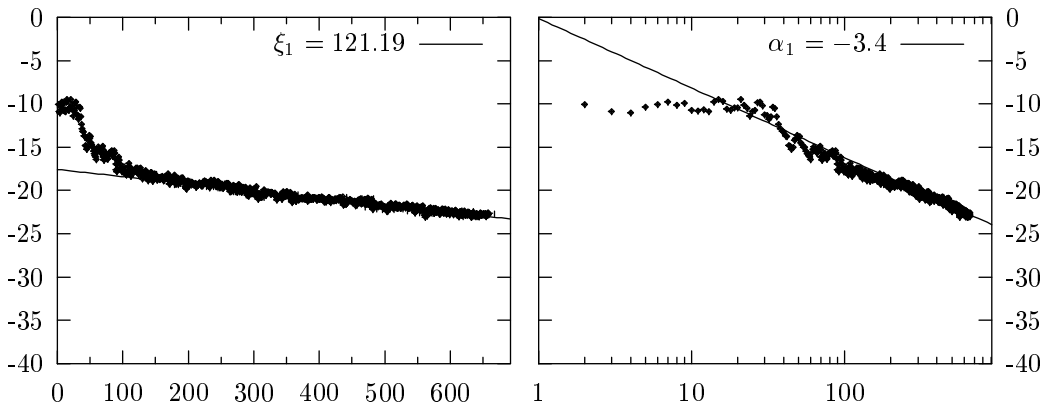


FIGURE 349. $\langle \log t_N \rangle_E$ vs. $N$ in 3D, $W = 24$, $E \in [12.5, 13.5]$

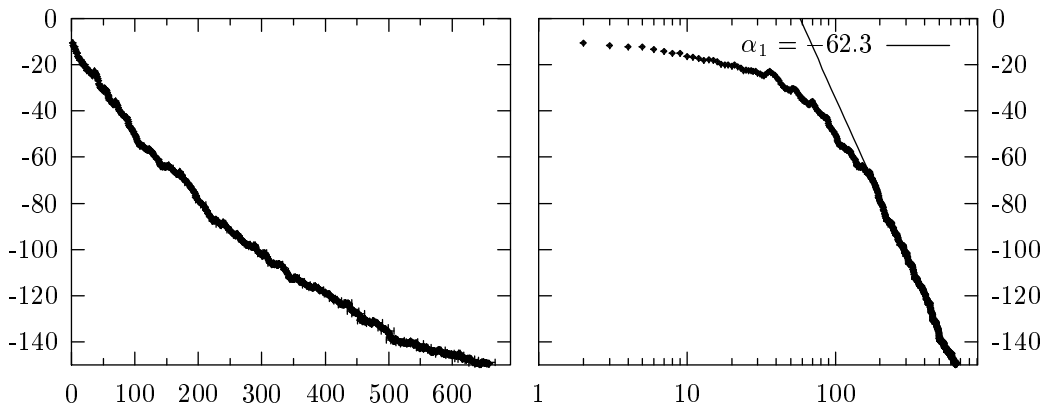


FIGURE 350. $\langle \log t_N \rangle_E$ vs. $N$ in 3D, $W = 24$, $E \in [13.5, 14.5]$

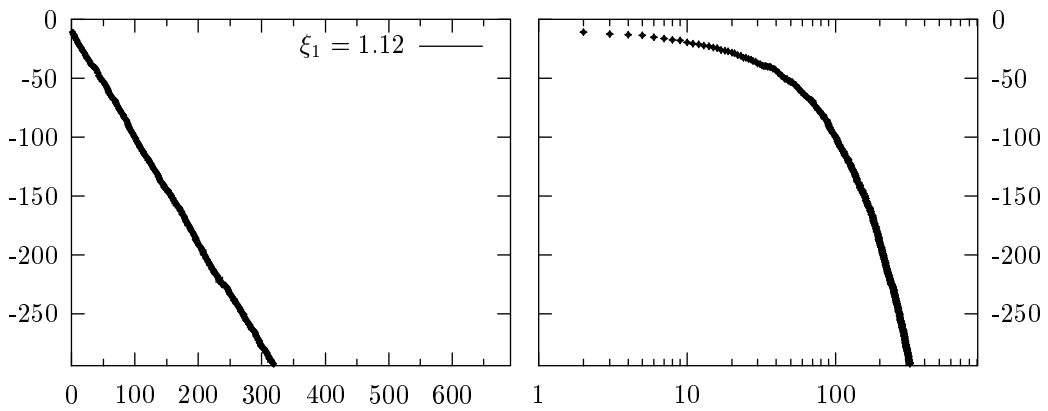


FIGURE 351. $\langle \log t_N \rangle_E$ vs. $N$ in 3D, $W = 24$, $E \in [14.5, 15.5]$

# BIBLIOGRAPHY

E. Abrahams, P. W. Anderson, D. C. Licciardello, and T. V. Ramakrishnan. Scaling theory of localization: absence of quantum diffusion in two dimensions. *Phys. Rev. Lett.*, 42:673–6, 1979.

N. I. Akhiezer. *The classical moment problem and some related questions in analysis*. Hafner Pub. Co., New York, 1965.

B. L. Altshuler, D. L. Maslov, and V. M. Pudalov. Metal-insulator transition in 2d: resistance in the critical region. *cond-mat/0003032*, 2000.

G. M. Amdahl. Limits of expectation (vector processing, massively parallel processing and Gallium Arsenide devices). *International Journal of Supercomputer Applications*, 2:88–94, 1988.

*ISO/IEC/ANSI International Standard, Programming Languages—C++*. American National Standards Institute, New York, 1998.

P. W. Anderson. Absence of diffusion in certain random lattices. *Physical Review*, 109:1492–05, 1958.

P. W. Anderson, D. J. Thouless, E. Abrahams, and D. S. Fisher. New method for a scaling theory of localization. *Phys. Rev. B*, 22:3519–26, 1980.

J. F. Annett, W. Matthew, C. Foulkes, and R. Haydock. A recursive solution of Heisenberg's equation and its interpretation. *J. Phys. C*, 1994.

W. T. Arnold and R. Haydock. A parallel, object-oriented implementation of the dynamic recursion method. In D. Caromel, R. R. Oldehoeft, and M. Tholburn, editors, *Computing in Object-Oriented Parallel Environments. Second International Symposium, ISCOPE '98. Proceedings*, pages 199–206, Berlin, Germany, 1998. Springer-Verlag.

N. W. Ashcroft and N. D. Mermin. *Solid state physics*. Holt, Rinehart and Winston, New York, 1976.

D. Belitz and T. R. Kirkpatrick. The Anderson-Mott transition. *Rev. Mod. Phys.*, 66:261–380, 1994.

E. Berger. The Hoard memory allocator. URL: `http://www.cs.utexas.edu/users/emery/hoard/`, 2000.

P. T. Boggs, R. H. Byrd, J. E. Rogers, and R. B. Schnabel. *User's Reference Guide for ODRPACK Version 2.01, Software for Weighted Orthogonal Distance Regression.* U.S. Department of Commerce, National Institute for Standards, Gaithersburg, MD 20899, 1992.

B. Bulka, M. Schreiber, and B. Kramer. Localization, quantum interference, and the metal-insulator transition. *Z. Phys. B*, 66(1):21–30, 1987.

T. S. Chihara. *An introduction to orthogonal polynomials.* Gordon and Breach, New York, 1978.

D. Cortesi, A. Evans, W. Ferguson, J. Hartman, and S. Thomas. *Topics in IRIX Programming.* Silicon Graphics, Inc., URL: `http://techpubs.sgi.com`, 1999.

D. Cortesi and J. Fier. *Origin2000 and Onyx2 Performance Tuning and Optimization Guide.* Silicon Graphics, Inc., URL: `http://techpubs.sgi.com`, 2nd edition, 1998.

J. K. Cullum and R. A. Willoughby. *Lanczos algorithms for large symmetric eigenvalue computations Vol. I Theory.* Birkhäuser, Boston, 1985.

P. P. Edwards, R. L. Johnston, C. N. R. Rao, D. P. Tunstall, and F. Hensel. The metal-insulator transition: a perspective. *Phil. Trans. R. Soc. Lond. A*, 356: 5–22, 1998.

T. J. Godin. *A phase transition in the low temperature conductance of two dimensional systems.* PhD thesis, University of Oregon, 1988.

T. J. Godin and R. Haydock. Evidence of a pseudo-mobility-edge for electrons in disordered layers. *Phys. Rev. B*, 46:1628–34, 1992.

A. R. Hamilton, M. Y. Simmons, M. Pepper, E. H. Linfield, P. D. Rose, and D. A. Ritchie. Reentrant insulator-metal-insulator transition at $B = 0$ in a two-dimensional hole gas. *Phys. Rev. Lett.*, 82(7):1542–5, 1999.

R. Haydock. The recursive solution of the Schrödinger equation. In H. Ehrenreich, F. Seitz, and D. Turnbull, editors, *Solid State Physics*, volume 35, page 215. Academic Press, New York, 1980.

R. Haydock. Asymptotic forms for the states of weakly disordered systems. *Phil. Mag. B*, 53:545–59, 1986.

R. Haydock. Convergent method for calculating the properties of many interacting electrons. *Phys. Rev. B*, 61:7953–64, 2000.

R. Haydock and D. B. Kim. Recursive solution of Liouville's equation. *Comp. Phys. Comm.*, 1995.

V. Heine. Electronic structure from the point of view fo the local atomic environment. In H. Ehrenreich, F. Seitz, and D. Turnbull, editors, *Solid State Physics*, volume 35, page 1. Academic Press, New York, 1980.

J. Heinrich. *Origin and Onyx2 Programmer's Reference Manual.* Silicon Graphics, Inc., URL: `http://techpubs.sgi.com`, 1996.

J. Heinrich. *Origin and Onyx2 Theory of Operations Manual.* Silicon Graphics, Inc., URL: `http://techpubs.sgi.com`, 1997.

J. Hubbard. Electron correlations in narrow energy bands. *Proc. R. Soc. Lond. A*, 276:238–57, 1963.

J. Hubbard. Electron correlations in narrow energy bands; II. the degenrate band case. *Proc. R. Soc. Lond.*, 277:237–59, 1964a.

J. Hubbard. Electron correlations in narrow energy bands; III. an improved solution. *Proc. R. Soc. Lond.*, 281:401–19, 1964b.

M. Janssen. Statistics and scaling in disordered mesoscopic electron systems. *Physics Reports*, 295(1-2):1–91, 1998.

P. D. Kirkman and J. B. Pendry. The statistics of one-dimensional resistances. *J. Phys. C*, 17:4327–44, 1984.

S. Kleiman, D. Shah, and B. Smaalders. *Programming With Threads.* Prentice Hall, 1996.

B. Kramer, K. Broderix, A. Mackinnon, and M. Schreiber. The Anderson transition: new numerical results for the critical exponents. *Physica A*, 167(1):163–74, 1990.

S. V. Kravchenko, G. V. Kravchenko, J. E. Furneaux, V. M. Pudalov, and M. D'Iorio. Possible metal-insulator transition at $B = 0$ in two dimensions. *Phys. Rev. B*, 50(11):8039–42, 1994.

S. V. Kravchenko, W. E. Mason, G. E. Bowker, J. E. Furneaux, V. M. Pudalov, and M. D'Iorio. Scaling of an anomalous metal-insulator transition in a two-dimensional system in silicon at $B = 0$. *Phys. Rev. B*, 51(11):7038–45, 1995. Copyright (1995) by the American Physical Society.

R. Landauer. Spatial variation of currents and fields due to localized scatterers in metallic conduction. *IBM J. Res. Dev.*, 1:223–31, 1957.

R. Landauer. Electrical resistance of disordered one-dimensional lattices. *Phil. Mag.*, 21:863–7, 1970.

R. Landauer. Can a length of perfect conductor have a resistance? *Physics Letters A*, 85A:91–3, 1981.

I. M. Lifshitz. Structure of the energy spectrum of impurity bands in disordered solid solutions. *Soviet Physics JETP*, 17(8):1159–70, 1963.

A. MacKinnon and B. Kramer. The scaling theory of electrons in disordered solids: additional numerical results. *Z. Phys. B*, 53(1):1–13, 1983.

A. Malony and S. Shende. Performance technology for complex parallel and distributed systems. In G. Kotsis and P. Kacsuk, editors, *Proc. Third Austrian-Hungarian Workshop on Distributed and Parallel Systems, DAPSYS 2000*, pages 37–46, Norwell, MA, 2000. Kluwer.

N. F. Mott. *Metal-insulator transitions.* Taylor & Francis, London, New York, 2nd edition, 1990.

C. M. M. Nex. The recursion method: processing the continued fraction. *Comp. Phys. Comm.*, 34:101–22, 1984.

P. Ordejón. Order-n tight-binding methods for electronic-structure and molecular dynamics. *Computational Materials Science*, 12:157–91, 1998.

B. N. Parlett. *The symmetric eigenvalue problem.* Classics in Applied Mathematics. SIAM, Philadelphia, 1998.

W. H. Press, S. A. Teukolsky, W. T. Vetterling, and B. P. Flannery. *Numerical recipes in C : the art of scientific computing.* Cambridge University Press, 2nd edition, 1999. Reprinted with corrections.

S. Shende. Profiling and tracing in Linux. In *Proceedings of the Extreme Linux Workshop No. 2, USENIX, Monterey CA*, 1999.

S. Shende, A. D. Malony, J. Cuny, K. Lildlan, P. Beckman, and S. Karmesin. Portable profiling and tracing for parallel, scientific applications using C++. In *Proceedings of the SIGMETRICS Symposium on Parallel and Distributed Tools*, pages 134–45, 1998.

B. I. Shklovskii, B. Shapiro, B. R. Sears, P. Lambrianides, and H. B. Shore. Statistics of spectra of disordered systems near the metal-insulator transition. *Phys. Rev. B*, 47:11487–90, 1993.

J. A. Shohat. *The problem of moments.* American Mathematical Society, New York, 1943.

M. Y. Simmons, A. R. Hamilton, T. G. Griffiths, A. K. Savchenko, M. Pepper, and D. A. Ritchie. Metal-insulator transition at $B = 0$ in an ultra-low density two-dimensional hole gas. *Physica B*, 249-251:705–9, 1998a.

M. Y. Simmons, A. R. Hamilton, M. Pepper, E. H. Linfield, P. D. Rose, D. A. Ritchie, A. K. Savchenko, and T. G. Griffiths. Metal-insulator transition at $B = 0$ in a dilute two dimensional gaas-algaas hole gas. *Phys. Rev. Lett.*, 80(6): 1292–5, 1998b.

B. Stroustrup. *The C++ Programming Language.* Addison-Wesley, 3rd edition, 1997.

R. L. Te and R. Haydock. Accuracy of the recursion method. *Phys. Rev. B*, 49: 10845–50, 1994.

D. J. Thouless. Electrons in disordered systems and the theory of localization. *Physics Reports C*, 13:93–142, 1974.

T. Vojta and F. Epperlein. Electronic transport in disordered interacting systems. *Ann. Phys.*, 7:493–7, 1998.

M. von Laue. Die Freiheitsgrade von Strahlenbündeln. *Annalen der Physik*, 44(4), 1914.

J. H. Wilkinson. *The algebraic eigenvalue problem.* Clarendon Press, Oxford, 1985.

K. G. Wilson and J. Kogut. The renormalization group and the epsilon expansion. *Physics Reports*, 12c(2):75–200, 1974.

A. D. Zdetsis, C. M. Soukoulis, E. N. Economou, and G. S. Grest. Localization in two- and three-dimensional systems away from the band center. *Phys. Rev. B*, 32:7811–7816, 1985.

I. K. Zharekeshev and B. Kramer. Scaling of level statistics at the disorder-induced metal-insulator transition. *Phys. Rev. B*, 51:17239–42, 1995.

I. K. Zharekeshev and B. Kramer. Asymptotics of universal probability of neighboring level spacings at the Anderson transition. *Phys. Rev. Lett.*, 79:717–20, 1997.

I. K. Zharekeshev and B. Kramer. Advanced Lanczos diagonalization for models of quantum disordered systems. *Comp. Phys. Comm.*, 121-122:502–4, 1999.

J. M. Ziman. *Principles of the theory of solids*. Cambridge University Press, 2nd edition, 1979.